University of Venda
Creating Future Leaders

University of Venda

SCHOOL OF ENVIRONMENTAL SCIENCES
DEPARTMENT OF MINING AND ENVIRONMENTAL GEOLOGY

PALEOENVIRONMENTAL CONDITIONS UNDERPINNING KAOLINITISATION OF LWAMONDO AND ZEBEDIELA KAOLIN DEPOSITS

BY

RAPHALALANI AVHATAKALI
STUDENT NO: 11584229

A RESEARCH DISSERTATION SUBMITTED TO THE DEPARTMENT OF MINING AND ENVIRONMENTAL GEOLOGY, SCHOOL OF ENVIRONMENTAL SCIENCES, UNIVERSITY OF VENDA, IN FULFILLMENT OF THE MASTER OF EARTH SCIENCE IN MINING AND ENVIRONMENTAL GEOLOGY.

SUPERVISOR: PROF G.E. EKOSSE

CO-SUPERVISORS: PROF J.O. ODIYO
PROF J.S. OGOLA

SEPTEMBER, 2017

DECLARATION

I, Raphalalani Avhatakali (Student Number: 11584229), do hereby declare that this dissertation for Master of Earth Sciences in Mining and Environmental Geology degree at the University of Venda, hereby submitted by me, is my own original work; has not been previously submitted for degree work at this or any other university; that all reference material contained therein has been duly acknowledged.

Undersigned,

--------------------------------- ----------------------------
Student's signature Date
A Raphalalani

---------------------------------- -----------------------------
Supervisor's signature Date
Prof G.E. Ekosse

--------------------------------- -----------------------------
Co-supervisor's signature Date
Prof J.O. Odiyo

-------------------------------- -----------------------------
Co-supervisor's signature Date
Prof J.S. Ogola

DEDICATION

I would like to dedicate this work to my family, especially my mother and father who always believed in me and raised me to someone who values education and, also to my friends, who are always there for me, giving me unwavering support, prayers and encouragement. I also want to dedicate this project to my grandparents whose dreams have been fulfilled through me.

ACKNOWLEDGEMENT

I would like to give my sincere and deepest gratitude to the Almighty God for guiding and protecting me all the days of my life especially providing me with strength that I needed during the compilation of this dissertation.

I thank Prof G.E. Ekosse who is my supervisor, and my co-supervisors: Prof J.O. Odiyo and Prof J.S. Ogola for their advice and encouragement that motivated me to carry on with the research. May the Almighty God continue to bless them.

I am most appreciative to the Lwamondo and Zebediela bricks management for giving me an opportunity to conduct research at their mine more especially Mr A Molomo and Mr D Ramarumo for their guidance and assistance. May Almighty God bless them.

I thank National Research Foundation (NRF) and Research Publication Committee (RPC) for supporting me financially.

I thank Mr M.P Tshidada from the Department of Soil Science who assisted me when I was conducting physico-chemical analyses.

I am grateful to Mr G Phindihama from Department of Ecology and Resource Management, University of Venda, who assisted me when I was carrying out Fourier Transform Infrared Spectrophotometry analyses.

I thank the staff of the Department of Hydrology and Water Resource, University of Venda, where clay size fraction were separated.

I am grateful to the staff of Ithemba Labs who assisted with the carrying out of X-ray diffractometry and those of XRD Analytical and Consulting for carrying out phase identification and quantification.

I thank Ms N Baloyi from the University of Johannesburg for assisting me when I was carrying out Scanning Electron Microscopy analyses

I thank the staff of the Department of Geological Sciences, University of Cape Town for carrying out stable isotopes analyses.

I am grateful to the staff of the Central Analytical Facilities, University of Stellenbosch for carrying out major oxides and trace elements analyses.

I also give thanks to my friend Ms Nenita Ntumba Bukalo who took her time to support me through fieldwork, laboratory work and academically.

I thank Mr M Oyebanjo who took his time and assisted me when I was doing my field work.

I thank all my friends for being there for me and supporting me when I was doing my research.

Last but not the least, I thank my father (Raphalalani Mashudu), my mother (Raphalalani Emily), my grandparents and my siblings who has always been there by my side while I was carrying out this research, supporting me spiritually, socially and financially. May Almighty God bless all of them.

ABSTRACT

In the present study, the physico-chemical, applications, mineralogy, geochemistry and stable isotope of Lwamondo and Zebediela kaolin is documented, in order to understand the genesis, paleoenvironmental conditions and possible utilization. Mineral identification studies were conducted using X-ray diffractometer (XRD), Fourier transform infrared spectrophotometer (FTIR) and scanning electron microscope with energy dispersive X-ray micro analysis (SEM-EDX). Major oxides were identified by X-ray Florescence (XRF) whereas trace elements were identified by Laser Ablation Inductively Coupled Plasma-Mass Spectrometer (ICP-MS). Hydrogen and oxygen isotopic composition were determined by δ^{18}O and δD isotopic measurements.

Kaolinite was dominant mineral in all the kaolin samples whereas muscovite, quartz, goethite, hematite, smectite, anatase occurred in minor to trace quantities. The chemical data show that the kaolins are composed mainly of SiO_2 and Al_2O_3 due to the presence of quartz and kaolinite, with minor to trace amounts of other elements such as Ca, Na, Cr, K, Fe, Mn, Mg, P and Ti which affected the kaolin application negatively. Lower concentration of Ca, Na, K, Fe, Mn, Mg, and Ti show the extent of the kaolinitisation. The samples were enriched in Ni and depleted in some other trace elements. The chondrite-normalised rare earth elements patterns show enrichmnent in Heavy Rare Earth Elements (HREE) than Light Rare Earth Elements (LREE) with slight positive Eu anomaly. The Rare Earth Elements (REE) pattern and the content of other trace elements show evidence of weathering processes related to kaolinitisatioon.

Kaolin genesis is explained using kaolin mineralogy, particle morphology, structural order (functional group), major and trace elements geochemical data. The data suggest that kaolin is derived from the intensive chemical weathering of intermediate to mafic rocks deposited in non-marine environment. The stable isotopes were used to determine the paleoenvironmental conditions which influenced kaolinitisation of Lwamondo and Zebediela kaolins. Stable isotopes mean values for kaolinite from both Lwamondo and Zebediela were as follows: δ^{18}O for Lwamondo= +18.57‰ and for Zebediela = +16.67 ‰

and δD for Lwamondo = -65‰ and for Zebediela = -64‰. The calculated mean temperatures were 26.94 ºC for Lwamondo kaolin and 36 ºC for Zebediela kaolin. Low temperatures were inferred from stable isotope values to have been involved in the kaolinitisation wherein hydrothermal processes were eliminated. The data suggests that kaolin was formed in a weathering environment. The kaolin is found to be suitable for brick making and based on the physico-chemical, mineralogical and chemical data it was suggested that the kaolin could also be used in producing low temperature ceramics, refractory materials, pottery and stoneware.

Keywords: geochemistry, kaolinite, mineralogy, paleoenvironmental conditions, stable isotope

TABLE OF CONTENTS

LIST OF FIGURES

LIST OF TABLES

LIST OF ACRONYM AND ABBREVIATION

XRD	X-ray diffractometry
FTIR	Fourier Transform Infrared Spectrophotometry
SEM-EDX	Scanning Electron Microscopy-energy dispersive
XRF	X-ray Fluorescence
LA ICP-MS	Laser Ablation Inductively Coupled Plasma-Mass spectrometry
DWAF	Department Water Affair and Forestry
pH	potential of hydrogen
EC	Electrical Conductivity
ClF_3	Chlorine Fluoride
CIW	Chemical Index of Weathering
CIA	Chemical Index of Alteration
GPS	Global Positioning System
H_2O_2	Hydrogen Peroxide
TAS	Total Alkali Silica
KCl	Potassium chlorine
H_2O	Water
Na_2Co_3	Sodium Carbonate
LOI	Loss on Ignition
BIF	Banded Iron Formation
Wt %	weight percentage

CHAPTER 1

INTRODUCTION

1.1 Background

Kaolin is an important industrial mineral, which is used in many industrial applications such as paper filling and coating, refractory, ceramics, fibreglass, cement, rubber, plastics, paint, catalyst and in many other uses (Murray, 2002). Brick making, pottery chinaware and the construction industries are major consumers of kaolin (Ekosse, 2005). World kaolin utilization is distributed as follows; paper filling and coating (45%), refractory (16%), ceramic (15%), fibreglass (6%), cement (6%), rubber and plastics (5%), paint (3%), catalyst (2%) and others (2%) (Diko, 2011). Knowledge about kaolin genesis and quality has a direct bearing on its industrial applications (Ekosse, 2000).

According to Njoya *et al*. (2006), kaolin quality and genesis play important roles in its exploitation, and the economy and development of technology. The value price of kaolin is determined by its grade. Kaolin exploitation around the world remains a financially sustainable profit making mining industry that continues to contribute positively to national economies (Ekosse, 2010). Exploitation and beneficiation of kaolin for other industrial applications add more economic value to the mineral (Ekosse, 2000). The total world production of kaolin is estimated to be 39 million tons per year (Murray, 2002).

Kaolin deposits occur in a wide range of lithologies such as laterites, bauxites and altered igneous and metamorphic rocks and form in different depositional environments such as tropical soils and flood plain deposits (Baioumy, 2013a). Kaolin deposits could be primary or secondary depending on their genesis. Primary kaolin could be formed by groundwater movement, weathering or by the action of hydrothermal fluids (Heckroodt, 1991). Secondary kaolins are sedimentary in origin and are formed by the deposition of kaolinite which was formed elsewhere. Kaolins of sedimentary origin have higher economic value as compared to kaolin of primary origin (Ekosse, 2000).

Kaolin occurrences are generally common and reported in all the continents of the world except Antarctica, but deposits of economic significance are relatively few. Studies carried out by Ekosse (2010) covered more than 250 kaolin deposits and occurrences in Africa including those from countries such as Algeria, Botswana, Burundi, Cameroon, Egypt, Nigeria, South Africa, Tanzania and Zimbabwe.

Seventeen kaolin deposits and occurrences were reported in South Africa including those occurring in Fishhoek Noordhoek Valley, Kommetjie, Brakenfell, Sommerset West, Gansbai, Albertina/Riversdale, George/Mossel Bay, Vanrhynsdorp/Bitterfontein, Garies, Inanda, Ndwedwe, Nelspruit, Grahamstown, Koster, Potchefstroom, Bronkhorstsruit and Polokwane. Kaolin is also known to occur in parts of Limpopo Province. Two of the occurrences in the Province are in Lwamondo and Zebediela for which this research was focused due to their geological and economic significances.

This study concentrated on the paleoenvironmental conditions underpinning the kaolinitisation of the two selected kaolin occurrences in the Limpopo Province (Lwamondo and Zebediela), South Africa. Kaolins are significant in interpreting paleoenvironments because they provide an insight on the ancient environmental conditions under which the mineral was formed and they are thus used as indicators in reconstructing the ancient environments.

1.2 Statement of the problem

Kaolin deposits are widely distributed in Africa. Studies carried out by Ekosse (2010) on several kaolin deposits and occurrences in Africa including South Africa reviewed their geology, mineralogy and applications but did not adequately consider paleoenvironments in their formation. Clay minerals could serve as an indicator in reconstructing paleoenvironments.

Kaolins give better information on the ancient environment under which they are formed and not many studies have been carried out in South Africa except for a few of the kaolins of Western Cape. Stable isotopes have not been used to characterize

South African kaolins including Lwamondo and Zebediela kaolins in studying paleoenvironments and how clay minerals are used to improve paleoclimatic reconstruction (Thiry, 2000).

Kaolin is an important industrial mineral; Lwamondo and Zebediela kaolins are of economic interest and it is important to understand their environments of formation for their efficient exploitation.

1.3 Justification of the study

Kaolinitisation is the process of the formation of kaolinite through alteration of plagioclase and K-feldspar (Pirajno, 2009). Research and publication on paleoenvironmental conditions influencing kaolinitisation in Africa particularly in South Africa, including the Limpopo Province (Lwamondo and Zebediela kaolins), have not been conducted and documented. There was therefore a need to carry out this study in order to outline the paleoenvironmental conditions influencing the kaolinitisation of Lwamondo and Zebediela kaolins and to generate new findings that could contribute to knowledge of paleo-environmental reconstruction using kaolin as an indicator.

Research on paleoenvironmental conditions for kaolinitisation of Lwamondo and Zebediela kaolins are relatively scarce. The study sheds light on the conditions of kaolin formation in the selected study sites and it contributes to the rationalisation of the Lwamondo and Zebediela mining operations and to the exploration of new deposits.

1.4 Research questions

- What are the physico-chemical characteristics of Lwamondo and Zebediela kaolins and their applications?
- What are the mineralogy and geochemistry of Lwamondo and Zebediela kaolins?
- How can trace elements elucidate the genesis of Lwamondo and Zebediela kaolin?

- What are the paleoenvironmental conditions responsible for the kaolinitisation of Lwamondo and Zebediela kaolins?

1.5 Objectives

The main objective of the research was to establish the paleoenvironmental conditions underpinning the kaolinitisation of Lwamondo and Zebediela kaolins. The specific objectives were:

- To determine the physico-chemical characteristics and applications of Lwamondo and Zebediela kaolins.
- To determine the mineralogy and geochemistry of Lwamondo and Zebediela kaolins.
- To elucidate on the genesis of Lwamondo and Zebediela kaolins using trace elements.
- To reconstruct the paleoenvironment of formation of the Lwamondo and Zebediela kaolins.

1.6 Description of the study areas

1.6.1 Location

The two study areas for this research are located in Thulamela and Lepelle-Nkumpi Municipalities in Limpopo Province, South Africa. The Lwamondo Kaolin occurs in Thulamela in the Vhembe District of Limpopo Province, and more precisely at longitude 30° 23' 23" E and latitude 23° 00' 16' N. It is 14.7 km from Thohoyandou town. The Zebediela Kaolin is located in Lepelle-Nkumpi Municipality, within the Capricorn District of Limpopo Province. It is located at longitude 29° 23' 28" E and latitude 24° 16' 56" N. It is 62.8 km from Polokwane (Figure 1.1). Polokwane is the capital and principal economic centre of the Province.

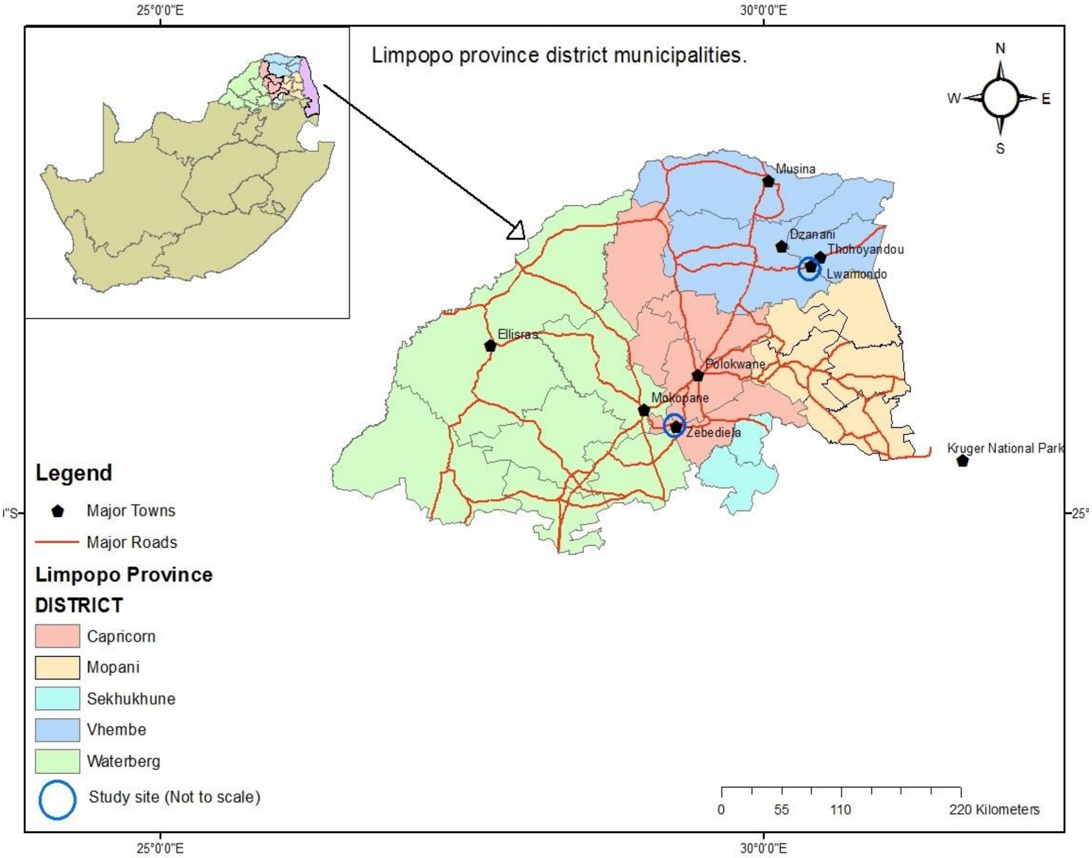

Figure 1.1: Location of the two study sites – Lwamondo and Zebediela in Vhembe and Capricorn Districts, respectively.

1.6.2 Climate

The temperature in Lwamondo area is strongly influenced by seasonal conditions and topography, as most part of the area is surrounded by Soutpansberg Mountain. The summer season (warm and wet) starts from December to February with warm temperatures ranging from 16°C - 40°C and most of the rainfall occurs during this season reaching 2000 mm annually. The winter season (cool and dry) occurs from May to August, the temperature is high and ranges from 12°C to 22°C. Due to the extreme topographic diversity and altitude changes over short distances within the Lwamondo study area, climate (especially rainfall and mist precipitation) varies dramatically (Kabanda, 2003).

The temperature at Zebediela is influenced by seasonal conditions and the changes in the two main physiographic areas, a northern mountainous and a southern flat region (Springbok flats). It also enjoys two seasons: summer and winter. It has a semiarid to semi-humid climatic regime. It has an average daily temperature of 17-27°C in summer and 4-20°C in winter. Average rainfall ranges from 350-650 mm (Diko, 2011).

1.6.3 Topography and drainage

Lwamondo is characterized by slopes of Soutpansberg ranges and the valleys are found between the eastern and western ranges, whereas the flow of the valley becomes flat at the central part of study area (DWAF, 2004). Zebediela consists of two main physiographic regions, a northern mountainous area which is part of the Strydpoort Range and a southern flat area which is known as the Springbok flats.

The community around Lwamondo area rely on Dzindi River for domestic, agricultural and recreational purpose. The Dzindi River is also used by the nearby community for different purposes such as streams or channels are constructed from the river for agricultural purpose. The key rivers in Zebediela area are the Mogoto, Rooisloot and Nkumpi which are used by the nearby community for domestic, agricultural and recreational purposes.

1.6.4 Soil type

The soil type of Lwamondo area is derived from the basalt and diabasic dykes which are fine textured, clayey, well weathered and generally deep (Brandl, 2000). The main soil types of the Zebediela area is predominantly reddish-brown to red sandy loams and have very little profile differentiation. Sandstone and granite may also contribute to the red colour of soil.

1.6.5 Landuse

The landuse in Lwamondo is settlement, agriculture, livestock rearing and mining. Kaolin deposit at Lwamondo covers an area of about 2700 m^2 at an average thickness of 28 m and half of the deposit has already been mined (Diko, 2011). The kaolin is currently mined under the trade name “Vhavenda Bricks” with its main use being brick making.

The landuse in Zebediela is settlement, mining, livestock farming, agriculture and tourism. There are Zebediela citrus estates, the Wolkberg Wilderness, Lekgalameetse nature reserve and Bewaarskloieloof reserve. Zebediela kaolin outcrop covers an area of about 3 km^2, average thickness of 130 m and an estimated volume of 390 000 000 m^3. Open pit mining is on-going with only 40 % of the deposit having been mined (Diko, 2011). Mining operations are currently carried out under the trade name “Zebediela Bricks”.

1.7 Study limitations

This study focuses mainly on paleoenvironmental reconstruction using kaolin as an indicator.

CHAPTER 2

LITERATURE REVIEW

2.1 Geology of study areas

2.1.1 Geology of Lwamondo

The geology of the Lwamondo area was dominated by the Soutpansberg Group. The Soutpansberg Basin was formed million years ago and it overlies the eastern part of the Palala Shear zone and part of the Kaapvaal Craton. The collision between the Kaapvaal Craton from the south and the Limpopo Mobile Belt from the north formed the Palala Shear Belt (Brandl, 2000). Initially, the Soutpansberg rocks were formed as a flat featureless landscape and later the area block-faulted and uniformly tilted to the north (Diko, 2011).

The Soutpansberg rocks belong to the Proterozoic and rest on the gneisses of the Limpopo Mobile Belt and Bandelierkoop Complex (Table 2.1 and Figure 2.1). The Soutpansberg outcrops along its eastern and northern part covered by the sedimentary rocks of the Karoo Supergroup. Many sills and dykes occur throughout the Soutpansberg and the sills were mainly emplaced along the interface of shale and competent quartzite whereas the dykes are of intrusive origin and intruded along fault planes (Barker, 1979). The Soutpansberg Group represents a volcano-sedimentary succession and it is subdivided into seven formations: Tshifhefhe Formation, Sibasa Formation, Funduzi Formation, Willies Poort Formation, Nzhelele Formation, Stayt and Mabiligwe Formation and only four Formations: Tshifhefhe, Sibasa, Fundudzi and Wyllie’s Poort Formations occur within the vicinity of the Lwamondo kaolin (Diko, 2011).

The basal discontinuous Tshifhefhe Formation is few meters thick and made up mainly of strongly epidotised clastic sediments, including Shale, greywacke and conglomerate. The Sibasa Formation is mainly a volcanic succession with rare discontinuous intercalations of clastic sediments, having a maximum thickness of about 3 000 m (Brandl, 2000).The volcanics comprise basalts, which were subaerially extruded, and minor pyroclastic rocks (Council for Geosciences, 2002). The basalts are amygdaloidal, massive and generally epidotised. The clastic sediments which include quartzite, shale and minor conglomerate, can reach locally a maximum thickness of 400 m (Brandl, 2000). The overlying Fundudzi Formation is developed only in the eastern part of the Soutpansberg, and wedges out towards the west (Figure 2.1). It consists mainly of argillaceous and arenaceous sediments with a few thin pyroclastic horizons. Near the top of the succession, about 50 m thick layer of epidotised basaltic lava was intercalated with these sediments. The uppermost unit is represented by the Wyllies Poort Formation. Resistant pink quartzite and sandstone with minor pebbles dominated the succession, reaching a maximum thickness of 1500 m. Conspicuously absent from the study area is the Stayt Formation which is correlative of the Sibasa Formation and the Nzhelele and Mabiligwe Formations which are the youngest units within the Soutpansberg Group.

Table 2.1: Lithostratigraphy of the Soutpansberg Group

PHANEROZOIC	**ERATHEN**	**GROUP**	**FORMATION**	**LITHOLOGY**
	UNDIFFERENTIATED KAROO SEQUENCE			
PROTEROZOIC	**MOKOLIAN**	**SOUTPANSBERG**	Willies Poort	Pink quartzite and sandstone with minor pebbles (max 1500m)
			Fundudzi	Epidotised basaltic lava intercalated with sediments (max 50m)
			Sibasa	Basalts, pyroclastic rocks, rare discountinuous intercalations of clastic sediments (400m)
			Tshifhefhe	Clastic sediments, shale, greywacke, conglomerate (max 9m)
ARCHEAN BASEMENT COMPLEX			Hout Plaats gneiss and granite	

Source: (Brandl, 2000)

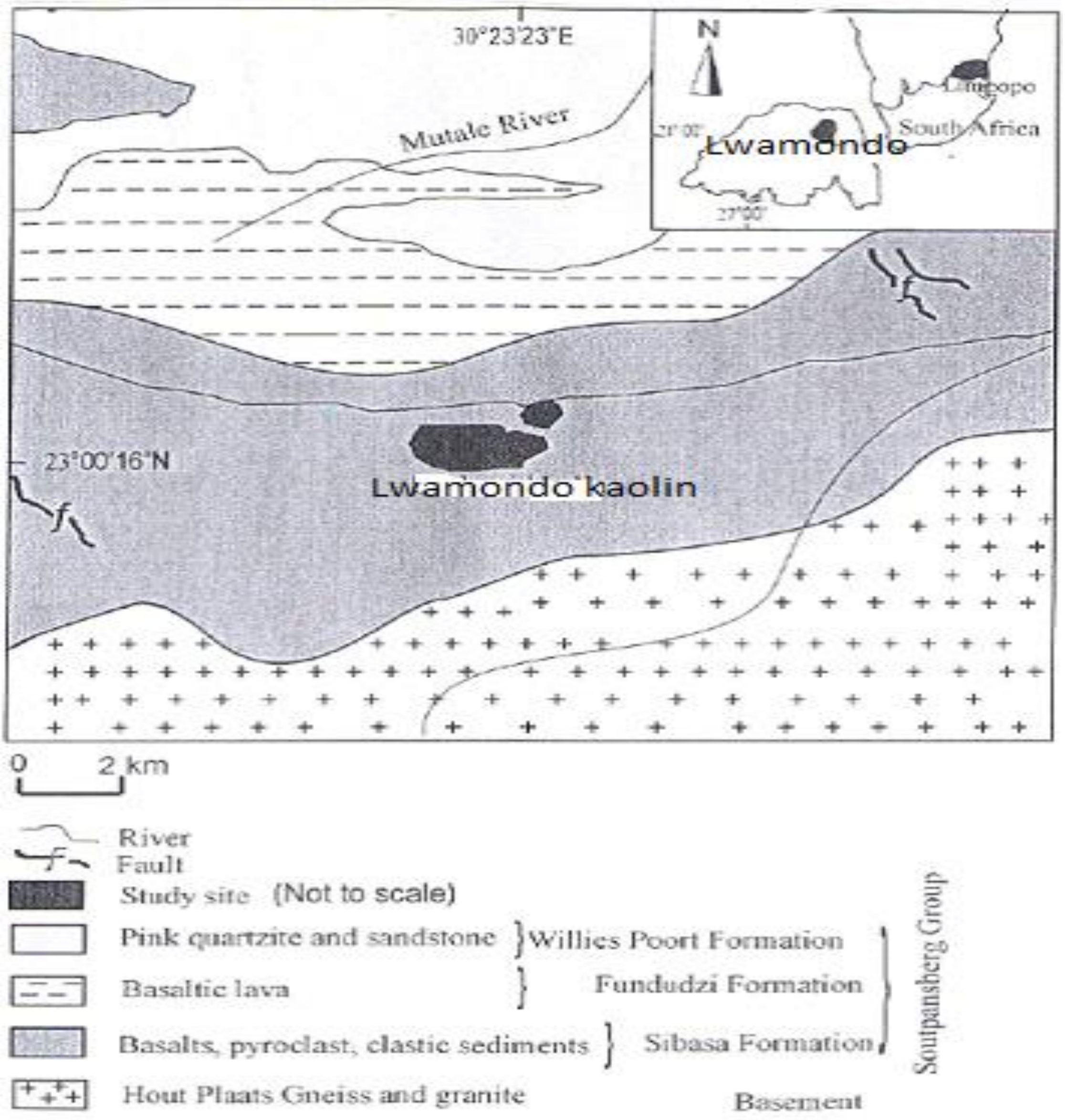

Figure 2.1: Geologic setting of Lwamondo kaolin occurrence (Diko, 2011).

2.1.2 Geology of Zebediela

The geology of Zebediela is made up of rocks that belong to the Transvaal Supergroup. The Transvaal Supergroup is preserved in three separate basins; the Transvaal, Kanye (Botswana) and Griqualand West basin (Catuneanu and Eriksson, 1999). The Transvaal basin is situated in the centre of the Kaapvaal Craton and extends from South Africa into easternmost Botswana. The Bushveld complex is situated largely within the confines of the Transvaal basin. As a result, the Transvaal rocks have undergone contact metamorphism, mostly producing hornfels and quartzites from clastic protoliths and asbestos deposits from Banded Iron Formation (BIF). The Transvaal Supergroup is intruded by mafic and granitic rocks of the Bushveld Complex at 2060 to 2050 Ma (Hartzer, 1995).

The Transvaal Supergroup is subdivided into four main lithostratigraphic units i.e. the Protobasinal rocks, Black Reef Quartzite Formation, Chuniespoort Group and Pretoria Group (Eriksson and Reczko, 1995). Traditionally, the Rooiberg Group has also been included within the Transvaal Supergroup. The area is covered by surficial sediments of the Karoo (Table 2.2 and Figure 2.2) and in the northern part of the Transvaal Supergroup, the area is controlled by ENE and NNW trending faults which are common throughout the Kaapvaal Craton (Diko, 2011). The stratigraphy of the Transvaal basin is discussed below (Figure 2.2).

Protobasinal rocks

Protobasinal term is used for the lowermost stratigraphical subdivision of the Transvaal Supergroup and the Transvaal basin occurs as dicrete units around the margins of the preserved basins: Godwan Group, Buffelsfotein Group, Wolkberg Group and Tshwene-Tshwene basin. The basin-fills of the protobasinal rocks comprise three main lithological associations: volcanic rocks, fault-related continental sedimentary deposits and basinal deposits. The Bimodal volcanics are found in the whole of the protobasinal succession. Fault-related sedimentary rocks (mostly coarse, ranging from boulder conglomerates to sandstones) and the volcanic lithologies (basaltic) characterise the lower Godwan and Wolkberg Groups and the entire Buffelsfontein and Tshwene-Tshwene basin.

Table 2.2: Stratigraphy of Zebediela

PHANEROZOIC	ERATHEM	GROUP/SUBGROUP	FORMATION	LITHOLOGY
	JURASSIC	KAROO SEQUENCE	Letaba	Volcanic rocks (basalts, pyroclast)
	TRIASSIC		Clarens	Red creamy sandstone (fine-grained)
PROTEROZOIC	VALINAN	Chuniespoort	Malmani	Dolomite, chert, limestone, chert breccias with interbed shale, sandstone, quartzite
		BLACK REEF		Lava, tuff, quartzite, shale, sandstone, volcanic rocks
		WOLKBERG		Sandy and tuffaceous shale, mudstone, arkose, conglomerate, volcanic rocks.

Source: (Diko, 2011)

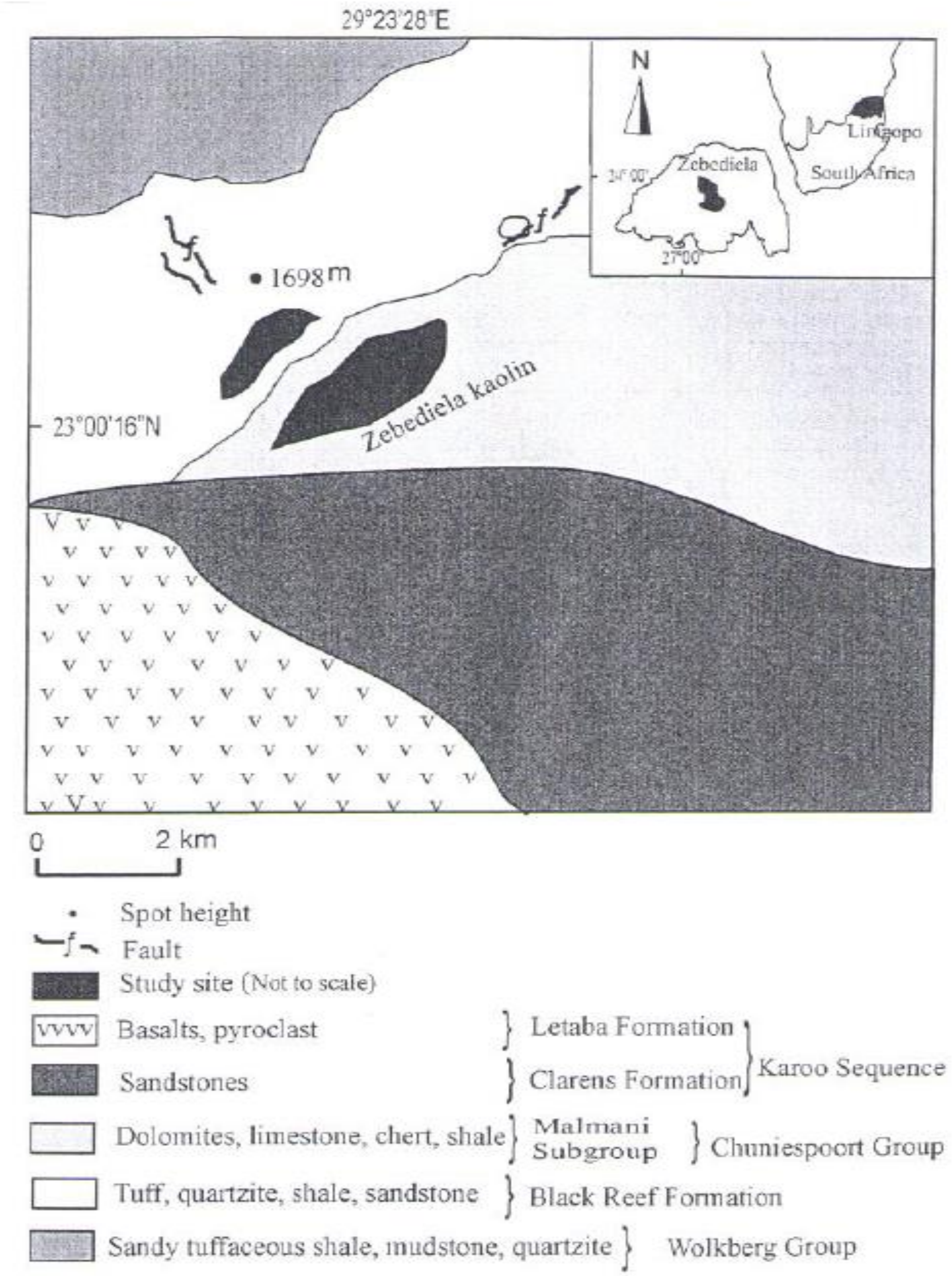

Figure 2.2: Geologic setting of Zebediela Kaolin occurrences (Diko, 2011).

Black Reef Quartzite Formation

The Black Reef Quartzite Formation is preserved around the margins of the Transvaal basin and in the Crocodile River, Marble Hall and Dennilton fragments where the Bushveld intrusive surrounded the occurrences of the Transvaal rocks (Eriksson *et al.*, 2001). The Godwan basin undergoes pre-Black Reef deformation and similarly pre-

Black Reef deformation occurred in the Johannesburg dome area (Eriksson *et al.*, 1995). The Black Reef rocks are overlain by transgressive black shale, which is considered to represent the advance of the Chuniespoort Group area. In most areas, the basal Black Reef generally upward-fining Conglomerates into mature quartz arenites and mudrocks, this upward-fining sequence being followed by upward-coarsening sandstones.

Chuniespoort Group

The Chuniespoort Group covers a large area in the preserved marginal portions of the Transvaal basin as well as more restricted outcrops in the Marble Hall, Dennilton and Crocodile River fragments (Eriksoon *et al.*, 1995). The Chuniespoort Group comprises a basal Malmani Subgroup which comprises five formations (Oaktree, Monte Christo, Lyttelton, Eccles and uppermost Frisco Formations) of dolomite which attains a maximum thickness of about 2100 m at the Crocodile River.

The Pretoria Group

The Pretoria Group covers a large area in the centre of the Transvaal basin, including isolated outcrops surrounded by Bushveld intrusive at the Crocodile River, Dennilton, Marble Hall and Makeckaan fragments. The upper formation in the south of the preserved basin with the Magaliesberg Formation has been removed by erosion having been affected by the intrusion of the Bushveld Complex. Five post Magaliesberg formations occur in the southeast of the basin with the single formations occurring in the Pretoria and far between Transvaal/Botswana regions. The Pretoria Group comprises predominantly alternating mudrock and sandstone formations, interbedded basaltic-andesitic lavas and subordinate conglomerates, diamicitites and carbonate rocks. Most of the sandstones have been recrystallized to quartzite and mudrocks of the Timeball Hill, Strubenkop, Silverton, Vermont, Nederhost and Houtenbek formations also contain thin tuffaceous interbeds (Erikson *et al.*, 1993 and 1995). The Timeball Hill, Daspoort and Magaliesberg Sandstones are mature. The major part of the Pretoria Group consists of the Hekpoort Andesite formation and sheet-like mudrocks of the Timeball Hill and Silverton formations and the interbedded basaltic lavas and pyroclastic rocks of the Machadodorp Member.

2.2 Kaolin minerals

Kaolin is both a rock and a mineral term. Kaolin means that the rock comprises predominantly of mineral kaolinite and/or one of the other kaolin minerals. As a mineral term, kaolin is defined as the group name given for the minerals kaolinite, dickite, nacrite and halloysite. Kaolinite is the most abundant kaolin mineral whereas dickite, nacrite and halloysite are relatively rare and are commonly formed by hydrothermal alteration and occur in sedimentary and residual deposits in association with kaolinite (Murray, 2007). Kaolin is a common phyllosilicate mineral, widely employed as raw material in ceramics, paper, filling, coating, refractory, fiberglass, cement, rubber, plastics, paints, catalyst, pharmaceuticals and agricultural industries (Murray, 2007; Ekosse, 2010).

Kaolin deposits are classified as primary (residual or hydrothermal) or secondary (erosion and transportation of clay particles and their deposition in lacustrine, paludal, deltaic and lagoonal environments) depending on their genesis (Ekosse, 2010). Primary kaolin could be hydrothermal, residual or mixed residual and hydrothermal. The primary kaolins originated in situ by alteration of alumina-silicate rocks such as granite and rhyolites, parent minerals being feldspars (Equation 2.1) and muscovite (Equation 2.2). The alteration of the parent materials (feldspar such as microcline and micas such as muscovite) contained in the gneisses and granitoids eventually led to the formation of the kaolins (Shemang *et al.*, 2007). The alteration caused by action of hydrothermal fluids, surface weathering or groundwater movement below the surface.

$2KAl_3Si_3O_1O\ (OH)_2 + 2H^+ + 3H_2O \rightarrow 3Al_2Si_2O_5\ (OH)_4 + 2K^+$-----------------------Eqn 2.1
K-feldspar kaolinite

$2KAlSi_3O_8 + 2H^+ + 9H2O \rightarrow Al_2Si_2O_5(OH)_4 + 2K^+ + 4H_4SiO_4$-----------------------Eqn 2.2
Muscovite kaolinite

Secondary kaolins are of sedimentary origin, they were eroded, transported and deposited as beds or lenses associated with other sedimentary rocks. Most secondary origin kaolin deposits were formed by the deposition of kaolinite which had been formed elsewhere (Baioumy, 2013a). Whereas some secondary deposits were formed from arkosic sediments that were altered after deposition, primarily by groundwater (Murray and Keller, 1993). Secondary kaolin could also be formed by the alteration of feldsphatic arenites in sedimentary rocks such as arkose, resulting mostly from groundwater activity (Ekosse, 2010). Some of the secondary kaolins were authigenic due to the action of underground meteoric water after deposition of arkosic or sandy materials (Galan, 2006). According to Ruiz (2007), kaolin minerals are formed typically under low temperature and pressure conditions.

Kaolin physico-chemical properties including pH, particle size, particle shape, natural and fired colours, electrical conductivity (EC), cation exchange capacity, surface area, relative density, and melting point ar presented in Table 2.3. Kaolins are usually fine (<2 µm) in particle size and are white or cream in colour (Ekosse, 2005).

Table 2.3: Physico-properties of kaolin minerals

Property	**Kaolinite**
PH value	6.8-7.3
Particle shape	Pseudo hexagonal crystalline plate or book
Particle size	60 wt % - 90 wt % >2µm
Natural color	White or near white, gray
Fired color	Pure white
Relative density (RD)	2.67
Melting point (^{0}C)	1850
Surface area (m_2/g)	10-18
CEC (meq/100g)	2-10
True CEC (meq/100g)	3-15

Source: (Ekosse, 2005)

2.2.1 Kaolinite

Kaolinite is a dominant clay mineral in kaolin constituting about 90% of kaolin deposits and it occurs in a wide variety of sedimentary and metamorphic rocks together with ancillary minerals such as feldspar, quartz, smectite and goethite (Ekosse, 2012). Kaolinite in the deposit occurs in different forms such as in irregular platelets, well-developed irregular flakes and pseudo-hexagonal stacks (Ekosse, 2001).The structural formula for kaolinite is $Al_2Si_2O_5(OH)_4$ and theoretical chemical composition is SiO_2=46.54%; Al_2O_3=39.50% and H_2O=13,96%. Kaolinite structure has a balanced charge (Murray, 2007).

According to Murray (2007), two sheets are combined to form a unit in which the tips of silica tetrahedrons are joined with the octahedral sheet. All of the oxygen of silica tetrahedrons point in the same direction so that the oxygen and/or hydroxyls, which may be present to balance the charges are shared by the silicon in the tetrahedral sheet and the aluminium in the octahedral sheet (Figure 2.3).

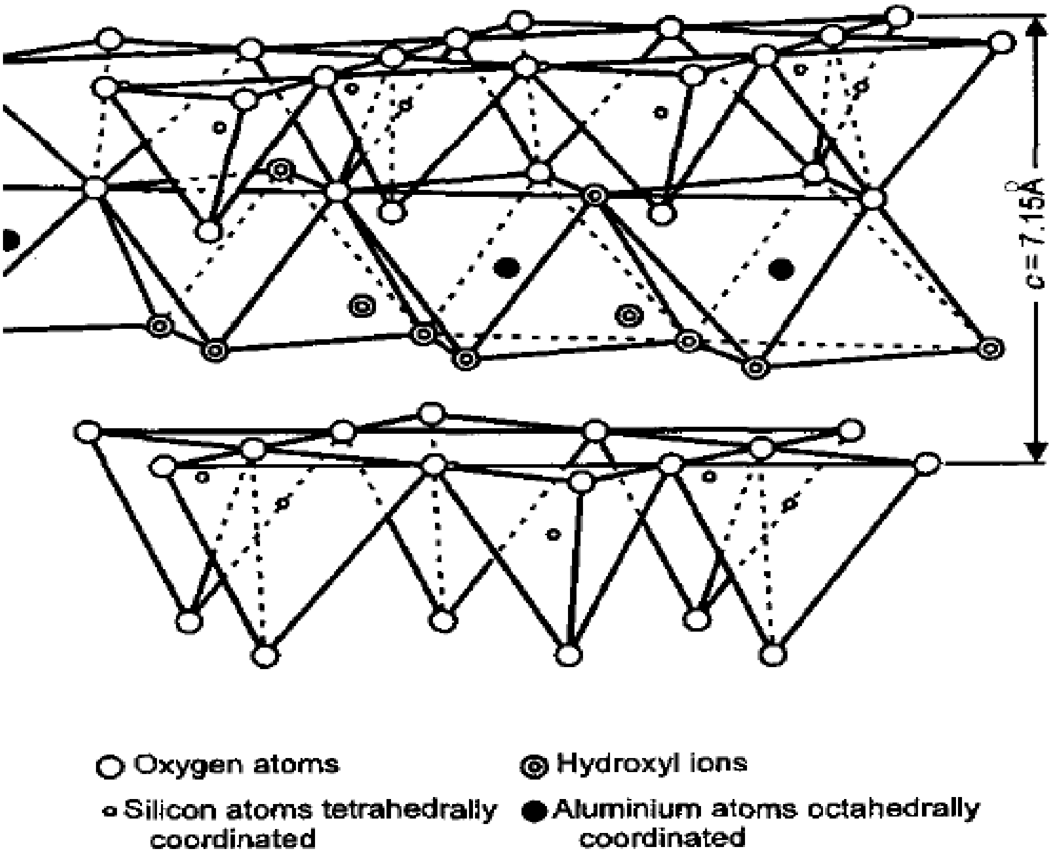

Figure 2.3: Kaolinite structure (Murray, 2007).

Abundant fossil content in kaolinite indicates that it is formed under warm humid climate in a continental palustrine-fluvial environment and the content of SO_2 is the indicator of hydrothermal activity (Dominquez *et al.,* 2008). Mostly Hydrothermal kaolinite are associated with a high temperature minerals such as illite, illite-smectite, mixed layer mineral, dickite, nacrite, topaz and pyrophyllite and are characterised by a very fine grained, hexagonal booklet, tightly packed and low porosity whereas the residual kaolin deposits contain only kaolinite and quartz minerals and are characterised by the absence of high temperature minerals, loosely packed, porous and coarse grain particles (Ismail *et al*., 2014).

2.2.2 Dickite

In dickite, the unit cell consists of two unit layers (Murray, 2007). Dickite has the same 1*M* stacking sequence of layers as kaolinite, but the vacancy alternates regularly between B and C. Dickite is a product of hydrothermal alteration of volcanic rocks and can also form under sedimentary conditions (Mizota and Longstaffe, 1996).

2.2.3 Nacrite

Nacrite has the *R* sequence of layers. The octahedral vacancy alternates regularly between B and C, but any other octahedral sheet is rotated 180°. Nacrite shows a greater interlayer separation and smaller lateral dimensions than dickite and nacrite.

2.2.4 Halloysite

Halloysite is regarded as a hydrated kaolinite phase. Halloysite occurs in two forms: one hydrated in which there is a layer of water molecules between layer, and one dehydrated (Murray, 2007). Halloysite has mainly irregular layer stacking but with a limited tendency for $2M_1$ stacking in small domains. The presence of interlayer water may be related to the presence of small amounts of Al that are balanced by exchangeable cations. Hallyosite is found in hydrothermal and residual deposits but it is rare in kaolins of secondary origin. Dickite and Nacrite are normally restricted to hydrothermal occurrences (Murray and Keller, 1993).

2.3 Factors affecting the formation of kaolin minerals

2.3.1 Parent rocks

Kaolin is generally derived from altered feldspars and muscovite. According to Madi *et al*. (2013), parent rocks are altered by water or hydrothermal fluids through faults and fractures, presence of quartz veins in kaolin may suggest that hydrothermal fluid have intensified the process of alteration. Kaolin deposits may also be derived from alteration of various rocks like igneous rocks such as granite, rhyolite and from volcanic rocks such as trachytes, trachyandesites, andesites and dacites (Papoulis and Katagas, 2008) and it can also be derived from sedimentary rocks such as arkosic sandstone.

Granite

Granite is one of the principal parent rocks of kaolinite (Ekosse, 2012). Under favorable conditions which include high rainfall, rapid drainage, tropical climate, a low water table and adequate supply to leach the soluble components, granite weather readily to kaolinite and quartz (Murray and Keller, 1993). Buwambo kaolin formed from the rock from which the feldspar was altered, rock was medium grained granite, with 60 wt % feldspar (Nyakairu *et al*., 2001).

Sandstone

Sandstone contains quartz and some detrital feldspars and mica grains, which are favourable parent phases for kaolinite formation. High porosity and permeability of the sandstones favoured migration of fluids which enhanced the formation of secondary diagenetic minerals (Diko and Ekosse, 2012).

2.3.2 Climatic conditions

According to Linlin *et al*. (2011), the formation and preservation of clay minerals depend upon the elements of paleo-environment, of which the main key factors are paleo-climate and paleo-water. A climate which is warm and humid with heavy rainfall contribute to the strong chemical weathering of feldspar and mica group and consequently minerals are easily hydrolyzed to kaolinite. A high rainfall, subtropical or tropical climate is therefore the most active environment in which to form residual kaolin (Harvey and Murray, 1997).

According to Manju *et al.* (2001), kaolinite could be formed under tropic weathering conditions characterized by alternate wet and dry seasons with high humidity and moderately high temperature (Figure 2.4). These conditions with periodic rainfall promote rapid chemical breakup of the parent material. Kaolin minerals are formed at relatively low temperatures and pressures. According to Thiry (2000), high temperature and high rainfall increases the rate of breakdown of the primary mineral to kaolin minerals

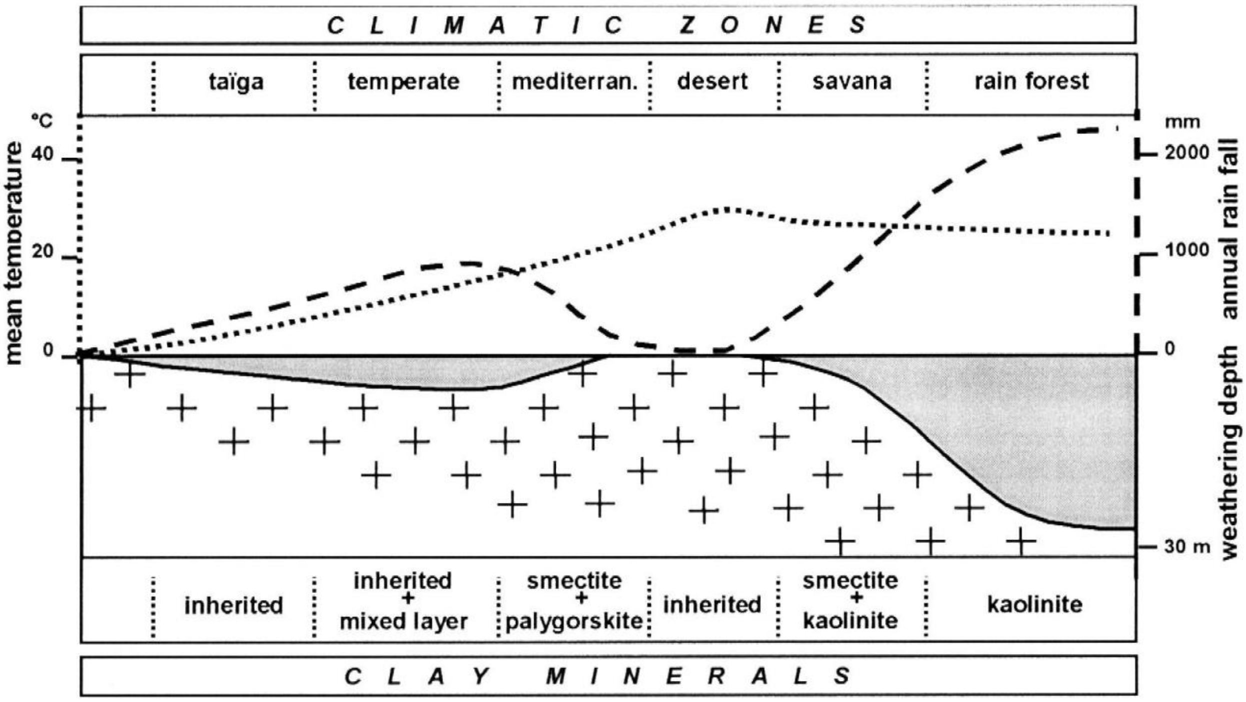

Figure 2.4: Climatic Zone of Clay Minerals (Thiry, 2000).

2.3.3 Hydrothermal alteration

Hydrothermal alteration involves water-rock interaction at temperatures above 50°C in association with volcanic activity or plutonism (Galan and Ferrel, 2013). The formation of kaolinite minerals is apparently enhanced by acidic conditions at low temperature and pressure, while the formation of smectite or mica is favoured by alkaline conditions, depending on the concentration of magnesium or potassium (Heckroodt, 1991). At more elevated temperatures and pressures, the relationship becomes complicated, for example, mica can form under acidic conditions, while kaolinite or pyrophyllite can form in the presence of excess potassium, depending on the particular conditions (Heckroodt, 1992). Alteration may vary from alkaline to acidic as a function of pH and the relative abundances of the alkalis and alkaline earths with respect to hydrogen.

As temperature increases, the mineral paragenesis may change from halloysite to kaolinite to pyrophyte in acidic environment (Galan and Ferrel, 2013). Chemical composition, temperature and pH of the fluid and petrography of the host rocks also influence the clay assemblages formed. According to Harvey and Murray (1997), climate, topography and permeability of the parent rock and temperature alteration are important factors promoting the alteration of the primary minerals to kaolinite and other clay minerals. The most striking examples of hydrothermal alteration were the production of pure kaolin and silica (Galan and Ferrel, 2013). According to Cravero *et al*. (2001), minor and trace elements are useful in interpreting the origin of the alteration.

2.3.4 Weathering

Weathering involves physical disintegration and chemical decomposition and it depends primarily on climate zonation, which determines the intensity of physical and/or chemical weathering. Kaolinite is produced during weathering under tropical or sub-tropical wet climatic conditions (Boulvais *et al*., 2000). Rocks rich in feldspar are commonly weathered/altered to kaolinite. In order to form elements like Na, K, Ca, Mg and Fe must be leached away by the weathering or alteration process. The leaching is favoured by acidic conditions (low pH). Granitic rocks rich in feldspar, are a common source for kaolinite (Odoma *et al*., 2013).

2.3.5 Tectonic and terrain conditions

The height of the terrain affects the strength of weathering. The mechanical sedimentary differentiation of clay minerals is clearly affected by terrain conditions (Linlin, 2011). High content of detrital kaolin in sedimentary sequences is an indicator of intense weathering of source terrains under humid tropical conditions. According to Galan and Ferrel (2013), in zones of intense tectonic activity when flysch is produced, the sedimentary clay minerals assemblages can reflect the composition of the parent rocks directly because active tectonics retard the formation of soils.

2.4 Paleoenvironmental reconstruction using kaolin

The paleoclimatic interpretation of clay minerals including kaolinite requires knowledge of the potential source areas, as well as of the mode and strength of transport processes. The paleoclimatic interpretation of clays is based on the assumptions that they are detrital and have not been altered by diagenesis, that their source areas can be identified and that they represent secondary products of continental weathering (Thiry, 2000).

2.4.1 Stable isotopes

Isotopes are atoms of the same element that differ in atomic mass. Stable isotopes are isotopes that do not undergo radioactive decay. The aluminosilicate framework of a clay mineral contains both hydrogen and oxygen. In addition to the framework oxygen and hydrogen, many types of clay contain loose structural water occupying space between aluminosilicate layers. Varying amounts of water are also typically absorbed on clay surfaces. The isotopic composition of this water contains no information about clay-forming processes or environments.

Hydrogen and Oxygen isotopes have widely been used to examine the environmental conditions prevailing during kaolinite formation (Santos *et al*., 2006, Sheppard and Gilg, 1996). According to Dudek (2012), the climatic constraints of kaolinite (i.e. tropical weathering) are no longer valid without isotopic data due to the reported widespread cold kaolinite weathering. Kaolinite line (KL) (Savin and Epstein, 1970) and Supergene-Hypogene line (SHL) (Sheppard *et al*., 1969) for δD- $\delta^{18}O$ stable isotopes of kaolinite, and the Meteoric Water Line (MWL) (Craig, 1961) (Figure 2.5) are used in interpreting paleoenvironments for kaolinitisation (Ekosse, 2008a; Gilg *et al*., 2003). According to Baioumy (2013b), kaolinites in weathering profiles allow establishment of a straight linear equation known as kaolinite line as well as estimating the isotope fractionation factor. Supergene and Hypogene line (S/H) used to distinguish between clay minerals formed under the earth surface and high burial temperatures. H and O isotopic compositions of kaolinitic rocks in all types of deposit are similar (from alteration profiles, from sedimentary deposits and from those after granites) and are consistent with a supergene origin: $\delta^{18}O_{kaol}$ = 20.2‰ ±1‰, δD_{kaol} = -55‰ to -67‰ (Boulvais *et al*., 2000).

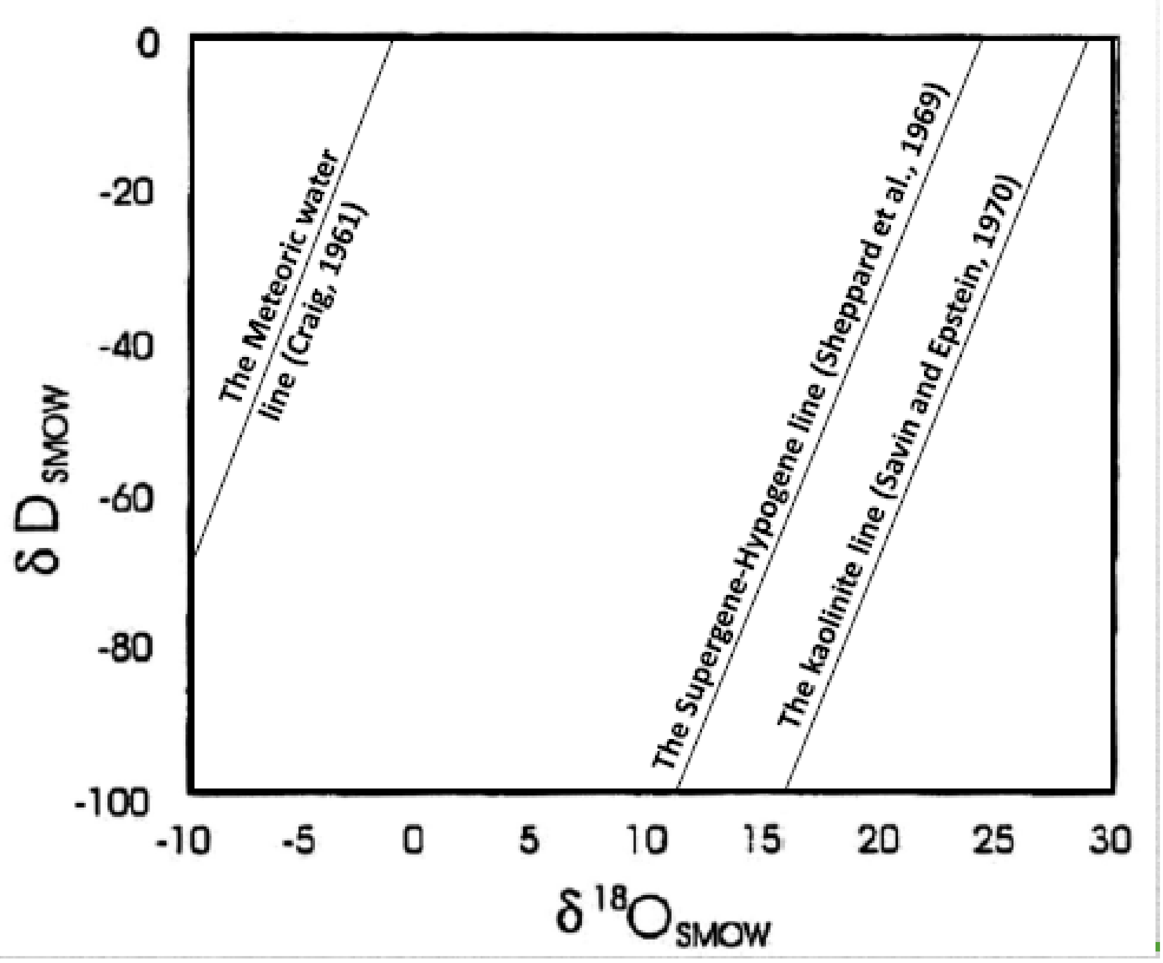

Figure 2.5: δD and $\delta^{18}O$ diagram: Kaolinite line, supergene/hypogene line and meteoric water line (Gilg *et al*., 1999).

Values of δD (-80 to -40‰) and δ^{18}O (+17 to +23‰) are associated with kaolinite formed in hot climates, whereas lower values are associated with kaolinite formed during weathering at high latitude or altitudes, or at a long distance from the coast, where meteoric water was more depleted of δD and δ^{18}O, and temperatures were generally lower (Mizota and Longstaffe, 1996). The hydrothermal kaolin has very low isotopic values, and the sedimentary kaolin has higher δ^{18}O value although there is some overlap particularly between the kaolinite from residual deposit (+15 to +19‰) and kaolinite of sedimentary origin (+19 to +23‰).

The H-and-O isotope compositions of meteoric waters, and therefore supergene clays, are determined by climatic factors of which annual mean air temperature is by far the principal variable outside of tropical island and monsoon climates (Rozanski *et al.*, 1993). We can therefore compare the climate during kaolinitisation with that of the present by determining changes in the isotopic composition of the meteoric waters. The H-and-O isotope composition of meteoric water during kaolinitisation are calculated from isotopic compositions of the kaolinite using the point of intersection of the meteoric water line (δD= δ δ^{18}O+10) with the curve for water in equilibrium with this kaolinite.

The isotopic composition and temperature of the water from which kaolinite formed in equilibrium can be determined from the following equations, which are based on the combination of experimental and theoretical data (Sheppard and Gilg, 1999):

(1) The meteoric-water equation: $\delta D= \delta\, \delta^{18}O+10$---------------------------------Eqn 2.3
(2) The equilibrium hydrogen isotope fractionation factor (α) between kaolinite and water: $1000 \ln \alpha_{kaol\text{-}water} = 2.76 \times 10^{6} T^{-2} - 6.75$----------------------------------Eqn 2.4
(3) The equilibrium oxygen isotope fractionation factor (α) between kaolinite and water: $1000 \ln \alpha_{kaol\text{-}water} = 2.76 \times 10^{6} T^{-2} - 6.75$----------------------------------Eqn 2.5

This approach is applied to clay minerals that are formed in open systems with high water-rock ratios and relatively low temperatures, such as surface alterations and low-temperature hydrothermal systems (Delgado and Reyes, 1996).

2.4.2 Mineralogy

Clay minerals reflect weathering conditions imparted on the source rock and can be used for the interpretation of marine depositional process and kaolinite used as an indicator for provenance, paleoenvironments and paleoclimate (Chamley, 1989). Particle size distributions allow determination of the environment of deposition and environmental reconstruction (Lario *et al*., 2002).

X-ray diffraction (XRD) is regarded as a definitive tool for identifying minerals in geological material, especially those containing significant clay minerals proportions (Moore and Reynolds, 1997). X-ray diffraction is used to determine the mineralogical composition of the raw material components as well as qualitative and quantitative phase analysis of multiphase mixtures. X-ray diffraction analysis of clay minerals may be based on the evaluation of a bulk sample of the whole material mounted in randomly oriented powder form (Ruan and Ward, 2002). XRD patterns of kaolin were obtained on a powder X-ray diffractometer Model Philips with CuK$_{\alpha}$ radiation having a scanning speed of 0.04 $^{0}/_{s.}$ Fourier transform infrared spectrophotometry (FTIR) was used as an alternative method for determining qualitative/quantitative mineralogy.

The SEM was used to determine morphological and microchemical analyses of the kaolin samples. The samples were carbon coated in order to make the minerals surface conductive. In Identifying mineral morphology and mode of occurrence, crushed carbon coated minerals were examined directly with scanning electron microscopy without polishing (Folorunso *et al.*, 2014).

2.4.3 Geochemical composition

The chemical composition for major oxides of kaolin are determined by XRF. The abundance of trace elements in sediments allows for a reconstruction of paleodepositional conditions. By using trace elements concentration it is possible to assess whether they are relatively enriched or depleted in order to reconstruct paleoenvironmental conditions (Werne *et al.*, 2003; Lyons *et al*., 2003). Trace elements in fine grained sediments, which are relatively rich in organic matter, are useful for paleoenvironmental reconstruction.

The chemical composition for trace elements of kaolin were determined by LA-ICP-MS According to Kogel and Lewis (2001) the ICP-MS is capable of analysing a wide range of isotopes and is highly sensitive.

2.5 Paleoenvironmental reconstruction of selected known kaolin deposits

This section presents a brief description of selected known kaolin deposits based on their paleoenvironmental reconstruction.

2.5.1 Hydrogen and Oxygen isotopic composition of sedimentary kaolin deposits, Egypt: Paleoclimatic implications

According to Baioumy (2013b), the objectives of the study was to provide Hydrogen and Oxygen isotopic compositions on the clay fractions of samples representing different ages, lithologies and localities of the sedimentary kaolin deposits from Egypt to examine the paleoclimatic conditions under which the deposits were formed. The methodology used was sedimentation to determine the grain size distributions. Mineralogical composition analysed by X-ray diffraction (XRD) using a PHILIPS PW1800 and quantitative mineralogical compositions were determined using the Rietveld program BGMN and chemical composition. Samples for H and O isotopic composition were selected based on their mineralogical and geochemical composition. The extraction of H for isotopic analysis follows the principle of Begeleisen *et al.* (1952). Oxygen was extracted from clays using BrF_5 and converted to CO_2 by reacting with hot graphite.

The results from the analysed data indicated that the grain size distributions reveal that the clay fractions represent the major components of sedimentary kaolin deposits of all ages, types and lithologies ranging from 62.3 to 98.4 wt %. Samples of both deposits plot close to the weathering kaolinite line. According to Sheppard *et al.*

(1969), the H and O isotopic compositions as well as the plot of the values close to the kaolinite line marks the isotopic composition of kaolinite in equilibrium with meteoric water at 20°C and indicates that the kaolinite in both Carboniferous and Cretaceous deposits in Egypt formed by meteoric water weathering of the source rock(s).

Stable isotopes were used to reconstruct the paleoclimate and the results were as follows: The δD and $\delta^{18}O$ values in this study suggest that the kaolinite of the Carboniferous and Cretaceous deposits were formed under the warm-temperate to tropical conditions. The δD and $\delta^{18}O$ values of clay fractions from Egypt are almost identical indicating their formation under similar paleoclimatic condition. Data also suggest the formation of both deposits in equilibrium with meteoric water from which they formed under water-temperate to tropical condition.

2.5.2 Origin and geochemical evolution of Nuevo Montecastelo kaolin deposits, Spain

The purpose of the study was to provide an insight into a large-scale kaolinitisation of Variscan granitiods in the Alberian massif based on mineralogical, geochemical and stable isotope data from Nuevo Montecastel kaolin deposit, to provide constraints on the genesis of the kaolin deposit and conditions of mineral formation and to improve understanding of geochemical behaviour of major and trace elements during granite kaolinitisation. It was outlined that the study was contribute to the exploration of new deposits in the region and to rationalization of the mining operations.

According to Fernandez-Caliani *et al*. (2010) the methodology of the study include the mineralogical analysis which was determined by XRD, where in the selected samples were examined by SEM using secondary electron (SE) to describe the textural and morphological features and the accessory heavy minerals were determined by Back-Scattered Electron (BSE) and energy dispersive X-ray (EDX) and the primary minerals were identified in thin sections of the parent rocks through optical microscopy. Major elements concentrations were determined by ICP-OES and trace elements were determined by ICP-MS. Stable hydrogen and oxygen isotopes analyses were performed on the samples.

According to Fernandez-Caliani *et al.* (2010), the results showed that the stable isotope values of studied kaolin indicated its formation in a weathering environment at the Earth-surface temperature and the climate during kaolinitisation was warmer than at present. The hydrogen isotope signature of the paleometeoric water suggested that the kaolinitisation process took place during Early Tertiary times. Geochemical and Mineralogical composition of the studied profile is consistent with the residual kaolin deposit derived from granite during a supergene event. The Chemical Index of Alterations (CIA) and Chemical Index of Weathering (CIW) indices increase upward in the profile revealing the weathering extent and the supergene origin of the kaolinitisation process. It was found that there was no geological and geochemical evidence of hydrothermal alteration. It was concluded that the Nuevo Montecastelo kaolin were formed in situ by alteration of granites under favourable conditions of climate and drainage to leach the most soluble components.

CHAPTER 3

MATERIALS AND METHODS

This chapter explains the procedures followed in sampling in the field and the methods used in sample and data analysis (Figure 3.1).

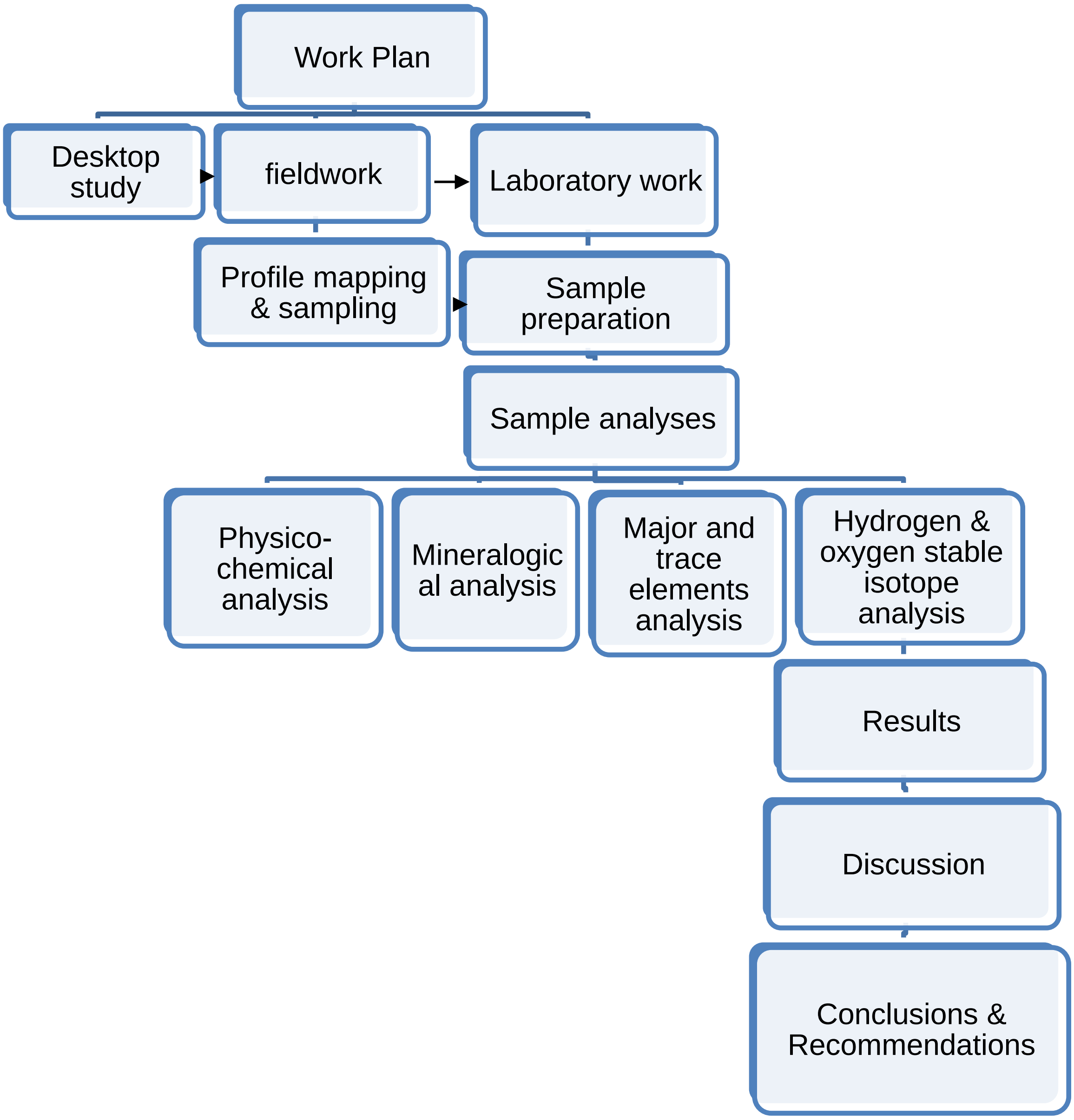

Figure 3.1: Flow chart of research work.

3.1 Desktop study

The desktop study was conducted through surfing the internet, searching books and journal articles in order to review the existing published data for the preliminary assessment of site conditions, conceptual design and literature review of appropriate analytical techniques.

3.2 Field methods

3.2.1 Profile mapping

Profile mapping was carried out around the kaolin outcrops in order to investigate their stratigraphic relationships with surrounding rocks as well as the paleoenvironmental changes that occurred. Profile mapping was performed with the aid of Global Positioning System (GPS), tape measure and trowel. The generated data were recorded.

3.2.2 Sampling

The method of sampling was judgemental (Ekosse *et al.*, 2005). The samples number and sampling distance depended on the availability of exposed outcrop as well as size and orientation of the kaolin occurrences (Ekosse, 2000 and 2001). Samples were obtained with the aid of an auger, machete, shovel and hammer and Global Positioning System (GPS) coordinates were taken (Table 3.1). Kaolin samples were collected from different sites within the Lwamondo and Zebediela study areas (Figures 3.2 and 3.3) for physico-chemical, mineralogical, major elements, trace elements, stable isotope, and diagnostic analyses and labelled accordingly. The distance between each sampling site depended on the availability of kaolin outcrop. Nine samples were collected from each study site and coded as LWA for Lwamondo Kaolin and QZEB for Zebediela Kaolin.

Table 3.1: Global Positioning System (GPS) Coordinates of the Lwamondo and Zebediela kaolin samples

	Sample No	GPS coordinates
Lwamondo	LWA1	S 23º 00' 01.0" E 30º 23' 15.1"
	LWA4	S 23º 00' 01.3" E 30º 23' 14.2"
	LWA6	S 23º 00' 02.8" E 30º 23' 09.9"
	LWA7	S 23º 00' 02.9" E 30º 23' 09.4"
	LWA8	S 23º 00' 06.2" E 30º 23' 13.9"
	LWA9	S 23º 00' 06.3" E 30º 23' 13.9"
Zebediela	Q1ZEB1	S 24º 16' 48.3" E 29º 23' 42.8"
	Q3ZEB1	S 24º 16' 53.6" E 29º 23' 27.4"
	Q4ZEB1	S 20º 25' 49.7" E 28º 27' 56.6"

Figure 3.2: Sampling of Lwamondo kaolin.

Figure 3.3: Sampling of Zebediela Kaolin.

3.3 Laboratory work

All the samples were air-dried and separation of the mineral particles into various size fractions was done by sieving. Each samples was treated with Hydrogen Peroxide (H_2O_2) to remove the organic matter followed the procedure described by Van Reeuwijk, 2002. 20 g of sample was weighed and put in the beaker, 15 ml of water and H_2O_2 was added and covered the beaker with a watch-glass, it was allowed to stand overnight. The beaker were placed on a hot plate and carefully boiled for an hour to remove remaining H_2O_2, The beaker was removed from the hot plate and allow to cool.

The sand fraction was obtained through dry sieving, and both the silt and clay fractions were determined by the hydrometer method. For the fractionation of the samples, separation was achieved through the application of Stoke's Law. The dispersing agent, commercially known as calgon (Sodium Hexametaphosphate ($(NaPO_3)_6$) and Soda (Na_2CO_3) was prepared.10 ml of deionized water plus 10 ml of dispersant were mixed with 10 g of the bulk sample in a beaker and stirred electronically for 15 minutes. The content was washed over a 63 µm sieve and collected in a 500 ml beaker. The silt and clay size fraction collected in a beaker was dispersed again, stirred and allowed to stand for 10 min (Van Reeuwijk, 2002).

Clay size fraction (<2 µm) for mineralogical, geochemical and stable isotope analyses was obtained by sedimentation and centrifuge method as described by Van Reeuwijk (2002). In order to separate sand from silt and clay the supernatant was decanted and transferred into the centrifuge tubes and centrifuged (Figure 3.4) for 3 min at 300 rpm. The supernant containing the clay fraction was decanted and allowed to stand for 5 – 10 min. the clear water was siphoned while the residue was oven-dried at 105 ºC for 4 hours. Dried samples were crushed gently in an agate mortar and packaged for mineralogical, geochemical and isotopic analyses.

Figure 3.4: Centrifuge for separation of particles.

3.3.1 Physico-chemical analyses

The following physico-chemical tests were conducted using bulk samples: colour, particle size determination, hydrogen ion concentration (pH) and electrical conductivity (EC).

3.3.1.1 Colour

Colour was determined using the Munsell Soil-Color Chart (2010). According to Munsell classification scheme, full attributes of colour include hue, value and chroma. Hue refers to the identity of a colour as it relates to the light spectrum. Munsell divided the hue circle into five principal hue spectra; red, yellow, green, blue, and purple, along with five intermediate hues halfway between adjacent principal hues (Kuehni, 2002). Each of this 10 steps is broken into 10 sub-steps, so that 100 hues are given integer values (Figure 3.5).

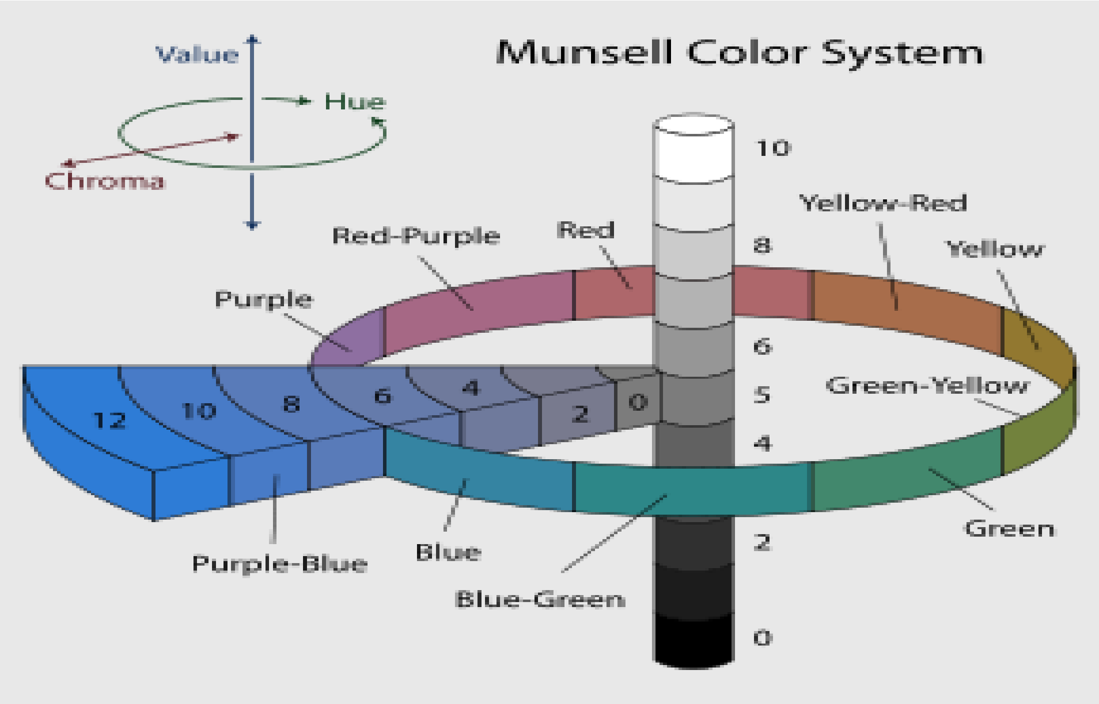

Figure 3.5: Munsell Color System depicting Hue, Value and Chroma (Cleland, 2005).

The kaolin raw samples were aerated for 24 hour to dry. Using a spatula; clayey aggregates were mounted on white cardboard sheets (Ekosse, 2001). The hue/value/chroma and colour of the mounted samples were obtained by visually comparing them to those of recorded standard soils in the Munsell Soil-Colour Charts.

3.3.1.2 Particle size distribution and texture

The particle size determination of the samples was conducted using the hydrometer method in accordance with Stoke's Law as described by Van Reeuwijk (2002). The dispersing agent, commercially known as calgon (Sodium Hexametaphosphate $(NaPO_3)_6$) and Soda (Na_2CO_3) were prepared. 10 ml of deionized water plus 10 ml of dispersant were mixed with 10 g of the bulk sample in a beaker and stirred electronically for 15 minutes.

Time for the suspension in sedimentation cylinder to equilibrate thermally and record temperature was allowed. The sedimentation cylinder was close with a rubber stopper and shaken well. After the mixing was completed, the hydrometer was carefully lowered into the suspension and reading was taken when the hydrometer was stable but not later than 50 seconds after completion of the mixing. The hydrometer was removed, rinsed and wiped dry.

The hydrometer was reinserted carefully about 10 seconds before each reading and readings were taken at 5 and 120 minutes. The hydrometer was removed and cleaned after each reading. The reading R each time was recorded. The reading and temperature were recorded by hydrometer in the blank solution. Based on distribution of particle sizes, the texture was determined and classified into one of the classes of the textural triangle (Figure 3.6). The clay, silt and sand percentage were calculated (Bouyoucos, 1962):

% clay = calculated hydrometer reading at 120 min x 100/wt of samples--------Eqn 3.1

% silt = calculated hydrometer reading at 40 sec x 100/ wt of sample------------Eqn 3.2

% sand = 100 - (% silt - % clay)--Eqn 3.3

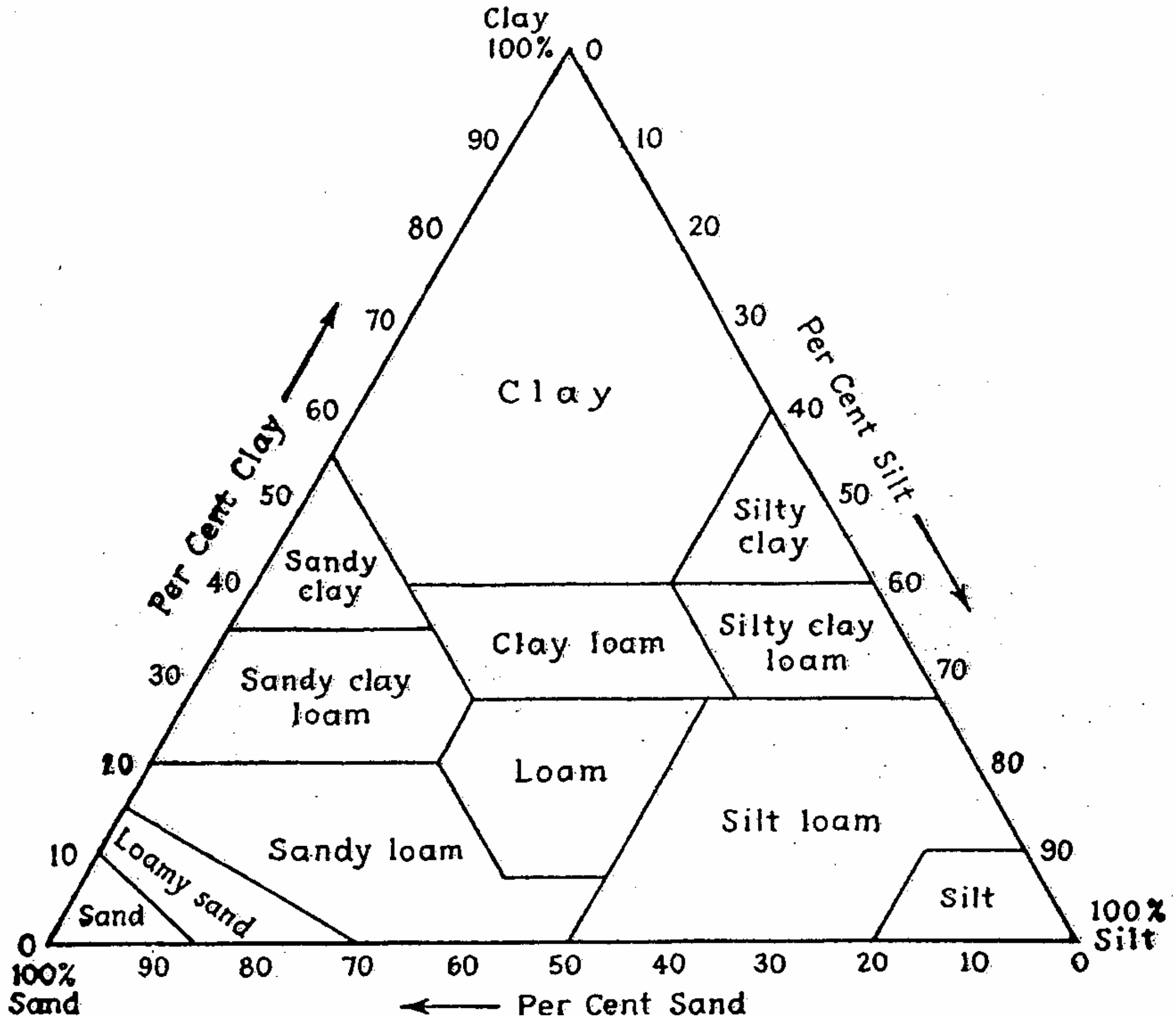

3.6: Textural triangle used to classify texture of earthy materials.

3.3.1.4 Hydrogen ion concentration (pH)

The hydrogen ion concentration (pH) is a measure of the acidity or alkalinity of a solution. Hydrogen ion concentration ($pH_{(KCl)}$) was determined by pH meter Basic 20 following the protocol described by Van Reeuwijk (2002). Buffering solution of pH 7.0 and 4.0 were used to calibrate the pH meter. 20 g of bulk sample was weighed in a 100 ml polythene wide-mouth bottle. 50 ml of KCl solution was added and the bottle capped. It was shaken for two hours. Before opening the bottle for measurement, it was again shaken by hand once or twice. The electrode was immersed in the upper part of suspension for the pH to be recorded under stabilised condition (Figure 3.7).

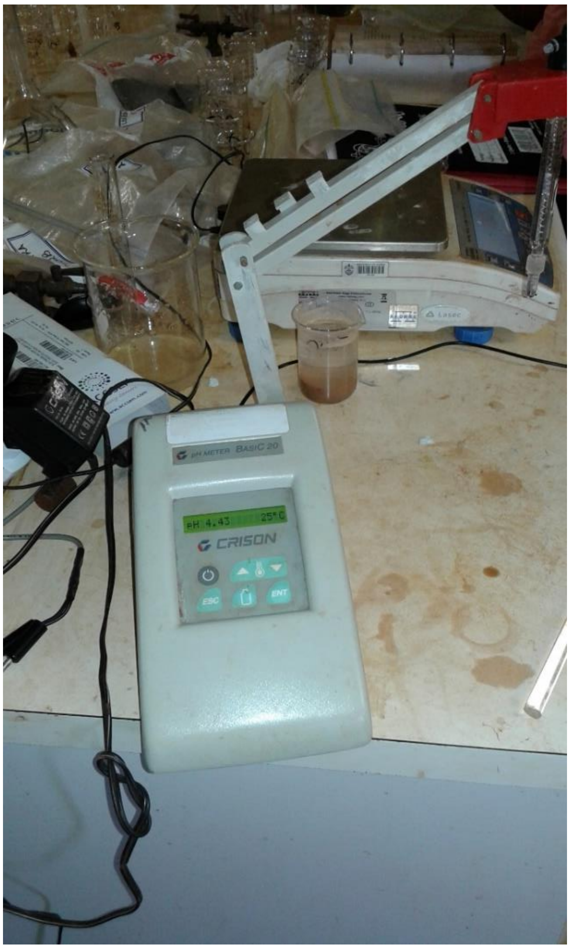

Figure 3.7: A display of the pH meter used in the experiment.

3.3.1.5 Electrical conductivity (EC)

Electrical conductivity is the measure of the ability of a material to allow the transport of an electric charge. The electrical conductivity (EC in H_2O) was determined by conductimeter Basic 30 (Figure 3.8) following the protocol described by Van Reeuwijk (2002). Twenty millilitres of distilled water was mixed with 10 g of weighed sample in a beaker. The mixture was stirred for 15 minutes and the EC measured under stable condition.

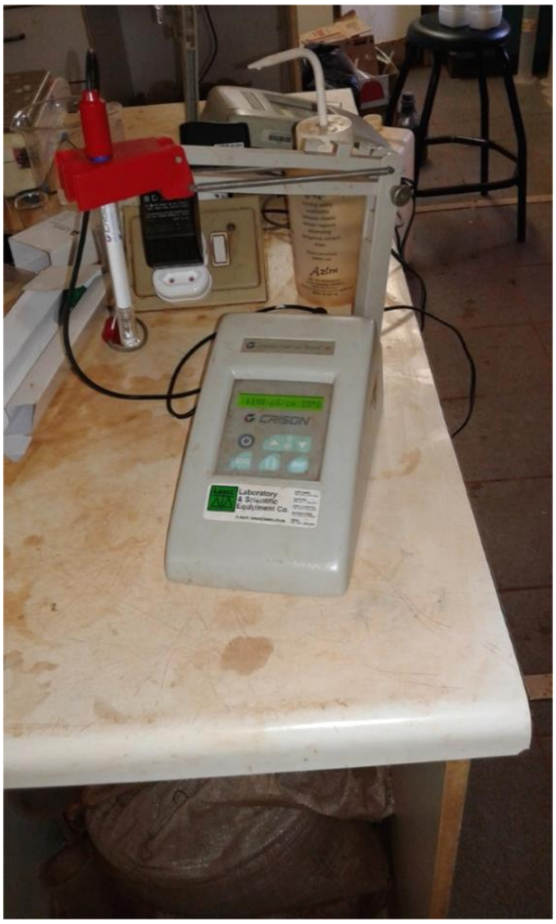

Figure 3.8: A display of the EC meter used in the experiment.

3.3.2 Mineralogical analyses

X-ray diffractometry (XRD), Fourier Transform Infrared (FTIR) Spectrophotometry, Scanning Electron Microscopy (SEM) were used to determine the mineral phases, functional groups and morphological characteristics of the 18 bulk, silt and clay size fraction samples.

3.3.2.1 Mineral phases

3.3.2.1.1 X- ray diffractometry (XRD)

The mineral phases within the samples were identified by powdered X-ray diffractometry (Figure 3.9). XRD preparations were made randomly by side loading to ensure the absence of any preferred orientation of the kaolinite particles (Hughes and

Brown, 1979; Cuadros and Linares, 1995). The samples were subjected to X-ray diffraction firstly using the Philips PW 3710 XRD, operated at 40 Kv and 45 Ma, with a Cu-kα radiation and graphite monochromator (Dudek, 2012). Samples were scanned from 2° 2θ to 40° 2θ and recorded their diffractograms. Xpert data collector/identify software was used to obtain and interpret XRD spectra (Folorunso *et al*., 2014).

Figure 3.9: X-ray diffractometer used for minerals identification.

In XRPD diffraction peaks occur when the paths of the diffracted X-ray is equal to an integer multiple of the path difference expressed by Bragg's equation as follows:

$n\lambda=2d\sin\theta$ --Eqn 3.4

Where n= integer, λ=wavelength, d= interatomic spacing, θ =diffraction angle

Origin software (OriginPro 2016 64Bit) was used to interpret the XRD results. Origin is a data analysis and graphing software which was produced by OriginLab Corporation and runs on Microsoft Windows.

3.3.2.1.2 Fourier transform infrared spectrophotometry (FTIR)

Fourier transform infrared spectrophotometry (FTIR) (Figure 3.10) is a complementary method for determining mineralogy. The spectra were recorded in the region of 4000-400 cm^{-1} (Olaremu, 2015). The absorbance/transmittance bands of each component in the mixture are proportional to the pure mineral spectrum. This is known as Beer's law, expressed as follows:

A = $\sum_{i=1}^{n} \mathcal{E}i\ 1\ ci$ --Eqn 3.5

Where A is the absorbance of a band, $\mathcal{E}i$ is the absorptivity of component I, 1 is the absorption path length (pellet thickness), and ci is the concentration of component i.

Figure 3.10: Fourier Transform Infrared Spectrophotometry.

The infrared spectra of the sample were collected using attenuated total reflection (ATR) module with a Nicolet model 360 FTIR at 0.5cm^{-1} nominal. The MIRacle were used to acquire the ATR spectra for clay size fraction in MIR region, the single reflection horizontal ATR accessory from PIKE technologies. About 5g of the dried samples were homogenized in spectrophotometric grade KBr in an agate mortar and hand pressed at 3mm pellets. In order not to pull the crystallinity of kaolinite in the samples, the mixing was set to 3 min allowing for minimal grinding as suggested by Tan (1996). The peaks were reported based on percentage transmittance to given wavelengths.

3.3.2.2 Mineral morphology

3.3.2.2.1 Scanning electron microscopy (SEM)

Morphological analysis of the clay fraction samples was performed using JOEL JSM-5800 W scanning electron microscope equipped with energy dispersive X-ray micro analysis (SEM-EDX) at the University of Johannesburg. Small amount of <2 µm fraction of kaolin powder was poured on the carbon tape which is attached to the machine to coat the sample (Figure 3.11) (Ekosse 2001). Airgun was used to blow the excess powder to ensure that small pieces of the powder remain on the tape and it was put in the SEM chamber for analysis. The SEM machine was operated at 20kV and 10 Kv (Figure 3.12). The magnification of X6000 and X10000 was used to capture picture of the sample. Particle images were obtained with the aid of a secondary electron detector.

Figure 3.11: Carbon coating equipment to prepare samples for SEM analysis.

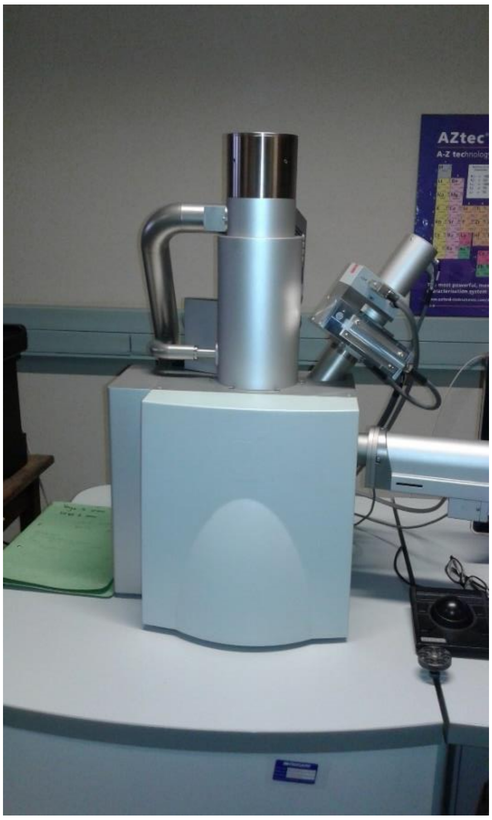

Figure 3.12: Scanning Electron Microscope used for morphological characterisation.

3.3.3 Geochemical analysis

Major and trace elements of 18 bulk, silt and clay size fraction of the kaolin samples were determined experimentally by XRF and ICP-MS.

3.3.3.1 X-ray fluorescence (XRF)

Chemical analyses for major elements concentration as well as Loss on Ignition (LOI) for bulk, silt and clay fractions of kaolin samples, were determined using XRF at the Central Analytical Facilities (CAF), University of Stellenbosch. Pulverised kaolin samples were analysed for major elements using Axios instrument (PANalytical) with a 2.4 KWatt Rh X-ray tube (Figure 3.13).

Figure 3.13: X-ray Fluorescence Spectrometer used for major oxides analysis.

Detailed procedures for sample preparation for the analytical technique were followed. Samples were crushed to fine powder in a tungsten carbide ball mill for about 10 min, fusion bead method was used: 1 g of milled sample were weighed and placed in an oven at 110 ºC for one hour to determine H_2O. It was placed in the oven at 1000 ºC for one hour to determine Loss on ignition (LOI). 10 g Claisse flux was added and fused in M4 Claisse fluxer for 23 minutes. 0.2 g of Na_2CO_3 was added to the mix and the sample + flux + Na_2CO_3 was pre-oxidized at 700 ºC before fusion. The major oxides concentrations were recorded (Madukwe et al., 2016).

Apart from concentrations of major oxides obtained, Si/Al, Fe/Ti and Ti/Al ratios were equally calculated. The CIA and CIW values were calculated based on Equations 3.6 and 3.7.

$$CIA = [(Al_2O_3) / (Al_2O_3 + CaO + Na_2O + K_2O)] * 100 \text{ ----------------------------------Eqn 3.6}$$

$$CIW = [(Al_2O_3) / (Al_2O_3 + CaO + Na_2O)] * 100 \text{--Eqn 3.7}$$

3.3.3.2 Laser Ablation inductively coupled plasma-mass spectrometry (LA-ICP-MS)

Laser Ablation Inductively Coupled Plasma Spectrometry (LA-ICP-MS) analyses (Figure 3.14) was used for trace elements analyses. The laser was used to vaporize the surface of the solid sample, whereas the vapour, and any particles, were then transported by the carrier gas flow to the ICP-MS. The detailed procedures for sample preparation for the analytical techniques are reported below.

Pressed pellet method for trace element analysis, 8 g of milled sample was weighed and it was mixed thoroughly with three drops of Mowiol wax binder, the pellet was pressed with pill press to 15 ton pressure and it was dried in an oven at 100ºC for half an hour before start analysing (Madukwe et al.,2016) .

Figure 3.14: Laser Ablation ICP-MS used for trace element analyses.

3.3.4 Stable isotopes analysis

Oxygen and hydrogen isotopic composition of clay size fraction of the kaolin samples were determined by oxygen and hydrogen isotopes using equipment set-up in Figures 3.15 and 3.16. Kaolinite grains >2 mm in length for O and H isotopes analysis were separated. Minerals separates of the primary silicate minerals present in the kaolinite rich samples were prepared by hand from the > 500 µm fraction, washed in acetone, crushed to powder and dried at 110ºC (Harris *et al*., 1999). The processed kaolinite was dried at 100ºC before analysis. Six samples of kaolin were used to determine the isotopic composition of the absorbed water.

Figure 3.15: Experiment setup used for sample preparation for stable isotopes analyses.

Figure 3.16: Stable isotope instrument used for oxygen and hydrogen isotopic composition analyses.

3.3.4.1 Oxygen isotopes

Oxygen isotope ratios of the <2 µm fraction of kaolin samples were determined after degassing under vacuum on the silicate line at 200ºC for two hours. Kaolinite was reacted with ClF_3 (Borthwick and Harmon, 1982) in conventional silicate line and the O_2 converted to CO_2 using hot platinized Carbon rod. Duplicate splits of the NBS-28 quartz standard were run with each sample and used to normalise the raw data to the SMOW scale using a value of 9.64 per mil for NBS-28 (Coplen, 1993). All delta (δ) values are reported in per Mil (‰) relative to SMOW. The overall reproducibility of replicate O analyses is ±0.1‰.

3.3.4.2 Hydrogen isotopes

Hydrogen isotope analyses of absorbed water extracted in the manner described above were made using a variation of the closed tube Zn reduction method (Coleman *et al*., 1982) described by Diamond and Harris (1997). Hydrogen extraction for isotopic analysis followed the principle of Bigeleisen *et al* (1952). After degassing at 180°C in a vacuum to remove absorbed moisture, water was extracted from kaolin by heating in a Mo crucible with an induction furnance to >1500°C. The water was converted to hydrogen gas by reduction over hot Uranium. The yields was determined manometrically. The reproducibility is ±2‰. O and H isotopic compositions will be reported using the δ notation with respect to Standard Mean Ocean Water (SMOW) (Boulvais *et al*., 2000).

3.4 Data analyses

Descriptive statistics were applied to analyse the generated data from the physico-chemical, mineralogical, geochemical and isotopic results using appropriate software such as Microsoft excel, Triplot and Origin. The generated data were presented in graphic and tabular form.

CHAPTER FOUR

RESULTS

4.1 Field observations

The geology of the Lwamondo area was dominated by the Soutpansberg Group. The Soutpansberg rocks belong to Proterozoic eon. Lwamondo kaolin occurred within the Sibasa Formation - volcanic succession. The volcanic rocks comprises basalts, which were subaerially extruded and minor pyroclastic rocks. The basalts were amyqdaloidal, massive and generally epidotised. One quarry was studied. An overburden having an average thickness of 2-3 m rests on the kaolin deposit and consists of reddish brown soil. Kaolin was exposed in the lower portion of the quarry. The lithology of the country rocks were basalt, clastic sediments include shale and minor conglomerates and minor pyroclastic rocks with a varicoured kaolin (white, brownish, red, pink and yellow). The kaolins were ferruginous (figure 4.1) and whitish (Figure 4.2).

Figure 4.1: Lwamondo ferruginous kaolin exposure.

Figure 4.2: Lwamondo whitish kaolin exposure.

The geology of Zebediela area comprised the Wolkberg Group followed by an uncorformity-bound Black Reef Quartzite Formation (BRQF), which in turn was overlain by the Chuniesport Group. The Chuniesport Group belongs to Proterozoic. Three quarries were studied namely: Quarry One, Quarry Three and Quarry Four. The thickness of the profile at Quarry four was up to 20 m (Figure 4.3). The lithology comprised of mudrocks, shale, brecia, chert as well as varicoloured kaolin. An iron rich vein, probaly the extention of the Penge Banded Iron Formation (BIF) cut across Quarry Four (Figure 4.5). Above the iron-rich vein was a brownish to reddish kaolin unit. Quarry Four, yellowish kaolin at the base was overlain by reddish brown, pale brown and light brown kaolin unit (Figure 4.3). These colours equally suggested high iron content in the deposit. Kaolin in quarry three was whitish in colour with no sedimentary structure identified (Figure 4.4) and quarry one kaolin was grayish and reddish in colour. Within Quarry four of the Zebediela kaolin formation was characterised by a major NNW-SE trending fault, truncated by numerous smaller veins.

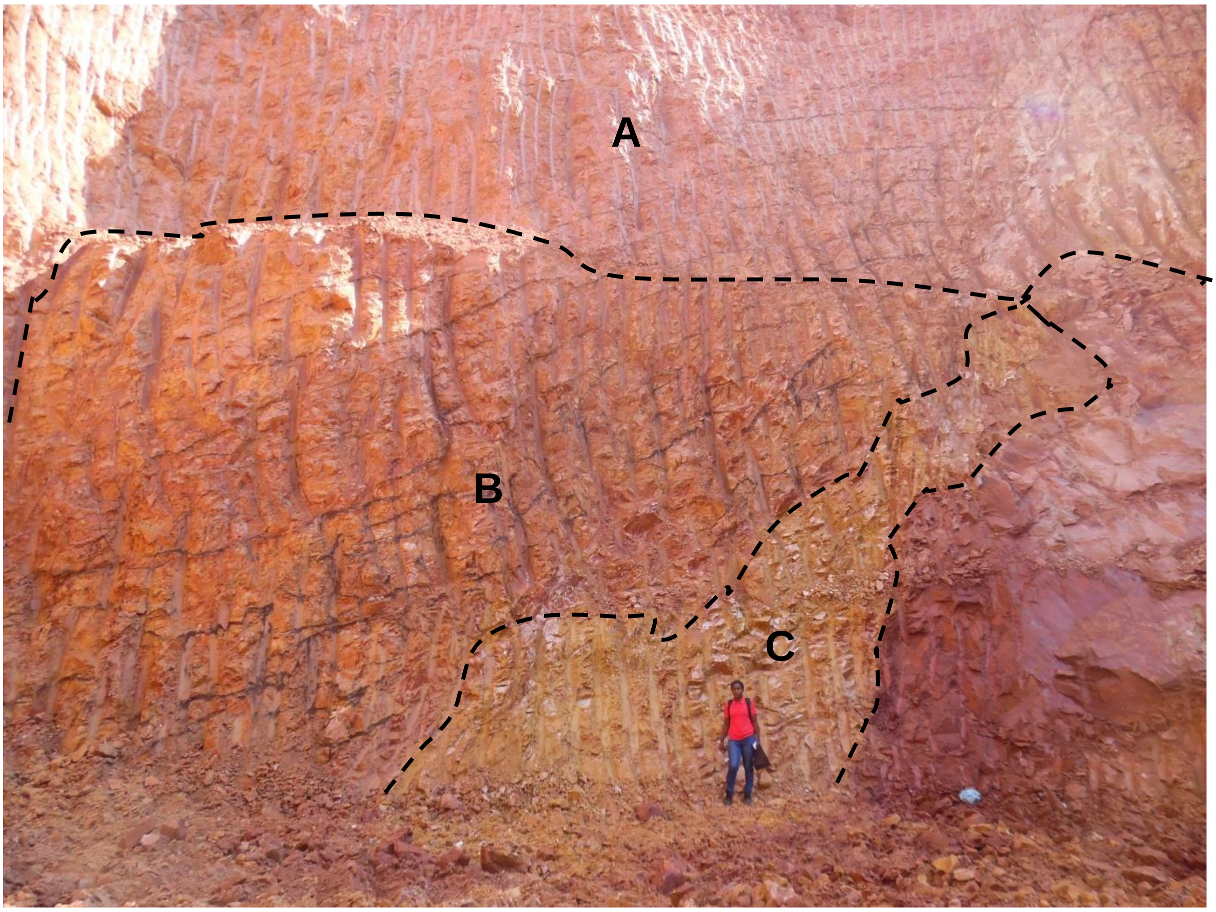

Figure 4.3: Zebediela kaolin exposure (A- hematite stained kaolin, B- Geothite stained kaolinite and C-Brownish kaolin).

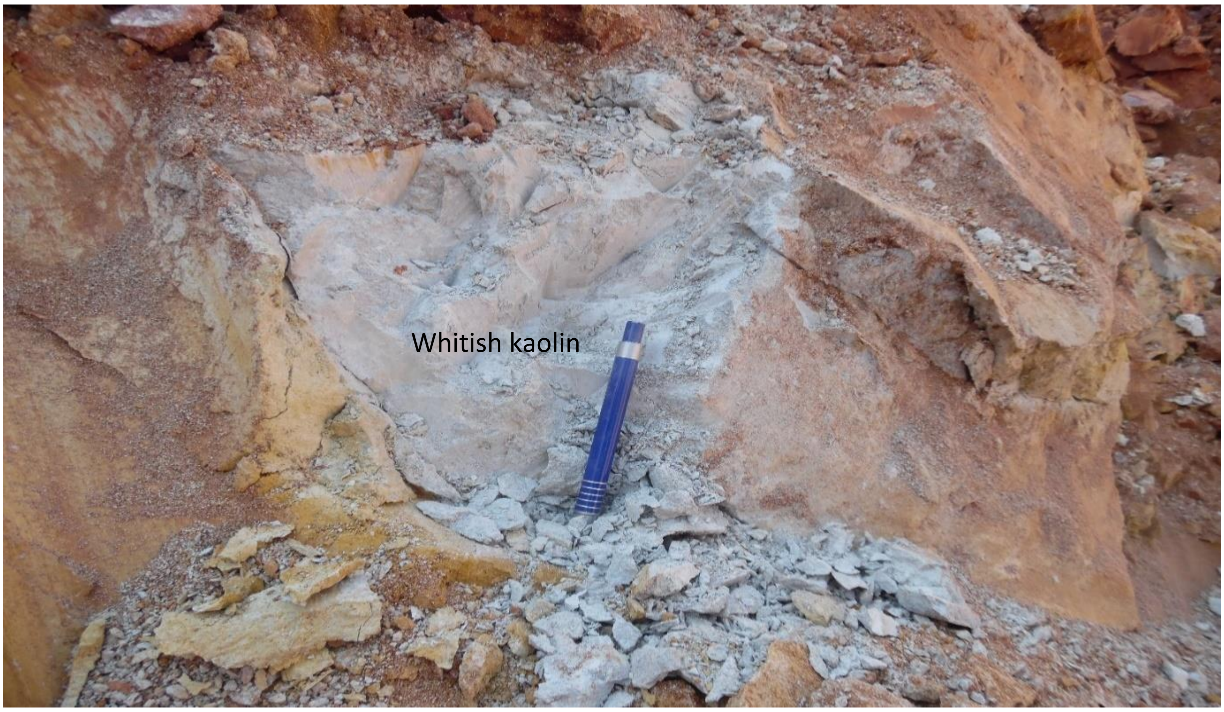

Figure 4.4: Zebediela kaolin exposure (whitish kaolin).

Figure 4.5: Zebediela Iron rich vein exposure(Quarry 4).

4.2 Physico-chemical properties

4.2.1 Colour

Lwamondo kaolin occurrence had various colours ranging from white to red (Table 4.1). Four samples were whitish in colour and suggestive of relative enrichment in kaolinite as compared to other samples. Other samples had yellow, pink, brown and red colours with varying shades of brownish yellow, pale yellow and pale brown indicative of the presence of oxides of iron goethite.

Table 4.1: Hue, value, chroma and colour of representative raw kaolin samples from Lwamondo

Samples	Hue/value/chroma	Colour
LWA1	10YR/6/6	Brownish yellow
LWA2	10YR/8/1	white
LWA3	2.5YR/8/3	Pink
LWA4	5Y/8/2	Pale yellow
LWA5	N/9	white
LWA6	2.5Y/7/4	Pale brown
LWA7	N/9.5	Normal white
LWA8	N/9.5	Normal white
LWA9	10R/5/6	Red

Zebediela kaolin occurrence was mainly brownish in colour (Table 4.2). Two samples (Sample Q3ZEB1 and Q3ZEB2) were whitish in colour and were suggestive of relative abundance in kaolinite. Whereas other samples were light gray, light red and yellowish in colour. The abundance of the reddish brown and yellowish colour was suggestive of the predominance of hematite over goethite in kaolins from Zebediela kaolin.

Table 4.2: Hue, value, chroma and colour of representative raw kaolin samples from Zebediela.

Quarry	Samples	Hue/Value/Chroma	Colour
Quarry 1	ZEB1	10YR/7/2	light gray
	ZEB2	2.5YR/6/6	light red
Quarry 3	ZEB1	N/9	White
	ZEB2	N/8.5	White
Quarry 4	ZEB1	10YR/7/6	Yellow
	ZEB2	2.5YR/4/4	reddish brown
	ZEB3	2.5YR/4/3	reddish brown
	ZEB4	10YR/8/3	very pale brown
	ZEB5	7.5YR/6/3	light brown

4.2.2 Particle size and texture

The results of the texture of representative samples from Lwamondo kaolin are presented in Table 4.3 and Figures 4.6- 4.7. The sand content ranged from 20 wt % (sample LWA4) to 46 wt % (sample LWA1 and LWA3) with a mean value of 33.78 wt %. Silt content ranged from 24 wt % (sample LWA3) to 62 wt % (sample LWA4) with a mean value of 41.56 wt % and clay fraction ranged from 12 wt % (sample LWA7) to 36 wt % (sample LWA6) with a mean value of 24.67 wt % of the bulk samples. Samples LWA 1, LWA 2, LWA 5 and LWA 7 were identified as loam from the textural triangle (Figure 4.6). Samples LWA 4 and LWA 8 were identified as silt loam. Sample LWA 3 was sandy clay loam whereas samples; LWA 6 and LWA 9 were silty clay loam.

Table 4.3: Particle weight percent in relation to textural classification of Lwamondo kaolin samples.

Sample no	Sand (wt %)	Silt (wt %)	Clay (wt %)
LWA1	46	32	22
LWA2	38	40	22
LWA3	46	24	30
LWA4	20	62	18
LWA5	30	44	26
LWA6	30	34	36
LWA7	40	48	12
LWA8	22	54	24
LWA9	32	36	32

Figure 4.6: Particle size distribution of Lwamondo kaolin samples.

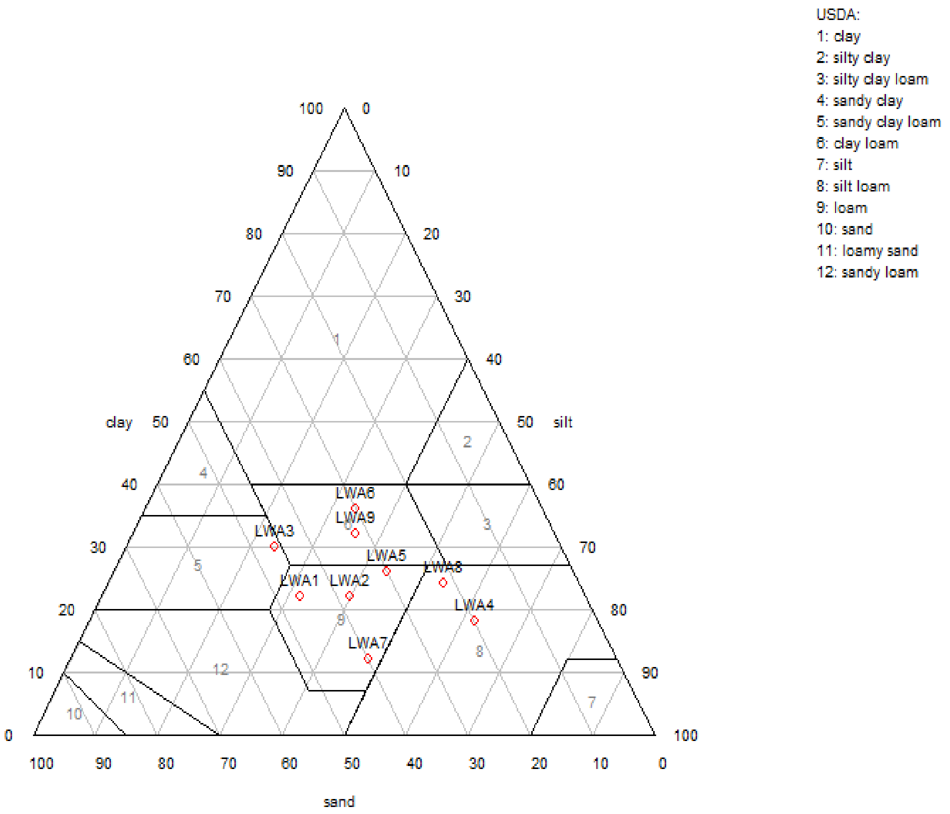

Figure 4.7: Textural triangle of Lwamondo kaolin samples (in wt %).

The results of the texture of representative samples from Zebediela kaolin was presented on the Table 4.4 and Figure 4.8. The sand content ranged from 10 wt % (sample Q3ZEB1) to 46 wt % (sample Q1ZEB2) with a mean value of 26.67 wt %. Silt content ranged from 24 wt % (sample Q4ZEB4) to 72 wt % (sample Q4ZEB2) with a mean value of 42 wt % and clay fraction ranged from 10 wt % (sample Q4ZEB2) to 46 wt % (sample Q4ZEB4) with a mean value of 31.33 wt % of the bulk samples. Q1ZEB1 and Q4ZEB4 were clay (Figure 4.9), Q4ZEB1 and Q4ZEB5 were clay loam, Q3ZEB1 was silty clay, Q3ZEB2 was silty clay loam. Q1ZEB2 was loam, Q4ZEB2 and Q4ZEB3 were silt loam.

Table 4.4: Particle weight percent in relation to textural classification of Zebediela kaolin samples.

Sample no	Sand (wt %)	Silt (wt %)	Clay (wt %)
Q1ZEB1	24	32	44
Q1ZEB2	46	30	24
Q3ZEB1	10	48	42
Q3ZEB2	18	50	32
Q4ZEB1	34	36	30
Q4ZEB2	18	72	10
Q4ZEB3	20	58	22
Q4ZEB4	30	24	46
Q4ZEB5	40	28	32

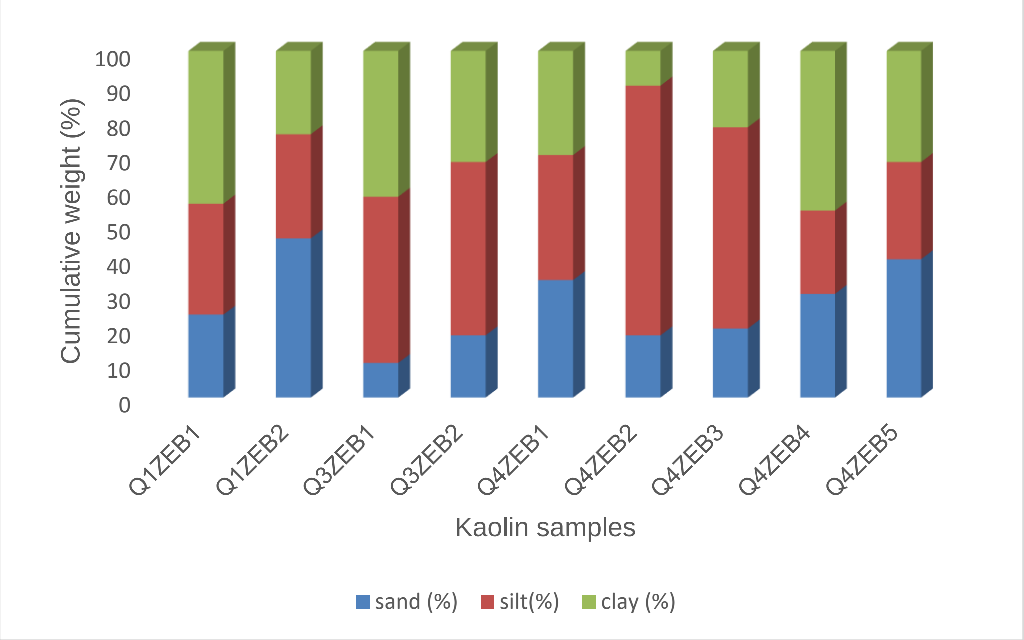

Figure 4.8: Particle size distribution of Zebediela kaolin samples.

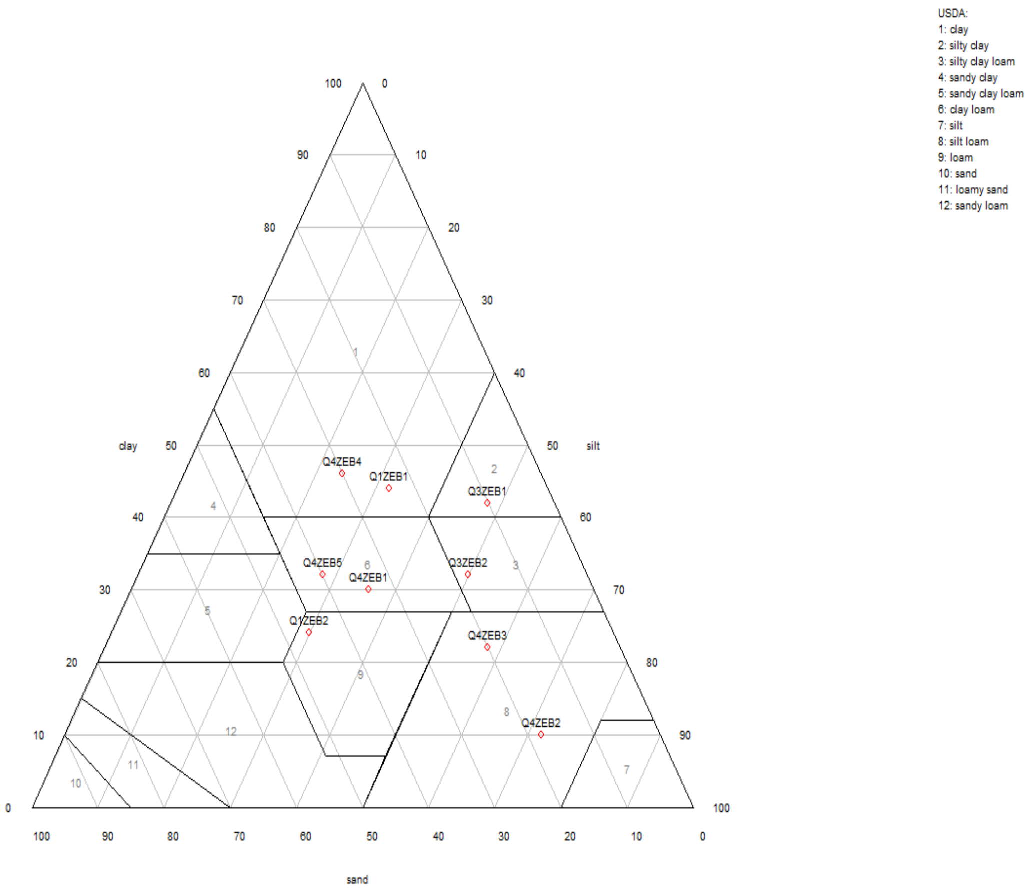

Figure 4.9: Textural triangle of Zebediela kaolin samples (in wt %).

4.2.3 Hydrogen ion concentration (pH)

The results of pH(KCl) of representative samples from Lwamondo kaolin are presented in Figure 4.10. The pH ranged from 3.59 (LWA1) to 5.04 (LWA7) (acidic) with a mean pH value of 4.30.

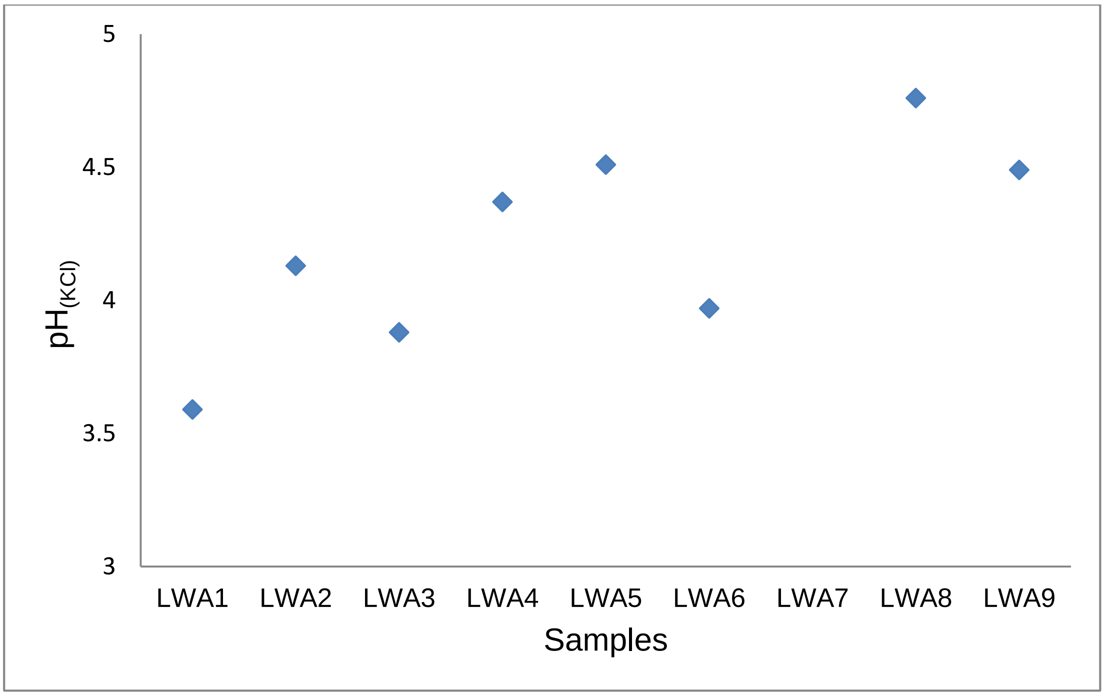

Figure 4.10: pH of Lwamondo kaolin samples.

The results of pH($_{KCl}$) of representative samples from Zebediela kaolin are presented in Figure 4.11. The pH was ranging from 3.48 (Q1ZEB1) to 4.50 (Q4ZEB1) (acidic) with a mean pH value of 3.88.

Figure 4.11. pH of Zebediela kaolin samples.

4.2.4 Electrical conductivity (EC)

The results of EC of representative samples from Lwamondo kaolin are presented in Figure 4.12. Generally, EC ranged between 24.0 µS/cm to 43.5 µS/cm; however, with an outlier at 376 µS/cm.

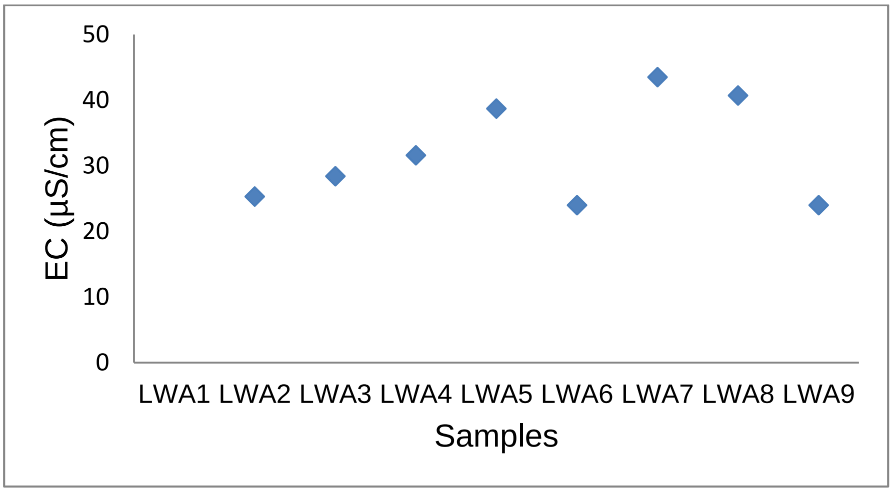

Figure 4.12: EC of Lwamondo kaolin samples.

The results of EC of representative samples from Zebediela kaolin are presented in Figure 4.13. The EC was between 15.0 µS/cm to 34.4 µS/cm. however, with an outlier at 321 µS/cm.

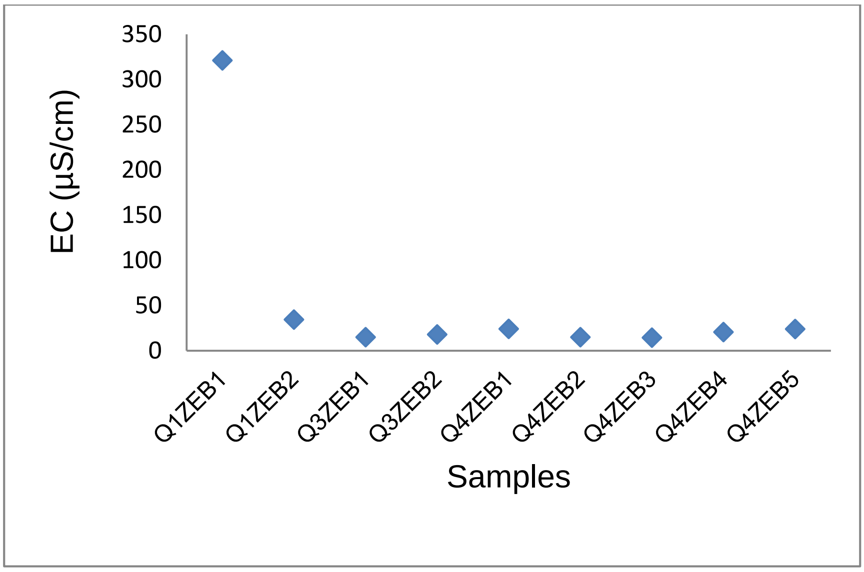

Figure 4.13. EC of Zebediela kaolin samples.

4.3 Mineralogy

4.3.1 Mineral phases

The results of semi-quantitative mineralogical analysis of Lwamondo bulk samples are summarised in Table 4.5 and Figure 4.14. Kaolinite was determined as the major mineral in all samples whereas anatase, plagioclase, microcline, muscovite and quartz occurred in major to minor quantities in most of the analysed samples. Rutile occurred as trace quantity in samples LWA2 and LWA 3 whereas goethite and hematite occurred in major quantity in sample LWA9.

Table 4.5: Semi-quantitative mineralogy of bulk samples from Lwamondo Kaolin Occurrences.

Sample No	**A**	**Cl**	**G**	**H**	**K**	**Mc**	**Mu**	**P**	**Q**	**R**	**S**	**T**
LWA1	++	+++	-	-	+++	-	-	-	++	-	+++	-
LWA2	-	-	-	-	+++	++	-	-	+	+	+	-
LWA3	-	-	-	-	+++	-	++	-	+++	+	+	-
LWA4	-	++	-	-	+++	+++	-	+++	-	-	++	-
LWA5	-	-	-	-	+++	+++	++	+++	+	-	+++	-
LWA6	++	++	-	-	++	-	-	-	++	-	+++	+++
LWA7	-	-	-	-	+++	+++	-	+++	+	-	-	-
LWA8	-	-	-	-	+++	++	++	+++	++	-	-	-
LWA9	-	-	+++	+++	+++	-	+++	-	++	-	-	-

(+++) Major, (++) Minor, (+) Trace, (-) not detected; A-Anatase, Cl-Clinoclore, G-Goethite, H-Hematite, K-Kaolinite, Mc-Microcline, Mu-Muscovite, P-Plagioclase, Q-Quartz, R-Rutile, S-Smectite, T-Talc.

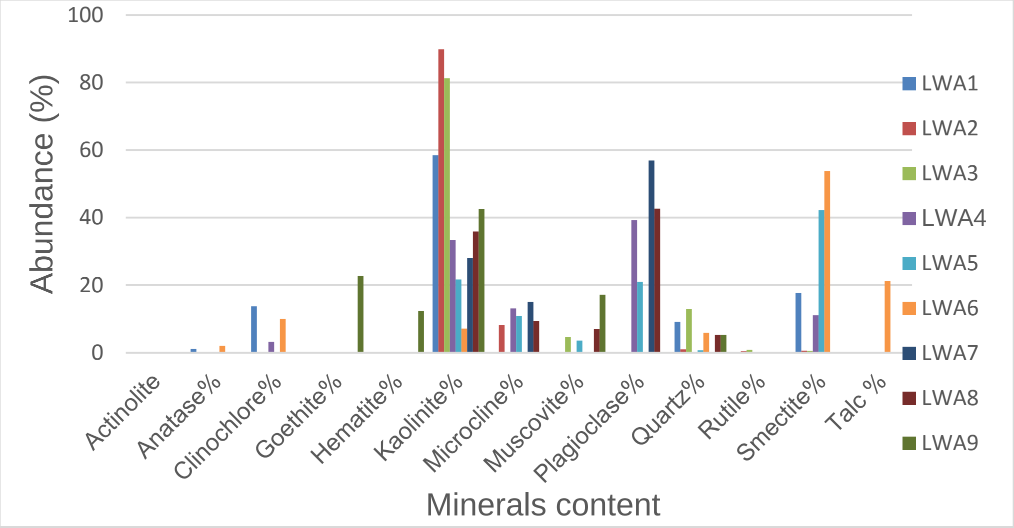

Figure 4.14: Mineral abundances in Lwamondo kaolin as determined by XRD.

The results of semi-quantitative mineralogical analyses of bulk samples of the Zebediela kaolin are shown in Table 4.6 and Figure 4.15.The table shows that kaolinite is the main constituent in all the samples (44.17-79.96 %) with quartz, muscovite and goethite in most of the samples. Traces of anatase were identified in the majority of the analysed samples with traces of hematite identified in two of the samples (Q4ZEB1 and Q4ZEB2).

Table 4.6: Semi-quantitative mineralogy of bulk samples from Zebediela Kaolin Occurrences.

Sample No	A	G	H	K	Mu	Q	S	T
Q1ZEB1	-	++	-	+++	-	+++	++	+++
Q1ZEB2	-	+++	-	+++	++	+++	-	-
Q3ZEB1	++	-	-	+++	+++	++	-	-
Q3ZEB2	-	-	-	+++	++	+++	-	-
Q4ZEB1	++	+++	-	+++	-	+++	-	-
Q4ZEB2	-	-	+	+++	+++	+++	-	-
Q4ZEB3	+	+++	++	+++	-	+++	-	-
Q4ZEB4	++	++	-	+++	++	+++	-	-
Q4ZEB5	++	++	-	+++	-	+++	-	

(+++) Major, (++) Minor, (+) Trace, (-) not detected; A-Anatase, G-Goethite, H-Hematite, K-Kaolinite, Mu-Muscovite, Q-Quartz, S-Smectite, T-Talc.

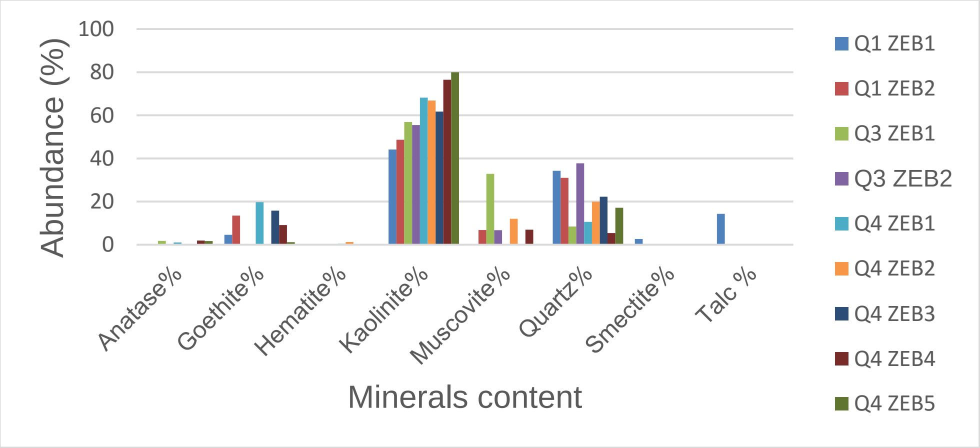

Figure 4.15: Mineral abundance in Zebediela kaolin as determined by XRD.

The results of semi-quantitative mineralogical analyses of silt size fraction samples of Lwamondo kaolin are shown in Table 4.7 and Figure 4.16 .kaolinite was the main constituent in all samples with microcline, plagioclase, quartz and smectite in some of the samples. Clinochlore, goethite and muscovite occurred in a minor quantity with anatase in a trace quantity.

Table 4.7: Semi-quantitative mineralogy of silt fraction samples from Lwamondo Kaolin Occurrences.

Sample No	A	CL	G	K	Mc	Mu	P	Q	S	T
LWA1	+	-	-	+++	+++	-	-	+++	+++	-
LWA2	+	-	-	+++	++	-	-	-	-	-
LWA3	+	-	-	+++	++	++	-	+++	-	-
LWA4	-	++	-	+++	+++	-	+++	++	-	-
LWA5	-	-	-	+++	+++	++	+++	-	-	-
LWA6	-	++	++	+++	-	-	-	++	+++	+++
LWA7	-	-	-	+++	++	-	+++	++	-	-
LWA8	-	-	-	+++	+++	-	+++	++	-	-
LWA9	+	-	+++	+++	-	++		++	-	-

(+++) Major, (++) Minor, (+) Trace, (-) not detected; A-Anatase, Cl-Clinoclore, G-Goethite, H-Hematite, K-Kaolinite, Mc-Microcline, Mu-Muscovite, P-Plagioclase, Q-Quartz, R-Rutile, S-Smectite, T-Talc.

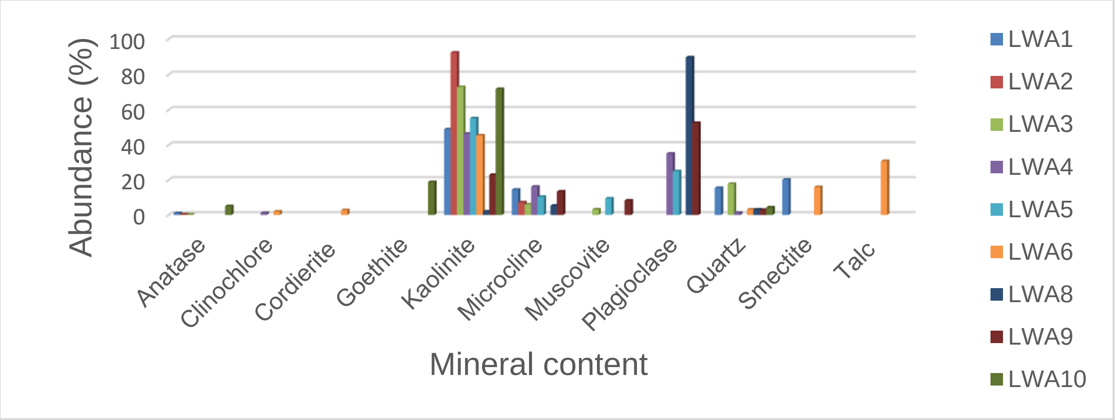

Figure 4.16: Mineral abundances in silt fraction of Lwamondo kaolin as determined by XRD.

The results of semi-quantitative mineralogical analyses of silt fraction samples of Zebediela kaolin are shown in Table 4.8 and Figure 4.17. Kaolinite and quartz was depicted as a main constituent in all the samples with goethite, talc and muscovite in some of the samples. Anatase occurred in a minor quantity.

Table 4.8: Semi-quantitative mineralogy of silt fraction samples from Zebediela Kaolin Occurrences.

Sample No	**A**	**G**	**K**	**M**	**Q**	**T**
Q1ZEB1		-	+++	-	+++	+++
Q1ZEB2	-	+++	+++	++	+++	-
Q3ZEB1	++	-	+++	+++	++	-
Q3ZEB2	++	-	+++	++	+++	-
Q4ZEB1	++	+++	+++	-	+++	-
Q4ZEB2	-	-	+++	+++	++	-
Q4ZEB3	-	+++	+++	-	+++	-
Q4ZEB4	++	++	+++	++	+++	-
Q4ZEB5	++	+++	+++	-	+++	-

(+++) Major, (++) Minor, (+) Trace, (-) not detected; A-Anatase, G-Goethite, H-Hematite, K-Kaolinite, Mu-Muscovite, Q-Quartz, S-Smectite, T-Talc.

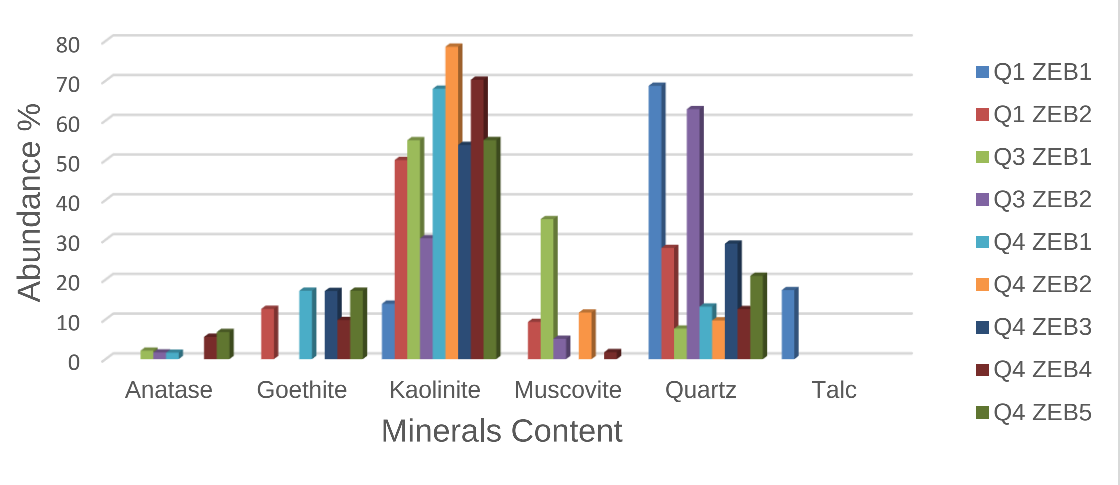

Figure 4.17: Mineral abundances in silt fraction of Zebediela kaolin as determined by XRD.

The results of the mineralogical analyses of Lwamondo kaolin clay fraction is summarized in Figure 4.18 and Table 4.9. The constituent minerals were reported as major, minor and trace depending on their concentration. Kaolinite was determined as the major mineral in all the samples whereas muscovite, microcline, plagioclase, smectite, clinochlore, goethite and talc were identified as a major to minor constituent in some of the samples. Goethite was identified in two samples (LWA 1 and LWA 9). Quartz was only identified in sample LWA 5 occurring in a trace quantity.

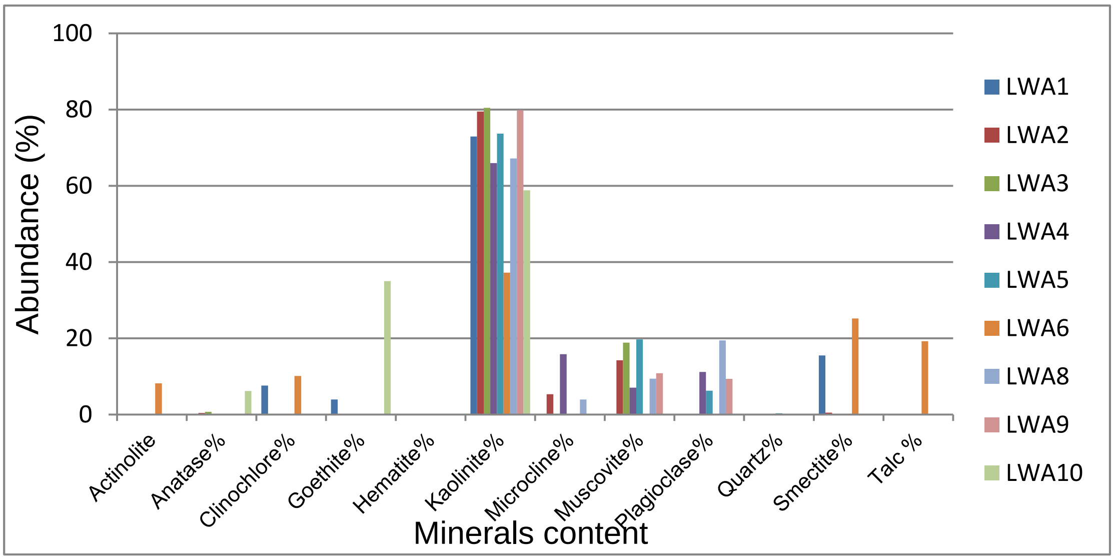

Figure 4.18: mineral abundance in Lwamondo clay size fraction kaolin as determined by XRD.

Table 4.9: Semi-quantitative mineralogy of clay fraction samples from Lwamondo Kaolin Occurrences.

Sample No	Ac	A	Cl	G	K	Mc	Mu	P	Q	S	T
LWA1	-	-	++	++	+++	-	-	-	-	+++	-
LWA2	-	+	-	-	+++	++	+++	-	-	+	-
LWA3	-	+	-	-	+++	-	+++	+++	-	-	-
LWA4	-	-	-	-	+++	+++	++	++	+	-	-
LWA5	-	-	-	-	+++	-	+++	-	-	-	-
LWA6	++	-	+++	-	+++	-	-	+++	-	+++	+++
LWA7	-	-	-	-	+++	++	++	++	-	-	-
LWA8	-	-	-	-	+++	-	+++	-	-	-	-
LWA9	-	++	-	+++	+++	-	-	-	-	-	-

(+++) Major, (++) Minor, (+) Trace, (-) not detected; Ac- Actinolite, A-Anatase, Cl-Clinoclore, G-Goethite, K-Kaolinite, Mc-Microcline, Mu-Muscovite, P-Plagioclase, Q-Quartz, S-Smectite, T-Talc

The results of semi-quantitative mineralogical analyses of clay fraction samples from Zebediela kaolin deposit are shown in Table 4.10 and Figure 4.19. Kaolinite was identified as the most dominant mineral in all the samples. Anatase, goethite, muscovite and quartz occurred in a major to trace quantity in most analysed samples. Smectite and talc were identified as major minerals in samples Q1ZEB1 and Q4ZEB5 whereas hematite occurred in minor quantities in both samples.

Table 4.10: Semi-quantitative mineralogy of clay size fraction samples from Zebediela Kaolin Occurrences.

Sample No	**A**	**G**	**H**	**K**	**Mu**	**Q**	**S**	**T**
Q1ZEB1	-	++	-	+++	-	++	-	+++
Q1ZEB2	-	+++	-	+++	+++	++	-	-
Q3ZEB1	-	-	-	+++	+++	-	-	-
Q3ZEB2	+	-	-	+++	+	-	-	-
Q4ZEB1	+	+++	++	+++	-	+	-	-
Q4ZEB2	-	++	-	+++	+++	-	-	-
Q4ZEB3	++	++	-	+++	-	++	-	-
Q4ZEB4	++	++	-	+++	++	+	-	-
Q4ZEB5	++	++	-	+++	-	-	+++	-

(+++) Major, (++) Minor, (+) Trace, (-) not detected; A-Anatase, G-Geothite, H-Hematite, K-Kaolinite, Mu-Muscovite, Q-Quartz, S-Smectite, T-Talc.

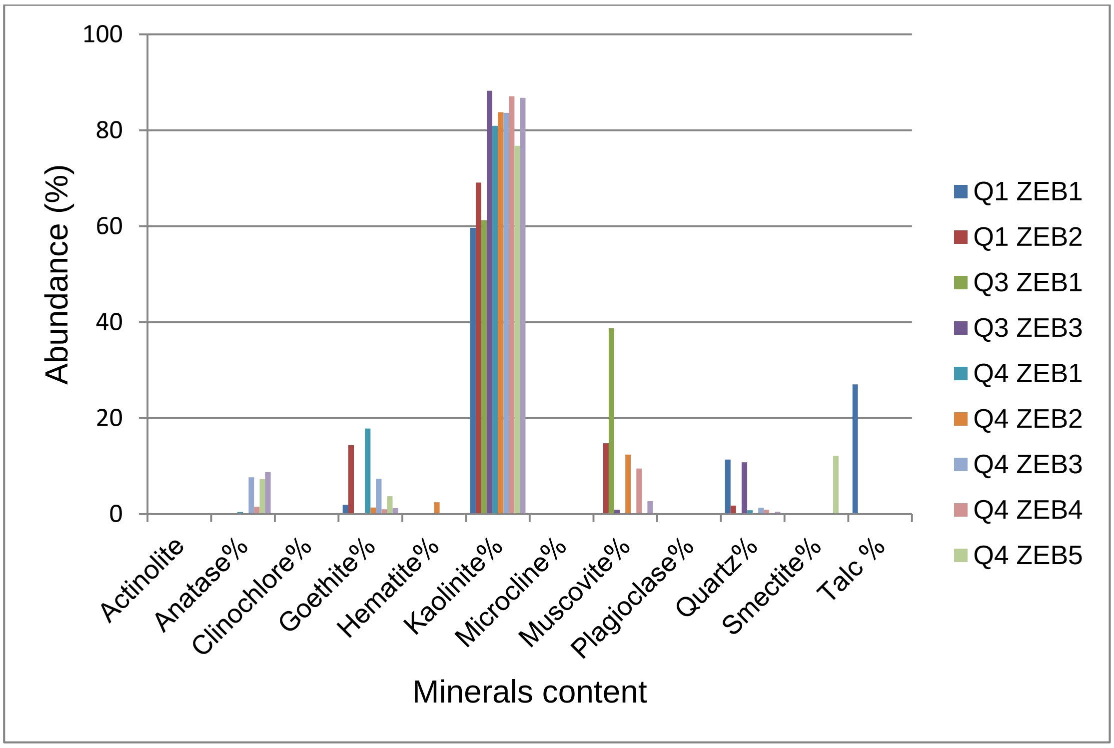

Figure 4.19: Mineral abundances in Zebediela kaolin as determined by XRD.

The diffractograms obtained from the XRD analysis of Lwamondo bulk kaolins samples in the region between 2°- 40° revealed kaolinite as a dominant mineral with muscovite in some of the samples (Figure 4.20). First and second kaolinite peaks observed at 12.28º and 24.78º. Highest plagioclase peak was observed at 28º in samples; LWA4, LWA5, LWA7 and LWA8. Peak observed at 26.8º in all samples except in LWA4 was assigned to quartz. Albite peaks observed at 21º in sample LWA4, LWA5, LWA7 and LWA8.

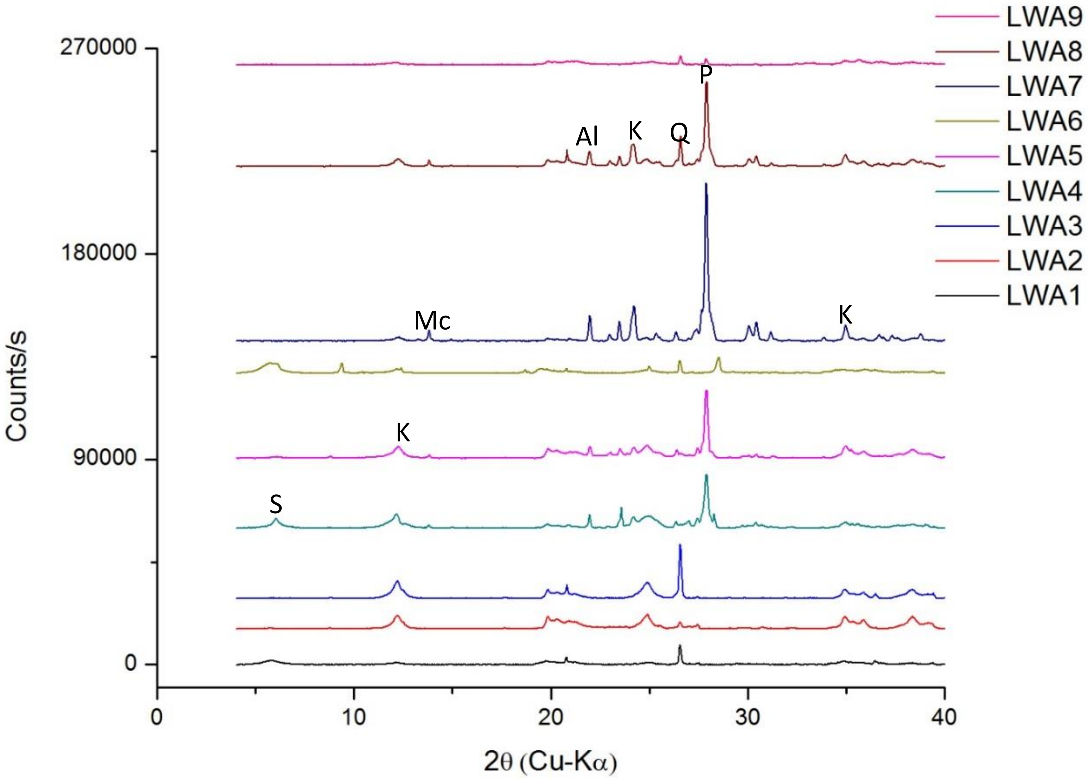

Figure 4.20: Diffractogram charts showing the mineralogical composition of Lwamondo kaolin. Note: Mc=Microcline, K=Kaolinite, Q=Quartz, S=Smectite, P=Plagioclase.

The diffractograms obtained from the XRD analysis of Lwamondo clay fraction kaolin samples in the region between 2°- 40° revealed kaolinite as a dominant mineral with muscovite peak observed at 8.84° and 34.99° in some of the samples (Figures 4.21 - 23). Microcline was present as major phase in samples; LWA2, LWA4, LWA7. Quartz was observed as trace mineral in LWA4. Goethite was observed at 21.4° and 36.8° as a major constituent in LWA9 and as minor phase at 36.80° in LWA1. Talc was observed as major phase in LWA6 at 9.4° and 28°.

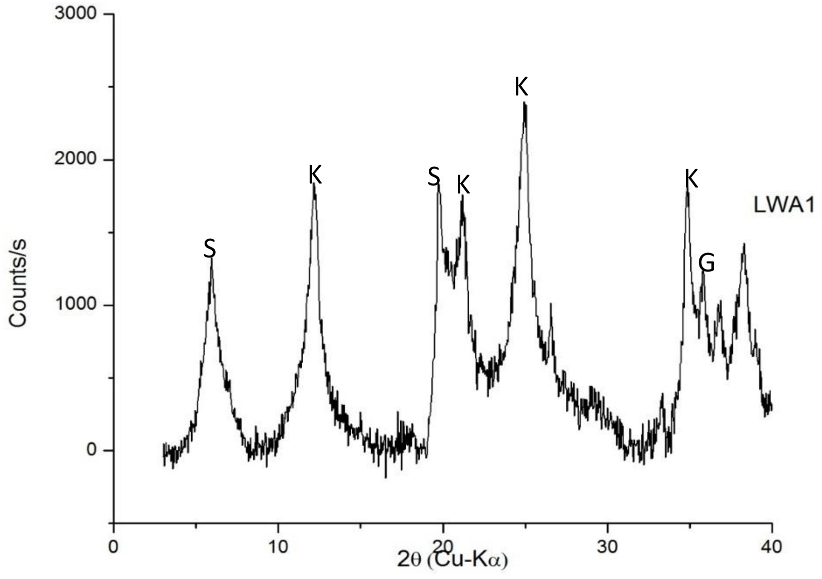

Figure 4.21: Diffractogram of Sample LWA1 obtained from Lwamondo Kaolin. Note: K= kaolin; S = smectite; Cl = chlorite.

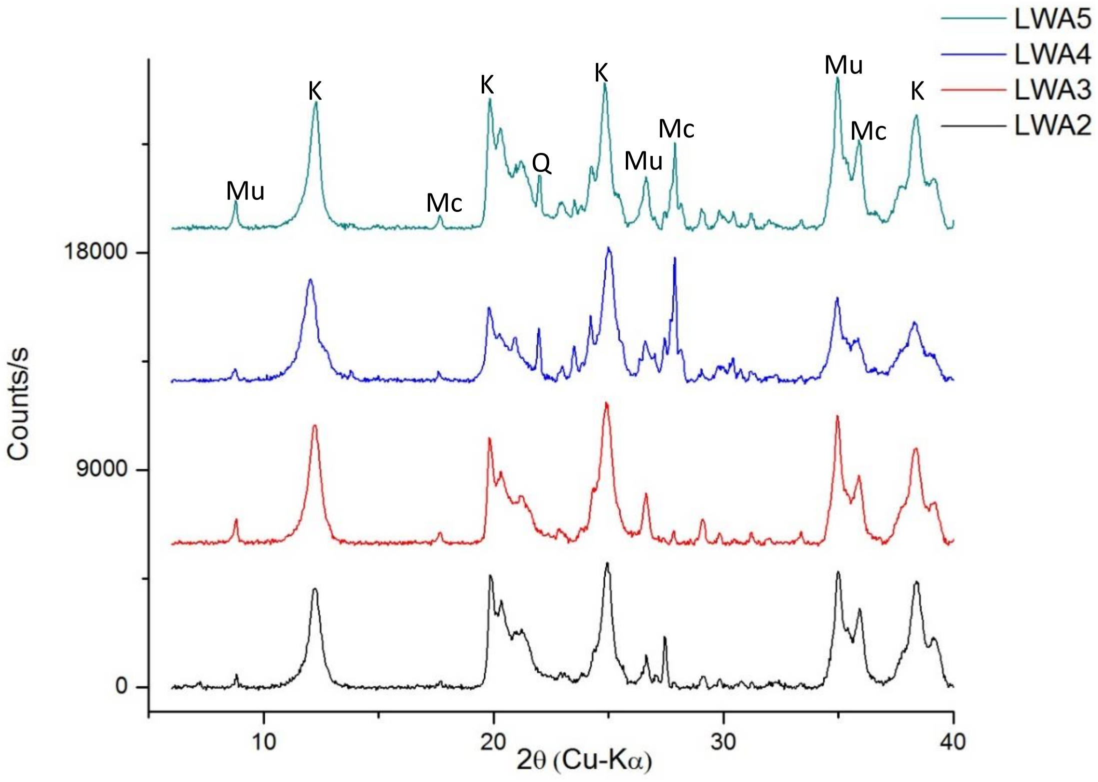

Figure 4.22: Diffractogram charts showing the mineralogical composition of Lwamondo kaolin. Note: Mu=Muscovite, Mc=Microcline, Q=Quartz, K=Kaolinite.

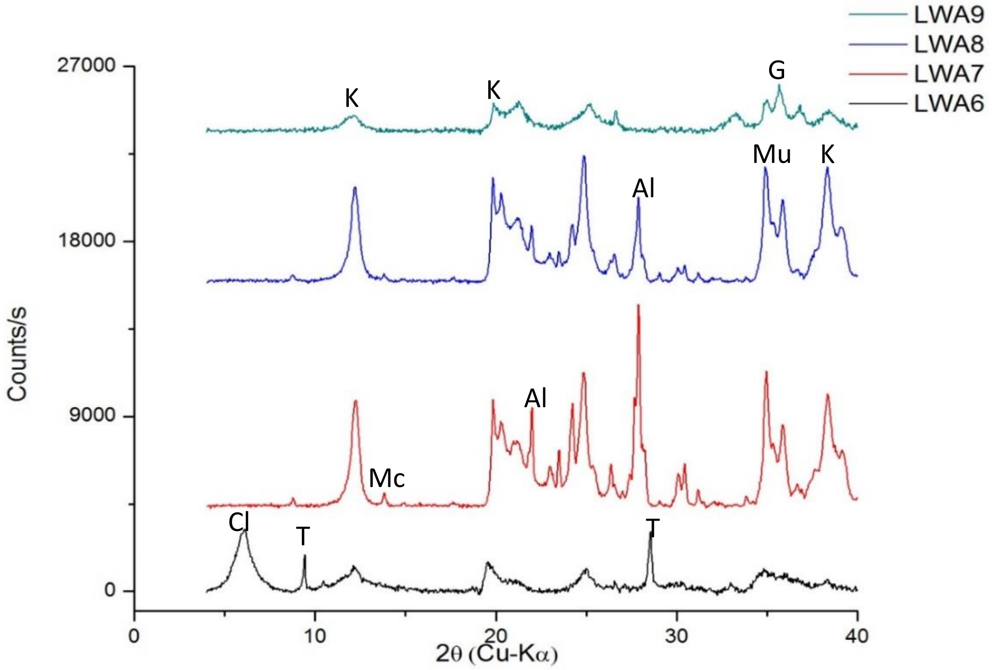

Figure 4.23: Diffractogram charts showing the mineralogical composition of Lwamondo kaolin. Note: Mu=Muscovite, Mc=Microcline, Al=Actilinote, K=Kaolinite, G=Geothite, Cl=Clinochlore.

The XRD pattern of Zebediela bulk kaolin samples characterized by weak kaolinite peaks (Figure 4.24). Most intense peaks observed at 26.8º were assigned to quartz. The kaolinite peaks were observed at 12.28º and 24.78º. Peak observed at 9.4º in sample Q1ZEB1 was assigned to Talc. Anatase peak was observed at 25.2º in some of the studied samples. Muscovite and Smectite occurred in a major to minor quantity in some of the samples.

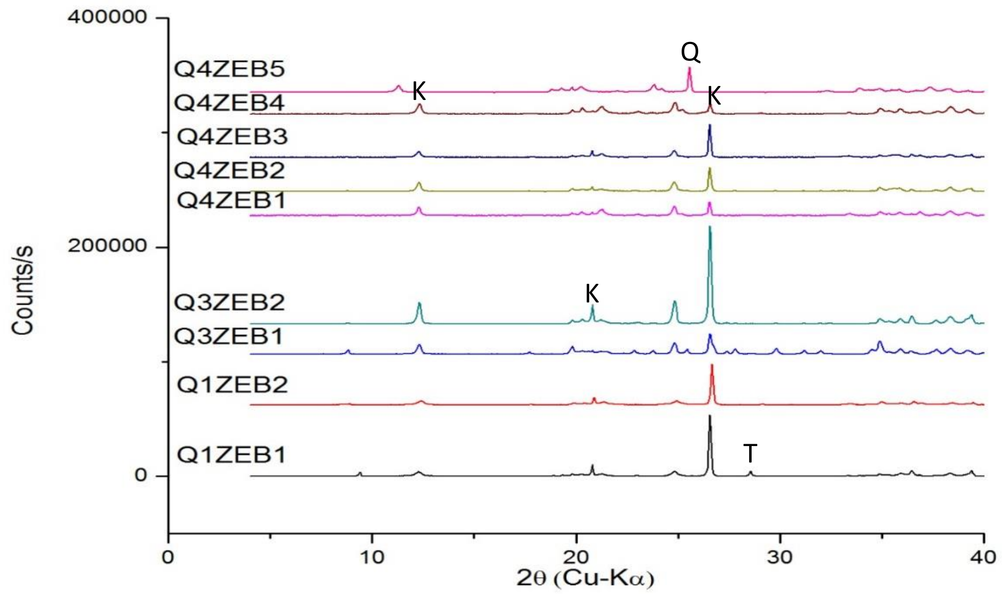

Figure 4.24: Diffractogram charts showing the mineralogical composition of Zebediela kaolin (K=Kaolinite, T=Talc, Q=Quartz).

The XRD pattern of Zebediela clay fraction kaolin samples was characterized by kaolinite peak occurred at 12.28° and 25º was the highest peak in most of the analysed samples (Figure 4.25). Talc was identified at 9.40° in sample Q1ZEB1. Montmorillonite peaks were identified at 5.88° and 17.75° at sample Q4ZEB5. Kaolinite peaks at sample Q3ZEB2 were identified whereas other peaks were very weak. Anatase peaks were identified in most of the studied samples but the strongest anatase peak was identified in sample Q4ZEB5. Goethite peak was identified at 21.29°.

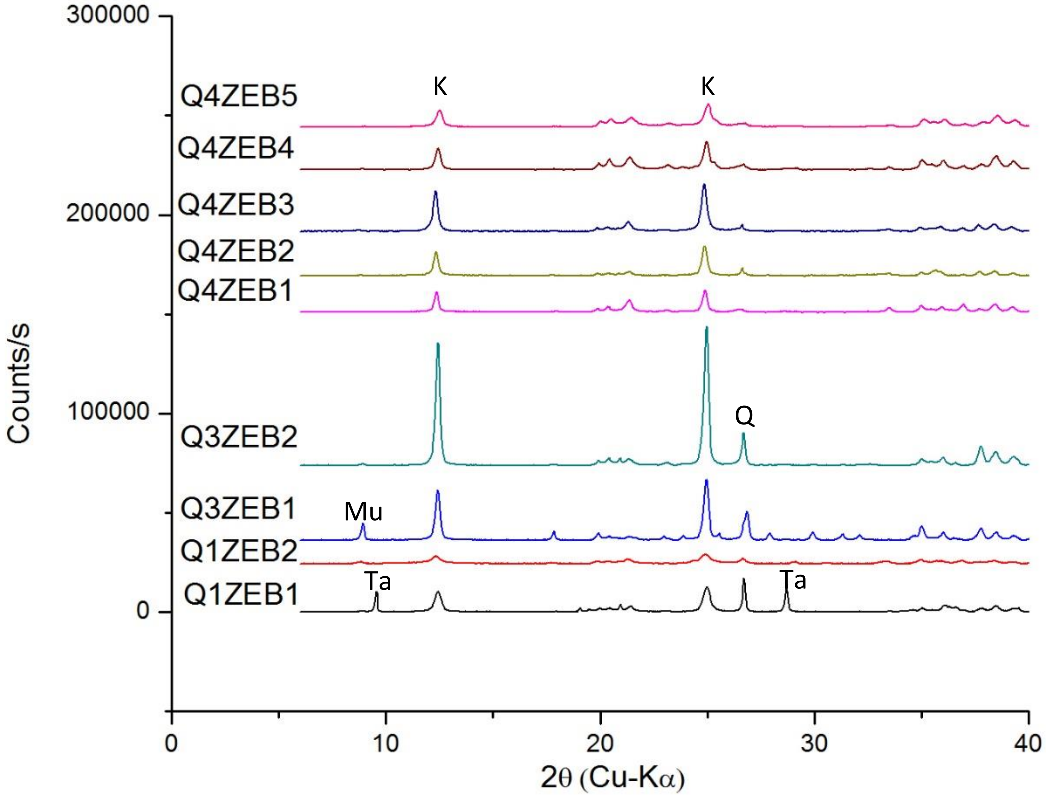

Figure 4.25: Diffractogram charts showing the mineralogical composition Clay fraction of Zebediela kaolin. Note: K=kaolinite, Q=Quartz, Mn=Microcline, Mu=Muscovite.

4.3.2 Functional groups

The assignment of the absorption bands in measure IR spectra was summarized in Table 4.11 and the IR spectra of clay kaolin samples from Lwamondo presented in the Figure 4.26. The absorption bands between 3689, 3669, 3651 and 3619 cm^{-1} region corresponding to OH stretching groups were observed in all samples except in samples; LWA1, LWA7 and LWA8 , supporting bands at 788 cm^{-1} (Si-O) and 681 cm^{-1} (Si-O) were observed in the samples which are diagnostic for kaolinite. Muscovite + quartz interference was identified in all samples except in LWA1 and LWA6.

Table 4.11: Assignments and infrared bands of selected clay size fraction of kaolin samples from Lwamondo kaolin deposit

Wavelength (cm^{-1})										
Theoretical Kaolinite	LWA1	LWA2	LWA3	LWA4	LWA5	LWA6	LWA7	LWA8	LWA9	Assignment
3689	-	3689	3689	-	3891	3689	3689	3687	3891	OH stretching of inner-surface hydroxyl groups1
3669	-	3667	3661	-	3661	3673	3667	3667	-	OH stretching of inner-surface hydroxyl groups2
3651	-	3657	3649	-	3640	3655	3651	3649	3653	OH stretching of inner-surface hydroxyl groups2
3619	-	3618	3618	-	3618	3616	3618	3618	3618	OH stretching of inner hydroxyl groups
1635	-	-		-	1635	-	1646	1633	-	H-O-H stretching; possibly smectite interference
1115	-	1111	1111	-	1111	-	1113	1113	111	Si-O stretching (longitudinal mode)
1027	-	1023	1023	1026	1026	-	1026	1023	1023	in-plane Si-O stretching
1005	-	-	1003	-	-	-	-	-	-	in-plane Si-O stretching
937	-	934	934	-	932	-	-	930	930	OH deformation of inner-surface hydroxyl group
788	777	785	789	-	787	-	785	787	787	Si-O
751	744	748	-	746	746	746	746	746	-	Si-O, perpendicular
681	679	683	679	-	677	-	-	-	-	Si-O, perpendicular
645	-	646	-	646	-	644	642	-	-	Si-O

(–)Very weak intensity or not detected

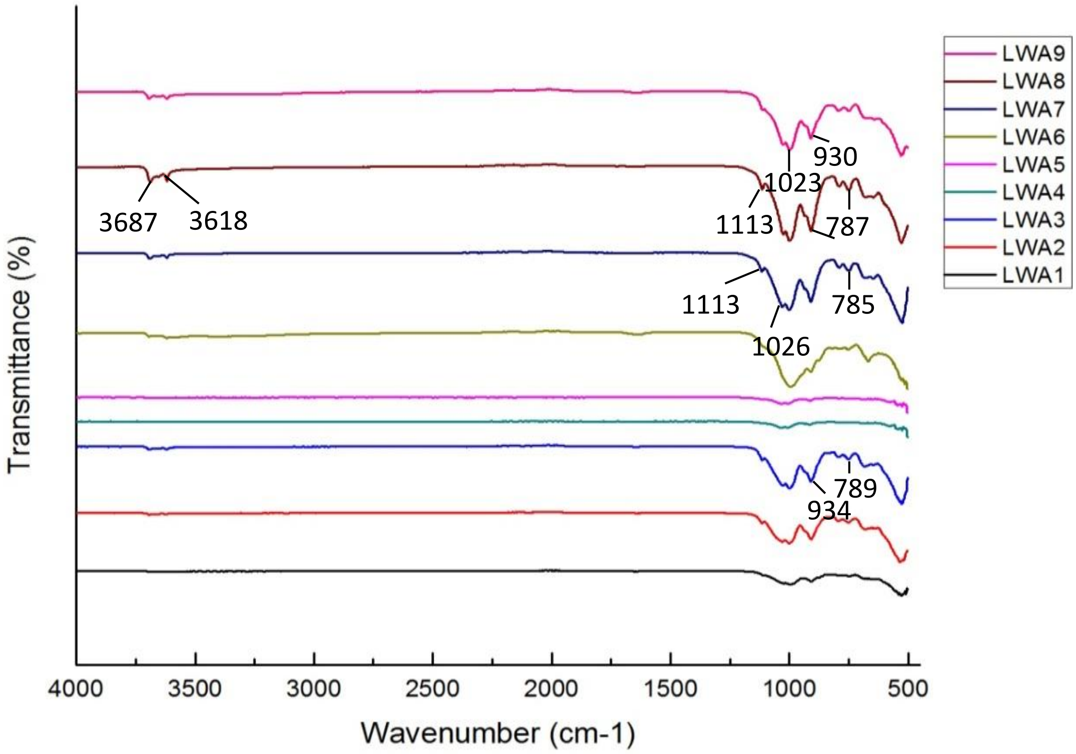

Figure 4.26: FTIR spectra of clay size fraction of the kaolin samples from Lwamondo kaolin deposit.

The assignment of the absorption bands in measure IR spectra was summarized in Table 4.12 and the IR spectra of clay fraction kaolin samples from Zebediela presented in Figure 4.27. The absorption bands 3689, 3669, 3651 and 3619 cm^{-1} corresponding to OH stretching groups were observed in all samples except in Q1ZEB1 where 3689 and 3619 cm^{-1} bands were not identified and Q3ZEB2 3669 cm^{-1} band was not identified. Supporting bands at 788 cm^{-1} (Si-O) were identified in all studied sample and bands 681 cm^{-1} (Si-O) were observed in the samples except in sample Q1ZEB1 which are diagnostic for kaolinite. Muscovite + quartz interferences was observed in all samples except in Q1ZEB1.

Table 4.12: Assignments and infrared bands of selected clay size fraction of kaolin samples from Zebediela kaolin deposit

Wavelength (cm^{-1})										
Theoretical kaolinite	Q1ZEB1	Q1ZEB2	Q3ZEB1	Q3ZEB2	Q4ZEB1	Q4ZEB2	Q4ZEB3	Q4ZEB4	Q4ZEB5	Assignment
3689	-	3685	3687	3689	3691	3689	3689	3691	3691	OH stretching of inner-surface hydroxyl groups1
3669	3669	3667	3665	-	3661	3661	3665	3665	3661	OH stretching of inner-surface hydroxyl groups2
3651	3651	3645	3647	3647	3647	3651	3647	3649	3649	OH stretching of inner-surface hydroxyl groups 2
3619	-	3612	3612	3618	3618	3616	3616	3618	3618	OH stretching of inner hydroxyl groups
1635	1644	1664	-	-	-	-	-	-	-	H-O-H stretching; possibly smectite interference
1115	-	-	-	-	1111	1109	1109	1111	1107	Si-O stretching (longitudinal mode)
1027	-	1023	1026	1026	1030	1028	1028	1030	1030	in-plane Si-O stretching
1005	-		1003	1001	1009	1003	1003	1009	1009	in-plane Si-O stretching
937	-	932	930	-	-	934	930	930	932	OH deformation of inner-surface hydroxyl group
912	-	-	-	-	911	-	-	911	911	OH deformation of inner hydroxyl group
788	777	791	791	787	787	785	789	785	785	Si-O
751	756	-	-	-	752	-	-	-	754	Si-O, perpendicular
681	-	681	687	689	687	687	689	685	683	Si-O, perpendicular
645	-	644	-	-	-	644	640	640	646	Si-O

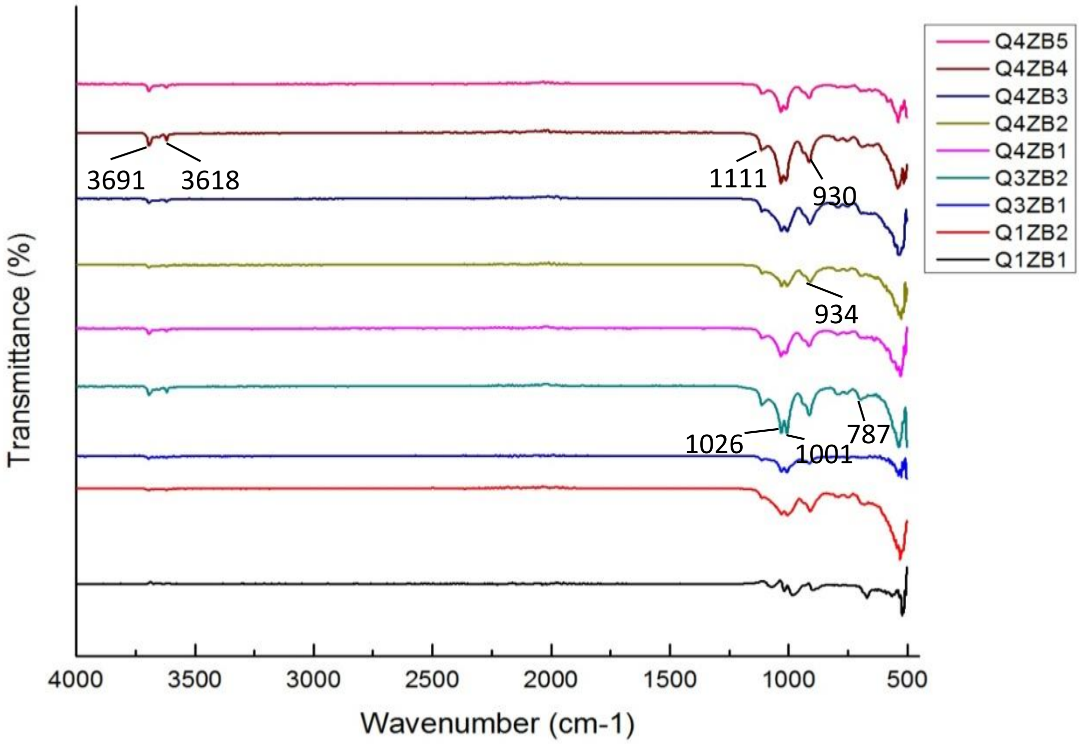

Figure 4.27: FTIR spectra of clay size fraction of the Zebediela kaolin samples.

4.3.3 Mineral morphology

The morphologies of the clay size fraction of 18 samples from Lwamondo and Zebediela Kaolins were well defined and could be classified under the following three groups:

1. Kaolinite booklets and stacks: LWA2, LWA3,LWA5, Q3ZEB1 and Q3ZEB2
2. Well developed and irregular flakes and platelets: LWA1, LWA4 (poorly ordered books) , LWA6, LWA7 (poorly ordered books), Q1ZEB1, Q1ZEB2, Q4ZEB1, Q4ZEB3, Q4ZEB4 and Q4ZEB5
3. Accordion morphology: LWA8 with halloysite detected

These are presented in Figures 4.27-4.41. Most of the studied samples show open texture and high porosity and pseudo-hexagonal structure retained in some samples.

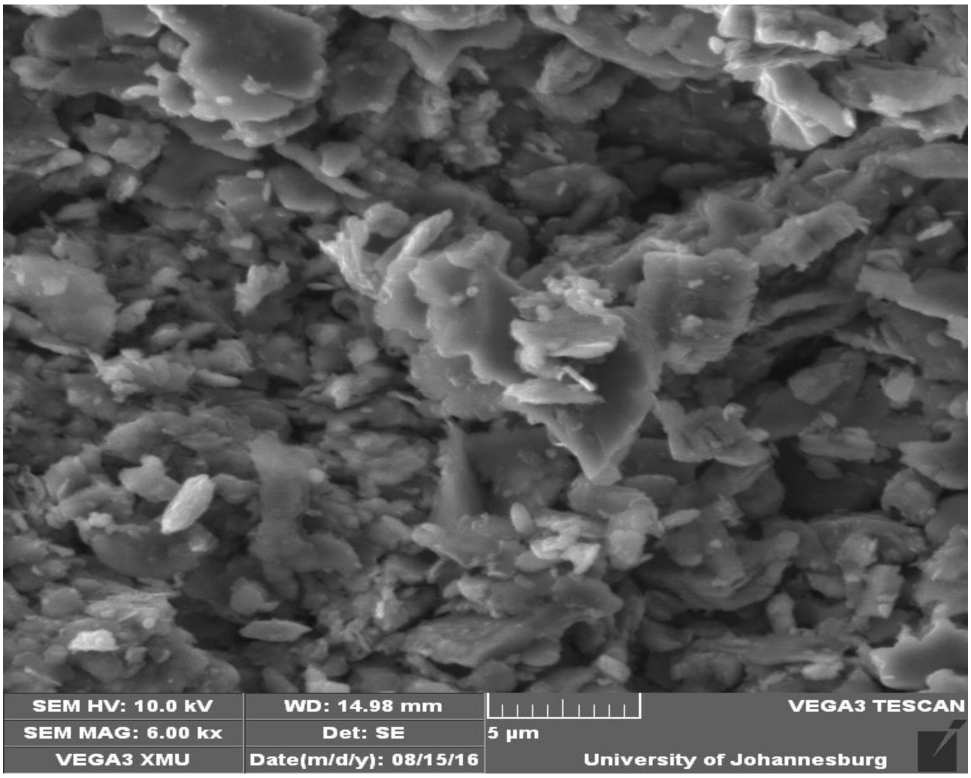

Figure 4.28: Scanning electron microscopy photograph of the clay fraction of sample LWA1 reflecting Irregular flakes and platelets of kaolinite.

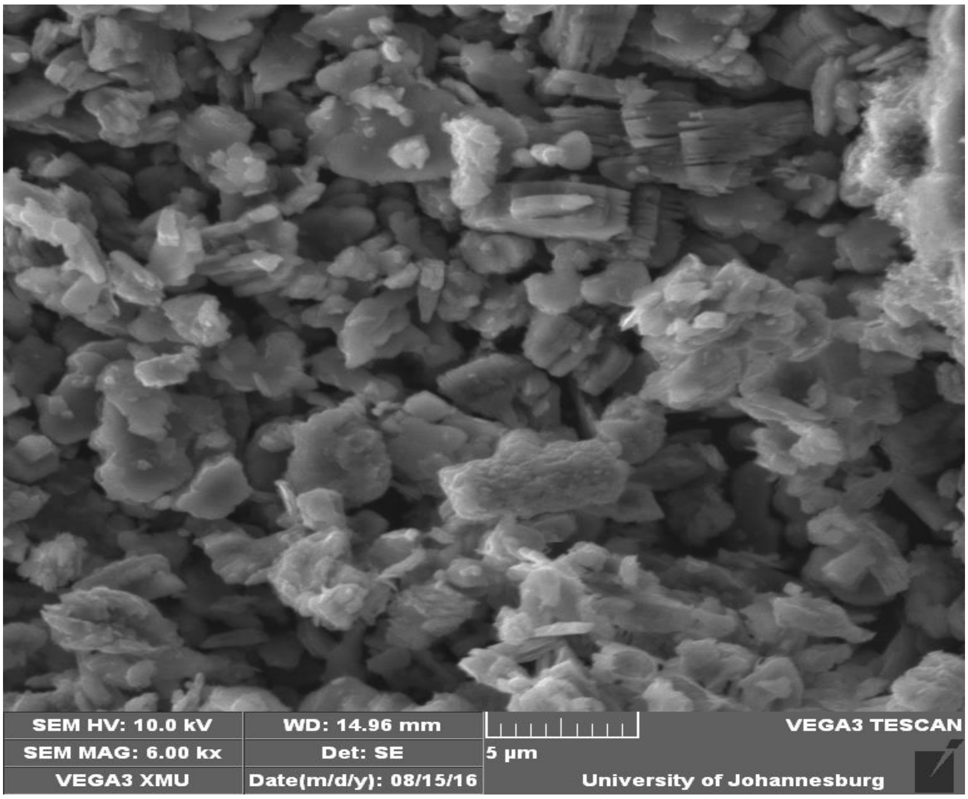

Figure 4.29: Scanning electron microscopy photograph of the clay fraction of sample LWA2 reflecting pseudo-hexagonal platelets of kaolinite.

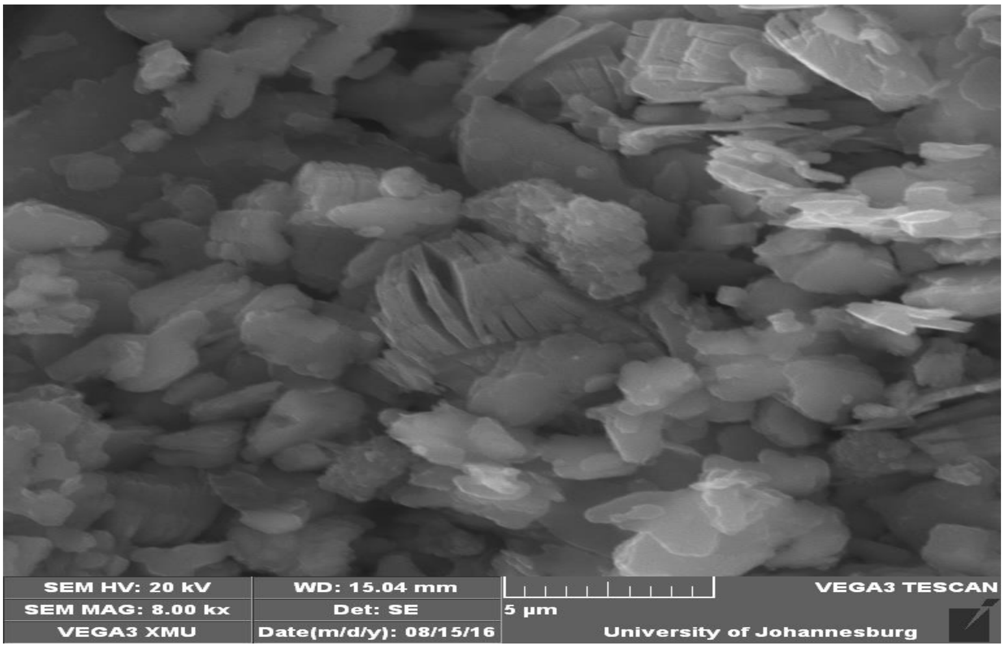

Figure 4.30: Scanning electron microscopy photograph of the clay fraction of sample LWA3 reflecting Kaolinite booklets and stacks.

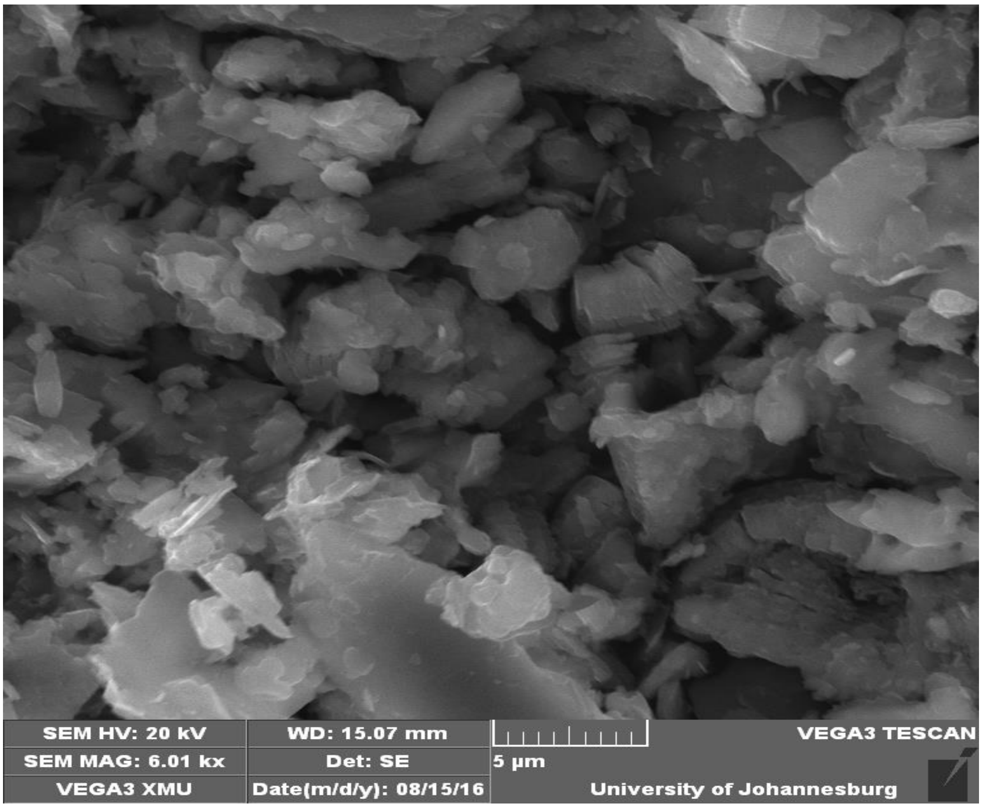

Figure 4.31: Scanning electron microscopy photograph of the clay fraction of sample LWA4 showing Irregular flakes and platelets of kaolinite.

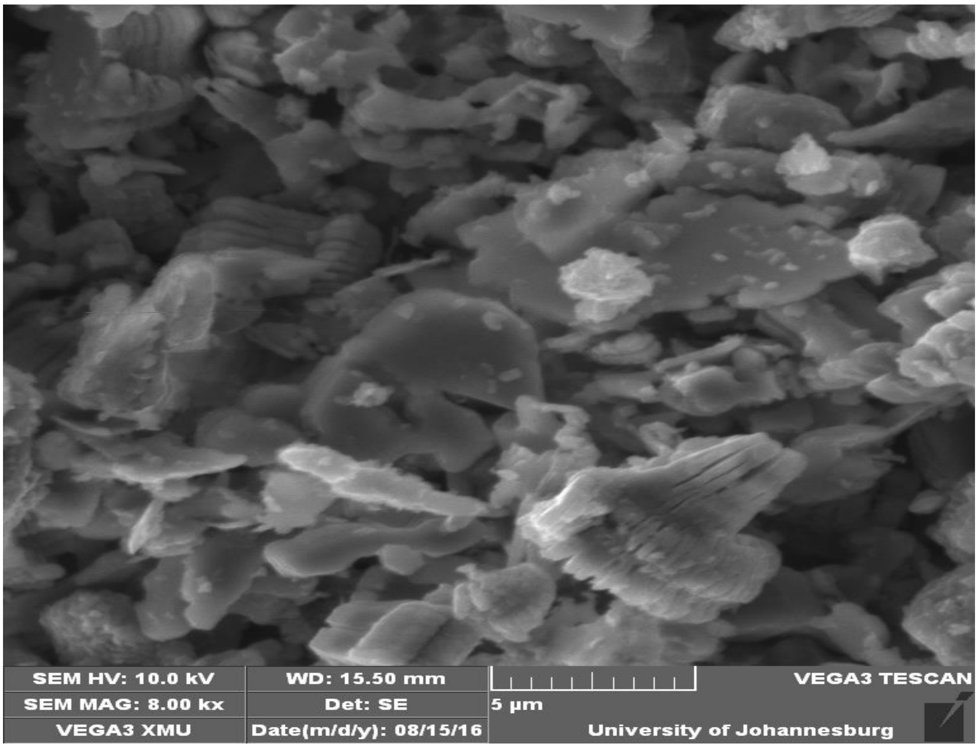

Figure 4.32: Scanning electron microscopy photograph of the clay fraction of sample LWA5 showing Kaolinite booklets and stacks.

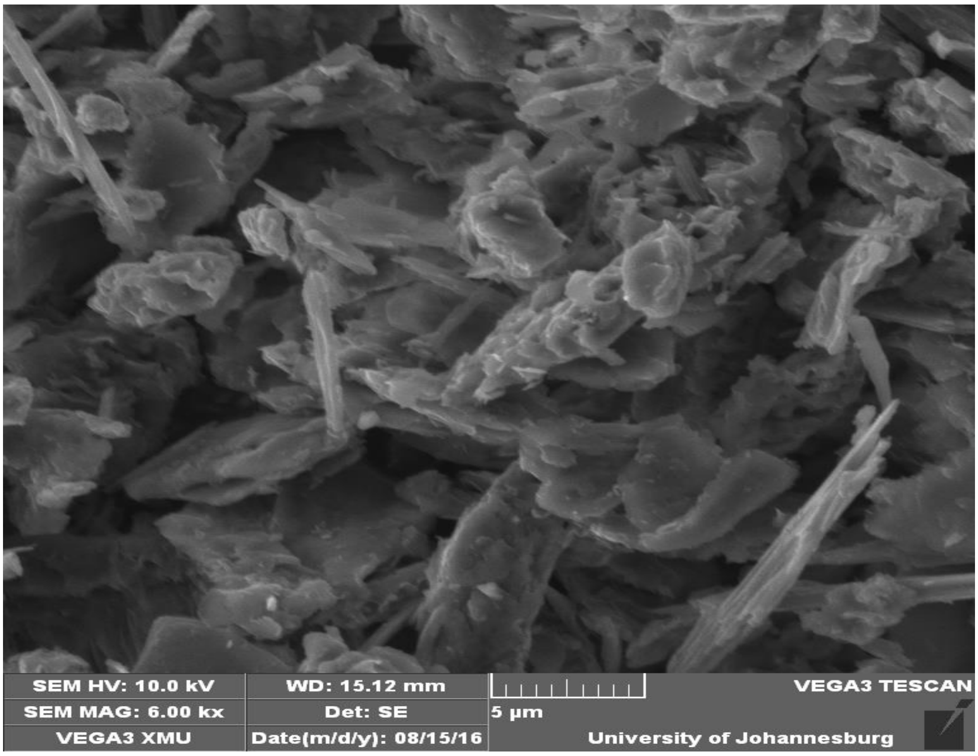

Figure 4.33: Scanning electron microscopy photograph of the clay fraction of sample LWA6 revealing irregular flakes and platelets.

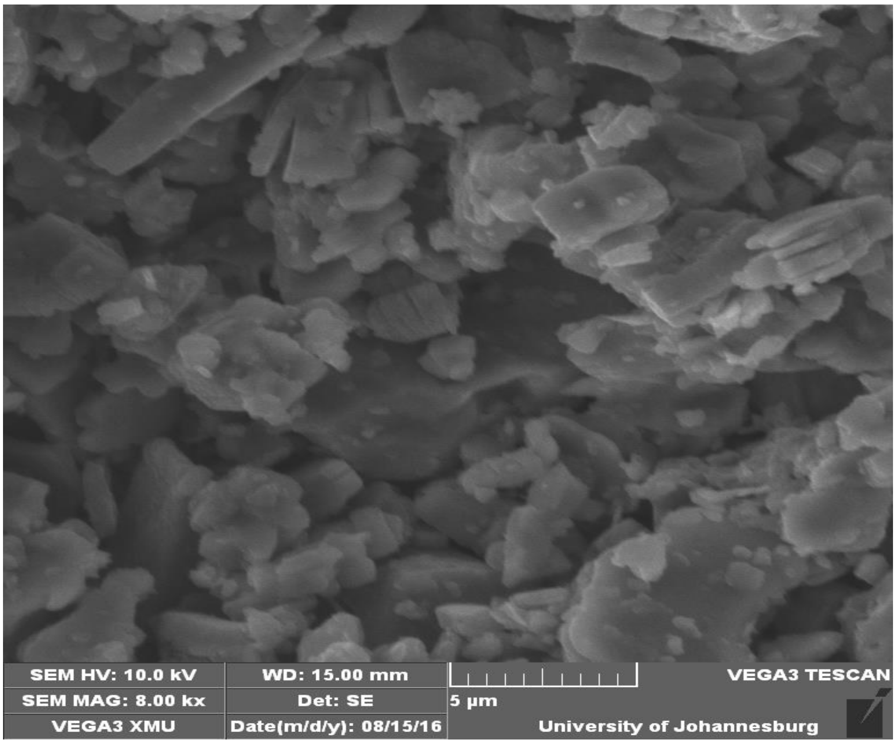

Figure 4.34: Scanning electron microscopy photograph of the clay fraction of sample LWA7 depicting irregular flakes and platelets.

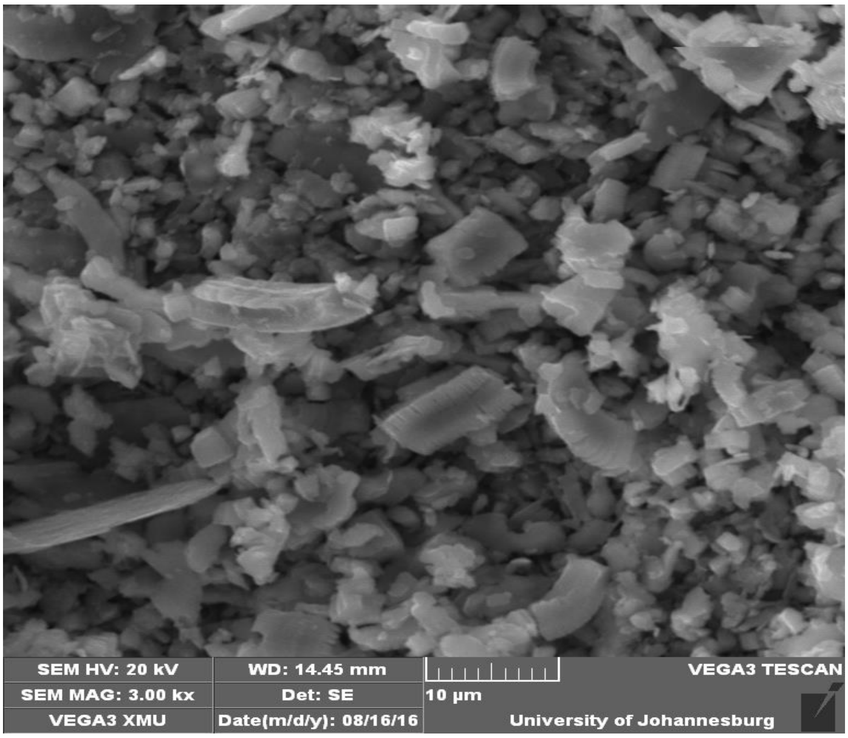

Figure 4.35: Scanning electron microscopy photograph of the clay fraction of sample LWA8 showing typical accordion morphology of kaolinite.

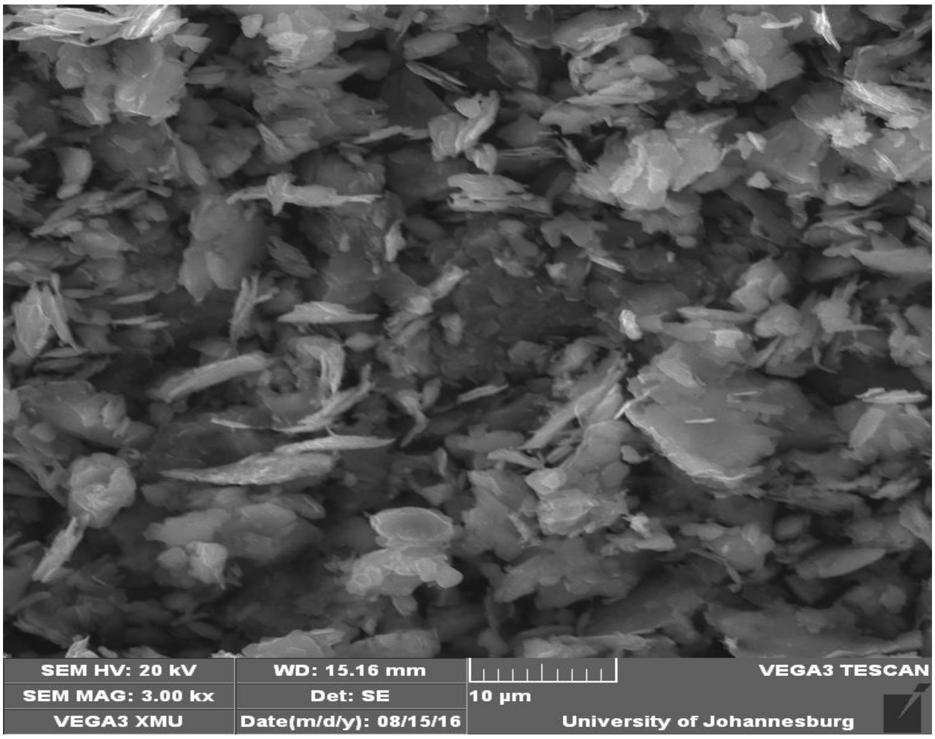

Figure 4.36: Scanning electron microscopy photograph of the clay fraction of sample Q1ZEB1 showing irregular flakes and platelets of kaolinite.

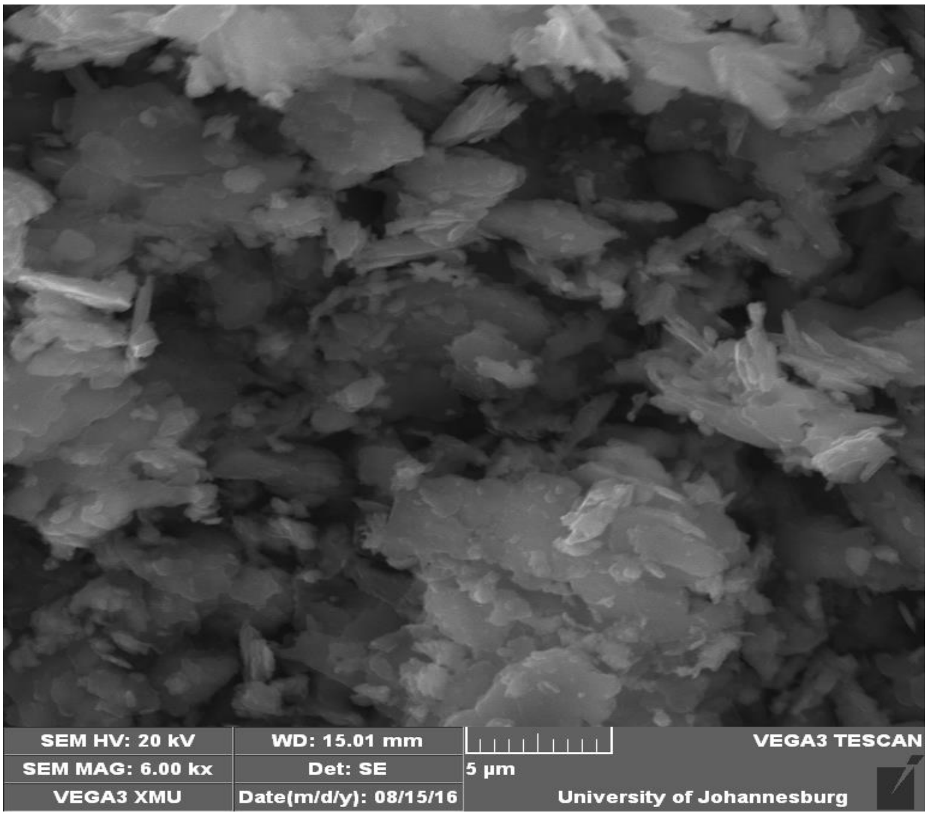

Figure 4.37: Scanning electron microscopy photograph of the clay fraction of sample Q1ZEB2 depicting irregular flakes and platelets of kaolinite.

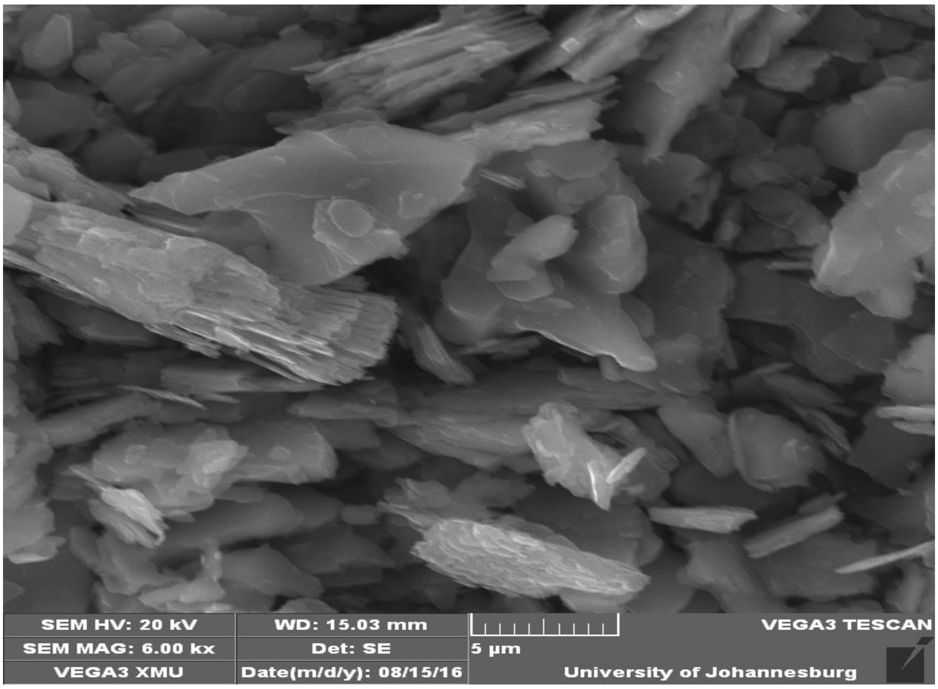

Figure 4.38: Scanning electron microscopy photograph of the clay fraction of sample Q3ZEB1 showing kaolinite booklets and stacks.

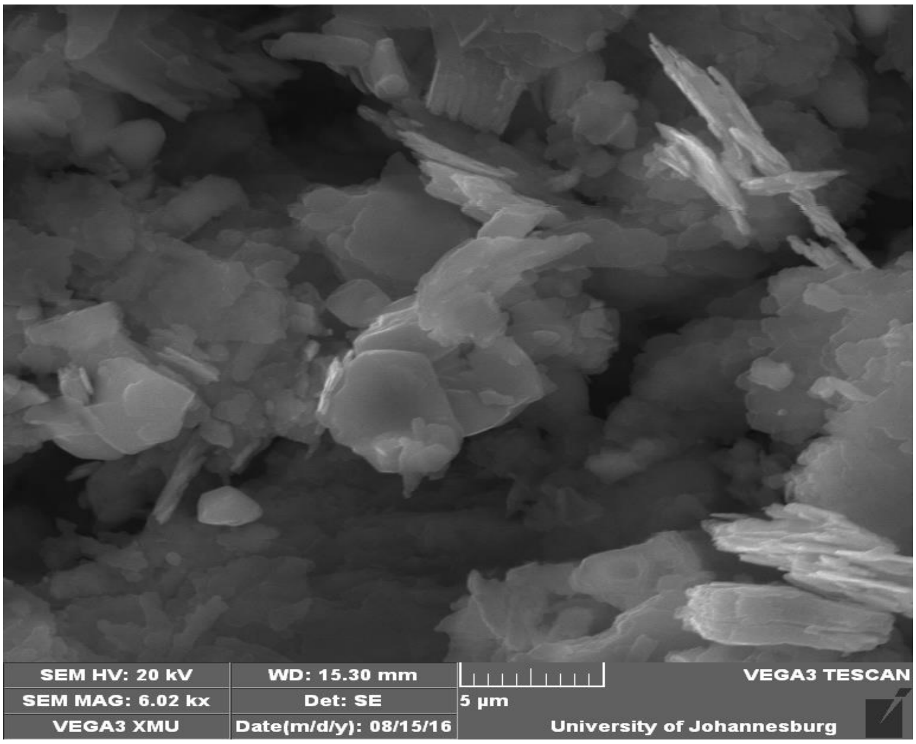

Figure 4.39: Scanning electron microscopy photograph of the clay fraction of sample Q3ZEB2 revealing kaolinite booklets and stacks.

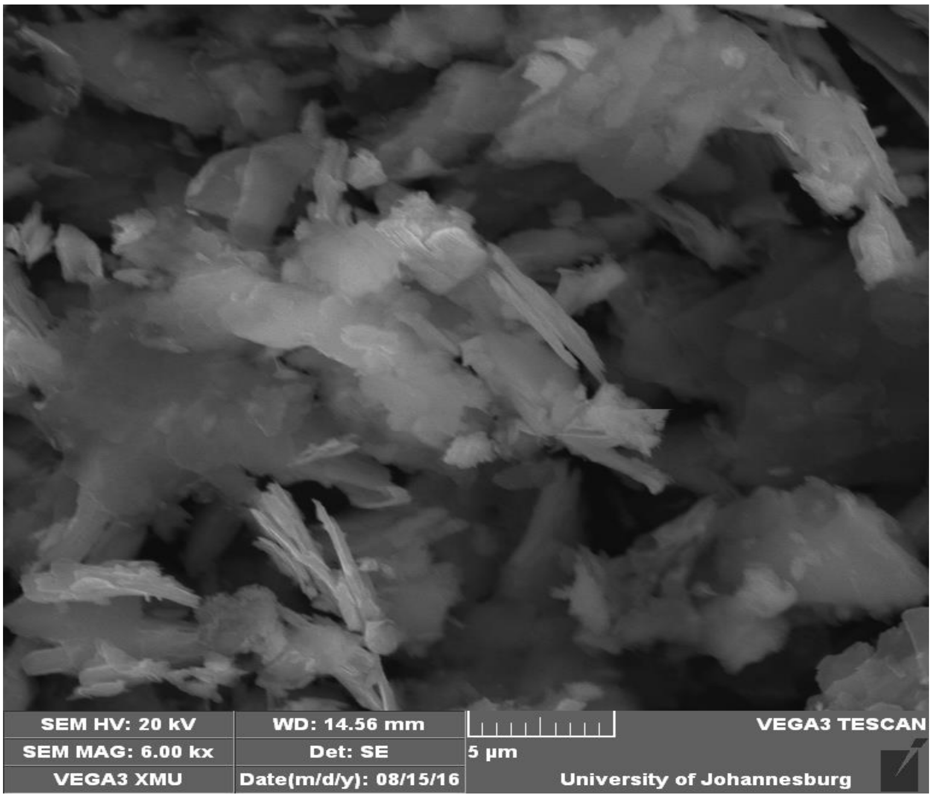

Figure 4.40: Scanning electron microscopy photograph of the clay fraction of sample Q4ZEB2 showing irregular flakes and platelets of kaolinite.

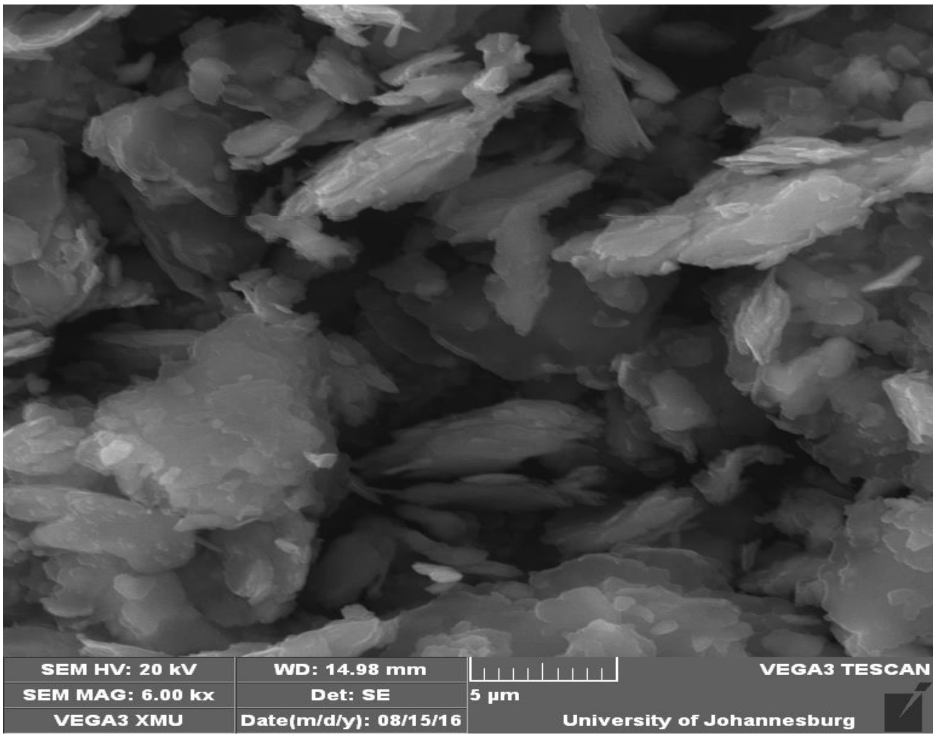

Figure 4.41: Scanning electron microscopy photograph of the clay fraction of sample Q4ZEB3 showing irregular flakes and platelets of kaolinite.

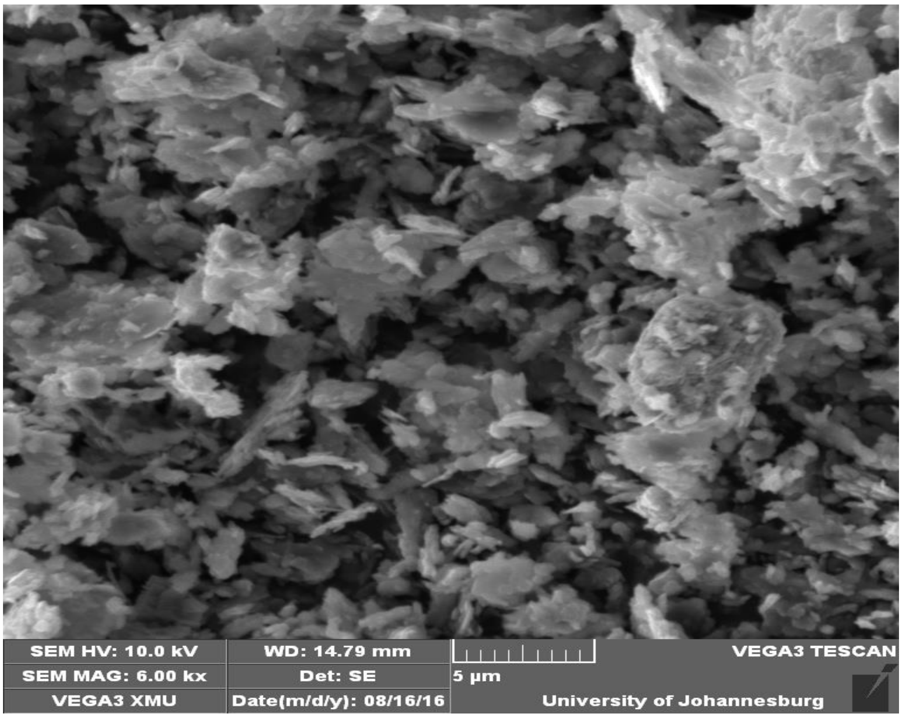

Figure 4.42: Scanning electron microscopy photograph of the clay fraction of sample Q4ZEB4 showing irregular flakes and platelets of kaolinite.

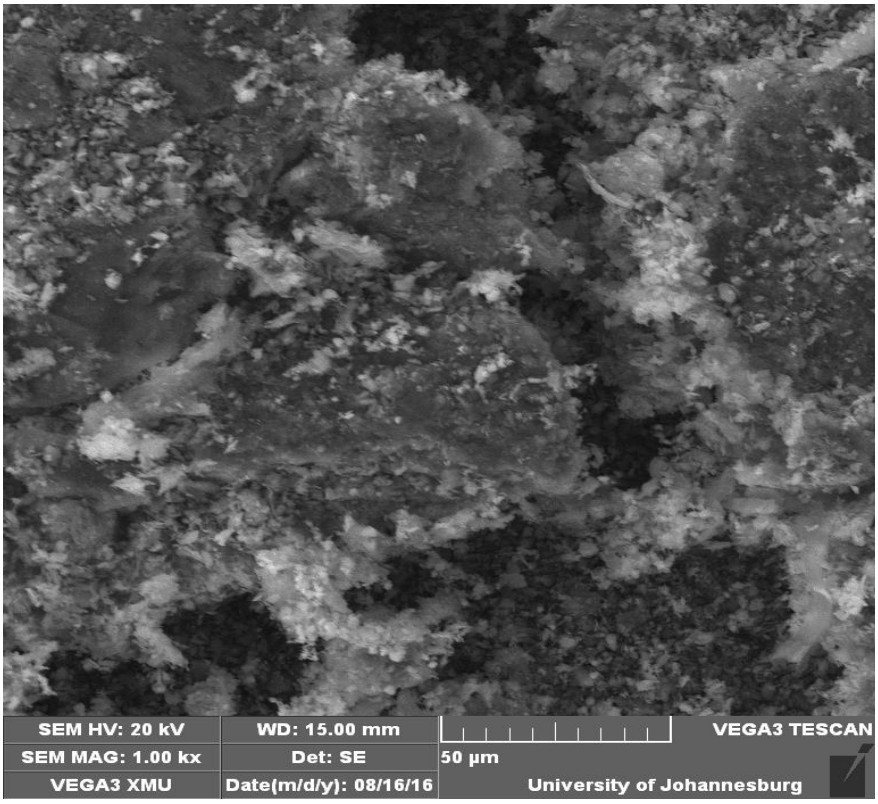

Figure 4.43: Scanning electron microscopy photograph of the clay fraction of sample Q4ZEB5 showing irregular flakes and platelets of kaolinite.

4.4 Geochemistry

4.4.1 Major oxides

The results of the geochemical analysis for bulk kaolin samples from Lwamondo are summarised in Figure 4.44 and Table 4.13. Silica content (SiO_2) ranged from 33.02 wt % (sample LWA9) to 64.49 wt % (sample LWA7) with a mean of 54.31 wt %. Alumina (Al_2O_3) content ranged from 10.13 wt % (LWA6) to 31.09 wt % (sample LWA2) with an average of 22.36 wt %. Iron content varied from 0.14 wt % (sample LWA7) to 30.24 wt % (sample LWA9) with an average of 7.88 wt %. Sample LWA1 (20.48 wt %), Sample LWA6 (10.96 wt %) and Sample LWA9 (30.24 wt %) was enriched in iron. Samples were depleted in other transition metals (Mn, Ti, Cr and Ni), alkaline and alkaline earth metals (Na, K, Mg and Ca), however, Sample LWA6 was enriched in Mg (12.56 wt %), whereas Sample LWA4 (4.03 wt %), Sample LWA7 (8.70 wt %) and Sample LWA9 (4.12 wt %) was enriched in Na. LOI ranged from 2.43 wt % (Sample LWA7) to 12.69 wt % (Sample LWA1) with a mean value of 9.10 wt %. The SiO_2/Al_2O_3 ratio varied from 1.71 (Sample LWA2) to 3.04 (Sample LWA3) whereas Fe_2O_3/TiO_2 ratio ranged from 6.26 (Sample LWA2) to 37.79 (LWA6) and TiO_2/Al_2O_3 ratio ranged from 0.00 (LWA8) to 0.23 (Sample LWA9).

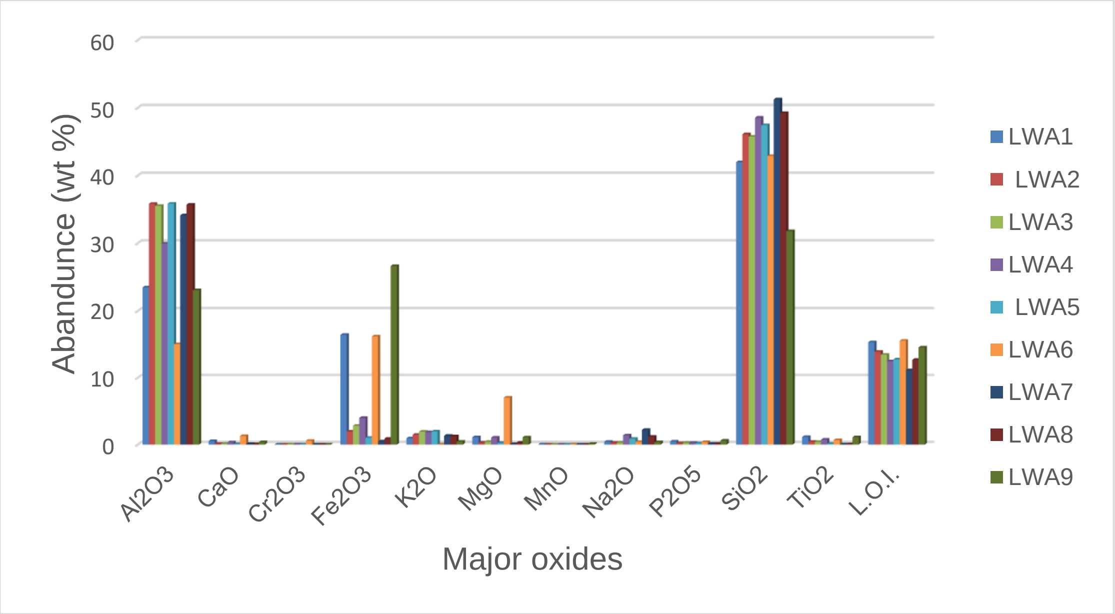

Figure 4.44: Major oxides abundance in Lwamondo bulk kaolin samples as determined by XRF.

Table 4.13: chemical composition in (wt %) and weathering indices of bulk samples from Lwamondo kaolin deposit

	Al_2O_3	**CaO**	**Cr_2O_3**	**Fe_2O_3**	**K_2O**	**MgO**	**MnO**	**Na_2O**	**P_2O_5**	**SiO_2**	**TiO_2**	**L.O.I.**	**Si/Al**	**Fe/Ti**	**Ti/Al**	**CIA**	**CIW**
LWA1	16.18	0.48	0.01	20.48	1.08	1.2	0.01	0.05	0.07	46.45	3.09	12.69	2.87	6.63	0.19	90.95	96.83
LWA2	31.09	0.19	0.01	1.94	2.05	0.34	0.01	0.07	0.02	53.08	0.31	12.06	1.71	6.26	0.01	93.08	99.17
LWA3	21.68	0.16	0.02	2.48	0.86	0.42	0.01	0.02	0.02	65.88	0.25	8.92	3.04	9.92	0.01	95.42	99.18
LWA4	25.63	0.94	0.01	2.36	2.92	0.87	0	4.03	0.03	56.68	0.28	7.14	2.21	8.43	0.01	76.46	83.76
LWA5	30.7	0.66	0.02	1.67	1.93	0.4	0.01	2.96	0.02	52.72	0.16	9.50	1.72	10.44	0.01	84.69	89.45
LWA6	10.13	1.13	0.46	10.96	0.01	12.56	0.08	0	0.02	53.82	0.29	11.13	5.31	37.79	0.03	89.88	89.96
LWA7	22.58	0.27	0	0.14	1.38	0.03	0	8.7	0.02	64.49	0	2.43	2.86	#DIV/0!	0.00	68.57	71.57
LWA8	24.35	0.22	0.01	0.63	2.06	0.24	0.01	4.12	0.02	62.68	0.03	6.18	2.57	21.00	0.00	79.19	84.87
LWA9	18.92	0.35	0.01	30.24	0.23	1.02	0.31	0.17	0.07	33.02	4.43	11.88	1.75	6.83	0.23	96.19	97.33
MEAN	22.36	0.49	0.06	7.88	1.39	1.90	0.05	2.24	0.03	54.31	0.98	9.10	2.43	8.02	0.04	86.05	81.24

The results of the concentrations of major elements in bulk kaolin samples from Zebediela are summarized in Figure 4.45 and Table 4.14. SiO_2 content ranged from 41.60 wt % (Sample Q4ZEB1) to 67.01 wt % (Sample Q3ZEB2) with an average of 52.61 wt %. The Al_2O_3 content ranged between 16.55 wt % (Sample Q1ZEB1), 32.20 wt % (Sample Q4ZEB4) with a mean of 23.61 wt %. Iron content (Fe_2O_3) ranged between 0.23 wt % (Sample Q3ZEB2), 20.16 wt % (Sample Q4ZEB3) with an average value of 10.69 wt %. Sample Q1ZEB1 had higher MgO concentration (4.65 wt %) whereas Sample Q3ZEB1 has higher K_2O concentration (4.87 wt %). LOI values ranged from 7.57 wt % (Sample Q4ZEB2) to 12.84 wt % (Sample Q4ZEB4) with an average of 9.73 wt %. The SiO_2/Al_2O_3 ratio varied from 1.32 (Sample Q4ZEB4) to 3.91 (Sample Q1ZEB1) whereas Fe_2O_3/TiO_2 ratio ranged from 0.13 (Sample Q3ZEB1) to 13.35 (Sample Q4ZEB3) and TiO_2/Al_2O_3 ratio ranged from 0.03 (Sample Q1ZEB1) to 0.10 (Samples Q3ZEB2, Q4ZEB4 and Q4ZEB5).

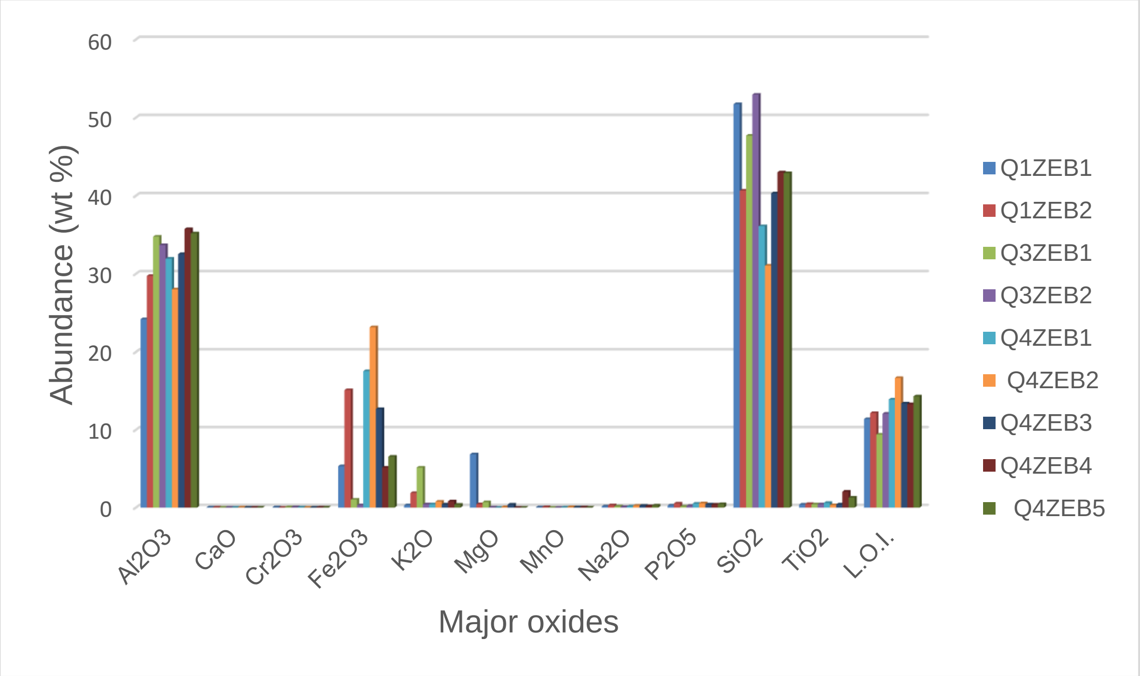

Figure 4.45: Major oxides abundance in Zebedeila bulk kaolin samples as determined by XRF.

Table 4.14: chemical composition in wt % and weathering indices of bulk samples from Zebediela kaolin.

	Al_2O_3	CaO	Cr_2O_3	Fe_2O_3	K_2O	MgO	MnO	Na_2O	P_2O_5	SiO_2	TiO_2	L.O.I.	Si/Al	Fe/Ti	Ti/Al	CIA	CIW
Q1ZEB1	16.55	0.09	0.04	4.98	0.38	4.65	0.21	bdl	0.06	64.71	0.46	8.44	3.91	10.83	0.03	97.24	99.46
Q1ZEB2	19.08	0.03	0	14.79	1.23	0.57	0.22	0.01	0.18	54.45	1.76	8.85	2.85	8.40	0.09	93.76	99.79
Q3ZEB1	31.21	0.02	0.04	1.01	4.87	0.71	0	0.09	0.05	50.8	2.65	8.25	1.63	0.38	0.08	86.24	99.65
Q3ZEB2	22.31	0.03	0.03	0.28	0.56	0.1	0	0	0.02	67.01	2.15	7.94	3.00	0.13	0.10	97.42	99.87
Q4ZEB1	28.77	0.03	0.03	14.9	0.3	bdl	0.15	0	0.23	41.6	2.26	12.73	1.45	6.59	0.08	98.87	99.89
Q4ZEB2	18.76	0.03	0.01	17.32	1.05	0.09	0.1	0.02	0.09	54.46	1.48	7.57	2.90	11.70	0.08	94.46	99.73
Q4ZEB3	17.68	0.04	0.02	20.16	0.27	0.34	0.2	0.02	0.19	51.34	1.51	9.21	2.90	13.35	0.09	98.17	99.66
Q4ZEB4	32.2	0.02	0.03	9.16	0.73	bdl	0.2	0	0.14	42.46	3.08	12.84	1.32	2.97	0.10	97.72	99.94
Q4ZEB5	25.96	0.05	0.04	13.68	0.31	0	0.04	0	0.16	46.66	2.52	11.71	1.80	5.43	0.10	98.63	99.81
MEAN	23.61	0.29	0.03	10.69	1.08	0.72	0.12	0.02	0.12	52.61	1.99	9.73	2.23	5.37	0.08	94.63	98.71

Results of geochemical analyses of silt fraction of Lwamondo kaolin is presented in Table 4.15 and Figure 4.46. SiO_2 content ranged from 36.64 wt % (Sample LWA9) to 65.72 wt % (Sample LWA7) with a mean value of 5.39 wt %. Al_2O_3 content ranged from 15.73 wt % (LWA6) to 34.9 wt % (LWA2) with an average of 25.38 wt %. Iron content varied from 0.12 wt % (LWA7) to 23.23 wt % (LWA9) with a mean value of 6.96 wt %. Samples LWA1, LWA6 and LWA9 were enriched in Fe_2O_3. All samples were depleted in other transition metals (Mn, Ti, Cr and P), alkaline and alkaline earth metals (Na, K, Mg and Ca), Sample LWA6 was enriched in MgO (0.05 wt %), whereas Sample LWA7 and LWA8 were enriched in Na_2O. LIO values ranged from 1.51 wt % (Sample LWA6) to 14.00 (Sample LWA6) with a mean value of 9.89 wt %. The SiO_2/Al_2O_3 ratio varied from 1.35 to 3.08 Fe_2O_3/TiO_2 ranged from 0.00 to 30.50 and TiO_2/Al_2O_3 ratio varied from 0.00 to 0.09.

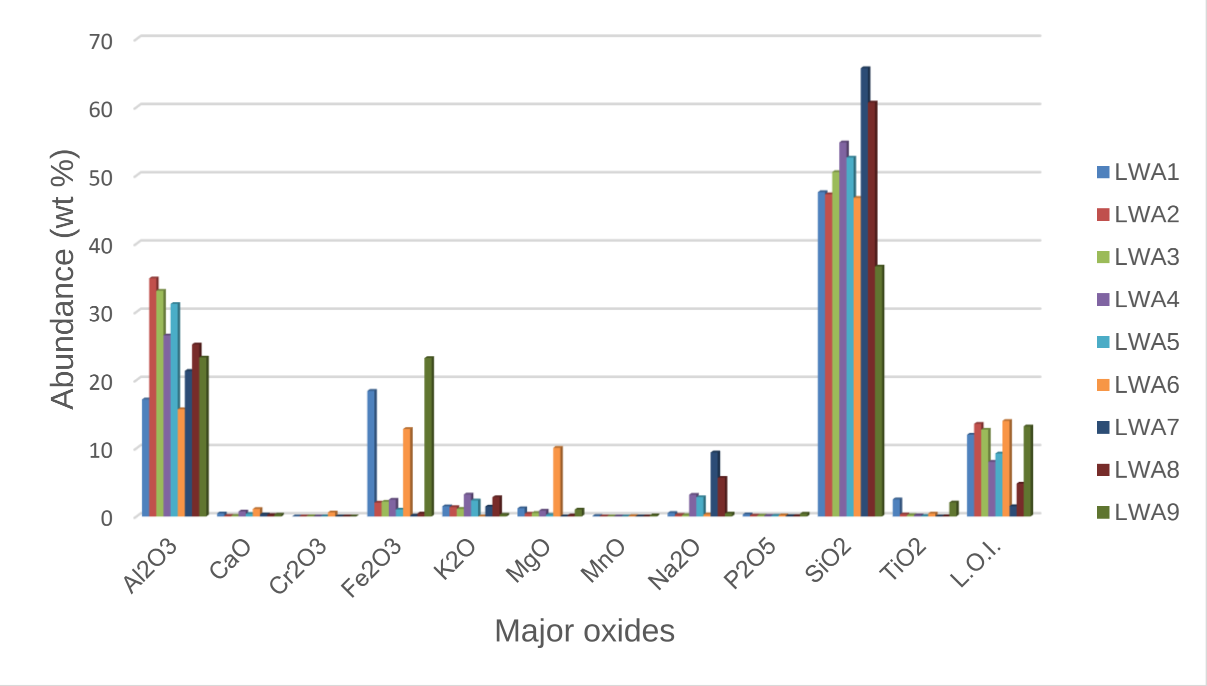

Figure 4.46: Major oxides abundance in silt fraction of Lwamondo kaolin as determined by XRF.

Table 4.15: Chemical composition (wt %) and weathering indices of silt fraction of Lwamondo kaolin.

	Al_2O_3	**CaO**	**Cr_2O_3**	**Fe_2O_3**	**K2O**	**MgO**	**MnO**	**Na_2O**	**P_2O_5**	**SiO_2**	**TiO_2**	**L.O.I.**	**Total**	**Si/Al**	**Fe/Ti**	**Ti/Al**	**CIA**	**CIW**
LWA1	17.15	0.44	0.01	18.41	1.48	1.2	0.08	0.51	0.31	47.55	2.5	11.99	101.63	2.77	7.36	0.15	87.59	94.75
LWA2	34.9	0.09	0.01	2.02	1.37	0.4	0.01	0.23	0.13	47.24	0.29	13.57	100.26	1.35	6.97	0.01	95.38	99.09
LWA3	33.08	0.1	0.02	2.15	1.11	0.51	0.01	0.19	0.12	50.49	0.2	12.71	100.69	1.53	10.75	0.01	95.94	99.13
LWA4	26.53	0.73	0.01	2.45	3.21	0.84	0.01	3.17	0.1	54.83	0.17	8.01	100.06	2.07	14.41	0.01	78.86	87.18
LWA5	31.15	0.37	0.02	1.01	2.34	0.24	0	2.82	0.11	52.61	0.07	9.23	99.97	1.69	14.43	0.00	84.92	90.71
LWA6	15.73	1.1	0.59	12.81	0.01	10.05	0.05	0.28	0.17	46.71	0.42	14.00	101.92	2.97	30.50	0.03	91.88	91.93
LWA7	21.33	0.29	bdl	0.12	1.45	0.01	0	9.38	0.05	65.72	bdl	1.51	99.86	3.08	0.00	0.00	65.73	68.81
LWA8	25.22	0.22	0.01	0.43	2.82	0.15	0.01	5.66	0.06	60.69	0.02	4.81	100.10	2.41	21.50	0.00	74.35	81.09
LWA9	23.3	0.27	bdl	23.23	0.25	1.01	0.16	0.43	0.4	36.64	2.05	13.19	100.93	1.57	11.33	0.09	96.08	97.08
Mean	25.38	0.40	0.10	6.96	1.56	1.60	0.04	2.52	0.16	51.39	0.72	9.89	100.60	2.16	13.03	0.03	85.64	89.98

Results of geochemical analyses of silt fraction of Zebediela kaolin is presented in Table 4.16 and Figure 4.47. The Al_2O_3 content ranged from 5.36 wt % (Sample Q1ZEB1) to 30.67 wt % (Sample Q4ZEB2) with an average of 22.10 wt %. The SiO_2 content varied from 42.83 wt % (Sample Q4ZEB4) to 82.81 wt % (Sample Q1ZEB1) with an average of 54.66 wt %. The iron oxide (Fe_2O_3) content ranged from 0.26 wt % (Sample Q3ZEB2) to 23.23 w % (Sample Q4ZEB3) with an average of 10.50 wt % The samples were depleted in all other elements such as CaO, Cr_2O_3, K_2O, MgO, MnO, Na_2O, P_2O_5 and TiO_2. However, Sample Q1ZEB1 was enriched in MgO (6.18 wt %), Samples QEZEB1, Q4ZEB4 and Q4ZEB5 were enriched in TiO_2. The LOI values ranged from 3.48 wt % to 12.29 wt % with an average of 8.91 wt %. The SiO_2/Al_2O_3 ratio ranged from 1.53 to 15.45, Fe_2O_3/TiO_2 ratio ranged from 0.17 to17.76 and TiO_2/Al_2O_3 ratio ranged from 0.02 to 0.17.

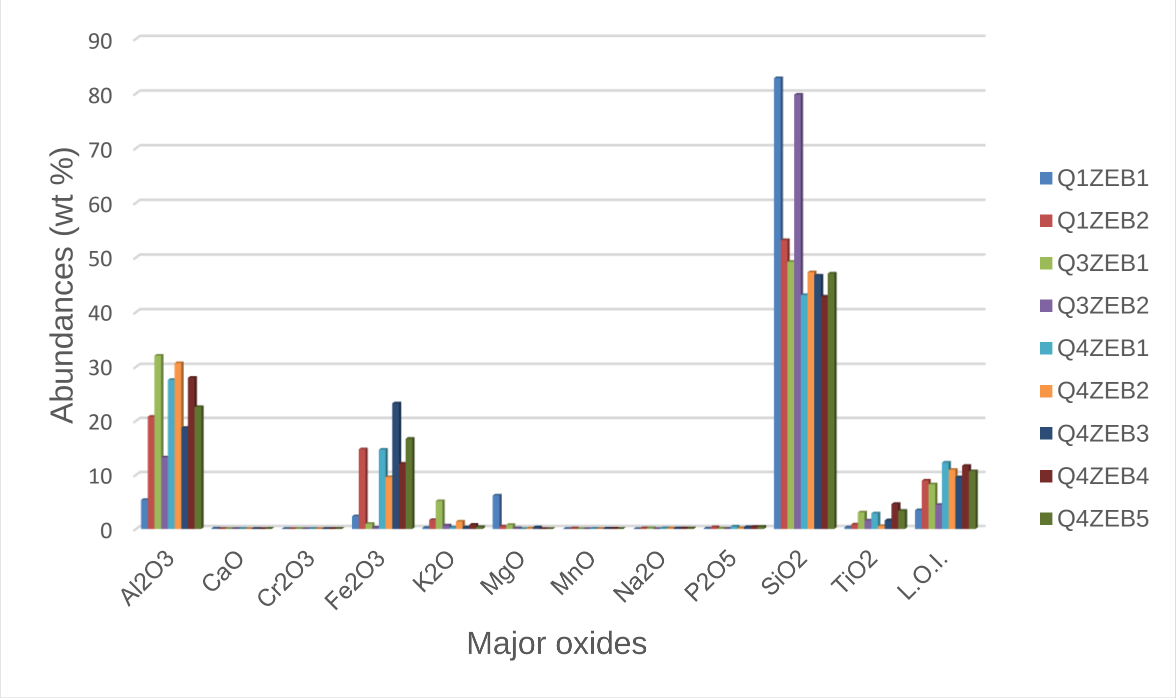

Figure 4.47: Major oxides abundance in silt fraction of Zebedilea kaolin as determined by XRF.

Table 4.16: Chemical composition (wt %) and weathering indices of silt fraction of Zebediela kaolin.

	Al_2O_3	CaO	Cr_2O_3	Fe_2O_3	K2O	MgO	MnO	Na_2O	P_2O_5	SiO_2	TiO_2	L.O.I.	Total	Si/Al	Fe/Ti	Ti/Al	CIA	CIW
Q1ZEB1	5.36	0.09	0.02	2.34	0.21	6.18	0.02	0	0.1	82.81	0.3	3.48	100.91	15.45	7.80	0.06	94.70	98.35
Q1ZEB2	20.76	0.02	0	14.73	1.66	0.48	0.11	0.15	0.32	53.17	0.83	8.95	101.18	2.56	17.75	0.04	91.90	99.19
Q3ZEB1	32.04	0.02	0.04	0.94	5.14	0.75	0	0.15	0.09	49.2	3.05	8.26	99.68	1.54	0.31	0.10	85.78	99.47
Q3ZEB2	13.24	0.03	0.01	0.26	0.64	0.15	0	0.01	0.06	79.79	1.56	4.45	100.20	6.03	0.17	0.12	95.11	99.70
Q4ZEB1	27.58	0.02	0.03	14.67	0.27	bdl	0.05	0.13	0.44	43.12	2.88	12.26	101.45	1.56	5.09	0.10	98.50	99.46
Q4ZEB2	30.67	0.01	0.01	9.59	1.36	0.1	0.03	0.12	0.17	47.29	0.54	10.94	100.83	1.54	17.76	0.02	95.37	99.58
Q4ZEB3	18.69	0.04	0.02	23.23	0.29	0.3	0.07	0.12	0.34	46.68	1.6	9.55	100.93	2.50	14.52	0.09	97.65	99.15
Q4ZEB4	27.97	0	0.04	12.07	0.78	bdl	0.08	0.11	0.39	42.83	4.62	11.67	100.56	1.53	2.61	0.17	96.92	99.61
Q4ZEB5	22.56	0.05	0.05	16.68	0.36	bdl	0.03	0.12	0.4	47.05	3.35	10.68	101.33	2.09	4.98	0.15	97.70	99.25
MEAN	22.10	0.03	0.02	10.50	1.19	1.33	0.04	0.10	0.26	54.66	2.08	8.91	100.78	3.87	7.89	0.09	94.85	99.31

Geochemical analysis results for clay fraction samples from Lwamondo kaolin are presented in Figure 4.48 and Table 4.17 revealed the following; SiO_2 ranged from 31.77 wt % (Sample LWA9) to 51.24 wt % (Sample LWA7) and mean of 44.99 wt % whereas, Al_2O_3 ranged from 15.01 wt % (Sample LWA6) to 35.80 wt % (Sample LWA2) and mean of 29.82 wt %. The alkali earth metals Mg ranged from 0.08 wt % (Sample LWA7) to 7.03 wt % (Sample LWA6) and Ca ranged from 0.06 wt % (Sample LWA8) to 1.28 wt % (Sample LWA6), whereas the alkalis; Na and K ranged from 0.27 wt % (Sample LWA2) to 2.19 wt % (LWA7) and 0.02 wt % (Sample LWA6) to 1.96 wt % (Sample LWA3). Fe_2O_3 varied from 0.47 wt % (Sample LWA7) to 26.62 wt % (Sample LWA9) with a mean of 7.81 wt % for iron oxide content. TiO_2 and P_2O_5 ranged from 0.02 wt % (Sample LWA7) to 1.14 wt % (Sample LWA1) and 0.13 wt % (Sample LWA8) to 0.60 wt % (Sample LWA9) whereas other transition metals, Cr_2O_3 from 0.01 wt % (Sample LWA1, LWA2,LWA8,LWA9) to 0.57 wt % (Sample LWA6). Loss on ignition values ranged from 11.12 wt % (Sample LWA7) to 15.30 wt % (Sample LWA1) with average of 13.52 wt %. The SiO_2/Al_2O_3 ratio ranged from 1.29 to 2.86, Fe_2O_3/TiO_2 ratio ranged from 4.62 to 24.15 and TiO_2/Al_2O_3 ratio ranged from 0.00 to 0.5.

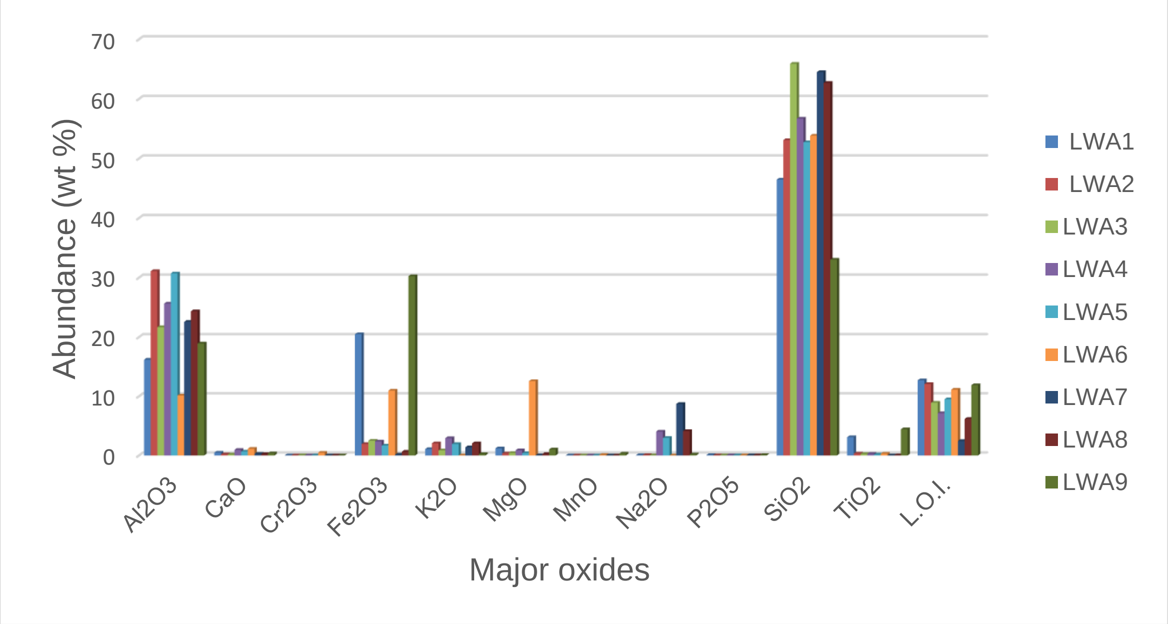

Figure 4.48: Major oxides abundance in Lwamondo kaolin clay fraction samples as determined by XRF.

Table 4.17: Chemical composition (in wt %) and weathering indices of clay fraction samples from Lwamondo kaolin deposit

	Al_2O_3	CaO	Cr_2O_3	Fe_2O_3	K_2O	MgO	MnO	Na_2O	P_2O_5	SiO_2	TiO_2	L.O.I.	Total	Si/Al	Fe/Ti	Ti/Al	CIA	CIW
LWA1	23.46	0.52	0.01	16.41	0.94	1.10	0.03	0.42	0.46	41.97	1.14	15.30	101.76	1.79	14.39	0.05	92.58	96.15
LWA2	35.80	0.12	0.01	1.94	1.46	0.29	0.01	0.27	0.21	46.09	0.42	13.89	100.51	1.29	4.62	0.01	95.09	98.92
LWA3	35.50	0.14	0.03	2.81	1.92	0.41	0.01	0.29	0.25	45.73	0.40	13.43	100.92	1.29	7.03	0.01	93.79	98.80
LWA4	29.95	0.33	0.02	3.99	1.85	1.04	0.01	1.38	0.26	48.54	0.74	12.46	100.57	1.62	5.39	0.02	89.38	94.60
LWA5	35.83	0.08	0.03	1.02	1.96	0.25	0.00	0.87	0.19	47.43	0.13	12.75	100.54	1.32	7.85	0.00	92.49	97.42
LWA6	15.01	1.28	0.57	16.18	0.02	7.03	0.04	0.40	0.39	42.87	0.67	15.54	100.00	2.86	24.15	0.04	89.83	8993
LWA7	34.11	0.09	0.01	0.47	1.31	0.08	0.01	2.19	0.14	51.24	0.02	11.12	100.79	1.50	23.50	0.00	90.48	93.73
LWA8	35.68	0.06	0.01	0.87	1.24	0.27	0.01	1.18	0.13	49.23	0.05	12.68	101.41	1.38	17.40	0.00	93.50	96.64
LWA9	2.06	0.36	0.01	26.62	0.44	1.07	0.11	0.36	0.60	31.77	1.11	14.53	100.04	1.38	23.98	0.05	95.21	96.97
MEAN	29.82	0.33	0.08	7.81	1.24	1.28	0.03	0.82	0.29	44.99	0.52	13.52	100.73	1.51	15.02	0.02	92.59	96.29

The results of the geochemical analysis of clay fraction kaolin samples from Zebediela are summarized in Figure 4.49 and Table 4.18. The SiO_2 content ranged from 13.06 wt % (Sample Q4ZEB2) to 52.94 wt % (Sample Q4ZEB2) with an average of 42.93 wt %. Al_2O_3 content ranged between 24.20 wt % (Sample Q1ZEB1) and 35.74 wt % (Sample Q4ZEB4) with a mean value of 31.76 wt %. Iron content (Fe_2O_3) ranged from 0.31 wt % (Sample Q3ZEB2) to 23.17 wt % (Sample Q4ZEB2) with an average of 9.65 wt %. Samples were depleted in other transition elements (Mn, Ti and Cr), alkaline and alkaline earth elements (Na, K, Mg and Ca), however, samples; Q4ZEB1, Q4ZEB4 and Q4ZEB5, MgO was below detection limit. Loss on ignition ranged from 9.39 wt % (Sample Q3ZEB1) to 16.67 wt % (Sample Q4ZEB2) with a mean of 12.95 wt %. The SiO_2/Al_2O_3 ratio ranged from 1.11 to 2.14, Fe_2O_3/TiO_2 ratio ranged from 0.72 to 72.41 and TiO_2/Al_2O_3 ratio ranged from 0.01 to 0.06.

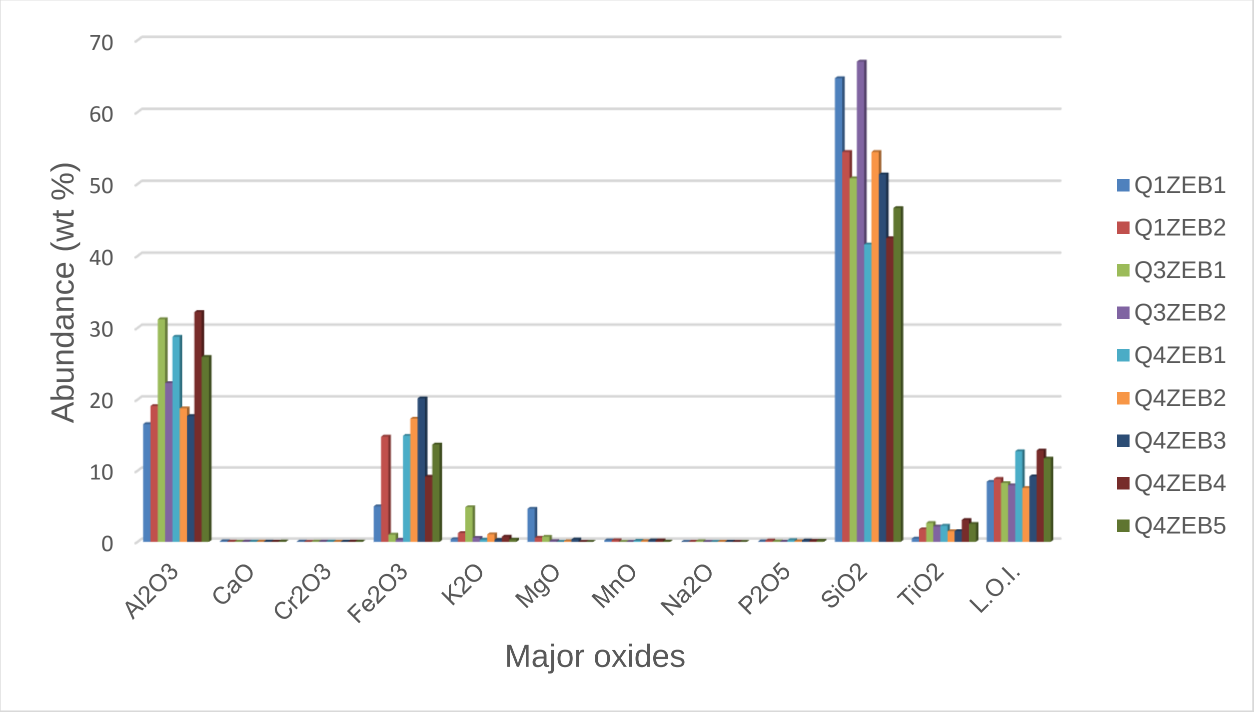

Figure 4.49: Major oxides abundance of clay fraction of Zebediela kaolin as determined by XRF.

Table 4.18: Chemical composition (in wt %) and weathering indices of clay fraction samples from Zebediela kaolin deposit

	Al_2O_3	**CaO**	**Cr_2O_3**	**Fe_2O_3**	**K_2O**	**MgO**	**MnO**	**Na_2O**	**P_2O_5**	**SiO_2**	**TiO_2**	**L.O.I.**	**Total**	**Si/Al**	**Fe/Ti**	**Ti/Al**	**CIA**	**CIW**
Q1ZEB1	24.2	0.03	0.04	5.33	0.3	6.85	0.04	0.17	0.28	51.73	0.39	11.38	100.74	2.14	13.67	0.02	97.98	99.18
Q1ZEB2	29.74	0.03	0	15.11	1.88	0.44	0.07	0.31	0.54	40.66	0.47	12.16	101.41	1.37	32.15	0.02	93.05	98.87
Q3ZEB1	34.77	0.01	0.05	1.03	5.14	0.7	0	0.16	0.15	47.69	0.42	9.39	99.51	1.37	2.45	0.01	86.75	99.51
Q3ZEB2	33.69	0.01	0.05	0.31	0.42	0.03	0	0.09	0.23	52.94	0.43	12.08	100.28	1.57	0.72	0.01	98.48	99.70
Q4ZEB1	31.95	0.01	0.03	17.54	0.43	bdl	0.03	0.15	0.51	36.11	0.61	13.90	101.27	1.13	28.75	0.02	98.19	99.50
Q4ZEB2	2.02	0.02	0.01	23.17	0.77	0.07	0.07	0.25	0.56	31.06	0.32	16.67	100.99	1.11	72.41	0.01	96.42	99.05
Q4ZEB3	32.54	0.01	0.01	12.67	0.41	0.39	0.04	0.25	0.41	40.31	0.41	13.40	100.85	1.24	30.90	0.01	97.98	99.21
Q4ZEB4	35.74	0.01	0.03	5.15	0.82	bdl	0.04	0.18	0.39	43	2.06	13.30	100.72	1.20	25.0	0.06	97.25	99.47
Q4ZEB5	35.19	0.01	0.02	6.55	0.38	bdl	0.01	0.27	0.46	42.9	1.29	14.30	101.38	1.22	5.08	0.04	98.16	99.21
MEAN	31.76	0.02	0.03	9.65	1.17	1.41	0.03	0.20	0.39	42.93	0.71	12.95	100.79	1.37	20.96	0.02	96.03	99.3

4.4.2 Trace elements

Trace and rare earth elements data of the bulk samples from Lwamondo kaolin deposit compared to chondrite of the upper continental crust values (UCC) are presented in Figures 4.50 - 4.51 and Tables 4.19 – 4.20. Sample LWA1 was enriched in Sc, V, Cr, Co, Ni, Cu, Y, Zr, Nb, Hf, Ta and depleted in all other trace elements. Sample LWA2 was enriched in Ni, Zr, Nb, Ba, Pb and depleted in other trace elements. LWA3 was enriched in in Cr, Ni and depleted in all other trace elements. Sample LWA4 was enriched in Ni, Sr, Zr, Ba, Pb, and Th and depleted in all other trace elements. Sample LWA5 was enriched in Cr, Ni, Ba and depleted in all other trace elements. Sample LWA6 was enriched in Sc, Cr, Co, Ni, Cu, Zn, Th and depleted in other trace elements. Sample LWA7 was depleted in all trace elements. Sample LWA8 was enriched in Ni, Zr, Hf, Pb and depleted in all other trace elements. Sample LWA9 was enriched in Sc, V, Co, Ni, Cu, Zn, Y, Zr, Nb, Hf, Ta and depleted in Cr, Rb, Sr, Cs, Ba, Pb, Th and U. The samples was enriched in LREE than HREE and Eu was positive.

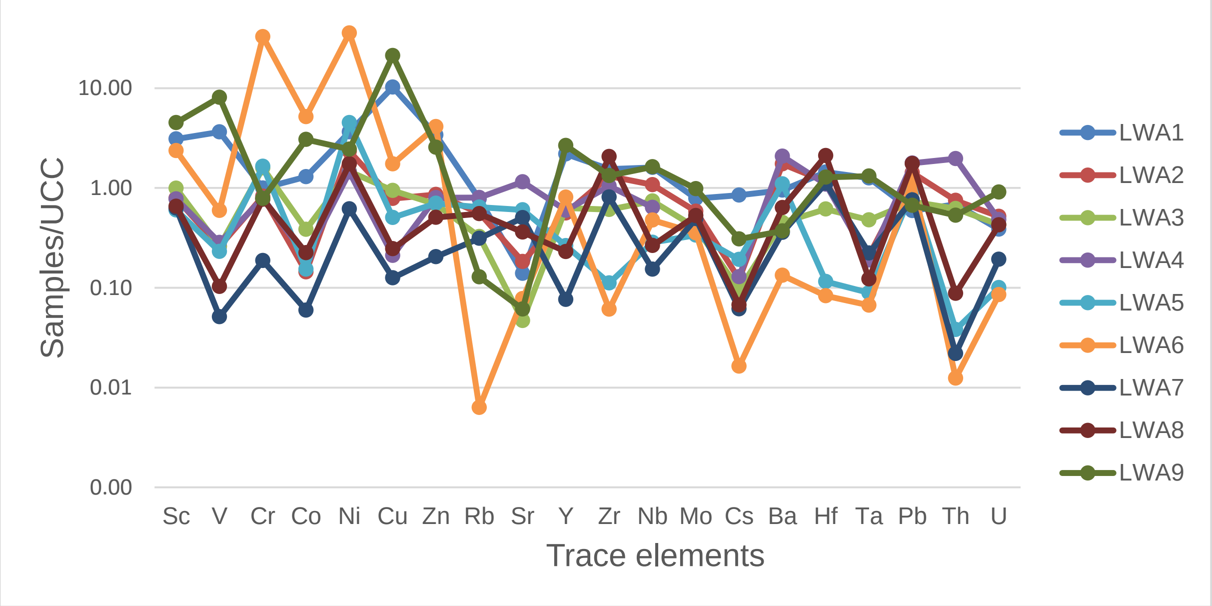

Figure 4.50: Trace elements plot of bulk samples of Lwamondo kaolin compared to UCC.

Table 4.19: Trace elements composition (in ppm) of bulk samples of Lwamondo kaolin

	LWA1	LWA2	LWA3	LWA4	LWA5	LWA6	LWA7	LWA8	LWA9	MEAN	UCC
Sc	43.25	11	13.88	10.86	8.4	33.02	8.78	9.14	63.1	22.38	14
V	353.05	25.1	25.25	27.5	22.4	57.66	4.96	9.98	782.75	145.41	97
Cr	91.45	75.75	145.95	72.6	151.3	3012	17.2	70.6	72.1	412.11	92
Co	22.34	2.49	6.65	3.56	2.65	89.5	1.03	3.87	52.9	20.55	17.3
Ni	170.75	109.5	68.65	67.7	211.5	1671	28.95	81.75	114.9	280.52	47
Cu	285.8	21.9	26.35	5.88	14.15	48.75	3.51	6.87	592.25	111.72	28
Zn	227.35	57.5	46	53.45	47	275.6	13.7	33.9	171.05	102.84	67
Rb	65.15	47.25	27.35	67.25	53.9	0.53	26.2	46.4	10.77	38.31	84
Sr	44.6	58.45	15	368.05	192.6	24.81	160.75	115.4	19.56	111.02	320
Y	45.97	11.76	13.23	12.5	5.54	16.95	1.6	4.82	55.81	18.69	21
Zr	298	253.4	117.25	201.75	21.5	11.74	156	397	256.2	190.32	193
Nb	19.23	12.92	8.85	7.63	3.42	5.7	1.84	3.17	19.5	9.14	12
Mo	0.86	0.64	0.44	BLD	0.37	0.39	0.54	0.58	1.08	0.61	1.1
Cs	4.15	0.6	0.47	0.63	0.94	0.08	0.3	0.33	1.51	1.00	4.9
Ba	591	1083	280.5	1294.5	684.5	83	223	395.5	230.7	540.63	624
Hf	7.62	6.12	3.25	5.77	0.61	0.44	5.9	11.15	6.79	5.29	5.3
Ta	1.13	0.19	0.43	0.17	0.08	0.06	0.2	0.11	1.18	0.39	0.9
Pb	10.05	24.1	12.38	30.1	15.65	20.24	12.86	29.8	11.35	18.50	17
Th	7.2	7.86	6.52	20.64	0.4	0.13	0.23	0.92	5.57	5.50	10.5
U	1.04	1.4	1.16	1.3	0.27	0.23	0.52	1.15	2.45	1.06	2.7
U/Th	0.14	0.18	0.18	0.06	0.68	1.77	2.26	1.25	0.44	0.19	
Ni/Co	7.64	43.98	10.32	19.02	79.81	18.67	28.11	21.12	2.17	13.65	
V/Cr	3.86	0.33	0.17	0.38	0.15	0.02	0.29	0.14	10.86	0.35	

Table 4.20: Rare earth elements (in ppm) of bulk samples of Lwamondo kaolin

	LWA1	LWA2	LWA3	LWA4	LWA5	LWA6	LWA7	LWA8	LWA9	UCC
La	32.57	48.05	50.65	68.85	5.06	18.56	5.14	4.14	28.13	31
Ce	44.61	73.8	70.75	123.5	6.09	2.58	8.61	26.3	62.65	63
Pr	7.8	10.41	10.28	15.37	1.1	4.01	0.82	0.99	7.71	7.1
Nd	33.75	39.5	38.5	55.3	3.31	16.7	2.12	2.51	33.8	27
Sm	7.53	5.05	6.52	10.1	0.83	3.69	0.51	0.74	9.23	4.7
Eu	2.36	1.45	1.7	1.75	0.49	0.95	0.38	0.39	2.51	1
Gd	8.12	4.32	3.66	6.58	0.88	3.07	0.38	0.74	9.66	4
Tb	1.27	0.49	0.5	0.65	0.16	0.53	0.1	0.15	1.59	0.7
Dy	8.7	2.17	2.25	2.91	0.81	3.17	0.31	0.71	10.6	3.9
Ho	1.8	0.5	0.42	0.41	0.15	0.63	0.11	0.17	2.24	83
Er	5.37	1.35	1.13	1.2	0.65	1.72	0.2	0.56	6.61	2.3
Tm	0.77	0.15	0.12	0.12	0.08	0.2	0.12	0.14	1.04	0.3
Yb	5.21	1.03	0.96	0.59	0.58	1.34	0.24	0.53	6.59	2
Lu	0.77	0.11	0.15	0.14	0.12	0.19	0.08	0.17	0.94	0.31

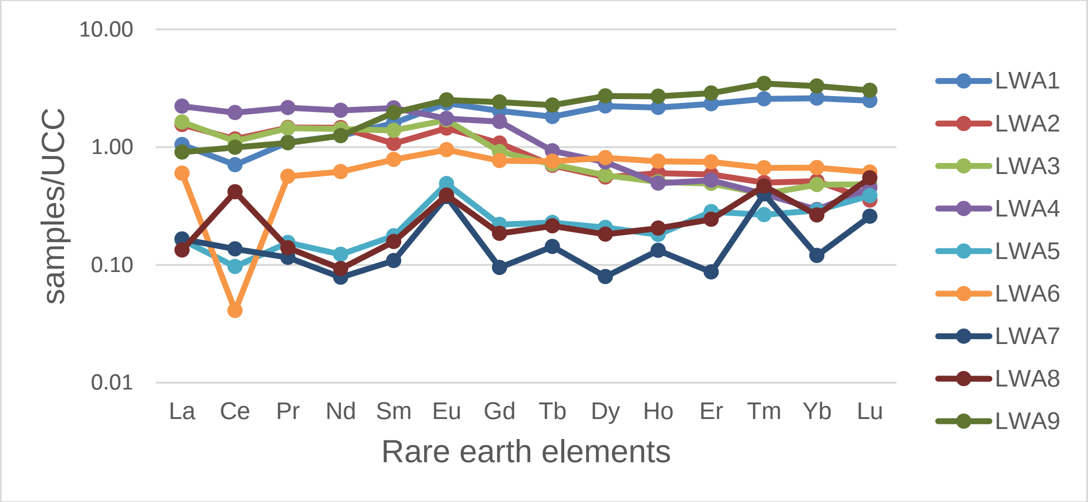

Figure 4.51: Rare earth elements plot of bulk samples of Lwamondo kaolin compared to UCC.

Trace and rare earth elements distribution in bulk samples of Zebediela kaolin deposit compared to chondrite of the upper continental crust (UCC) values are shown in Figures 4.52 - 4.53 and Tables 4.21 – 4.22. Sample Q1ZEB1 was enriched in Sc, Cr, Co, Ni, Cu, Zn, Cs and depleted in other trace elements. Sample Q1ZEB2 was enriched in Sc, V, Co, Cu, Zn, Y, Ba, Pb and depleted in other trace elements. Sample Q3ZEB1 was enriched in Sc, V, Cr, Cu, Rb, Y, Nb, U and depleted in other trace elements. Sample Q3ZEB2 was enriched in Sc, V, Cr, Ni, Y, U and depleted in other trace elements. Sample Q4ZEB1 was enriched in Sc, V, Cr, Co, Ni, Cu, Y, Nb, Mo, U and depleted in other trace elements. Sample Q4ZEB2 was enriched in Sc, V, Cr, Co, Ni, Cu, Zn, Y, Nb, Mo, U and depleted in other trace elements. Sample Q4ZEB3 was enriched in Sc, V, Cr, Co, Ni, Cu, Zn, Y and depleted in other trace elements. Sample Q4ZEB4 was enriched in Sc, V, Cr, Co, Ni, Cu, Zn, Y, Nb, Mo, U and depleted in other trace elements. Sample Q4ZEB5 was enriched in Sc, V, Cr, Ni, Cu, Y, Nb, and depleted in other trace elements. HREE was enriched than LREE. Eu anomaly was positive.

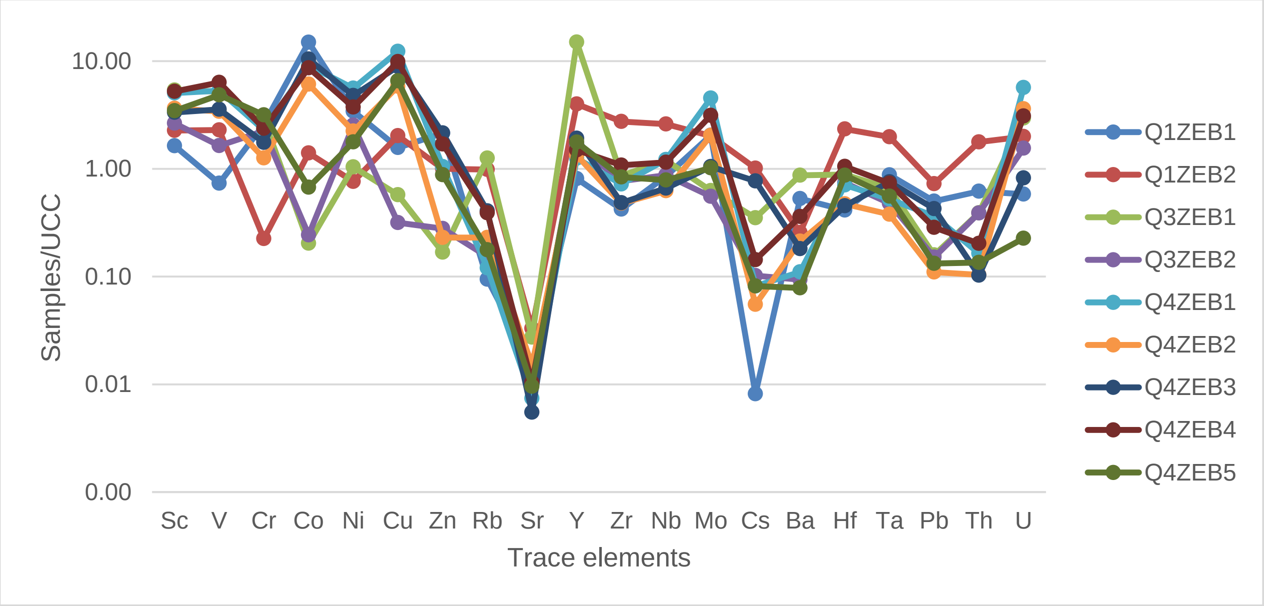

Figure 4.52: Trace elements plot of bulk samples of Zebediela kaolin compared to UCC.

Table 4.21: Trace elements composition (in ppm) of bulk samples from Zebediela kaolin.

	Q1ZEB1	Q1ZEB2	Q3ZEB1	Q3ZEB2	Q4ZEB1	Q4ZEB2	Q4ZEB3	Q4ZEB4	Q4ZEB5	MEAN	UCC
Sc	22.9	31.75	75.1	37	70.75	50.85	46.71	73.05	48.3	50.71	B
V	71.05	222.45	505.2	159.1	514.85	330.9	345.6	612.85	470.64	359.18	97
Cr	238.64	20.7	263.35	206.55	210.6	115.95	161.2	218	290.35	191.70	92
Co	258.25	24.21	3.52	4.2	157.15	105.5	180	149.45	11.64	99.32	17.3
Ni	160.9	35.8	48.85	119.2	262.75	105.25	224.75	175.4	83.4	135.14	47
Cu	44	56.8	16.05	8.86	343.8	163.35	248.95	275.8	183.1	148.97	28
Zn	143.5	67.15	11.25	18.65	70.15	15.4	143.6	113.75	58.9	71.37	67
Rb	7.91	82.7	105.6	12.85	10.11	19.32	34.12	32.75	14.84	35.58	84
Sr	4.84	10.55	8.75	3.62	2.37	4.84	1.76	3.32	3.06	4.79	320
Y	17.02	83.75	314.8	35.21	26.24	28.02	40.29	31.33	37.1	68.20	21
Zr	81.25	529.35	166.95	148.55	139.3	92.3	93.25	208.3	161.8	180.12	193
Nb	10.27	31.23	14.35	10.48	14.61	7.5	7.91	13.78	9.43	13.28	12
Mo	2.25	2.22	0.69	0.61	4.97	2.24	1.15	3.44	1.12	2.08	1.1
Cs	0.04	4.96	1.72	0.5	0.4	0.27	3.77	0.7	0.4	1.42	4.9
Ba	330.1	159.5	542.5	58.45	68.8	132.9	112.95	224.9	48.95	186.56	624
Hf	2.19	12.41	4.69	3.93	3.75	2.5	2.4	5.57	4.62	4.67	5.3
Ta	0.79	1.78	0.59	0.43	0.47	0.34	0.68	0.66	0.5	0.69	0.9
Pb	8.49	12.33	2.7	2.57	6.18	1.87	7.24	4.85	2.25	5.39	17
Th	6.5	18.63	4.09	4.08	1.72	1.09	1.08	2.13	1.42	4.53	10.5
U	1.57	5.37	7.97	4.19	15.32	9.73	2.22	8.33	0.61	6.15	2.7
U/Th	0.24	0.29	1.95	1.03	8.91	8.93	2.06	3.91	0.43	3.08	
Ni/Co	0.62	1.48	13.88	28.38	1.67	1.00	1.25	1.17	7.16	6.29	
V/Cr	0.30	10.75	1.92	0.77	2.44	2.85	2.14	2.81	1.62	2.85	

Table 4.22: Rare earth elements (in ppm) of bulk samples of Zebediela kaolin

	Q1ZEB1	Q1ZEB2	Q3ZEB1	Q3ZEB2	Q4ZEB1	Q4ZEB2	Q4ZEB3	Q4ZEB4	Q4ZEB5	UCC
La	29.15	68.5	10.85	12.81	7.34	9.22	15.83	11.19	12.59	31
Ce	48.2	116	35.63	64.95	60	15.4	65.15	52.6	6.2	63
Pr	6.49	17.7	5.62	6.15	2.47	3.25	5.34	3.8	3.96	7.1
Nd	26.65	72.6	31.05	27.85	11.9	17.05	24.5	17.45	19.91	27
Sm	0.34	14.6	21.05	7.84	3.78	6	6.62	4.53	4.95	4.7
Eu	1.12	3.56	5.26	1.38	1.16	0.98	1.97	1.4	1.77	1
Gd	3.86	13.5	53.05	6.83	4.06	5.87	6.95	4.96	6.37	4
Tb	0.6	2.16	9.31	1.09	0.77	0.88	1.1	0.84	0.99	0.7
Dy	3.57	14.7	53.6	6.36	5.17	5.29	7.44	5.7	6.66	3.9
Ho	0.66	3.03	9.76	1.32	1.02	1.03	1.42	1.23	1.31	83
Er	1.81	8.78	23.57	3.76	3.4	2.77	4.15	3.78	3.91	2.3
Tm	0.25	1.32	2.93	0.55	0.49	0.41	0.62	0.6	0.54	0.3
Yb	1.62	8.51	16.9	3.36	3.78	2.43	4.07	3.9	3.69	2
Lu	0.21	1.25	2.26	0.52	0.51	0.39	0.59	0.59	0.48	0.31

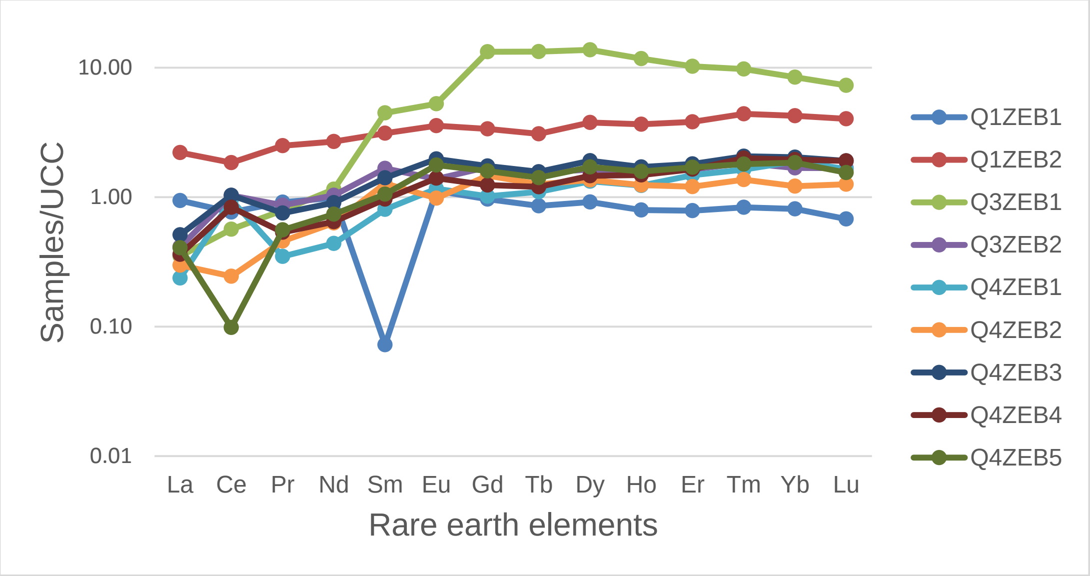

Figure 4.53: Rare earth elements plot of bulk samples of Zebediela kaolin compared to UCC.

Trace elements and rare earth elements distribution in silt fraction of Lwamondo kaolin compared to chondrite of the UCC values are presented in Figures 4.54 – 4.55 and Tables 4.23 – 4.24. Sample LWA1 was enriched in Sc, V, Co, Ni, Cu, Zn, Nb, Ta and depleted in all other trace elements. Sample LWA2 was enriched in Ni, Cu, Ba, Pb and depleted in all other trace elements. Sample LWA3 was enriched in Cr, Ni, Cu, Zr and depleted in all other trace elements. Sample LWA4 was enriched in Ni, Sr, Zr, Ba, Hf, Pb and depleted in other elements. Sample LWA5 was eniched in Cr, Ni, Ba, and depleted in all other elements. Sample LWA6 was enriched in Sc, Cr, Co, Ni, Cu, Zn and depleted all other trace elements. Sample LWA7 was enriched in Cr, Hf and depleted in all other elements. Sample LWA8 was enriched in Ni, Zr, Hf, Pb and depleted in all other trace elements. Sample LWA9 was enriched in Sc, V, Co, Zn, Y, Zr, Nb, Hf, Ta and depleted in all other trace elements. Eu anomaly was positive in all the samples except in Sample LWA4, whereas it was enriched in HREE than LREE.

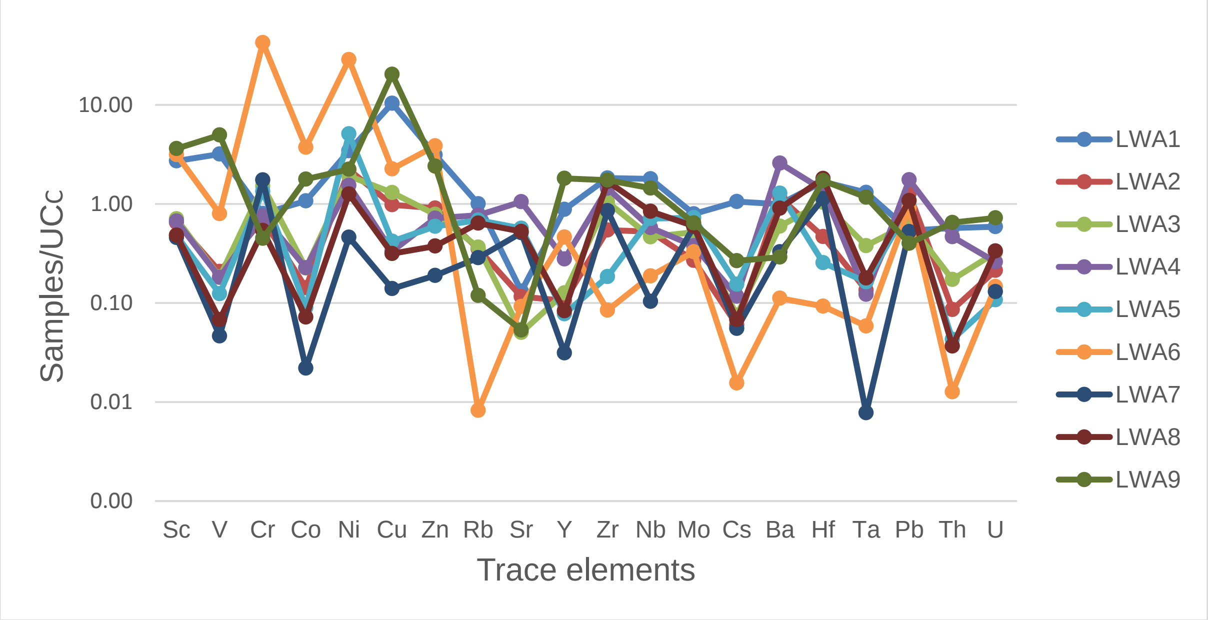

Figure 4.54: Trace elemnets plot of silt fraction of Lwamondo kaolin compared to UCC.

Table 4.23: Trace elements composition (in ppm) of silt fraction samples of Lwamondo kaolin

	LWA1	LWA2	LWA3	LWA4	LWA5	LWA6	LWA7	LWA8	LWA9	Mean	UCC
Sc	38	9.08	9.885	9.37	6.685	43.9	6.4	6.755	50.55	20.07	14
V	308.6	20.1	17.75	17.56	11.98	77.2	4.5	6.56	480.5	104.97	97
Cr	73.4	64.45	139.4	69.3	123	3892	160	49.5	41.25	512.48	92
Co	18.51	2.46	3.9	3.905	1.55	64.3	0.38	1.245	30.7	14.11	17.3
Ni	161	104	89.95	72.1	238.5	1343.5	21.6	58.9	104.9	243.83	47
Cu	289.4	27.35	36.3	9.3	11.75	63.1	3.9	8.8	567.6	113.06	28
Zn	209.5	60.6	52.5	47.9	39.6	258.15	12.65	25.15	160.7	96.31	67
Rb	84.15	29.45	30.7	64.45	57.45	0.69	24	53.6	9.965	39.38	84
Sr	41.95	37	16.1	336.6	181.05	29.34	163.3	168.25	17	110.07	320
Y	18.45	2.215	2.645	5.83	1.625	9.685	0.655	1.745	37.99	8.98	21
Zr	351.2	105.1	200.9	276.5	35.5	16.245	164.3	325	334.8	201.06	193
Nb	21.44	6.295	5.56	6.905	8.525	2.245	1.24	10.08	17.3	8.84	12
Mo	0.87	0.295	0.57	0.415	0.795	0.36	0.65	0.655	0.705	0.59	1.1
Cs	5.17	0.294	0.37	0.57	0.755	0.076	0.27	0.332	1.305	1.02	4.9
Ba	619	721	371.5	1605	797	69.55	204.5	563	181	570.17	624
Hf	8.86	2.48	5.49	7.33	1.35	0.49	5.97	9.53	9.11	5.62	5.3
Ta	1.17	0.121	0.34	0.109	0.15	0.05	0.007	0.16	1.05	0.35	0.9
Pb	9.13	21.6	10.8	29.7	15.9	15.37	8.9	18.35	6.78	15.17	17
Th	5.99	0.9	1.81	4.88	0.45	0.133	bdl	0.385	6.79	2.37	10.5
U	1.59	0.58	0.87	0.7	0.29	0.3955	0.35	0.9	1.945	0.85	2.7
U/Th	0.26	0.64	0.48	0.14	0.64	2.97	bdl	2.34	0.29	0.86	
Ni/Co	8.70	42.28	23.06	18.46	153.87	20.89	56.84	47.31	3.42	41.65	
V/Cr	4.20	0.31	0.13	0.25	0.10	0.02	0.03	0.13	11.65	1.87	

Table 4.24: Rare earth elements (in ppm) of silt fraction samples of Lwamondo kaolin

	LWA1	LWA2	LWA3	LWA4	LWA5	LWA6	LWA7	LWA8	LWA9	UCC
La	8.39	3.01	7.61	20.36	2.235	6.67	2.27	1.775	14.31	31
Ce	17.13	6.175	21.15	38.65	4.095	1.27	4.745	10.32	20.945	63
Pr	2.235	0.915	1.665	5.195	0.502	1.865	0.395	0.364	3.835	7.1
Nd	9.66	3.245	5.93	19	1.55	7.555	1.04	1.26	17.9	27
Sm	2.74	0.655	1.355	3.805	0.495	2.205	0.51	0.225	4.32	4.7
Eu	0.9	0.187	0.37	0.845	0.348	0.554	0.255	0.313	1.31	1
Gd	2.695	0.635	0.9	2.555	0.4	1.845	bdl	0.26	4.905	4
Tb	0.543	0.09	0.136	0.288	0.07	0.374	bdl	0.062	0.9955	0.7
Dy	4.01	0.45	0.455	1.37	0.337	2.39	0.17	0.275	6.885	3.9
Ho	0.856	0.09	0.101	0.209	0.126	0.469	0.013	0.124	1.56	83
Er	2.775	0.3	0.315	0.495	0.315	1.19	0.08	0.27	5.215	2.3
Tm	0.436	0.032	0.072	0.077	0.084	0.184	bdl	0.127	0.853	0.3
Yb	3.315	0.365	0.34	0.405	0.33	1.21	0.05	0.44	5.56	2
Lu	0.509	0.031	0.032	0.051	0.092	0.163	0.016	0.092	0.9125	0.31

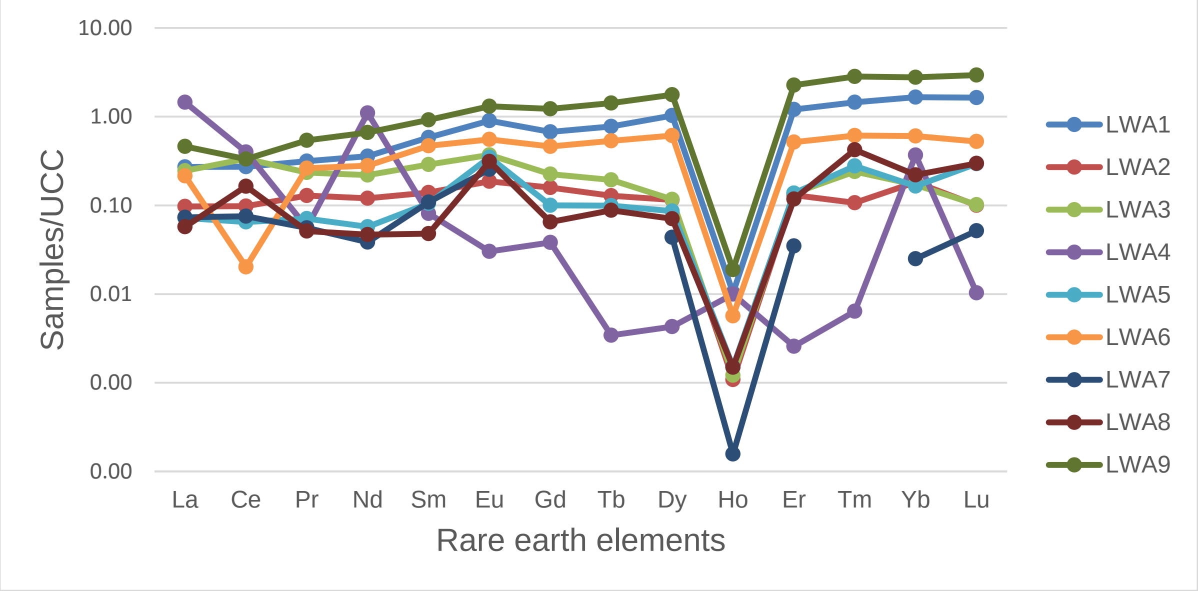

Figure 4.55: Rare earth elements plot of silt fraction of Lwamondo kaolin compared to UCC.

Trace and Rare earth elements distribution in a silt fraction of Zebediela kaolin compared to chondrite of the UCC values are shown in Figures 4.56 – 4.57 and Tables 4.25 – 4.26. Sample Q1ZEB1 was enriched in Cr, Co, Cu, Ta, Pb, U and depleted all other trace elements. Sample Q1ZEB2 was enriched in Sc, V, Co, Cu, Rb, Y, Zr, Nb, Mo, Hf, Ta, Pb, Th, U and depleted in all other trace elements. Sample Q3ZEB1 was enriched in Sc, V, Cr, Rb, Y, Hf, Pb, U and depleted in all other trace elements. Sample Q3ZEB2 was enriched in Sc, V, Cr, Ni, Nb, Hf, Pb, U and depleted in all other trace elements. Sample Q4ZEB1 was enriched in Sc, V, Vr, Cr, Co, Ni, Cu, Mo, Hf, Pb, U and depleted in all other trace elements. Sample Q4ZEB2 was enriched in Sc, V, Co, Ni, Cu, Hf, Pb, U and depleted in all other trace elements. Sample Q4ZEB3 was enriched in Sc, V, Cr, Co, Ni, Cu, Zn, Mo, Hf, Pb, U and depleted in all other trace elements. Sample Q4ZEB4 was enriched in Sc, V, Cr, Co, Ni, Cu, Zn, Y, Zr, Nb, Mo, Hf, Pb, Th, U and depleted in all other trace elements. Sample Q4ZEB5 was enriched in Sc, V, Cr, Ni, Cu, Y, Nb, Mo, Hf, Pb, U and depleted in all other trace elements. Eu anomaly was positite in all samples except in sample Q3ZEB1, Q3ZEB2 and Q4ZEB2. HREE was enriched than LREE.

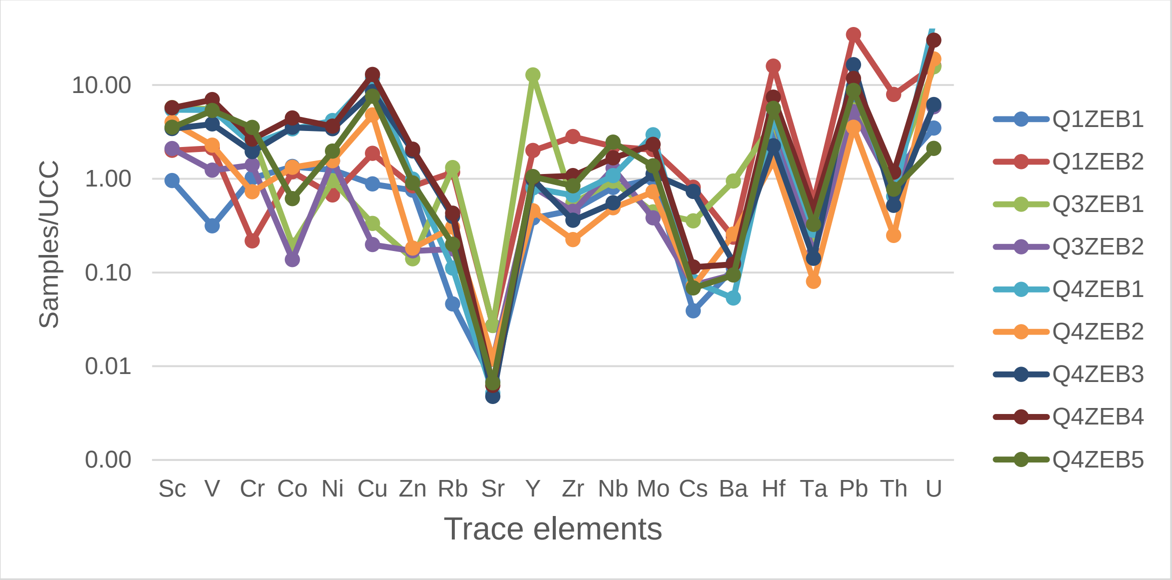

Figure 4.56: Trace elements plot of silt fraction of Zebediela kaolin compared to UCC.

Table 4.25: Trace elements composition (in ppm) of silt fraction samples of Zebediela kaolin

	Q1ZEB1	Q1ZEB2	Q3ZEB1	Q3ZEB2	Q4ZEB1	Q4ZEB2	Q4ZEB3	Q4ZEB4	Q4ZEB5	Mean	UCC
Sc	13.34	28.07	80	29.3	76.5	55.75	47.8	79.75	49.4	51.10	14
V	30.35	205.2	537.7	119.25	524.9	219.9	371.7	676.35	517.7	355.89	97
Cr	93.7	19.9	265.3	128.7	214.2	66.6	178.5	243.05	323.3	170.36	92
Co	23.3	20.46	3.385	2.365	58.7	22.805	61.1	76.75	10.57	31.05	17.3
Ni	58.45	31.4	44.6	72.55	195.75	72.8	160.2	170.2	92.45	99.82	47
Cu	24.55	52.1	9.285	5.535	331.6	133.45	237.8	360.95	212	151.92	28
Zn	50.5	56.05	9.35	11.35	66	12.15	132.2	137.8	60.25	59.52	67
Rb	3.86	98.35	109.9	14.95	9.325	25.5	33.15	35.9	16.76	38.63	84
Sr	2.19	8.685	8.655	3.78	1.655	3.805	1.515	1.99	2.115	3.82	320
Y	7.98	41.92	268.2	17.19	16.7	9.53	20.67	21.72	22.06	47.33	21
Zr	89.25	541.2	106.3	86.35	128.5	43.05	69.4	207.5	161.6	159.24	193
Nb	9.65	26.57	11.27	15.455	12.925	5.865	6.625	19.98	29.32	15.29	12
Mo	1.09	2.235	0.485	0.42	3.22	0.795	1.23	2.55	1.505	1.50	1.1
Cs	0.19	3.955	1.735	0.36	0.3935	0.348	3.57	0.558	0.334	1.27	4.9
Ba	68.85	147.9	587	59.25	33.2	159.6	79.35	76.4	58.4	141.11	624
Hf	2.455	12.67	3.17	3.745	3.64	1.235	1.785	5.92	4.48	4.34	5.3
Ta	0.54	1.31	0.583	0.365	0.645	0.184	0.325	1.092	0.746	0.64	0.9
Pb	1.915	11.32	1.785	1.705	3.19	1.165	5.415	3.865	2.87	3.69	17
Th	2.575	17.57	2.335	1.77	1.435	0.5485	1.15	2.595	1.71	3.52	10.5
U	1.105	5.135	4.98	1.865	15.36	6.045	1.97	9.57	0.673	5.19	2.7
U/Th	0.43	0.29	2.13	1.05	10.70	11.02	1.71	3.69	0.39	3.49	
Ni/Co	2.51	1.53	13.18	30.68	3.33	3.19	2.62	2.22	8.75	7.56	
V/Cr	0.32	10.31	2.03	0.93	2.45	3.30	2.08	2.78	1.60	2.87	

Table 4.26: Rare earth elements composition (in ppm) of silt fraction of Zebediela kaolin

	Q1ZEB1	Q1ZEB2	Q3ZEB1	Q3ZEB2	Q4ZEB1	Q4ZEB2	Q4ZEB3	Q4ZEB4	Q4ZEB5	UCC
La	8.505	17.54	4.155	4.8	2.39	1.26	5.65	2.41	3.455	31
Ce	14.92	82.65	15.01	21.1	24.95	4.405	24.61	22.52	4.9	63
Pr	1.675	4.16	2.285	2	0.909	0.553	2.465	0.985	1.1485	7.1
Nd	7.405	16.51	14.4	8.85	4.48	3.06	11.68	5.145	6.53	27
Sm	1.56	4.075	16.35	2.515	2.025	1.4	3.41	1.81	2.375	4.7
Eu	0.345	1.305	3.74	0.435	0.728	0.202	1.26	0.77	0.9	1
Gd	1.145	5.05	41.05	3.015	2.485	1.545	3.755	3.015	2.885	4
Tb	0.269	0.869	7.25	0.473	0.507	0.29	0.729	0.601	0.5835	0.7
Dy	1.385	6.805	46.15	2.75	3.68	1.76	4.535	4.675	4.2	3.9
Ho	0.334	1.58	8.12	0.65	0.786	0.365	0.919	1.028	0.948	83
Er	0.895	5.005	20.75	1.77	2.425	0.955	2.775	3.155	2.805	2.3
Tm	0.176	0.779	2.56	0.245	0.407	0.108	0.412	0.536	0.3955	0.3
Yb	1.015	5.72	14.49	1.73	2.785	0.89	2.805	3.76	2.815	2
Lu	0.171	0.85	1.865	0.279	0.424	0.136	0.384	0.556	0.3655	0.31

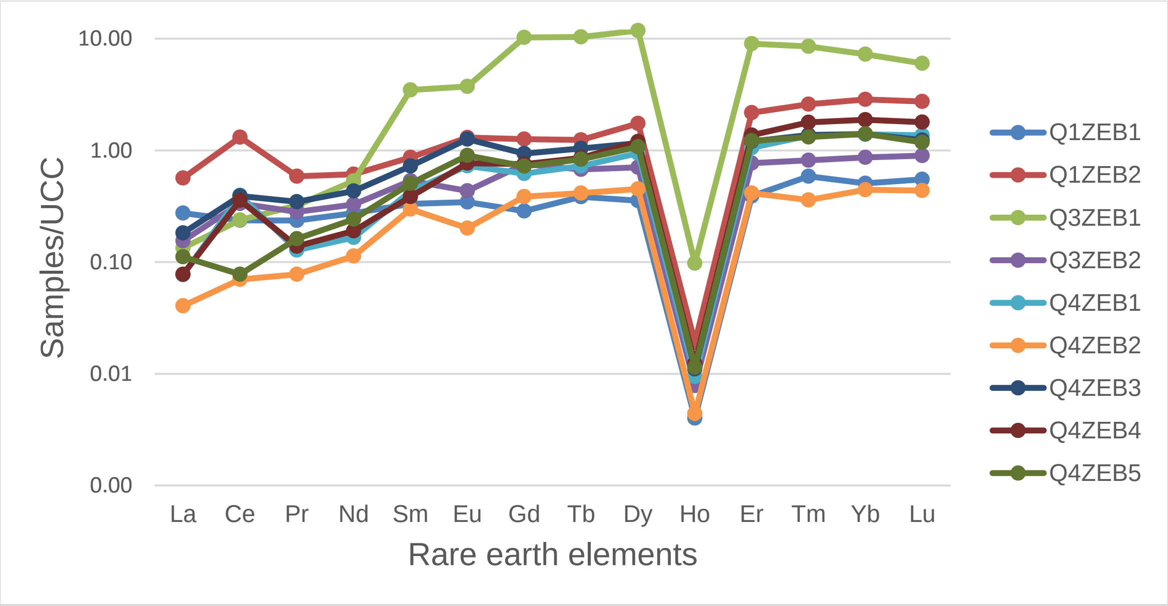

Figure 4.57: Rare earth elements plot of silt fraction of Zebediela kaolin compared to UCC.

Trace and rare earth elements distribution in clay fraction samples of Lwamondo kaolin deposit compared to chondrites UCC values are shown in Figures 4.58 – 4.59 and Tables 4.27 – 4.28. Sample LWA1 was enriched in Sc, V, Ni, Cu, Rb and depleted in Cr, Co, Zn, Sr, Y, Zr, Nb, Mo, Cs, B, Hf, Ta, Pb, Th and U. Sample LWA2 was enriched in Ni, Pb and depleted in Sc, V, Cu, Rb, Cr, Co, Zn, Sr, Y, Zr, Nb, Mo, Cs, B, Hf, Ta, Th and U. Sample LWA3 was enriched in Cr, Ni, Cu, Nb and depleted in Sc, V, Co, Zn, Sr, Y, Zr, Mo, Cs, B, Hf, Ta, Pb, Th and U. Sample LWA4 was enriched in Cr, Ni, Nb, Pb and depleted in Sc, V, Cu, Co, Zn, Sr, Y, Zr, Mo, Cs, B, Hf, Ta, Th and U. Sample LWA5 was enriched in Cr, Ni and depleted in Sc, V, Cr, Co, Cu, Zn, Rb, Sr, Y, Zr, Nb, Mo, Cs, B, Hf, Ta, Pb, Th and U. Sample LWA6 was enriched in Sc, Cr, Co, Ni, Cu, Zn and depleted in V, Sr, Y, Zr, Nb, Mo, Cs, B, Hf, Ta, Pb, Th and U. Sample LWA7 was enriched in Ni, Cr, Pb and depleted in Sc, V, Cu, Rb, Co, Zn, Sr, Y, Zr, Nb, Mo, Cs, B, Hf, Ta, Th and U. Sample LWA8 was enriched in Sc, V, Co, Ni, Cu, Zn, Y, Zr, Nb, Mo, Hf, Ta and depleted in Cr, Rb, Sr,Cs, Ba, Pb, Th and U. Sample LWA9 was enriched in Ni and depleted in Sc, V, Cu, Rb, Cr, Co, Zn, Sr, Y, Zr, Nb, Mo, Cs, B, Hf, Ta, Pb, Th and U. LREE was enriched than HREE and Eu anomaly was positive.

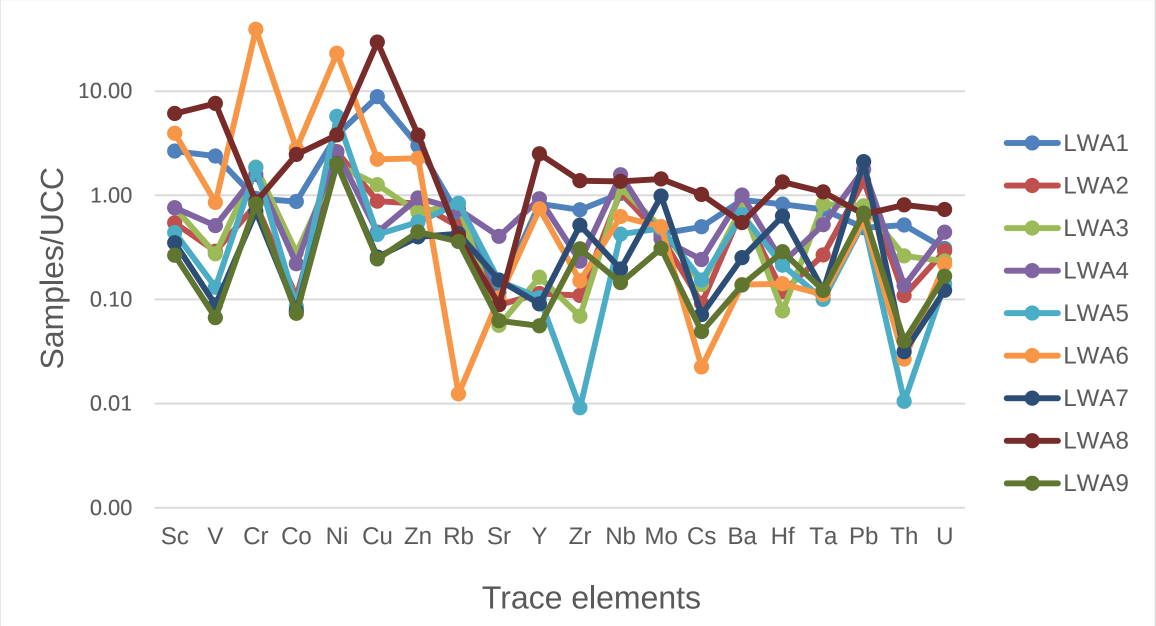

Figure 4.58: Trace elements plots of clay size fraction of Lwamondo kaolin samples compared to UCC.

Table 4.27: Trace elements composition (in ppm) in clay fraction of Lwamondo kaolin

	LWA1	LWA2	LWA3	LWA4	LWA5	LWA6	LWA7	LWA8	LWA9	Mean	UCC
Sc	37.2	7.62	10.57	10.62	6.14	54.95	4.89	85.45	3.71	24.57	14
V	230.4	28.1	26.55	49.55	12.7	82.65	8.59	738	6.47	131.45	97
Cr	85.6	74.95	171.55	145.45	168.9	3604	64.15	79.6	76.05	496.69	92
Co	15.07	1.83	4.85	3.8	1.48	48.55	1.35	42.7	1.27	13.43	17.3
Ni	178.75	123.25	92.95	122	269	1082.5	94.6	178.6	94	248.41	47
Cu	247	24.55	35.35	12.35	11.75	62.1	7.14	828	6.85	137.23	28
Zn	200.55	55.85	46	63.1	37.15	151.65	26.65	253	29.8	95.97	67
Rb	53.7	41.9	68.7	61.6	70.45	1.04	35.9	33.5	30.25	44.12	84
Sr	37.24	28.3	18.01	128.65	47.95	33.15	49	28.5	20	43.42	320
Y	17.41	2.39	3.43	19.4	2.18	15.53	1.9	52.4	1.17	12.87	21
Zr	140.05	21.1	13.32	44.98	1.76	29.04	99.5	266.35	59	75.01	193
Nb	12.45	12.97	14.17	18.87	5.07	7.5	2.35	16.3	1.74	10.16	12
Mo	0.47	0.44	0.54	0.42	0.53	0.55	1.08	1.58	0.34	0.66	1.1
Cs	2.44	0.45	0.68	1.18	0.75	0.11	0.35	4.98	0.24	1.24	4.9
Ba	562.5	450	484.5	626	404.5	86.55	157	340.5	85.75	355.26	624
Hf	4.35	0.63	0.41	1.2	1.13	0.75	3.35	7.1	1.52	2.27	5.3
Ta	0.66	0.24	0.74	0.47	0.09	0.1	0.11	0.97	0.11	0.39	0.9
Pb	8.29	23.35	13.45	30.13	9.4	9.79	35.75	11.15	11.43	16.97	17
Th	5.43	1.14	2.75	1.42	0.11	0.28	0.33	8.5	0.42	2.26	10.5
U	0.83	0.79	0.63	1.19	0.38	0.59	0.33	1.97	0.45	0.80	2.7
U/Th	0.15	0.69	0.23	0.84	3.45	2.11	1.00	0.23	1.07	1.09	
Ni/Co	11.86	67.35	19.16	32.11	181.76	22.30	70.07	4.18	74.02	53.65	
V/Cr	2.69	0.37	0.15	0.34	0.08	0.02	0.13	9.27	0.09	1.46	

Table 4.28: Rare earth elements composition (in ppm) of clay fraction of Lwamondo kaolin

	LWA1	LWA2	LWA3	LWA4	LWA5	LWA6	LWA7	LWA8	LWA9	UCC
La	10.14	3.43	6.61	38.55	2.73	12.43	12.89	30.79	2.52	31
Ce	16.87	4.41	19.13	14.33	3.83	1.46	15.51	30.13	8.82	63
Pr	2.55	0.76	1.5	10.55	0.48	3.54	1.53	8.14	0.42	7.1
Nd	10.81	3.08	6.41	42.35	1.71	13.67	4.51	36.4	1.17	27
Sm	2.66	0.77	1.45	10.2	0.31	3.65	0.83	9.35	0.22	4.7
Eu	0.92	0.27	0.5	2.74	0.09	1.04	0.6	2.43	0.15	1
Gd	2.7	0.61	0.8	6.64	0.45	3.17	0.46	8.6	0.21	4
Tb	0.5	0.07	0.11	0.84	0.1	0.53	0.09	1.52	0.09	0.7
Dy	3.69	0.53	0.57	4.33	0.54	3.49	0.4	10.4	0.23	3.9
Ho	0.75	0.09	0.19	0.69	0.15	0.62	0.13	2.19	0.08	83
Er	2.5	0.32	0.35	1.75	0.25	1.81	0.28	6.62	0.22	2.3
Tm	0.37	0.04	0.05	0.2	0.08	0.27	0.09	1.03	0.05	0.3
Yb	2.5	0.32	0.37	1.16	0.26	1.66	0.29	7.11	0.16	2
Lu	0.38	0.06	0.06	0.16	0.11	0.21	0.09	1.04	0.04	0.31

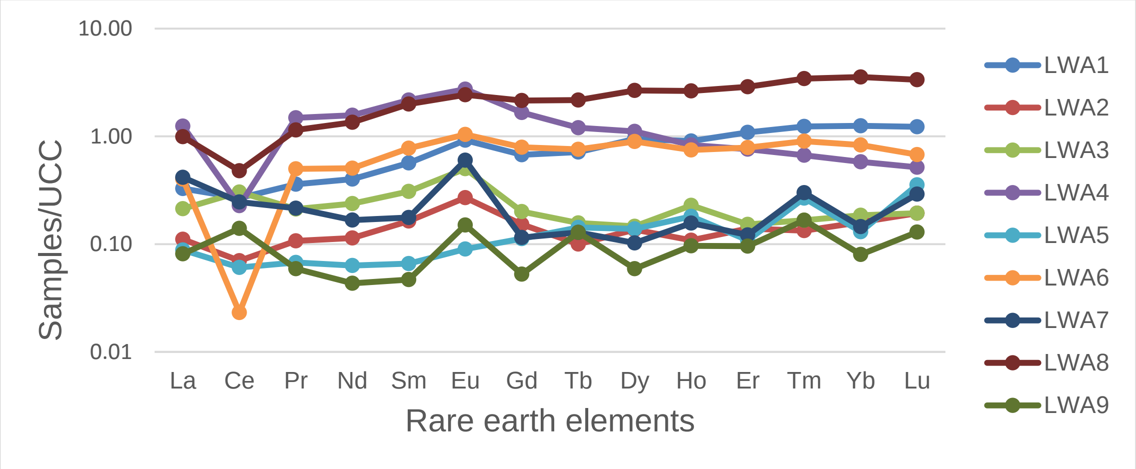

Figure 4.59: Rare earth elements plot of clay size fraction of Lwamondo kaolin samples compared to UCC.

Trace and rare earth elements distribution in clay fraction samples of Zebediela kaolin deposit chondrite UCC values are shown in Figures 4.60 – 4.61 and Tables 4.29 – 4.30. Sample Q1ZEB1 was enriched in Sc, Cr, Co, Ni, Cu, Zn, Mo and depleted in V, Rb, Sr, Y, Zr, Nb, Cs, Ba, Hf, Ta, Pb, Th, U. Sample Q1ZEB2 was enriched in Sc, V, Cu, Rb, Y, Mo, Th and depleted in Cr, Co, Ni, Zn, Sr, Zr, Nb, Cs, Ba, Hf, Ta, Pb, U. Sample Q3ZEB1 was enriched in Sc, V, Cr, Ni, Rb, Y, Hf, U and depleted in Co, Cu, Zn, Mo, Sr, Zr, Nb, Cs, Ba, Ta, Pb, Th. Sample Q3ZEB2 was enriched in Sc, V, Cr, Ni, Y, Zr, Hf, U and depleted in Co, Cu, Zn, Mo, Sr, Nb, Cs, Ba, Ta, Pb, Th. Sample Q4ZEB1 was enriched in Sc, V, Cr, Co, Ni, Cu, Zn, Mo, U and depleted Rb, Sr, Y, Zr, Nb, Cs, Ba, Hf, Ta, Pb, Th . Sample Q4ZEB2 was enriched in Sc, V, Cr, Co, Ni, Cu, Mo, U and depleted in Zn, Rb, Sr, Y, Zr, Nb, Cs, Ba, Hf, Ta, Pb, Th. Sample Q4ZEB3 was enriched in Sc, V, Cr, Co, Ni, Cu, Zn, Cs and depleted in Mo, Rb, Sr, Y, Zr, Nb, Ba, Hf, Ta, Pb, Th, U. Sample Q4ZEB4 was enriched in Sc, V, Cr, Co, Ni, Cu, Zr, U and depleted in Mo, Zn, Rb, r, Y, Nb, Cs, Ba, Hf, Ta, Pb, Th. Sample Q4ZEB5 was enriched in Sc, V, Cr, Ni, Cu and depleted in Zn, Rb, Sr, Y, Zr, Nb, Cs, Ba, Hf, Ta, Pb, Th, U. HREE was enriched than LREE and Eu anomaly was positive in all samples.

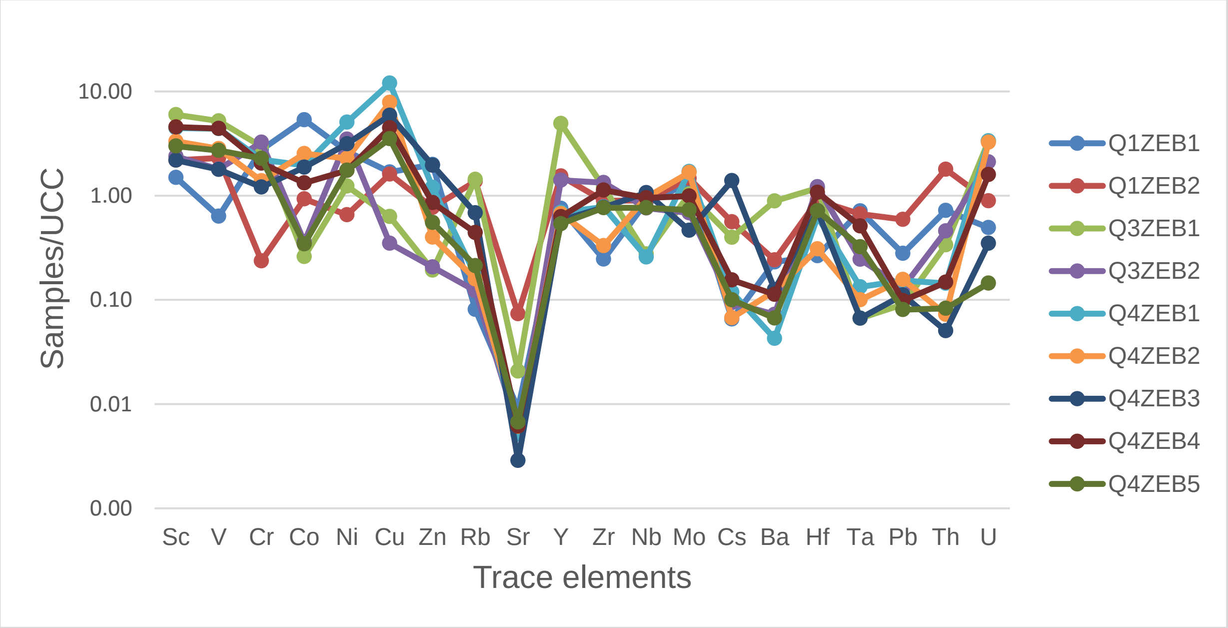

Figure 4.60: Trace elements plot of clay size fraction of Zebediela kaolin samples compared to UCC.

Table 4.29: Trace elements composition (in ppm) of clay size fraction of Zebediela kaolin

	Q1ZEB1	Q1ZEB2	Q3ZEB1	Q3ZEB2	Q4ZEB1	Q4ZEB2	Q4ZEB3	Q4ZEB4	Q4ZEB5	Mean	UCC
Sc	20.88	30.6	83.6	33.3	62.25	46.4	30.59	63.7	41.75	45.90	14
V	61.45	223	504	174.15	425.95	273.55	172.55	427.95	263.55	280.68	97
Cr	253.6	21.7	272.8	299	203.85	127.2	110.85	188.05	209.4	187.38	92
Co	92.25	16.08	4.5	6.23	33.77	43.75	32.4	22.89	5.95	28.65	17.3
Ni	124.8	30.75	57.9	163.3	237.9	106.8	147.2	81.85	82.2	114.74	47
Cu	47.15	45.05	17.65	9.75	335.5	219.15	165	125.25	98.45	118.11	28
Zn	133.35	51.65	12.9	13.85	80.2	26.75	130.75	57.35	36.95	60.42	67
Rb	6.8	115.2	120.05	10.28	14.55	13.28	57.3	37.15	17.84	43.61	84
Sr	2.9	23.54	6.62	1.81	1.65	1.95	0.92	1.96	2.15	4.83	320
Y	15.85	32.29	103.2	29.45	14.5	14.06	12.2	13.15	11.27	27.33	21
Zr	47.35	172.2	232.85	257	150.2	63.8	148.4	217.55	147.55	159.66	193
Nb	10.46	10.78	3.3	9.12	3.08	11.56	12.79	11.44	9.16	9.08	12
Mo	1.44	1.61	1.14	0.75	1.87	1.83	0.51	1.09	0.8	1.23	1.1
Cs	0.32	2.74	1.95	0.46	0.58	0.33	6.82	0.76	0.49	1.61	4.9
Ba	143.55	150.65	554	45.15	26.55	75.8	78.3	70.4	41.7	131.79	624
Hf	1.4	4.76	6.27	6.45	3.32	1.63	3.79	5.68	3.79	4.12	5.3
Ta	0.64	0.6	0.06	0.22	0.12	0.09	0.06	0.46	0.29	0.28	0.9
Pb	4.74	10.05	1.54	2.23	2.61	2.66	1.89	1.67	1.37	3.20	17
Th	7.57	18.74	3.53	4.8	1.51	0.76	0.53	1.55	0.87	4.43	10.5
U	1.33	2.4	9.01	5.67	9.02	8.76	0.94	4.29	0.39	4.65	2.7
U/Th	0.18	0.13	2.55	1.18	5.97	11.53	1.77	2.77	0.45	2.95	
Ni/Co	1.35	1.91	12.87	26.21	7.04	2.44	4.54	3.58	13.82	8.20	
V/Cr	0.24	10.28	1.85	0.58	2.09	2.15	1.56	2.28	1.26	2.48	

Table 4.30: Rare earth elements composition (in ppm) of clay size fraction of Zebediela kaolin

	Q1ZEB1	Q1ZEB2	Q3ZEB1	Q3ZEB2	Q4ZEB1	Q4ZEB2	Q4ZEB3	Q4ZEB4	Q4ZEB5	UCC
La	33.11	51.03	4.43	9.55	2.16	2.56	3.51	1.99	2.46	31
Ce	41.1	129	18.6	64.3	12.53	20.95	25.41	7.44	2.03	63
Pr	7.86	10.1	2.7	5.63	0.82	1.01	1.17	0.66	0.75	7.1
Nd	31.1	36.55	13.55	24.9	3.85	5.93	5.78	2.84	3.79	27
Sm	6.4	6.93	6.95	6.05	1.31	2.01	2.06	1.09	0.97	4.7
Eu	1.37	1.54	1.69	1.29	0.59	0.49	0.62	0.38	0.45	1
Gd	4.8	6.18	16	5.21	2.05	2.49	1.72	1.39	1.44	4
Tb	0.67	0.95	2.82	0.79	0.42	0.38	0.34	0.29	0.25	0.7
Dy	3.9	6.13	17	5.12	2.69	2.93	2.39	2.54	1.93	3.9
Ho	0.56	1.23	3.3	1.04	0.62	0.48	0.48	0.56	0.43	83
Er	1.72	3.85	7.95	2.95	2.02	1.27	1.32	1.68	1.29	2.3
Tm	0.21	0.52	1.17	0.52	0.34	0.21	0.26	0.3	0.23	0.3
Yb	1.34	3.47	6.4	3.5	2.79	1.23	1.78	2.51	1.78	2
Lu	0.19	0.55	0.93	0.5	0.42	0.18	0.35	0.4	0.28	0.31

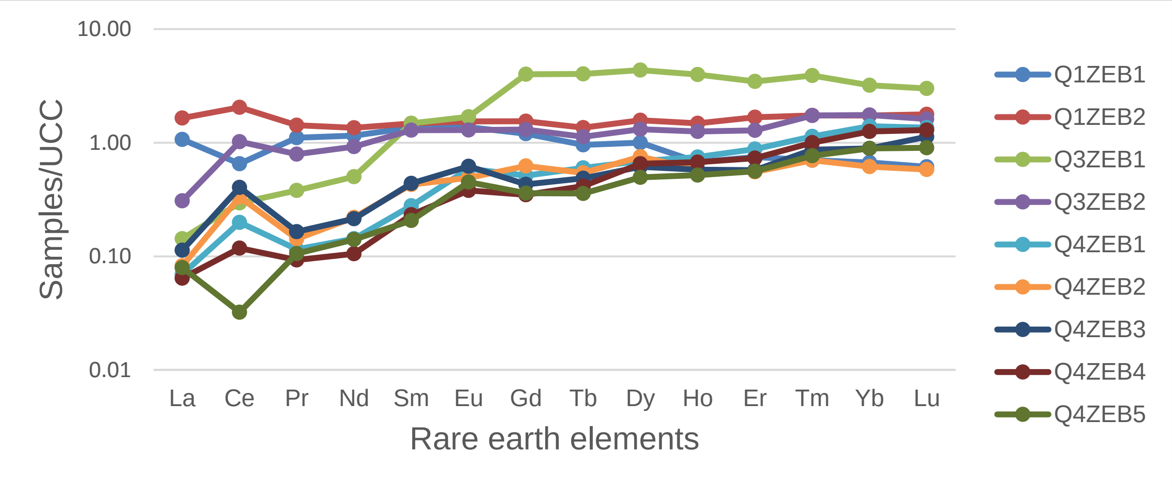

Figure 4.61: Rare earth elements plot of clay size fraction of Zebediela kaolin samples compared to UCC.

4.5 Stable isotopes

The stable isotopes values for kaolinite from Lwamondo were as follows: $\delta^{18}O$ values ranges from 17.4 to 19.2‰ and the δD ratios ranging from -54 to 84‰, with the mean $\delta^{18}O$ and δD values being 18.6‰ and -65.3‰, respectively (Table 4.31). The mean water content was 10.63%.

The stable isotopes values for kaolinite from Zebediela were as follows: $\delta^{18}O$ values ranges from 16.7 to +17.7‰ with the mean value of 16. 7‰ and the δD was ranging from -61 to-68 ‰ with a mean value of -65.3‰ (Table 4.31). The mean water content was 10.86%. The $\delta^{18}O$ and δD was plotted on a diagram below (Figure 4.63) where most of the samples was in a supergene field, the right hand of the supergene/hypogene line whereas one of the sample was in the hypogene field in the left of the supergene-hypogene line.

Table 4.31: H_2O yields, $\delta^{18}O$ and δD values of analysed clay fractions of Lwamondo and Zebediela kaolins

Sample No	**$\delta^{18}O$**	**δD**	**H_2O (%)**
LWA1	17.4	-84	8.48
LWA2	19.2	-58	12.05
LWA9	19.1	-54	11.37
Mean	18.6	-65	10.63
Q1 ZEB2	16.7	-68	10.16
Q3 ZEB2	17.7	-61	11.67
Q4 ZEB2	15.6	-63	10.74
Mean	16.7	-64	10.86

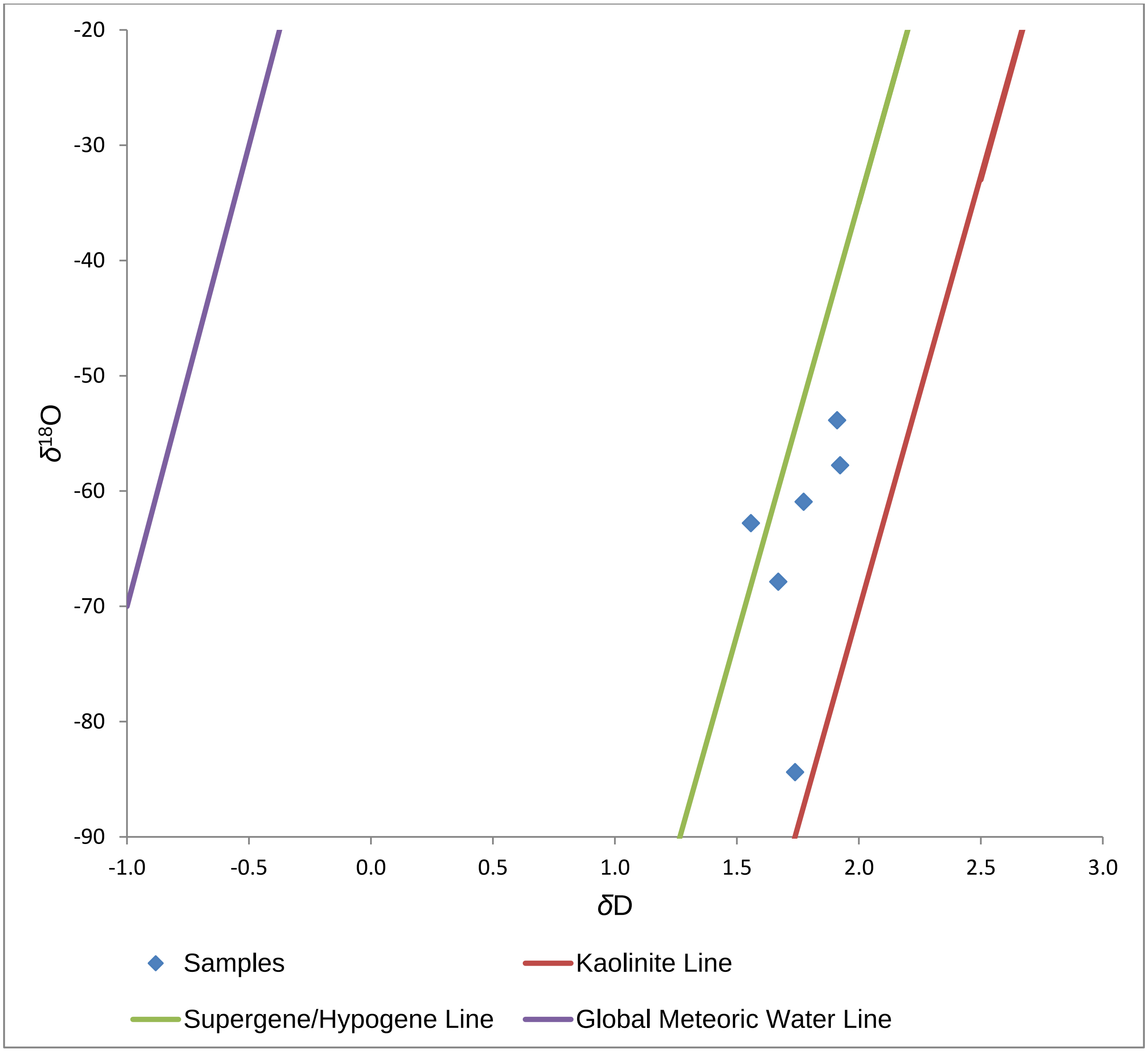

Figure 4.62: δ^{18}O versus δD diagram for <2 µm fraction of the Lwamondo and Zebediela kaolins. The meteoric water, supergene/hypogene and kaolinite weathering lines (KWL) are given for reference.

CHAPTER FIVE

DISCUSSION

5.1 Field observations

Lwamondo kaolin deposit is located in the Sibasa Formation and there are basalts which rest on the basements of the Hoot Plaats Gneiss and Granite. Observed kaolin deposit was ferruginous and whitish. Geology of the area infer that kaolin may have been formed from basalt and clastic sediments. The surrounding country rocks are believed to have provided the primary minerals for kaolinitisation.

The field observation from Zebediela kaolin is similar to the one reported by Ekosse (2008b; 2010) of the Kgwakgwe kaolins of Botswana.The thickness of the beds in Zebediela kaolin deposit shows different colours (pinkish, yellowing and reddish) and layerings which depict beds of sedimentary nature. The kaolin deposit is penetrated by reddish veins which probably mark groundwater passages. Surrounding country rocks are arkose, mudstone and shale which are considered to have provided primary minerals for kaolinitisation.

5.2 Physico-chemistry

Colour could be indicative of the mineral assemblages or presence of organic materials in clay (Diko and Ekosse, 2014). The common colour shades employed to infer the mineralogy are: white-cream attributable to the presence of kaolin, yellowish-brownish colour attributed to the presence of goethite, red to reddish brown colour were indicative of hematite and greyish colour suggesting the presence of organic matter (Ekosse, 2005).

Particle size and texture show that the smaller the particles the more the clay minerals. More wt % of finer particles indicate weathering in Lwamondo and Zebediela kaolin deposits; similar observations reported by Ngole *et al*.(2007).

The pH of clay minerals ranges from 2.64 to 5.48. The pH values of the Lwamondo and Zebediela kaolin samples were < 6.5 which showed that it does not contain dissolved salts (Murray, 1986; Ngole *et al.*, 2007; Ekosse 2000) and the EC values were between 10 and 50 µS/cm indicating that samples do not contain soluble salts (Ekosse, 2000) (Figure 5.1).The high acidity indicates an ongoing weathering process and intense hydrolysis processes (Manju *et al.*, 2001, Santos *et al.*, 2014). Acidic condition is of importance for the migration of several chemical elements in the course of kaolinitisation (Nyakairu *et al.*, 2001).

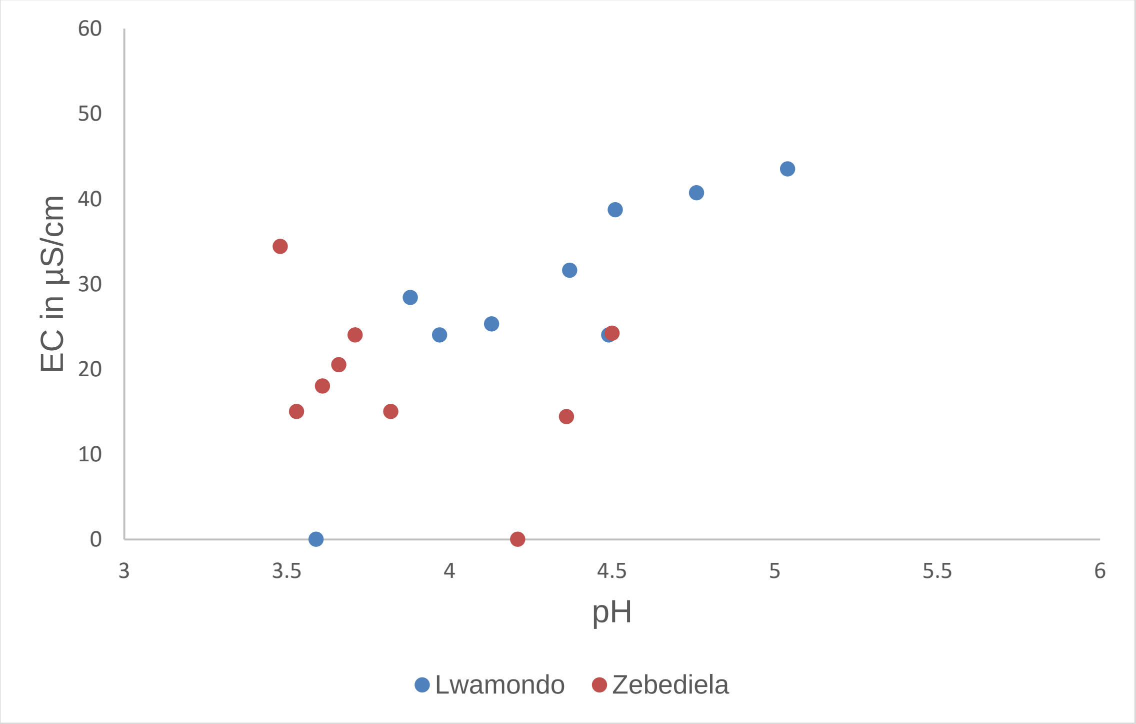

Figure 5.1: Relationship between pH and EC of samples from the Lwamondo and Zebedeila kaolins.

5.3 Mineralogy

Feldspars and muscovite are the most common parent materials for kaolin formation (Diko and Ekosse, 2012). Weathering of rocks rich in feldspar and micas forms kaolinite or smectite. The parent minerals are enriched in the bulk and silt samples but depleted in the clay fractions due to weathering/kaolinitisation. Parent minerals such as plagioclase, muscovite, microcline and quartz decrease as secondary minerals (kaolinite, smectite and goethite) increase (Figure 5.2-5.13). Quartz content reduces as the particle size becomes finer whereas clay minerals increase (Figures 5.5-5.6 and 5.10-5.11).

Clay minerals and goethite presence in the samples reflect the humid conditions. The abundance of kaolinite in the sediments is due to the decomposition of feldspars and other rocks during geologic times (Ngon Ngon *et al.*, 2012). The high content of kaolinite in the studied kaolin samples suggest the high degree of weathering of aluminium-rich rocks in the humid tropical environment (Mousa *et al.*, 2014). The transformation of K-feldspars into kaolin is indicated in equation 5.1 below:

$2KAlSi_3O_8 + 3H_2O \rightarrow 3Al_2Si_2O_5(OH)_4 + 4SiO_2 + 2K(OH)$------------------------------ Eqn 5.1
K-feldspar kaolinite

Out of nine samples from Lwamondo plagioclase occurred in four and its wt% in samples LWA4 and LWA5 decreased noticeably from bulk to clay fraction and in samples LWA7 and LWA8 decresed in bulk and clay fraction (Figure 5.2); which is indicative of alteration of the primary mineral to secondary mineral, Albite alteration is shown in Equation 5.2 and that of Anorthite is given in Equation 5.3 below.

$2NaAlSi_8O_8 + 3H_2O + 2CO_2 \rightarrow Al_2SiO_5(OH)_4 + H_4SiO_4 + 2NaHCO_3$--------------Eqn 5.2
Albite Water Carbon dioxide Kaolinite silicic acid Sodium bicarbonate

$CaAl_2Si_2O_8 + 3H_2O \quad 2CO_2 \rightarrow Al_2Si_2O_5(OH)_4 + Ca(HCO_3)_2$-------------------Eqn 5.3
Anorthite water Carbon dioxide Kaolinite Sodium bicarbonate

Muscovite was identified in seven of the samples from Lwamondo, and in only three of the samples was it present in the bulk, silt and clay fractions (Figure 5.3). In three of the samples, its presence was in the clay fraction only. This observation could be substantiated by physical weathering of the muscovite particles to smaller sizes and its possible alteration, as shown in equation 5.4.

$2KAlSi_3O_8 + 2H^+ + 9H_2O \rightarrow Al_2Si_2O_5(OH)_4 + 2K^+ + 4H_4SiO_4$-------------------------Eqn 5.4

Muscovite   Kaolinite

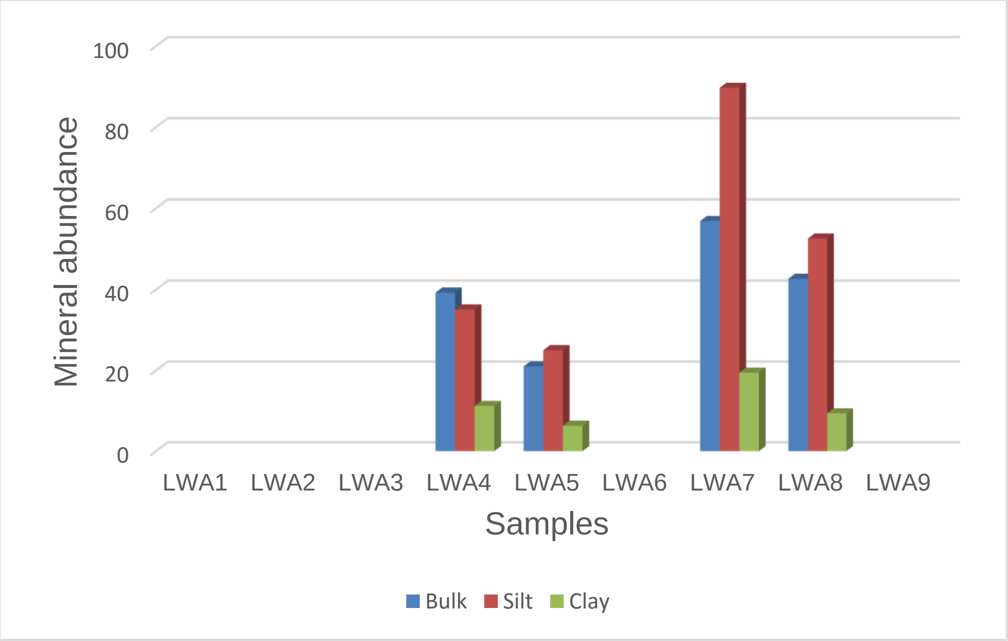

Figure 5.2: Plagioglase content in Lwamondo bulk, silt and clay kaolin samples.

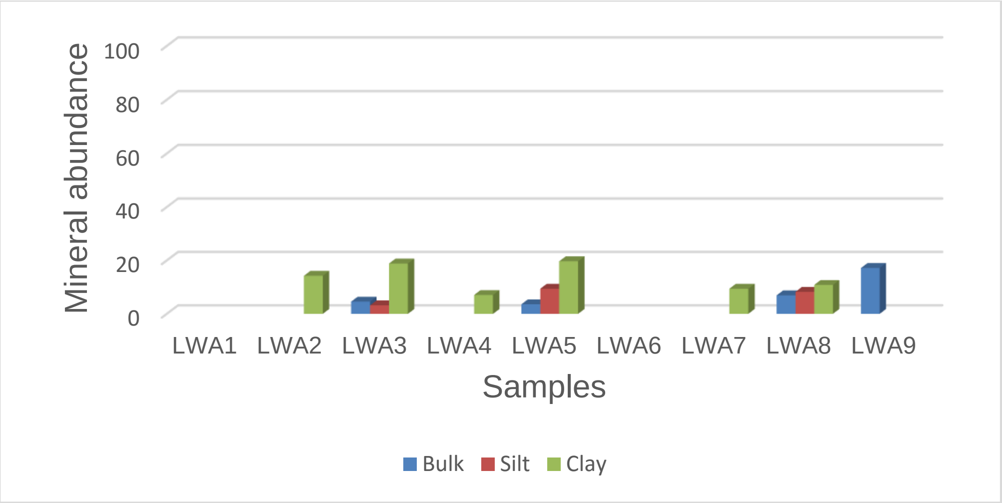

Figure 5.3: Muscovite content in Lwamondo bulk, silt and clay kaolin samples.

The reduction in presence of microcline from bulk to clay size fraction of Lwamondo kaolins was reflective of alteration of the primary minerals to kaolinite (Figure 5.4), as already depicted in the alteration of feldspars in Equation 5.1. The equation below is an endothermic reaction wherein an increase in temperature favours the conversion of microcline to kaolinite

$2KAlSi_3O_3 + 9H_2O\ H^+ \rightarrow Al_2Si_2O_5(OH)_4 + 2K^+ + 4H_4SiO_4$----------------------------Eqn 5.5
Microcline Kaolinite

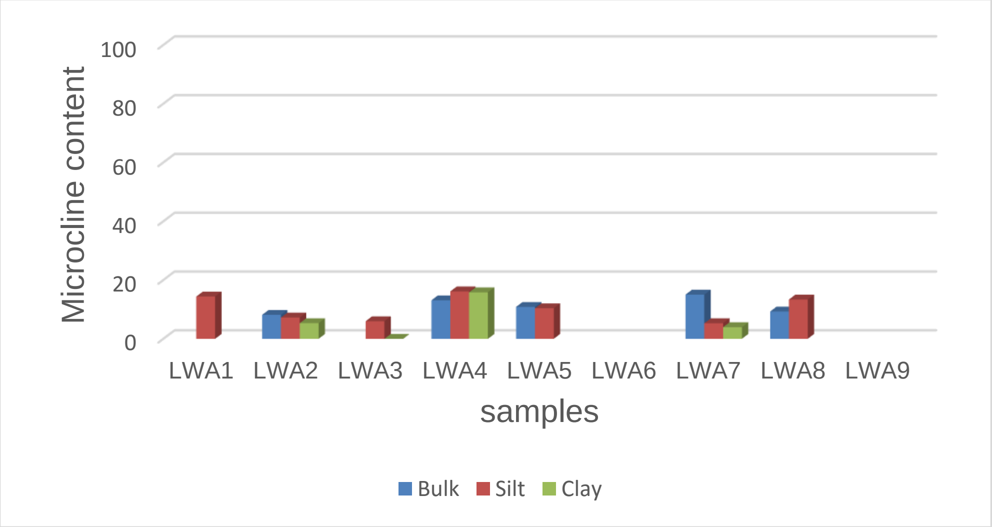

Figure 5.4: Microcline content in Lwamondo bulk, silt and clay kaolin samples.

Quartz was present in all the Lwamondo samples though in small quantities (Figure 5.5). In none of the samples was it present in all the three size fractions of bulk, silt and clay. Lwamondo kaolins contained more kaolinite in the clay fraction than the bulk and silt fractions (Figure 5.6). Increase in kaolinite content in the kaolins could be associated to the alteration of the plagioclase, muscovite and microcline to secondary minerals particularly kaolinite and smectite. Smectite in nine samples decreased in quantity from bulk to clay fraction (Figure 5.7). Goethite occurred in only two samples and more of it in silt and clay fraction than in the bulk (Figure 5.8).

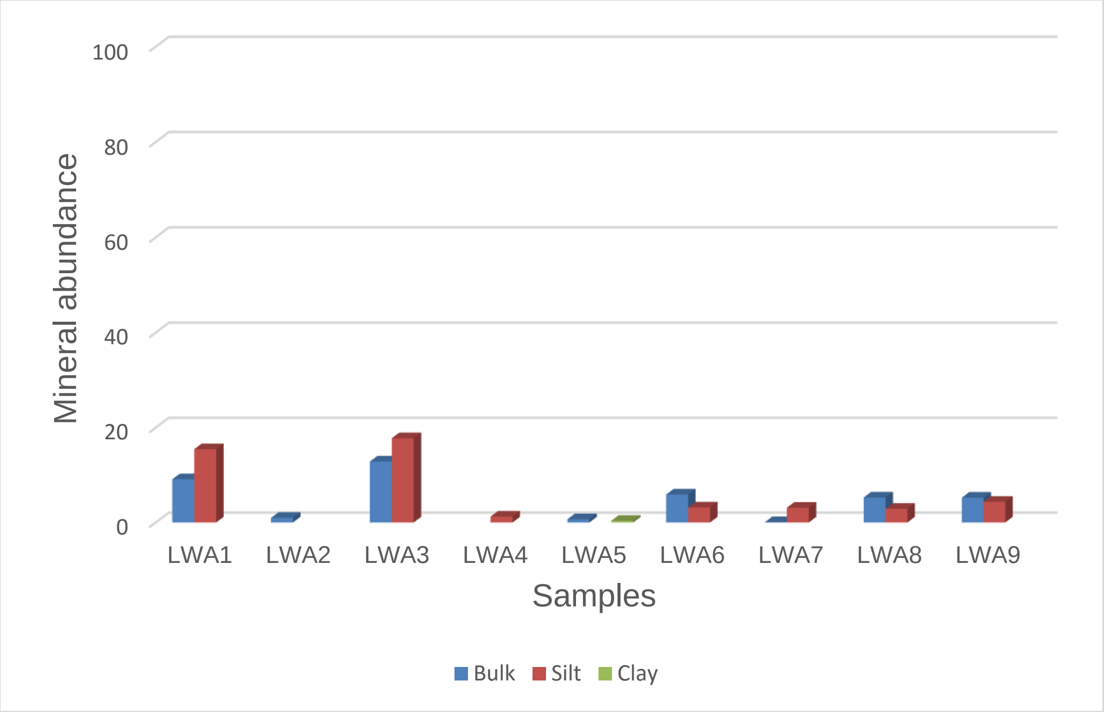

Figure 5.5: Quartz content in Lwamondo bulk, silt and clay kaolin samples.

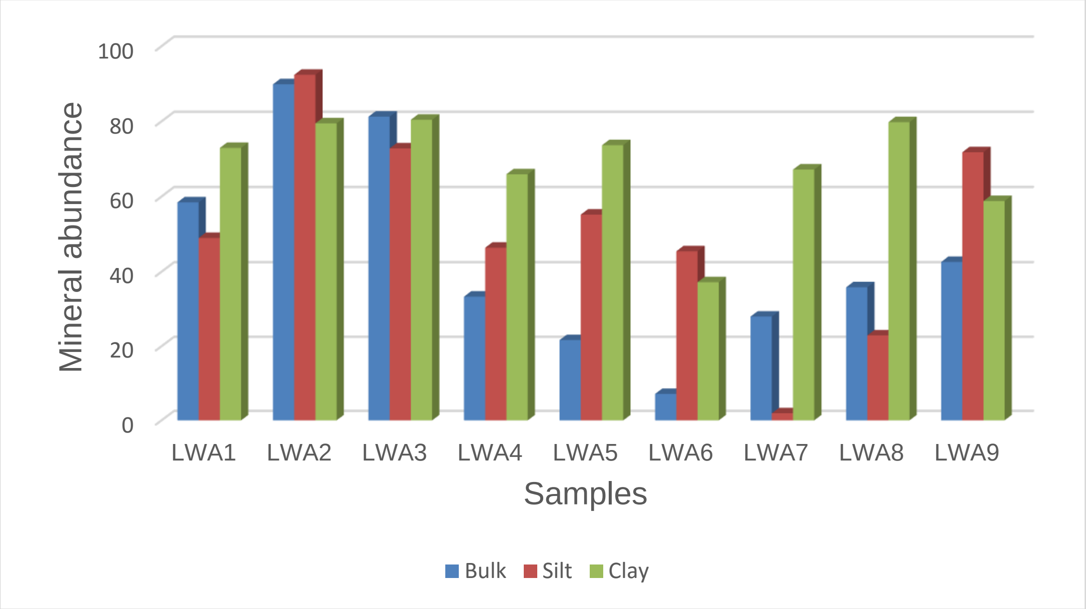

Figure 5.6: Kaolinite content in Lwamondo bulk, silt and clay fraction kaolin samples.

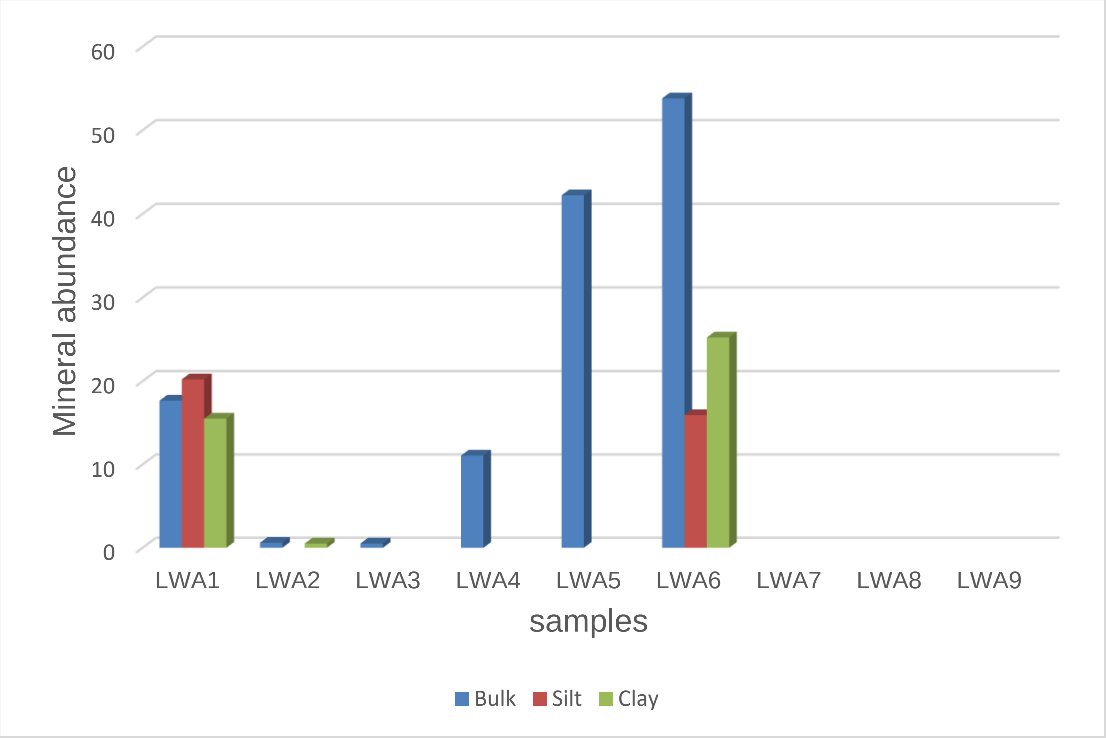

Figure 5.7: Smectite content in Lwamondo bulk, silt and clay kaolin samples.

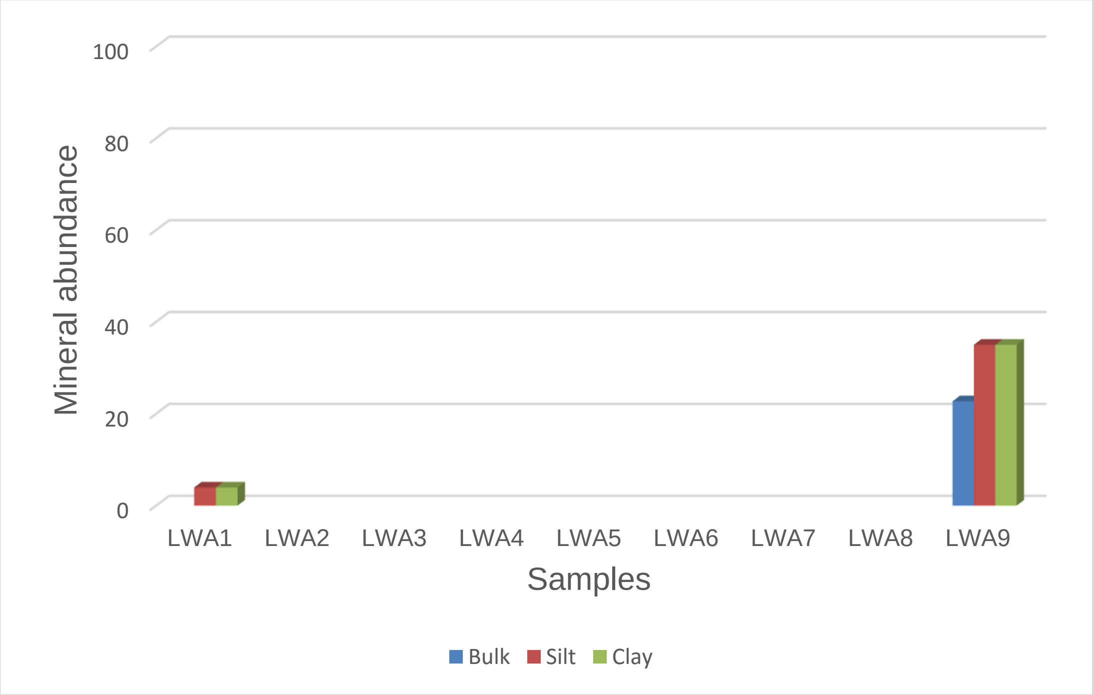

Figure 5.8: Goethite content in Lwamondo bulk, silt and clay kaolin samples.

Muscovite was identified in six of the nine samples from Zebediela kaolins, and in only five samples was it present in bulk, silt and clay size fractions (Figure 5.9). Its presence in bulk, silt and clay fractions could be substantiated as physical weathering of muscovite particles in smaller sizes and its possible alteration (Equation 5.4).

Quartz was present in all the Zebediela kaolin samples (Figure 5.10). In five samples its presence was in bulk, silt and clay fractions which could be due to its resistance during weathering. Zebediela kaolins contained high kaolinite content in clay size fraction than in bulk and silt fraction (Figure 5.11). Increase in kaolinite content in the kaolins could be associated to the alteration of the muscovite to secondary minerals particularly kaolinite and smectite.

Out of nine samples from Zebediela, smectite occurred in two samples, in silt and clay size fractions. Goethite was present in seven samples from the Zebediela kaolins (Figure 5.13). Its presence was high in bulk and silt fractions.

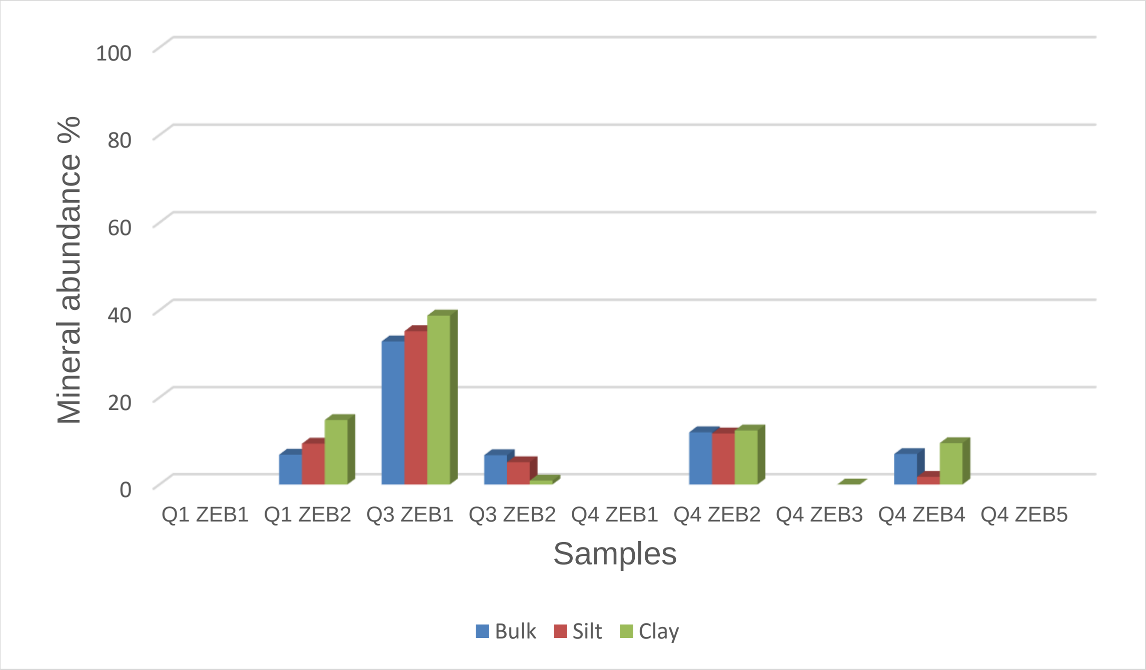

Figure 5.9: Muscovite content in Zebediela bulk, silt and clay kaolin samples.

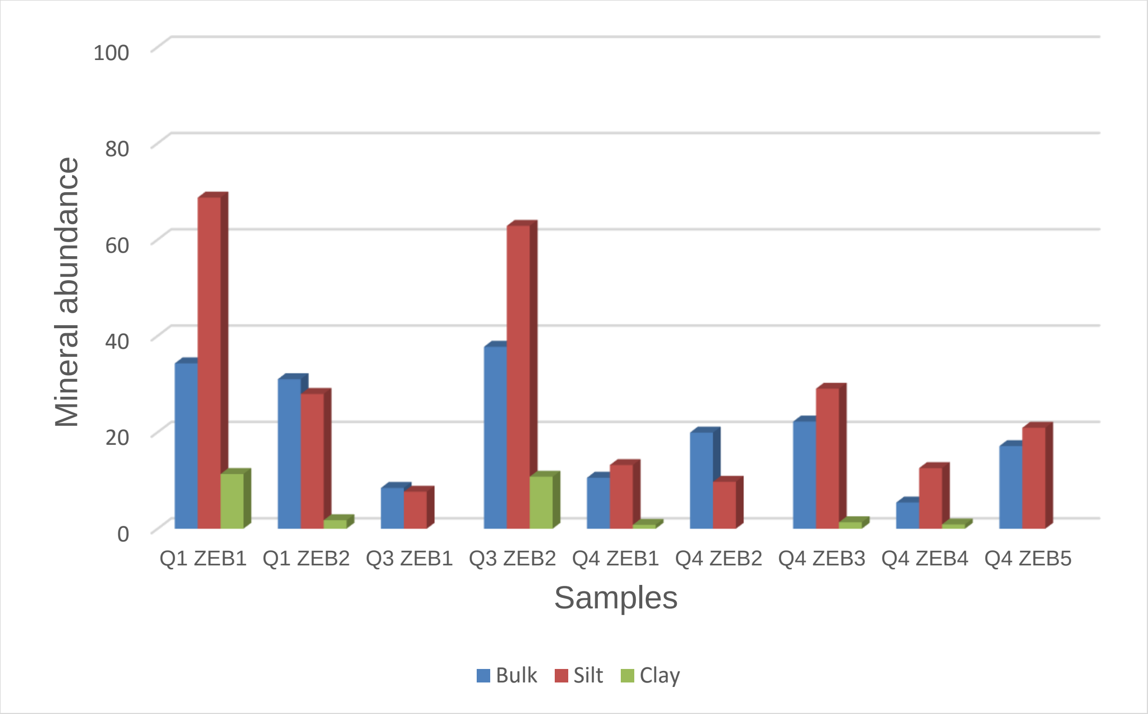

Figure 5.10: Quartz content in Zebediela bulk, silt and clay kaolin samples.

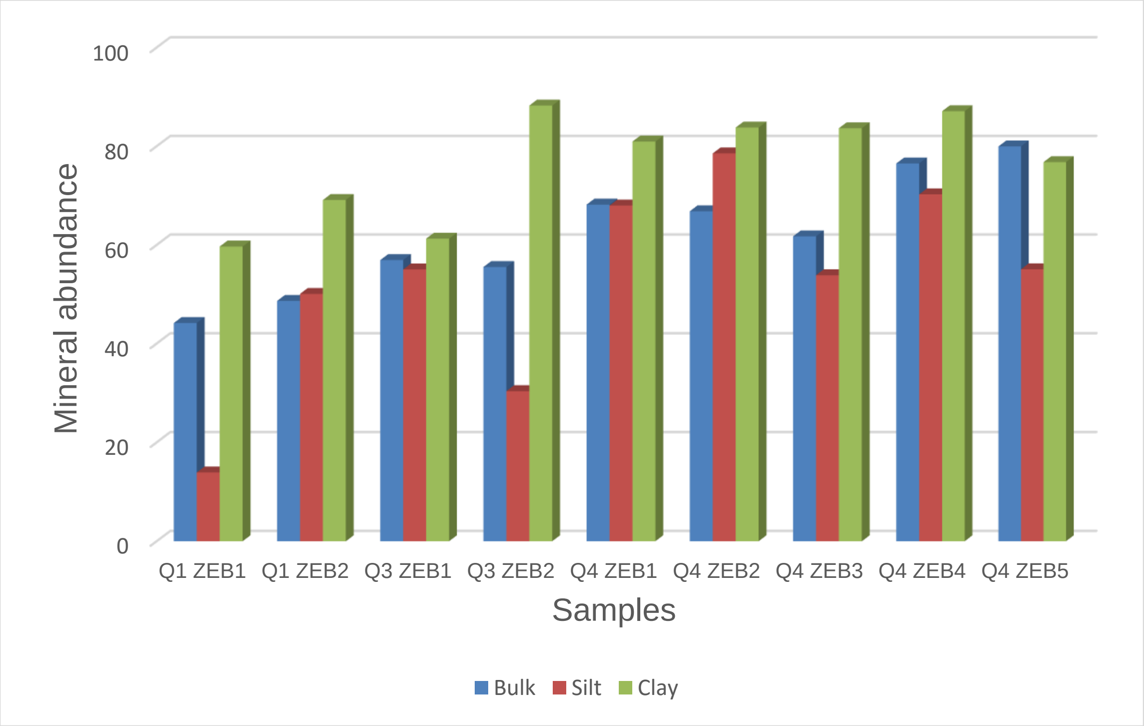

Figure 5.11: Kaolinite content in Zebediela bulk, silt and clay kaolin samples.

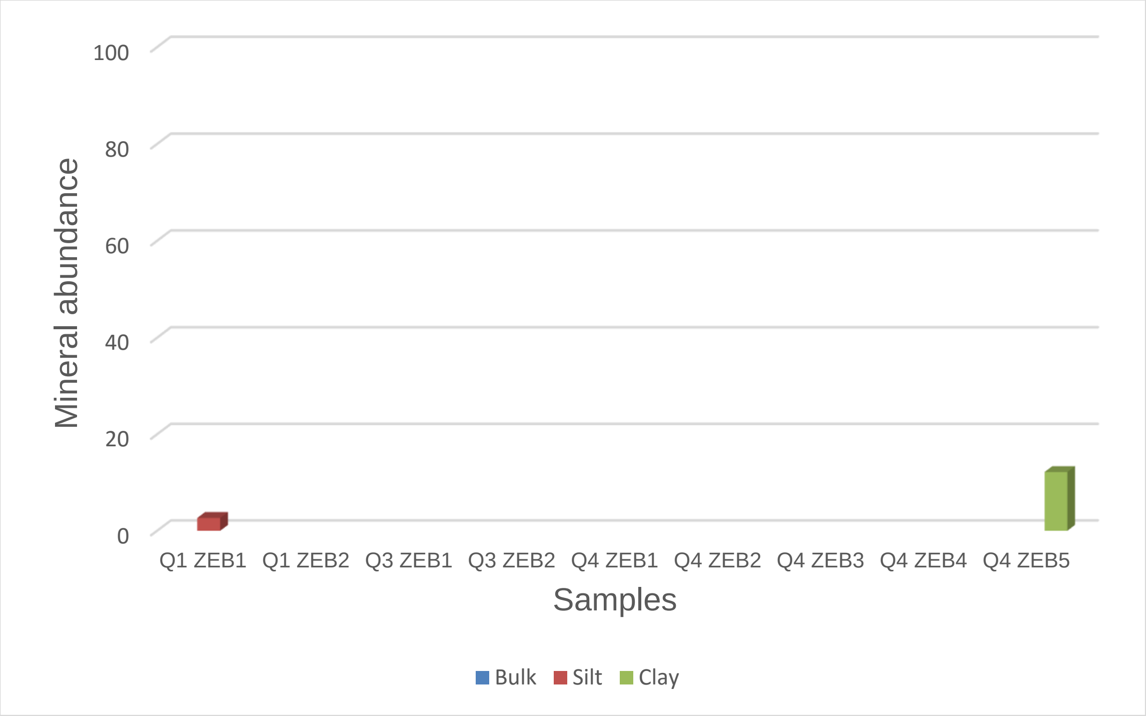

Figure 5.12: Smectite content in Zebediela bulk, silt and clay kaolin samples.

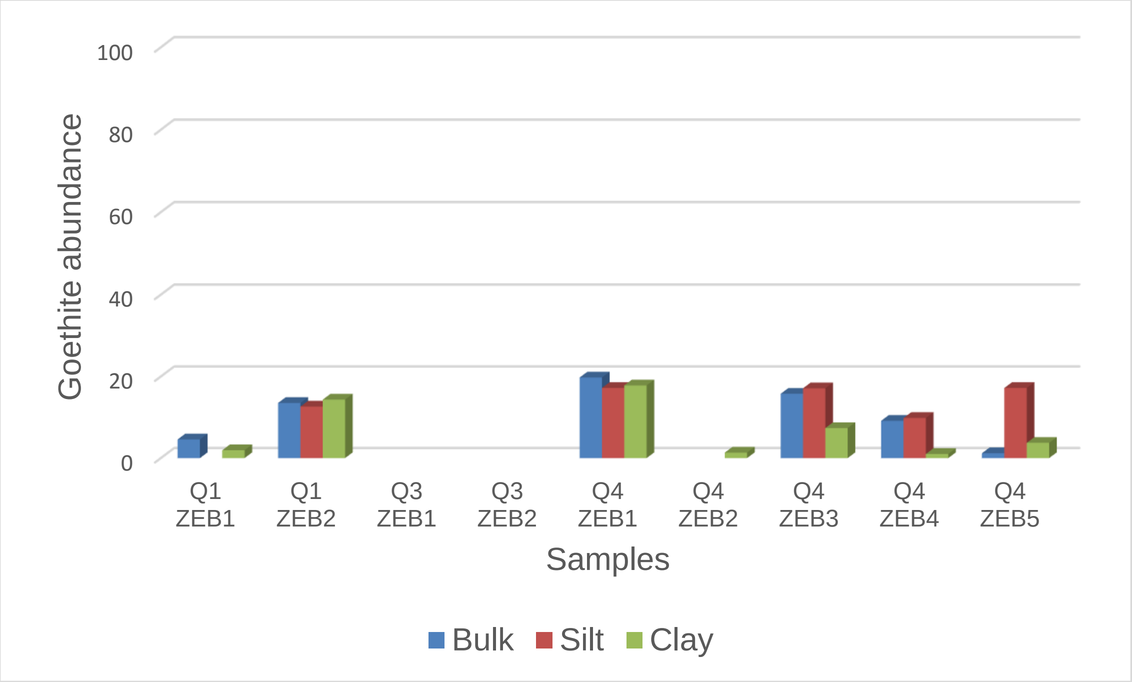

Figure 5.13: Goethite content in Zebediela bulk, silt and clay kaolin samples.

The SEM observations depicted that kaolinite in the studied samples consists of many stacks or books of kaolinite flakes which is typical to kaolinite formed from weathering processes (Ekosse, 2000). Kaolinite booklets and accordion morphologies observed in the representative samples from Lwamondo and Zebediela kaolin samples are suggestive of kaolin emplacement through weathering processes. The occurrence of irregular platelets and flakes suggests incomplete feldspar dissolution and precipitation of kaolins. Pseudo-hexagonal particle with angular to sub-angular edges identification in the samples inferred moderate kaolinitisation processes and moderate structural order (Lanson *et al.*, 2002).

The FTIR spectra were used as complementary indicators of kaolin mineralogy. The assignment of the absorption bands in measured IR spectra have been summarised in Table 4.9 and 4.10. The typical spectrum of kaolin display four clearly resolved absorption bands at about 3697, 3670, 3650 and 3620 cm^{-1} which reflect high structural ordering of the samples (Vaculikova *et al*., 2011) corresponding to 3689, 3669, 3651 and 3619 cm^{-1} for ATR spectra (Madejova and Komadel, 2001), and these characteristic bands were observed in the kaolin samples.

The bands observed around 3619 cm^{-1} have been assigned to the inner hydroxyls, and the bands observed around the other three characteristic bands are generally assigned to vibrations of the external hydroxyls (Saika *et al*., 2010). The bands around 3619 cm^{-1} and around other three characteristic bands were observed in all the samples except for samples LWA1, LWA4 and Q1ZEB1. The determination of the degree of structural disorder from the IR spectra of selected kaolinites based on empirical approach (IR-E) on the basis of resolution and relative intensities of the bands in OH stretching and bending regions (Vaculikova *et al*.,2011) proposed the following classification schemes for kaolinite disorder:

- Ordered; if the OH stretching and bending bands are clearly resolved.
- Partially ordered; if the individual OH bands at 3670 cm^{-1}, 3650cm^{-1} and 938 cm^{-1} had low intensities but could be identified.

- Poorly ordered; if only one band near 3660 cm^{-1} or inflexions near 3670 cm^{-1}, 3650 cm^{-1} and 938 cm^{-1} were observed in the spectra

The studied kaolin samples exhibit the bands near four characteristic bands at 3696, 3669, 3651 and 3620 cm^{-1}. The sharp doublet at 3696 and 3620 cm^{-1} corresponding to 3689 and 3619 cm^{-1} is characteristic for the kaolin group. The absorption bands observed between 3689, 3669, 3651 and 3619 cm^{-1} region corresponds to OH stretching groups. The OH-deformation bands of kaolinite were observed at around 937 and 911 cm^{-1}. Supporting bands at 788 (Si-O) and 681 cm^{-1} (Si-O) were observed in the samples which are diagnostic for kaolinite.

In sample LWA1 and sample LWA4 few peaks were identified and four characteristics peaks were not identified in both samples and it was regarded as a disordered sample. LWA2 and Q1ZEB1, Q1ZEB2, Q4ZEB1 and Q4ZEB2 individual OH bands at 3669, 3651 and 926 cm^{-1} were identified but their intensities were low and considered as partially ordered (Vaculikova *et al*., 2011). In samples; LWA6, LWA7, Q4ZEB4, Q3ZEB2 and Q3ZEB1, OH stretching and bending bands were clearly resolved, all four kaolinite characteristic bands were clearly resolved and are considered to be well ordered.

5.4 Geochemistry

5.4.1 Major oxides

SiO_2/Al_2O_3 ratios

The SiO_2/Al_2O_3 ratio reflect quartz and aluminosilicates abundance in weathered products. Low SiO_2/Al_2O_3 values indicate relative enrichment of argillites (kaolins) at the expense of quartz and vice versa (Wu *et a*l., 2011). The SiO_2/Al_2O_3 ratios of the studied kaolins are higher than 1.18 value reported for theoretical kaolinite (Ekosse, 2005), indicating that the kaolin also had other minerals apart from kaolinite.

Fe_2O_3/TiO_2 ratios

The Fe_2O_3/TiO_2 ratio employed to infer the mechanism of kaolin emplacement. Weathering enhances the presence of ferric oxides and hydroxides whereas TiO_2 is more concentrated as anatase by hydrothermal fluids. The sedimentary structures such as faults and fractures provide pathways for weathering processes and hydrothermal alteration. The Fe_2O_3/TiO_2 ratio can be used to infer the predominant kaolinitisation (Santos *et al*., 2000; Njoya *et al*., 2006). The mean values for Fe_2O_3/TiO_2 ratios of the studied kaolins were as follows: Lwamondo (15.02 wt %) and Zebediela (20.96 wt %), this is due to the presence of minerals such as goethite and hematite in some of he studied samples. Low Fe_2O_3/TiO_2 ratios were obtained for whitish kaolins.

Loss on Ignition

Samples with highest kaolinite content had the highest Al_2O_3 and LOI concentrations. Al_2O_3 increased as kaolinitisation increased and formation of hydrated clay minerals like kaolinite occured rather than goethite.The LOI of theoretical kaolinite is 13.9 wt %, the LOI from the studied kaolin deposits confirmed that samples contained other minerals such as smectite and goethite. LOI increases as particle sizes decreases (Figures 5.14 – 5.15).

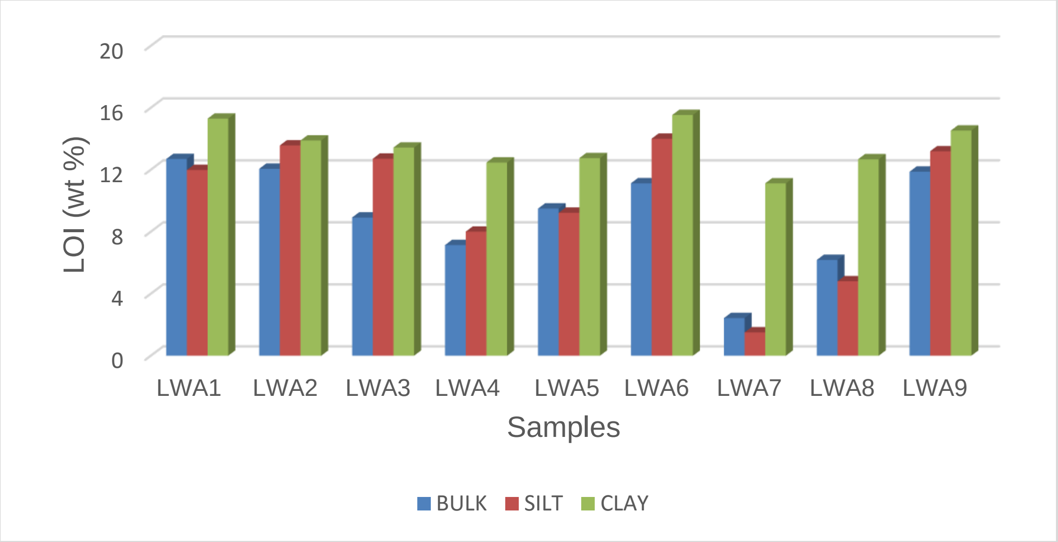

Figure 5.14: LOI in bulk, silt fraction and clay size fraction of Lwamondo kaolin samples.

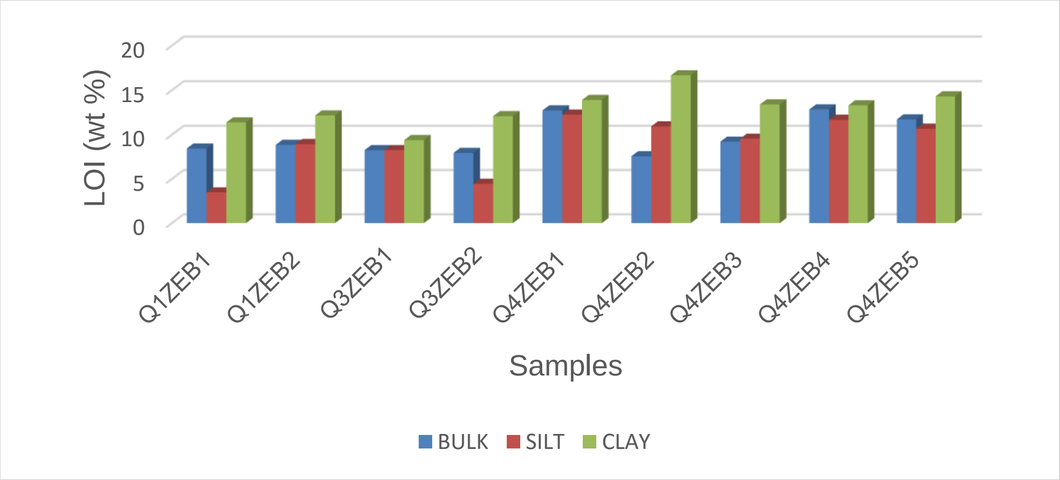

Figure 5.15: LOI of bulk, silt fraction and clay size fraction of Zebediela kaolin samples.

Harker variation diagrams

Harker variation diagrams of how major oxides vary compared to the Al_2O_3 content, which are largely a reflection of the feldspar content in kaolin samples (Figures 5.16-5.37). In case of Lwamondo kaolin, CaO vs Al_2O_3 showed strong positive correlation from bulk to clay size fraction, yielding to reduction in CaO. The SiO_2 vs Al_2O_3 reflected moderate to strong negative correlation from bulk to clay size fraction due to weathering. It revealed more scattered distribution suggesting moderate to strong chemical weathering (Figure

5.19). The Fe_2O_3 vs Al_2O_3 and TiO_2 vs Al_2O_3 variation showed moderate to strong negative correlation from bulk to clay size fraction (Figure 5.20), and is indicative of the low level depletion of Fe and Ti. The Fe_2O_3 vs Al_2O_3 demonstrated clustering groups which is reflective of possible formation from two different sources and there was no significant change in Fe; with the highest R^2 occurring in the clay fraction. However, there was a slight increase in the TiO_2 in the clay fraction.

The K_2O vs Al_2O_3 showed strong positive correlation with a reduction in K_2O. The Cr_2O_3 vs Al_2O_3 showed strong negative correlation with a slight reduction in Cr_2O_3 and Al_2O_3 increased in the clay fraction. The MgO vs Al_2O_3 showed strong negative correlation, and the MnO vs Al_2O_3 showed moderate negative correlation. The Na_2O vs Al_2O_3 showed moderate negative correlation in bulk and clay fraction. P_2O_5 vs Al_2O_3 showed moderate to strong positive correlation from bulk to clay fraction. Low concentrations of oxides favoured ions of Al^{3+} and Si^{2+} to be released from primary minerals; thus creating opportunity for kaolinisation to occur.

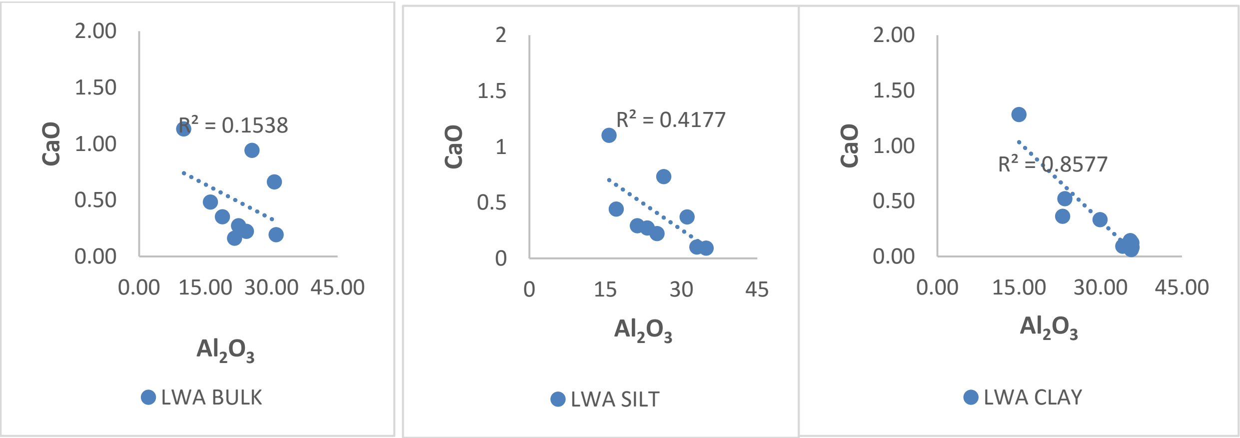

Figure 5.16: Harker variation diagram of CaO vs Al_2O_3 content for Lwamondo kaolin.

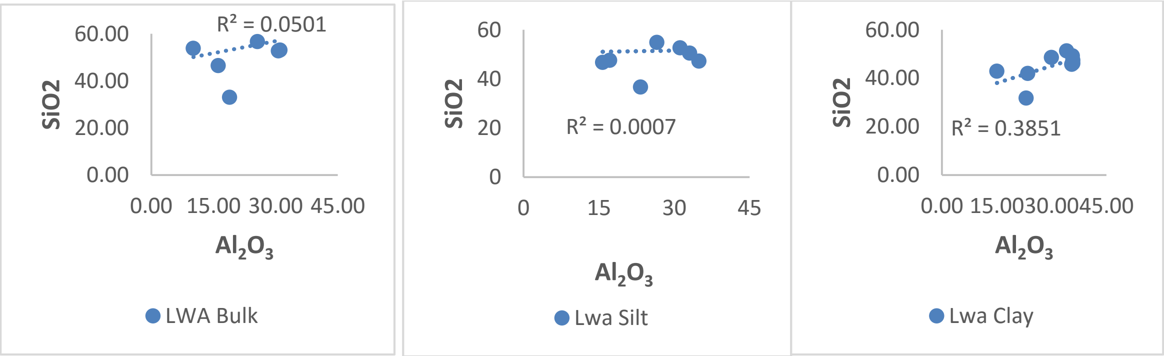

Figure 5.17: Harker variation diagram of SiO_2 vs Al_2O_3 content for Lwamondo kaolin.

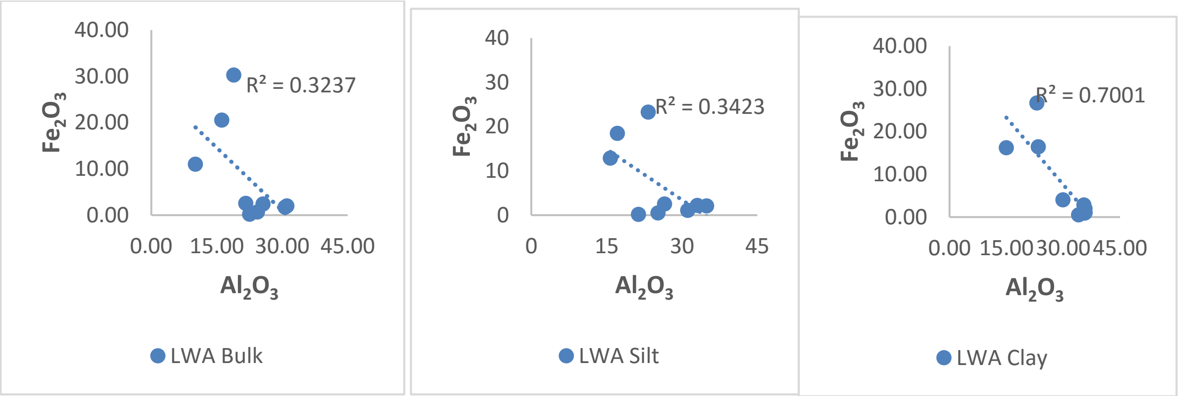

Figure 5.18: Harker variation diagram of Fe_2O_3 vs Al_2O_3 content for Lwamondo kaolin.

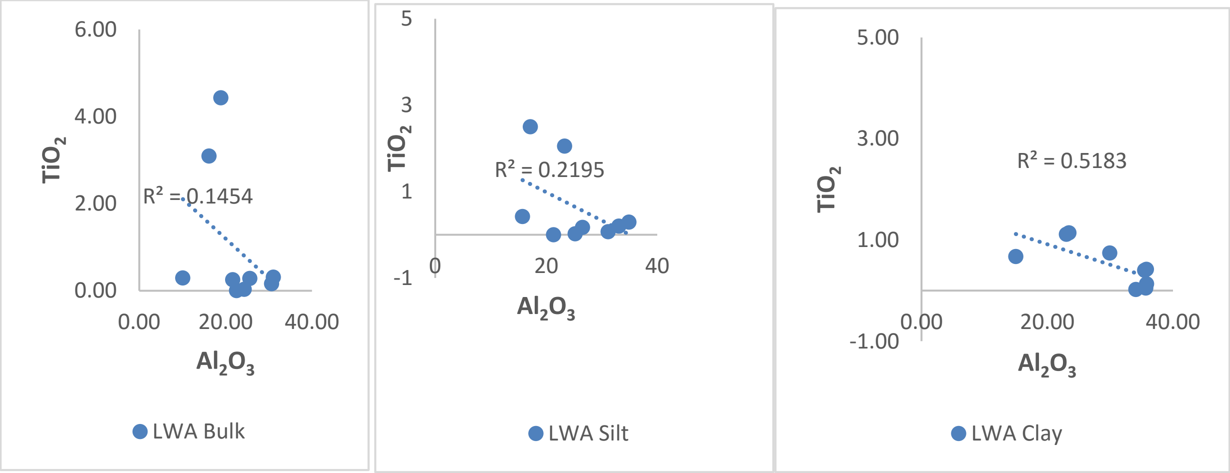

Figure 5.19: Harker variation diagram of TiO_2 vs Al_2O_3 content for Lwamondo kaolin.

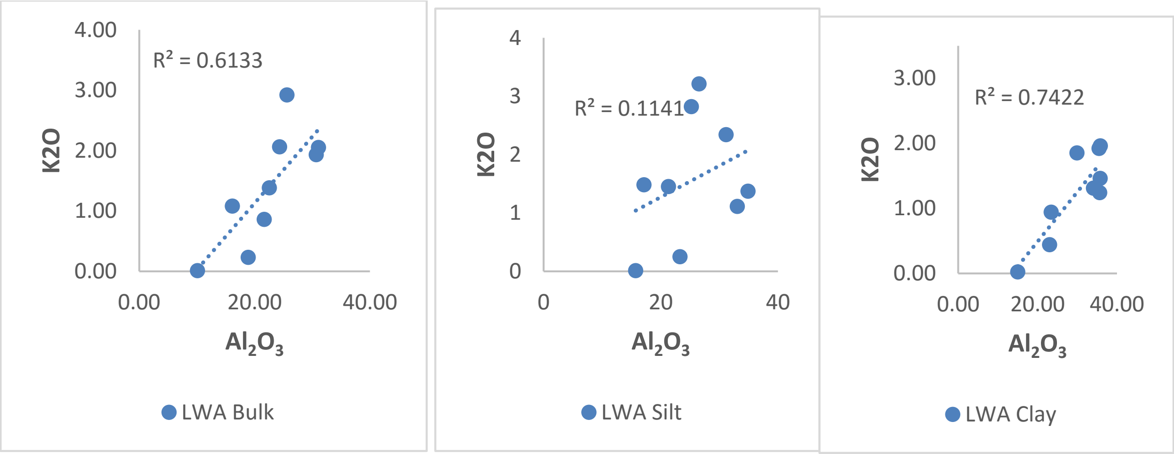

Figure 5.20: Harker variation diagram of K_2O vs Al_2O_3 content for Lwamondo kaolin.

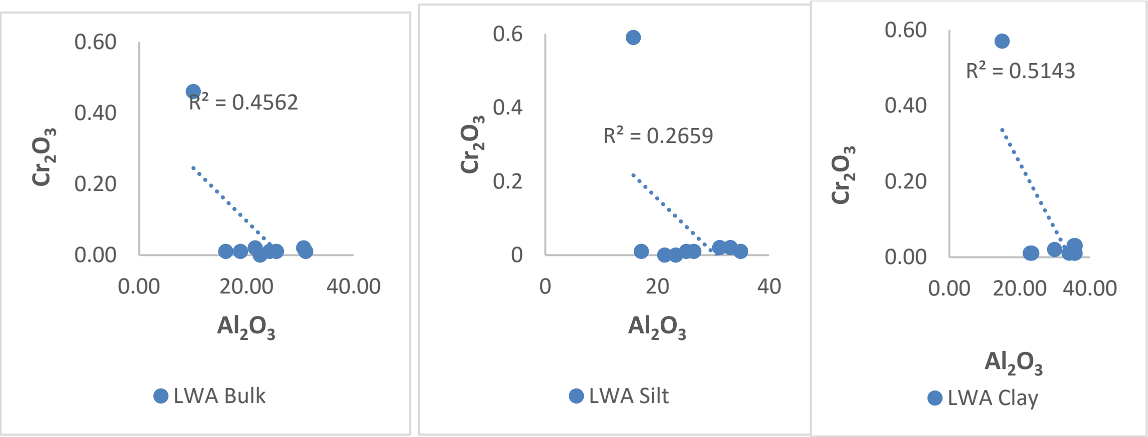

Figure 5.21: Harker variation diagram of Cr_2O_3 vs Al_2O_3 content for Lwamondo kaolin.

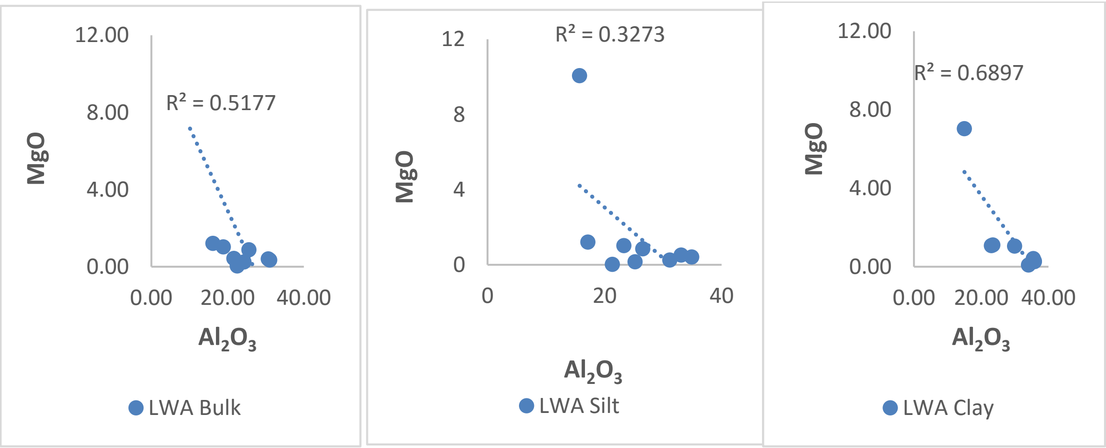

Figure 5.22: Harker variation diagram of MgO vs Al_2O_3 content for Lwamondo kaolin.

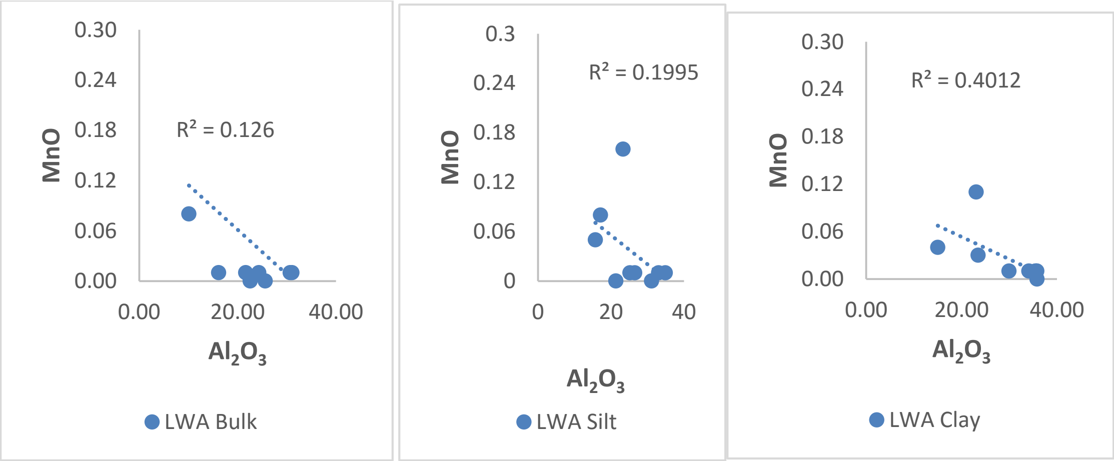

Figure 5.23: Harker variation diagram of MnO vs Al_2O_3 content for Lwamondo kaolin.

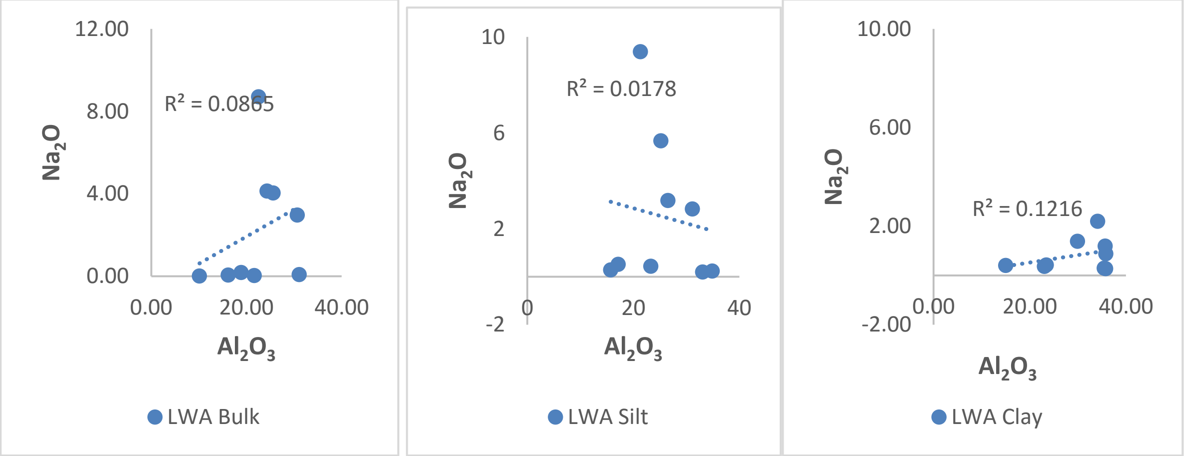

Figure 5.24: Harker variation diagram of Na_2O vs Al_2O_3 content for Lwamondo kaolin.

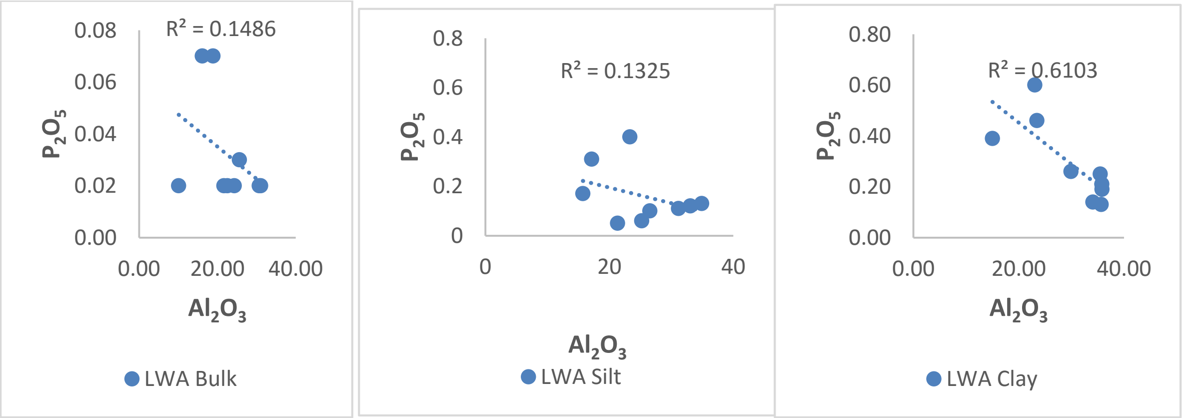

Figure 5.25: Harker variation diagram of P_2O_5 vs Al_2O_3 content for Lwamondo kaolin.

The Harker variation diagrams of Zebediela kaolin were almost similar to the Lwamondo kaolin (Figures 5.26 – 5.35). The CaO vs Al_2O_3 showed strong negative correlation from bulk to clay with a reduction in CaO (Figure 5.26). The Cr_2O_3 and Al_2O_3 reflected positive correlation in bulk and silt fraction (Figure 5.27). The Fe_2O_3 vs Al_2O_3 showed negative to positive correlation from bulk to clay (Figure 5.28), and is indicative of low level depletion in Fe. The K_2O vs Al_2O_3 demonstrated moderate positive correlation (Figure 5.29), yielding to the reduction in K, and the MgO vs Al_2O_3 showed strong negative correlation equally yielding to Mg reduction (Figure 5.30).

The MnO vs Al_2O_3 showed negative to weak positive correlation for bulk to clay fraction (Figure 5.31). The Na_2O vs Al_2O_3 showed weak positive correlation with decreasing Na values from bulk to clay suggesting moderate to strong chemical weathering (Figure 5.32). The P_2O_5 vs Al_2O_3 revealed weak positive correlation (Figure 5.33). The SiO_2 vs Al_2O_3 reflected strong positive correlation, with an increase in Al in bulk and clay fraction (Figure 5.34). The TiO_2 vs Al_2O_3 showed strong negative correlation from bulk to silt fraction and weak negative correlation in the clay fraction due to weathering (Figure 5.35). Depletion in Na, Mg, K, Ca, Cr and Mn ions favoured the formation of kaolinite.

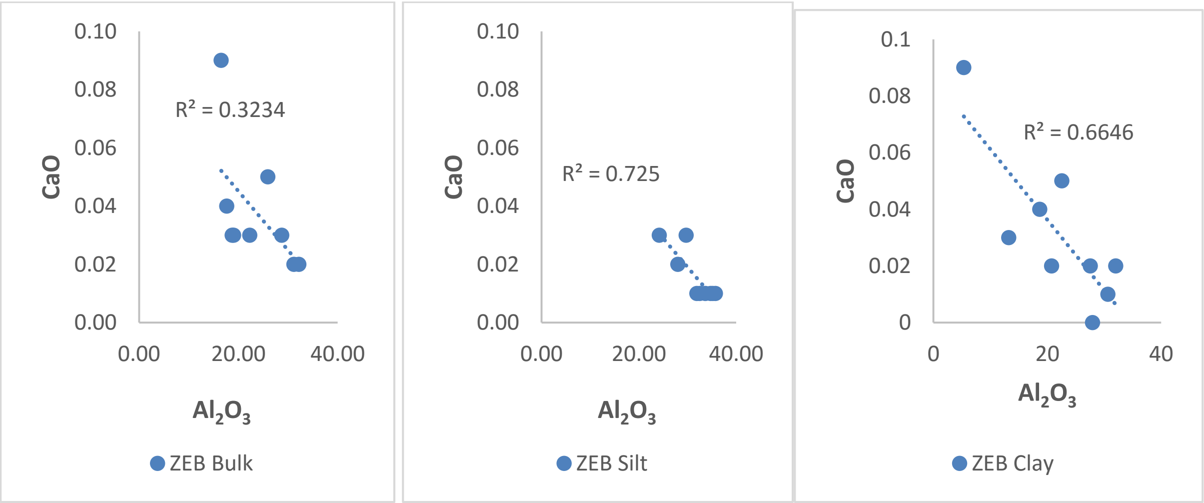

Figure 5.26: Harker variation diagram of CaO vs Al_2O_3 content for Zebediela kaolin.

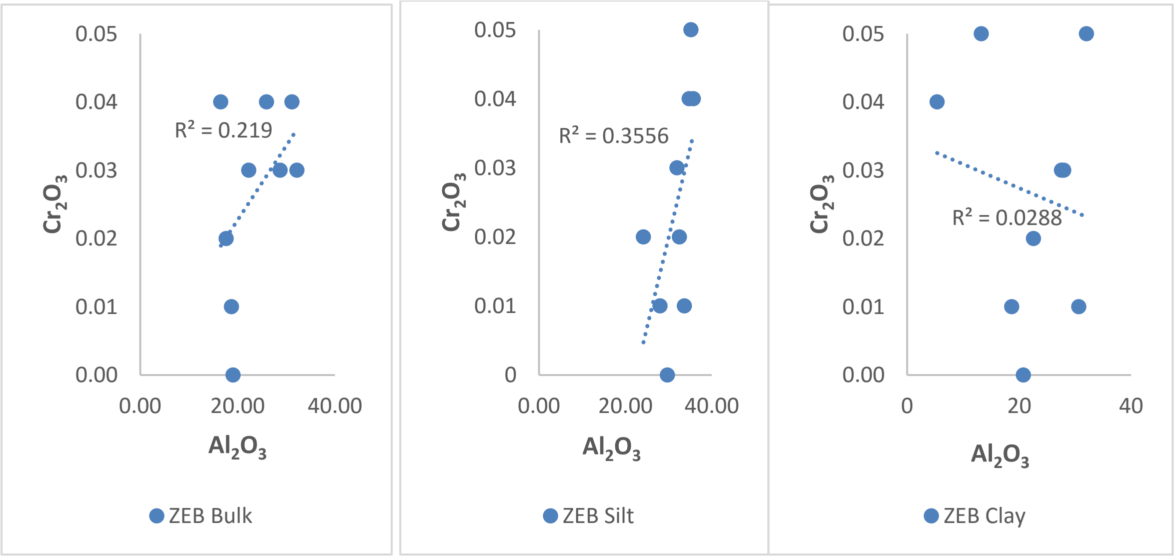

Figure 5.27: Harker variation diagram of Cr_2O_3 vs Al_2O_3 content for Zebediela kaolin.

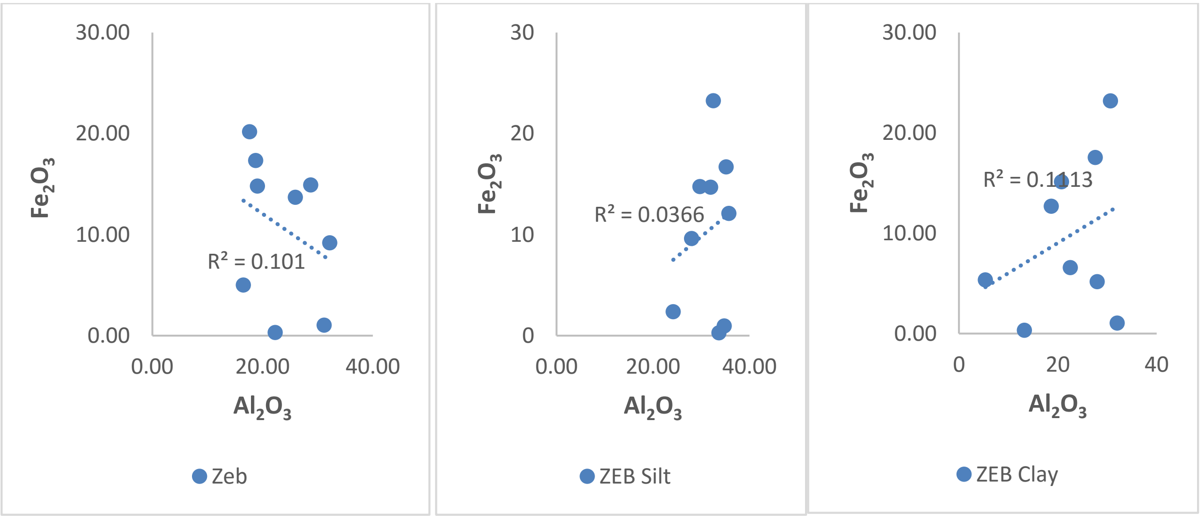

Figure 5.28: Harker variation diagram of Fe_2O_3 vs Al_2O_3 content for Zebediela kaolin.

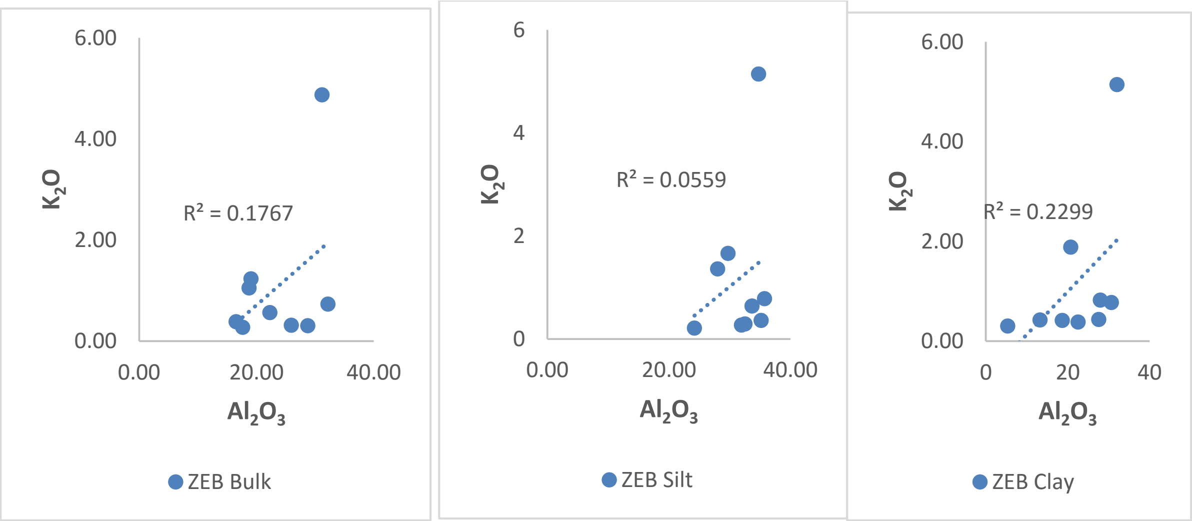

Figure 5.29: Harker variation diagram of K_2O vs Al_2O_3 content for Zebediela kaolin.

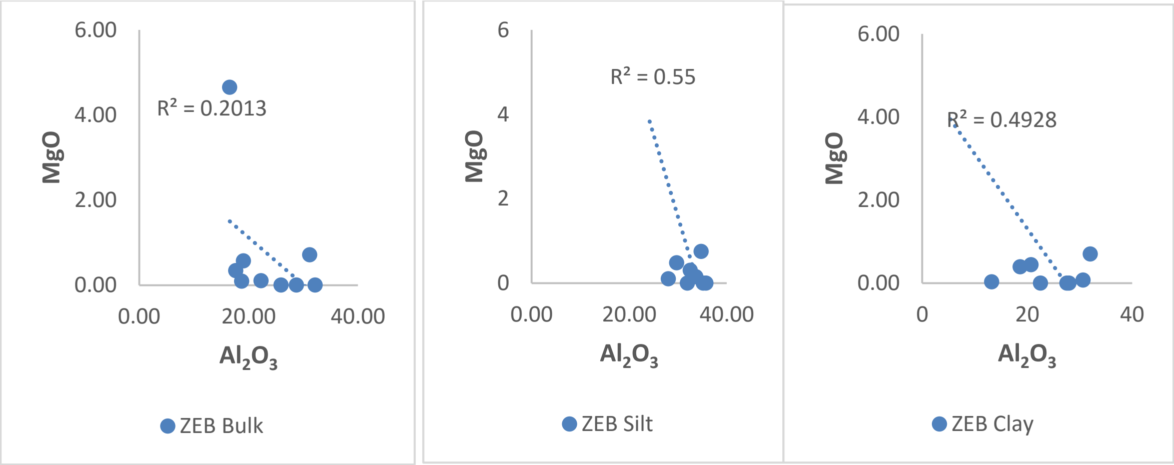

Figure 5.30: Harker variation diagram of MgO vs Al_2O_3 content for the Zebediela kaolin.

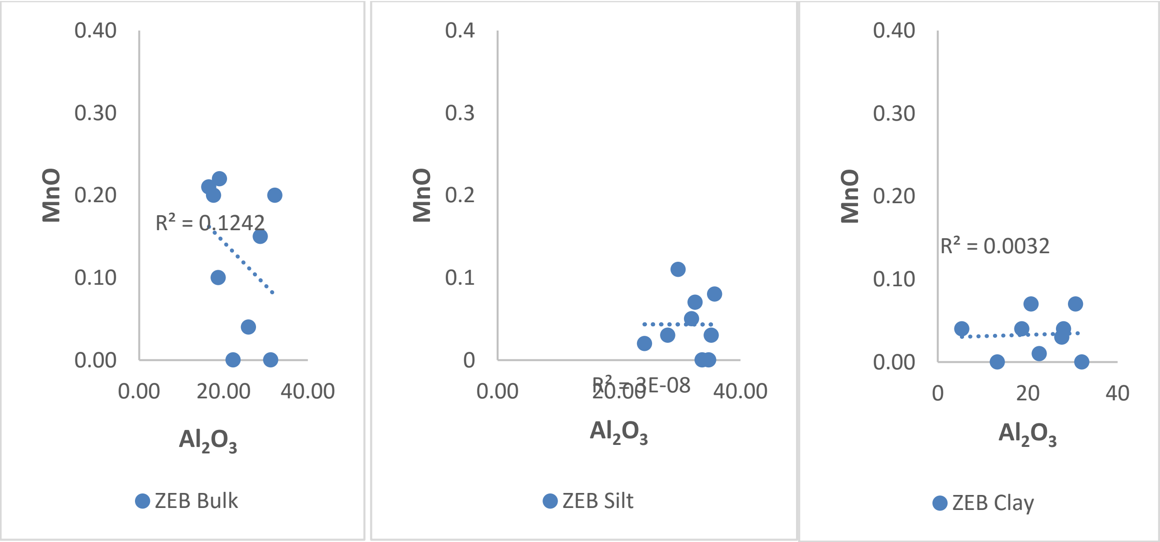

Figure 5.31: Harker variation diagram of MnO vs Al_2O_3 content for the Zebediela kaolin.

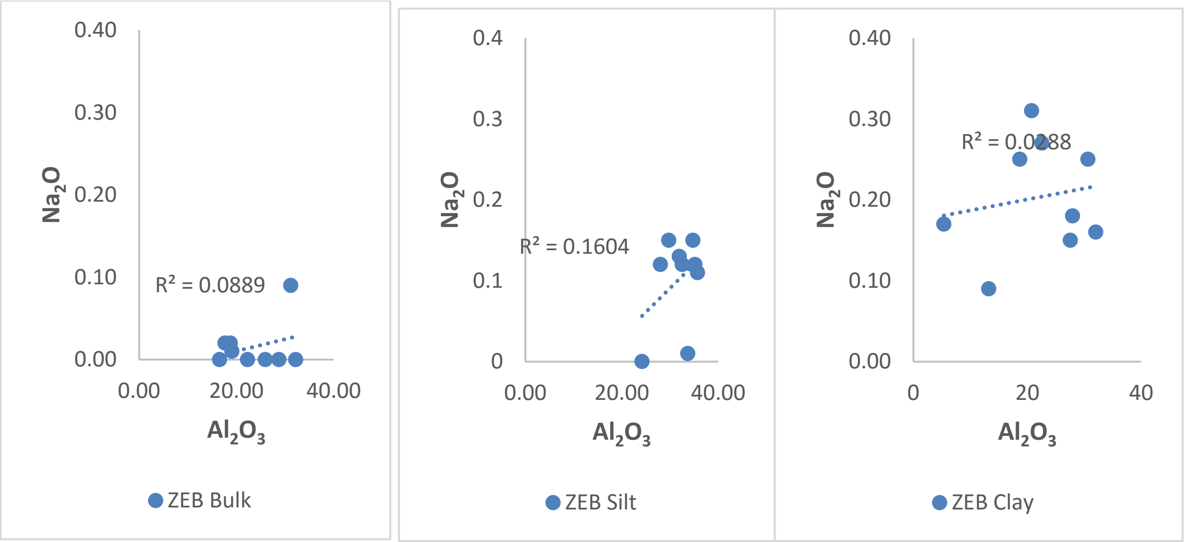

Figure 5.32: Harker variation diagram of Na_2O vs Al_2O_3 content for the Zebediela kaolin.

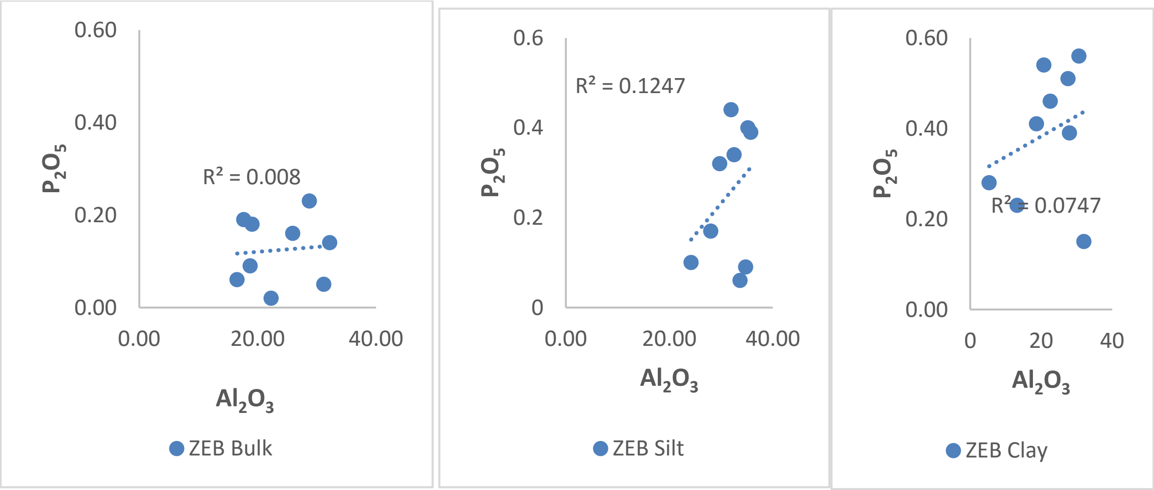

Figure 5.33: Harker variation diagram of P_2O_5 vs Al_2O_3 content for the Zebediela kaolin.

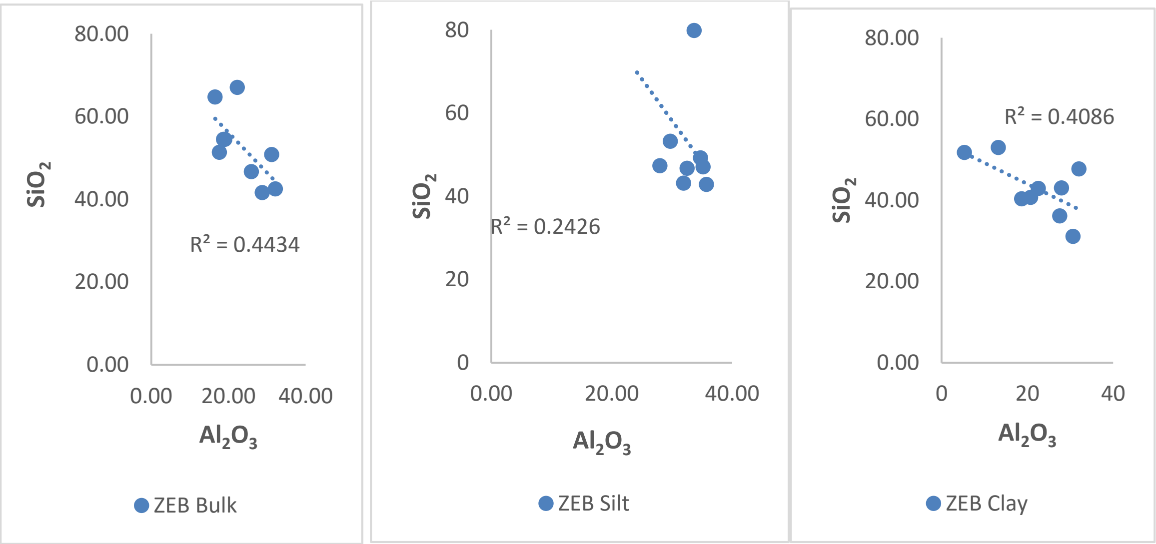

Figure 5.34: Harker variation diagram of SiO_2 vs Al_2O_3 content for the Zebediela kaolin.

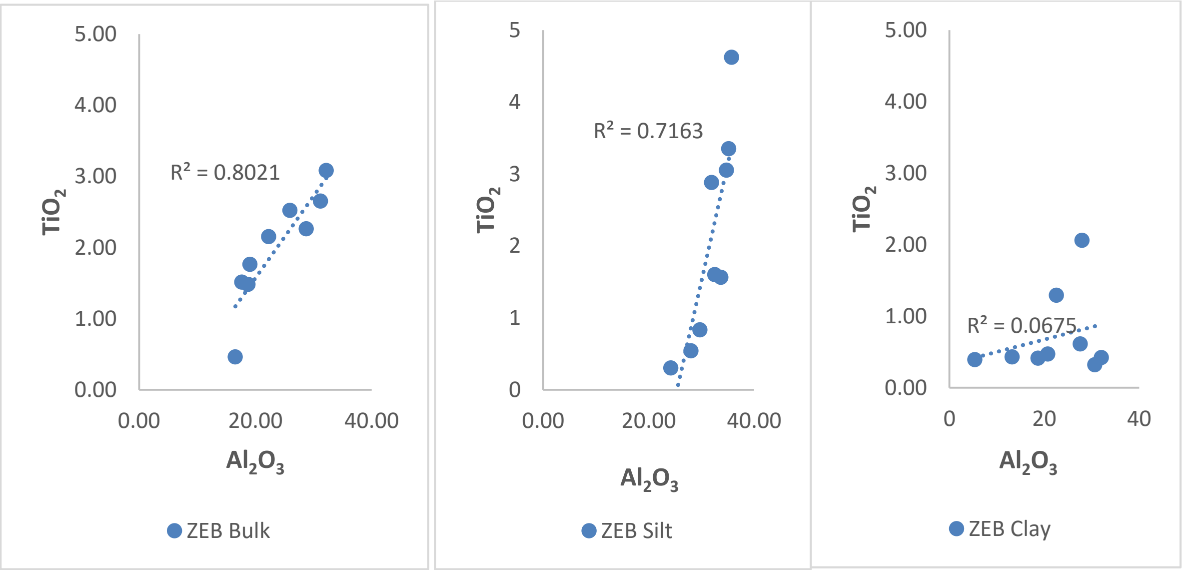

Figure 5.35: Harker variation diagram of TiO_2 vs Al_2O_3 content for the Zebediela kaolin.

5.4.2 Weathering trends and kaolinitisation

Kaolinite content and relatively high values of the CIA and CIW suggest intensive chemical weathering of the source rocks (Ojo *et al.*, 2014). Kaolinite was identified as a dominant mineral in the Lwamondo and Zebediela kaolin samples. The CIA values for Lwamondo kaolin of the bulk samples ranged from 68.57 to 96.19 wt % with an average of 86.05, for silt fraction ranged from 65.73 to 96.08 wt % with an average of 85.64 wt % and for clay size fraction ranged from 89.38 to 95.21 wt % with an average of 92.43 wt %. However, the CIA values for Zebediela kaolin of the bulk samples ranged from 86.24 to 98.87 wt % with an average of 94.65 wt %, for silt fraction ranged from 85.78 to 98.50 wt % with an average of 94.85 wt % and for clay size fraction ranged from 86.75 to 98.48 wt % with an average of 96.03 wt %.

The values recorded in the analysed samples were higher and reflected higher presence of kaolinite and less feldspar with extreme chemical weathering in the source area (Figure 5.36 and 5.37) (Ekosse, 2000; Ojo *et al.*, 2014; Mahjoor *et al.*, 2009; Mousa *et al.*, 2014). The high CIA value (>98 %) indicate the maturity of the kaolin deposit (Baioumy *et al.*, 2014).The high value of CIW for Lwamondo kaolin bulk samples ranged from 71.57 to 99.18 wt % with an average of 90.24 wt %, for silt fraction ranged from 68.81 to 99.13 wt % with an average of 89.98 wt % and for clay size fraction ranged from 89.93 to 98.92 wt % with an average of 96.29 wt %. However, the CIW values for Zebediela kaolin bulk samples ranged from 99.46 to 99.94 wt % with an average of 98.71 wt %, for silt fraction ranged from 98.35 to 99.70 wt % with an average of 99.31 wt % and for clay size fraction ranged from 98.87 to 99.70 wt % with an average of 99.32 wt %, these values support intensive weathering at the source area as indicated by CIA.

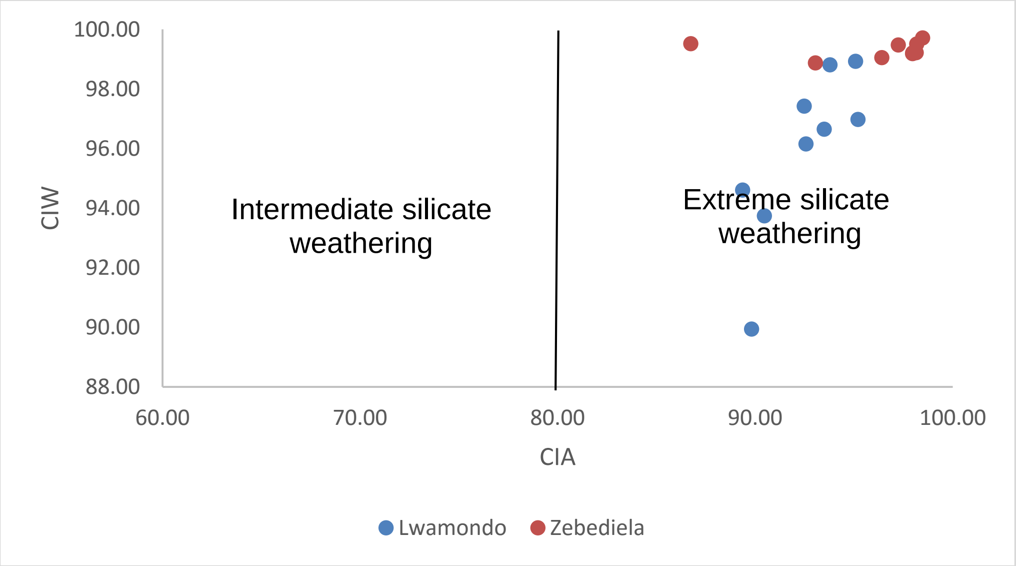

Figure 5.36: CIW versus CIA weathering trends of Lwamondo and Zebediela kaolins.

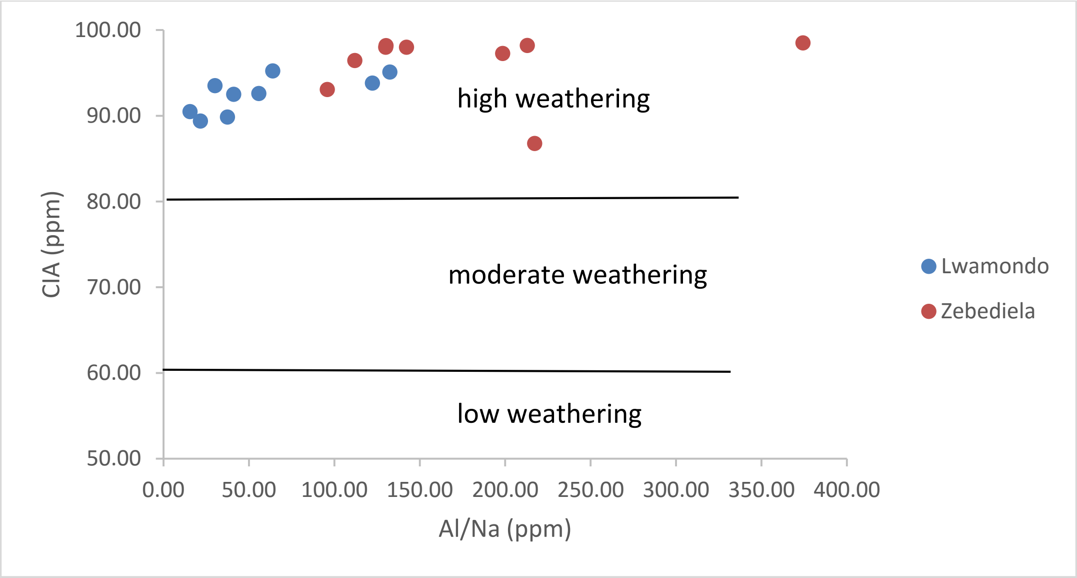

Figure 5.37: CIA versus Al/Na of Lwamondo and Zebediela kaolin showing weathering intensity.

The A-CN-K ternary diagram (Figure 5.38) used to deduce weathering trends, samples plot in a region that is clearly show variations in the Al_2O_3, CaO, Na_2O and K_2O concentration. The Lwamondo and Zebediela kaolin samples plotted closer to the Al_2O_3 contents dominated by kaolinite and suggest that the samples were generated from the sources affected by relatively high and intensive chemical weathering which resulted in the depletion of selectively leached elements (Ca, Na, K) from the weathering profiles (Ekosse, 2000; Ojo *et al.*, 2014; Mahjoor *et al.*, 2009; Mousa *et al.*, 2014).

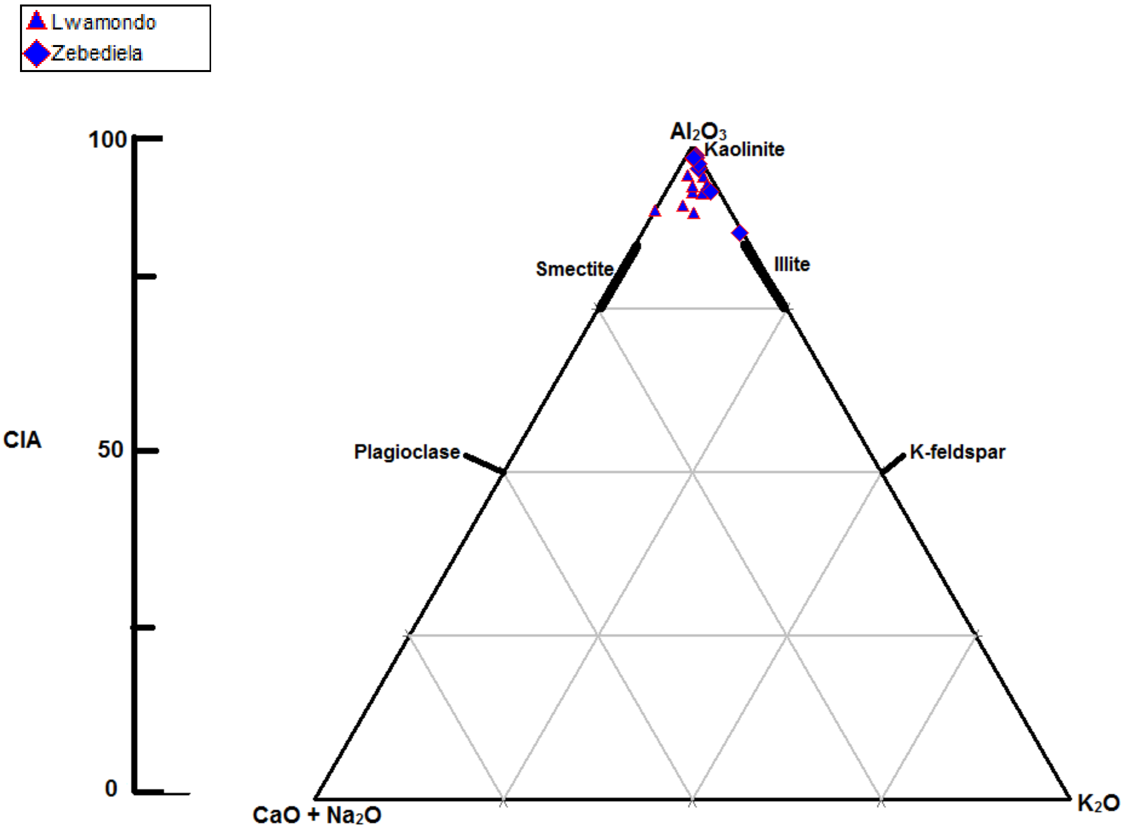

Figure 5.38: Al_2O_3-(CaO+Na_2O)-K_2O (A-CN-K) plot of Lwamondo and Zebediela kaolin samples.

5.5 Paleoenvironmental conditions

5.5.1 Genesis and depositional environment

Trace elements distribution in clays and sediments are influenced by weathering processes and nature of the parent rocks (Nesbitt *et al*., 1980; Wronkiewiez *et al.*, 1987). The higher concentration of Cr and V in the studied kaolin may be related to their low mobility during kaolinitisation process (Vidal, 1998). Lwamondo and Zebediela kaolins were also enriched in Ni except sample Q1ZEB2 which is related to it being easily mobilized during weathering. Ba and Sr were depleted in all the studied samples indicating that they were easily mobilised during weathering and removed from the environment (Nyakairu *et al.*, 2001; Mahjoor *et al.*, 2009). During kaolinitisation, Sc was slightly concentrated in the kaolin deposit and it was enriched in all samples except in samples LWA1, LWA6 and LWA8.

The Heavy REE are more enriched than Light REE in the weathered and sub-weathered zones (Zuoping and Chuanxian, 1996).The REE pattern showed enrichment in Heavy REE than light REE in all samples with slight positive Eu anomaly due to the presence of plagioclase in the kaolin samples. The REE pattern and the content of other trace elements show evidence of weathering process related to kaolinitisation in the Lwamondo and Zebediela kaolins.

The Total Alkali Silica (TAS) diagram based on Le Bas *et al*., (1986) (Figure 5.39), the possible source rocks for Lwamondo was basalts, whereas Zebediela source rocks ranged from Basalt (Picrobasalts) to basaltic andesite. Kaolinite was formed from the weathering profiles of the source rocks rich in feldspars, transported and deposited as kaolinite.

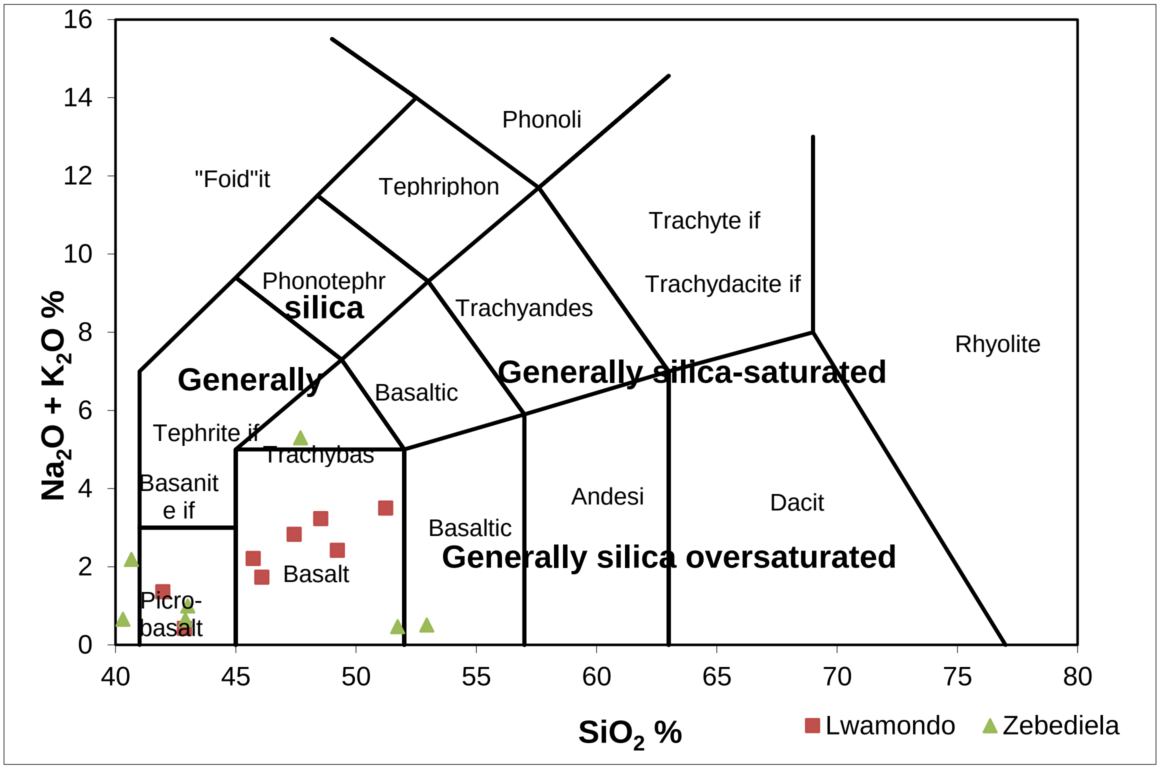

Figure 5.39: Chemical classification of kaolinitic samples from Lwamondo and Zebediela based on the TAS diagram.

The source rocks for the kaolin formation for Lwamondo and Zebediela based on Roser and Korsch (1988) was believed to be intermediate to mafic due to the occurrence of basalts, clastic sediments, shales and arkose in the study sites (Figure 5.40).

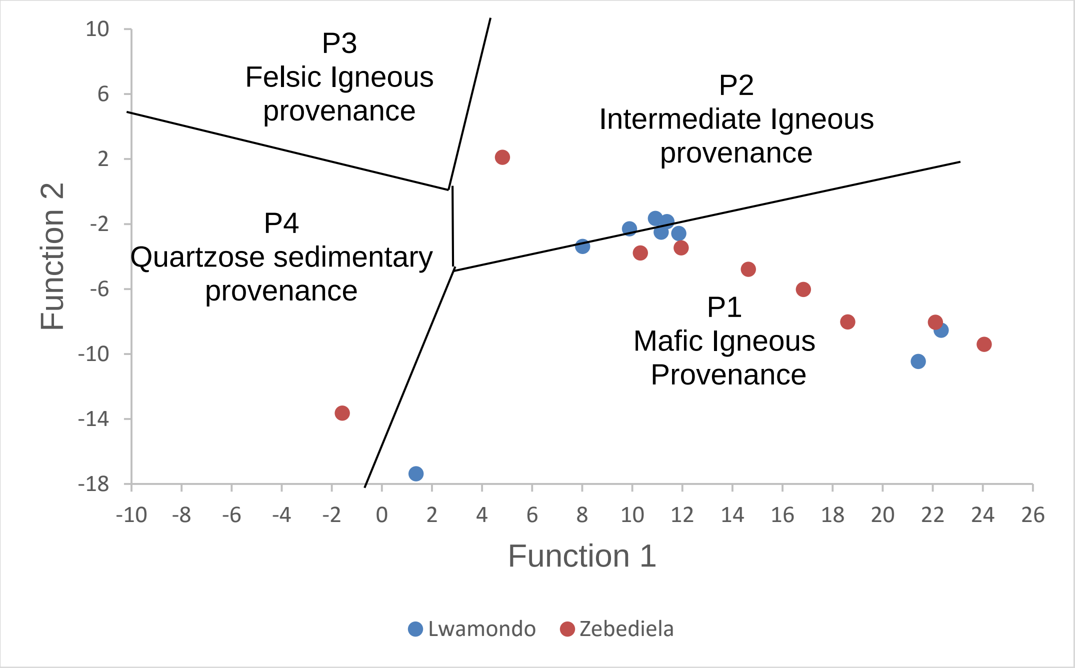

Figure 5.40: Major element provenance discriminant function diagram for the Lwamondo and Zebediela kaolin.

The relationship between MgO/Al_2O_3 and K_2O/Al_2O_3 was used to differentiate between clay formed under marine and non-marine (Roaldset, 1978). The application of this relationship on the studied samples revealed that most of the Lwamondo and Zebediela kaolin samples fell in non-marine environment (Figure 5.41). Redox sensitive elements such as Cu, Zn, V, Ni, Cr and U in sediments can be used to evaluate the paleoredox conditions (Jones and Manning, 1994; Madhavaraju and Ramasamy, 1999). Elemental ratios such as U/Th, Ni/Co and V/Cr are used as redox indicators (Jones and Manning, 1994; Rimner, 2004; Hallberg, 1976).

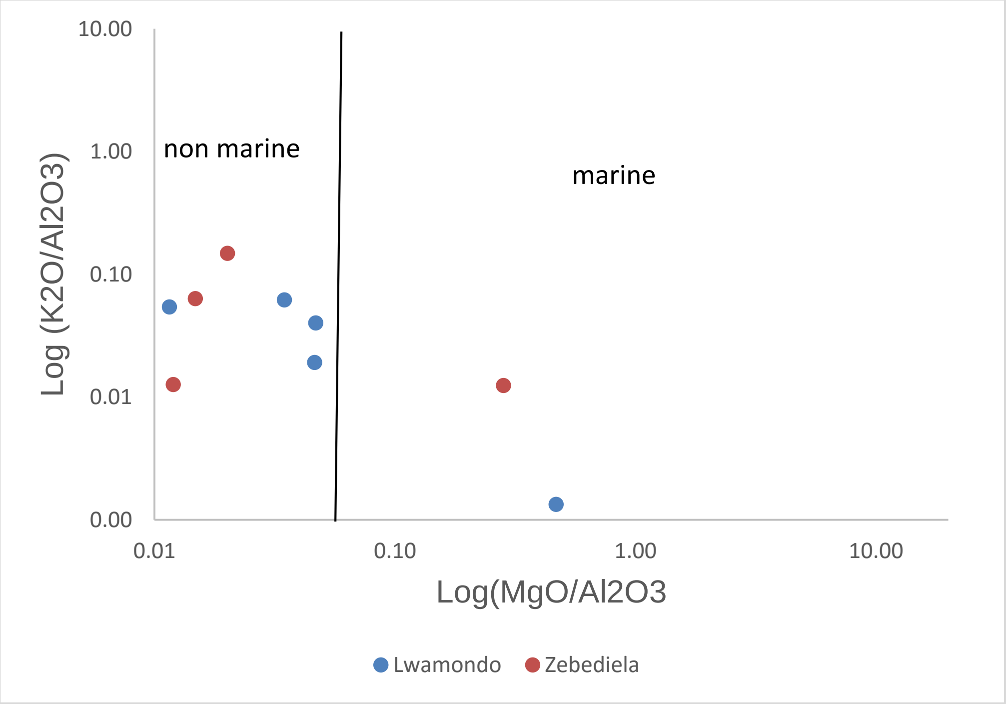

Figure 5.41: Environment of deposition for Lwamondo and Zebediela kaolins.

U/Th ratios below 1.25 suggest oxic condition of deposition, whereas values above 1.25 indicate suboxic and anoxic condition (Jones and Manning, 1994). Most of the Lwamondo kaolin showed low U/Th (0.15-3.45, average of 1.09) which indicate that the kaolin was deposited in an oxic environment whereas Zebediela kaolin display high U/Th ratios (0.18-11.5, average of 2.95 ppm), which indicate that the kaolin were deposited under the suboxic/anoxic conditions.

The V/Cr ratio below 2 indicates oxic, 2.0-4.25 to dysoxic and more than 4.25 to suboxic to anoxic conditions (Jones and Manning, 1994). The V/Cr ratios of the Lwamondo kaolin samples vary from 0.02-9.27, average of 1.40, indicating an oxic condition (Figure 5.42). Whereas, V/Cr ratios of the Zebediela kaolin vary from 0.24-10.28, with an average of 2.48, indicating an oxic conditions (Figure 5.42).

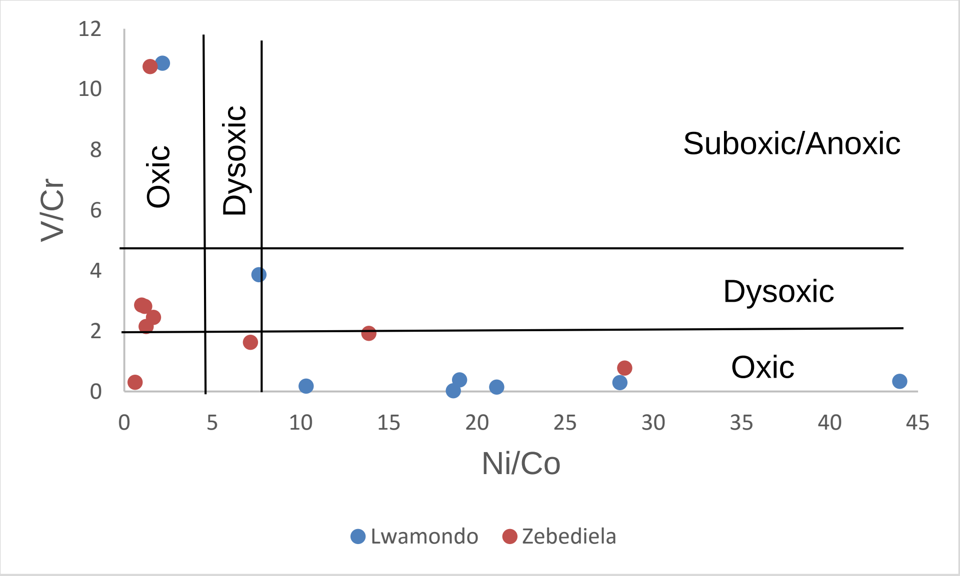

Figure 5.42: Cross plots of trace elements ratios (V/Cr vs Ni/Co) used as paleoredox proxies.

5.5.2 Stable isotopes

Kaolin can be formed through the interactions with modern local meteoric water. The isotopic composition of kaolinite was determined using the mean isotopic composition of modern meteoric water, and equilibrium fractionation factors between kaolinite and water (Equation 5.6 and 5.7) by Savin and Epstein (1970).

$$\alpha^{O}_{k\text{-}w} = \frac{\delta 18O_{k} + 1000}{\delta 18O_{w} + 1000} \text{--Eqn 5.6}$$

$$\alpha^{D}_{K\text{-}w} = \frac{\delta D_{k} + 1000}{\delta D_{w} + 1000} \text{ ---Eqn 5.7}$$

Where $\alpha^{O}_{k\text{-}w}$ and $\alpha^{D}_{K\text{-}w}$ are equilibrium fraction factors between kaolinite and water (meteoric water) with respect to oxygen and hydrogen (Lawrence and Taylor, 1971).

Isotopic composition of kaolinite was determined using modern mean annual temperature (Equation 5.8 and 5.9).

Hydrogen: 1000 In $\alpha_{kaolinite-water} = -2.2 \times 10^{6} \times T^{-2} - 7.7$---------------------------------Eqn 5.8

Oxygen: 1000 In $\alpha_{kaolinite-water} = 2.76 \times 10^{6} \times T^{-2} - 7.7$------------------------------------Eqn 5.9

Where, T is the temperature (ºK) and α kaolinite-water is equilibrium isotopic fractionation factors between kaolinite and water.

The stable isotope composition of kaolins, as well as other clay minerals, is a function of the isotopic composition of the water from which they were formed. The equilibrium isotopic fractionation factors between kaolinite and water were developed by Gilg and Sheppard (1996) and Sheppard and Gilg (1996) (Equation 5.10). These fractionation factors are a function of the temperature of kaolinitisation; therefore, the isotopic composition of kaolinite can provide information about its genesis (Fernandez-Caliani *et al.*, 2010).

$3.04\ 10^{6}\ T^{-2} = \delta^{18}O_{k} - 0.125\delta D_{k} + 7.04$ (Galan *et al*, 2016)--------------------- Eqn 5.10

Temperature of kaolinitisation (T) of the studied kaolins were calculated and presented in Table 5.1. Lwamondo kaolin deposit had a mean temperature of 26.94ºC ± 3.6 whereas Zebediela kaolin had a mean temperature of 36.58ºC ± 4.2. Kaolinite in equilibrium with the global meteoric water line, kaolinitisation temperature in Lwamondo kaolins (26.94ºC) whereas Zebediela kaolins kaolinitisation temperature (36.58ºC).

The position of the Q4ZEB2 in the hypogene filed could be interpreted as being formed in isotopic equilibrium with its parental fluid, without subsequent isotopic exchange with meteoric water (Clauer *et al.*, 2015).

Table 5.1: Temperatures of kaolinitisation (T) of the analysed samples

Samples	δ18O	δD	T (ºC)
LWA1	17.4	-84	21.82
LWA2	19.2	-58	28.14
LWA9	19.1	-54	30.87
MEAN	18.57	-65	26.94 ± 3.6
Q1ZEB2	16.7	-68	33.92
Q3ZEB2	17.7	-61	33.33
Q4ZEB2	15.6	-63	42.48
MEAN	16.67	-64	36.58 ± 4.18

The mean temperature of kaolinitisation determined using GMWL were used to determine mean stable isotope composition of the meteoric water in equilibrium with Lwamondo kaolin and Zebediela kaolin using Equation 5.8 and 5.9.The results of mean isotopic composition of meteoric water are shown in the Table 5.2 using GMWL equation, the mean isotopic composition of the meteoric water in equilibrium with Lwamondo kaolins is -5.33 and -33.2‰ for $\delta^{18}O_w$ and δD_w, whereas mean isotopic composition when in equilibrium with Zebediela kaolin -5.36 and -33.37‰ for $\delta^{18}O_w$ and δD_w (Table 5.2 and Figure 5.43).

The equilibrium fractionation factor of deuterium (D) between kaolinite and water (α_{k-w} D) of Lwamondo and Zebediela using the GMWL was 0.97 and 0.97. Whereas, the equilibrium fractionation factor of ^{18}O between kaolinite and water of Lwamondo and Zebediela was 1.024 and 1.022 (Table 5.2). Ekosse (2008) had around 40ºC for temperature of formation of Makoro and Kgwakgwe kaolin but Mizota and Longstaffe (1996) had lower values. This findings compared to the temperatures of formation of Lwamondo and Zebediela kaolins based on their stable isotopes values are indicative of low temperature of kaolinitisation; thus ruling out any possible hydrothermal processes.

Table 5.2: Mean isotopic composition of meteoric water and kaolinite-water fractionation factors

Samples	$\delta^{18}O$	δD	T (ºK)	$\delta^{18}O_w$	δD_w	$\alpha_{k-w}\ ^{18}O$	$\alpha_{k-w}\ ^{D}$
Lwamondo	18.6	-65	300.09	-5.33	-33.2	1.024	0.97
Zebediela	16.7	-64	309.73	-5.36	-33.37	1.022	0.97

The isotopic composition of Lwamondo and Zebediela kaolins indicate that they are of weathering origin and formed in a supergene environment. Kaolins of weathering origin have generally higher $\delta^{18}O$ (17 to 23‰) and δD (-80 to 40‰) values. This is supported by kaolin of weathering origin: Nuevo Montecastelo kaolins in Spain (Fernandez-Caliani *et al.*, 2010), Variscan kaolins in Spain (Clauer *et al*., 2015), Burela kaolin deposit in Spain (Galan *et al*., 2016), Lastarria kaolin in Chile (Gilg *et al*., 1999) and La Espingarda kaolin in Patagonia (Dominquez *et al*., 2016).

The major controlling factor in the clay mineral assemblages is the water composition in the environment of deposition (Buhmann and Buhmann, 1990). The 2:1 layer silicates are dissolved by fresh water and enhances kaolinite formation (Keller, 1976), whereas sea water preserves and promotes the genesis of mica, chlorite and smectite (Eberl, 1984). The mineralogy of the studied kaolin being dominated by kaolinite were indicative of relatively uniform chemistry from the processes of weathering, transportation, deposition and reworking of Lwamondo and Zebediela kaolins.

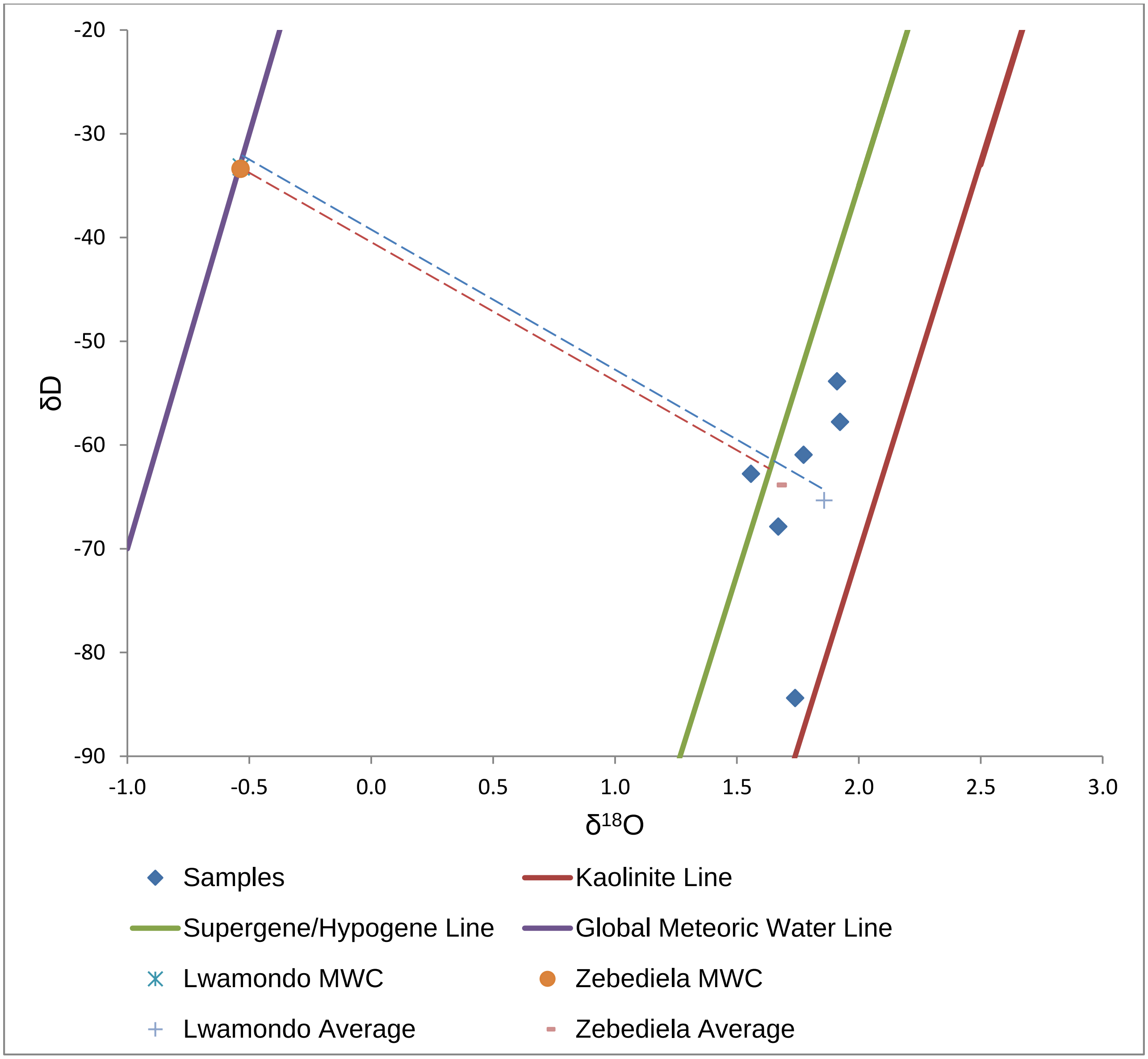

Figure 5.43: $\delta^{18}O$ versus δD diagram for <2 µm fraction of the Lwamondo and Zebediela kaolins. The meteoric water, supergene/hypogene and kaolinite weathering lines (KWL) are given for reference

5.7 Applications

Currently both Lwamondo and Zebediela kaolins are exploited for brick making. Focus is thus directed after the suitability of the kaolin in the brick industry. Ceramic strength of any clayey material is affected by the particle size distribution of argillaceous sediments and the grain particles of the sediments which are divided into three main classes based on their sizes: sand (50-1000 µm), silt (>2-50 µm) and clay (<2 µm). The higher wt % of finer particles is a very important property for some application and confer good binding properties (Sei *et al.*, 2007). Grain size distribution of the clay shows high percentage of fines and low silts which makes them suitable as fillers and coating materials in plant and paper industries.

The higher content of kaolinite in the studied samples makes them good for paints and ceramics. The higher SiO_2, Al_2O_3 and LOI in the studied clays compare favourably with the standard for ceramics and refractory bricks (Singer and Sonja, 1971). Low content of Fe_2O_3 and TiO_2 suggest their suitability for ceramic, refractory and sanitary wares.

According to particle size classification a diagram was developed to evaluate the suitability of clay materials in ceramic applications of studied kaolin's according to Winkler's scheme (Figure 5.44). Lwamondo and Zebediela kaolin were determined as suitable for common bricks, vertically perforated bricks, roofing tiles/ lightweight bricks and thin walled hallow bricks (Manoharan *et al.*, 2012; Ekosse and Mulaba, 2008).

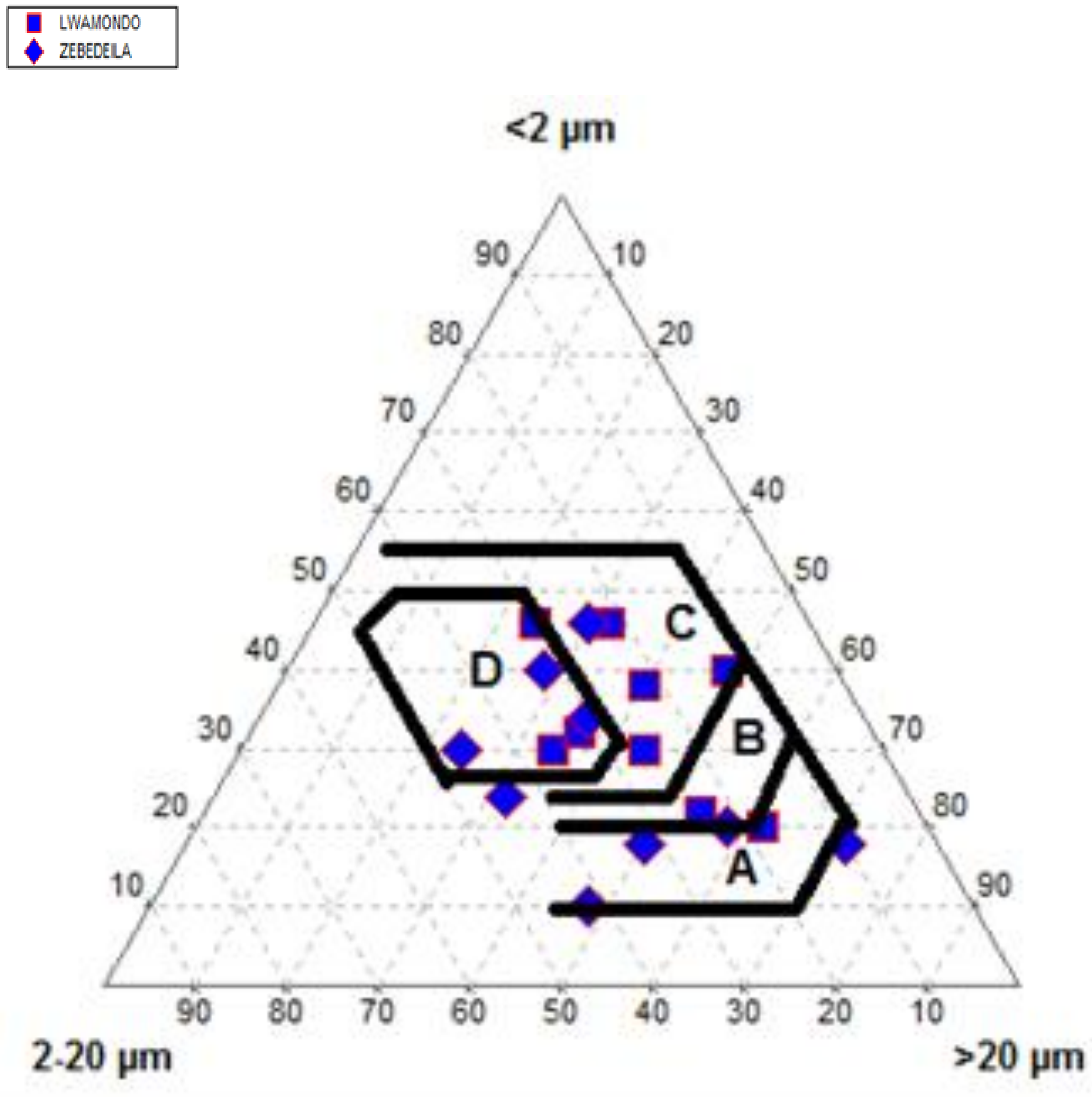

Figure 5.44: Grain size classification of studied kaolins according to Winkler's scheme. (A) Common bricks, (B) vertically perforated bricks, (C) roofing tiles and masonry bricks (D) hollow products (Dondi *et al*., 1992; Manoharan *et al*., 2012; Ekosse and Mulaba, 2008)

CHAPTER SIX

COCLUSION AND RECOMMENDATION

6.1 CONCLUSION

Based on the physico-chemical findings, Lwamondo and Zebediela kaolins have varying colour distribution from whitish to dark reddish brown, due to the presence of goethite and hematite. The particle size was finer indicating weathering in Lwamondo and Zebediela kaolins whereas the pH and EC values indicated that the samples does not contain soluble salts.

Mineralogicaly Lwamondo and Zebediela kaolins were dominated by kaolinite and quartz as a non-clay minerals and other clay minerals presence such as smectite and talc, minor of goethite, hematite, anatase. Occurrence of feldspar, plagioclase and micas are indicative of primary minerals which eventually weathered to kaolinite, smectite and goethite. FTIR results were complimentary to the X-ray diffractometry results. In terms of classifications, three morphological classes were identified and these included: kaolinite booklets and stacks, well developed and irregular flakes and platelets and accordion morphology. These classes reflect the formation and weathering characteristics of kaolinite in particular in the kaolin.

The chemical composition of the kaolins is essentially SiO_2 and Al_2O_3, with minor amounts of TiO_2, Fe_2O_3, MnO, MgO, K_2O and P_2O_3. TiO_2, Fe_2O_3, MnO and MgO affected kaolin colour negatively. Al_2O_3 content was lower than in the theoretical kaolinite due to the presence of quartz and clay impurities. The kaolinitic enrichments with chemically immobile major and trace elements reflect a strong chemical weathering in the source area. High CIA and CIW indices indicate that kaolin as derived during intense chemical weathering of the source area. The elemental ratios suggest that kaolin was deposited in non-marine environment, mostly under oxic humid conditions. The REE pattern shows enrichment in HREE than LREE with slight positive Eu anomaly and contents of other trace elements show evidence of weathering processes related to kaolinitisation of Lwamondo and Zebediela kaolin

The $\delta^{18}O$ and δD values of the kaolinite from the Lwamondo and Zebediela kaolin deposits suggest that they were formed during weathering consistent with supergene origin. The mean $\delta^{18}O$ and δD isotopic values of the studied samples indicate that the kaolin formation was in equilibrium with meteoric water at near surface temperature. The temperature of formation of Lwamondo and Zebediela kaolin based on their stable isotopes values are indicative of low temperature of kaolinitisation, ruling out any possible hydrothermal processes.

Application of the clay used in the manufacturing of bricks were suitable based on physico-chemical, mineralogical and geochemical data. Interpretation from the Winkler diagram indicates that Lwamondo kaolin could be used for common bricks, vertically perforated bricks, roofing tiles, masonry bricks and hollow products and Zebediela could be used for common bricks, roofing tiles, masonry bricks and hollow products.

6.2 RECOMMENDATIONS

- The study cover physico-chemical, mineralogy and geochemistry and give new contribution to their stable isotopic composition ($\delta^{18}O$ and δD), however there is a need for geochronological dating analyses in order to fully ascertain the ages of formation of kaolins.

- The possibility of using them for other applications such as for pottery, stoneware and low temperature ceramics is yet to be investigated.

- Other kaolins occurrences within the region of similar postulated ages should be investigated in order to have a regional paleoenvironmental reconstruction.

REFERENCES

Abou El-Anwar, E.A., Gomaa, M.M., 2016. Electrical, mineralogical, geochemical and provenance of Cretaceous black shales, Red Sea Coast, Egypt. Egyptian Journal of Petroleum 25. 323-332.

Baioumy, H.M., 2013a. Geochemistry and origin of the Cretaceous sedimentary kaolin deposits, Egypt: paleoclimate implications. Chemie der erde.

Baioumy, H., 2013b. Hydrogen and oxygen isotopic compositions of sedimentary kaolin deposits, Egypt: paleoclimate implications. Applied Geochemistry 29, 182-188.

Baioumy, H.M., 2014. Geochemistry and origin of the Cretaceous sedimentary kaolin deposits, Red Sea, Egypt. Chemie der Erde 74, 195-203.

Barker, O.B., 1979. A contribution to the geology of the Soutpansberg Group, Waterberg Supergroup, Northern Transvaal. University of the Witwatersrand, Johannesburg. Unpublished M.sc. Thesis.

Bigeleisen, J., Perlman, M.L., Prosser, H.C., 1952. Conversion of hydrogenic materials to hydrogen for isotopic analysis. Anal chem. 24, 1356-1357.

Borthwick, J., Harmon, R.S., 1982. A note regarding ClF_3 as an alternative to BrF5 for oxygen isotope nalysis. Geochim. Cosmochim. Acta 46, 1666-1668.

Boulvais, P., Vallet, J-M., Esteoure-Choux, J., Fourcade, S., Martineau, F., 2000. Origin of kaolinization in Brittany (NW France) with emphasis on deposits over granite: Stable isotopes (O, H) constraints. Chemical Geology 168, 211-223.

Bouyoucos, G.J., 1962. Hydrometer method improved for making particle size analysis of soils. Agron. J. 54, 464-465.

Brandl, G., 2000. Soutpansberg Group. Catalogue of South African Lithostratigraphic Units, SA Committee for stratigraphy, Council for Geoscience, 6-39-6-41.

Buhmann, C., Buhmann, D., 1990. Hydrogen-isotope geochemistry of diagenetic clay minerals from Cretaceous Sandstones, Alberta, Canada: evidence for exchange. Applied Geochemistry 5, 657-668.

Catuneanu, O and Eriksson, P.G., 1999. The sequencestartigraphic concept and the Precambrian rock record: an example from the 2.7 – 2.1 Ga Trnasvaal Supergroup, Kaapvaal Craton, Precambrian Research, 97, 215-251.

Chamley, H., 1989. Clay sedimenatology. Springer Verlag, Berlin, pp. 623 .

Clauer, N., Fallick, A.E., Galan, E., Aparicio, P., Fernandez-Caliani, J.C., Aubert, A., 2015. Stable isotopes constrains on the origin of kaolin deposits from Variscan granitoids of Galicia (NW Spain). Chem. Geol. 417, 90-101.

Clayton, R.N., Mayeda, T.K., 1963. The use of bromine pentafluoride in the extraction of oxygen from oxides and silicates for isotopic analysis. Geochim Cosmochim Acta 27, 43-52.

Cleland, T.M., 2005. A practical description of the Munsell color system, with suggestions for its use. Boston: Munsell Color Company <available online> http://www.applepainter.com. [Accessed 26 Sep 2012]

Coleman, M.L., Shepherd, T.J., Durham, J.J., Rouse, J.E and Moore G.R., 1982. Reduction of water with zinc for hydrogen isotope analysis. Anal. Chem. 54, 993-995.

Coplen, T.C., 1993. Normalization of oxygen and hydrogen isotope data. Chemical geology, vol 72, pp. 293-297.

Council for Geosciences. 2002. 1:250 000 Geological series, sheet 2228 Alldays.

Craig, H., 1961. Standards for reporting concentrations of deuterium and oxygen-18 in natural waters. Science 13, 1833-1834.

Cravero, M.F., Dominguez, E., Iglesias, C., 2001. Genesis and application of the Cerro Rubio kaolin deposit, Patagonia (Argentina). Applied Clay Science 18, 157-172.

Cuadros, J., Linares, J., 1995. Some evidence supporting the existence of polar layers in mixed-layer illite/smectite. Clays and Clay Miner. 43, 467-473.

Delgado, A., Reyes, E., 1996. Oxygen and hydrogen isotope compositions in clay minerals: A potential single-mineral geothermometer. Geochemical et Cosmochimica Acta 60 (21), 4285-4289.

Department Water Affairs and Forestry., 2004. Strategic framework for national water resource quality monitoring programmes.

Diamond, R.E and Harris, C., 1997. Oxygen and hydrogen isotope composition of Western Cape meteoric water: South African Journal of Science, vol 93, pp. 371-374.

Diko, M.L., 2011. Genesis and Ceramic Applications of selected kaolin occurrences from Limpopo Province, South Africa and South West Region. Unpublished Ph.D. thesis. University of Limpopo, Polokwane, South Africa.

Diko, M.L., Ekosse, G.E., 2012. Physiochemical and mineralogical considerations of Ediki sandstone-hosted kaolin occurrence, south west Cameroon. Internationsl Journal of the Physical Sciences 7(3), 501-507.

Diko, M.L., Ekosse, G.E., 2013. Characterisation of two kaolin facies from Ediki, Southwest Cameroon. Academic Journal 8(18), 698-704.

Diko, M.L., Ekosse, G.E., 2014. Soil ingestion and Associated Health Implications: A physico-chemical and mineralogical appraisal of Geophagic soils from Moko, Cameroon. Ethno Med, 8(1): 83-88.

Dominguez, E.A., Iglesias, C., Dondi, M., 2008. The Geology and Mineralogy of a range of kaolins from the Santa Cruz and Chubut Provinces, Patagonia (Argentina). Applied Clay Science. 40, 124-142.

Dominguez, E.A., Iglesias, C., Dondi, M., Murray, H., 2010. Genesis of the La Espingarda kaolin deposit in Patagonia. Applied Clay Science. 47, 290-302.

Dondi, M., Fabbri, B., Laviano, R., 1992. Characeristics of the clays clays utilized in the brick industry in Apulia and Basilicata (Southern Italy). Mineral Petrologica Acta 35, 181-191.

Dudek, T., 2012. Clay minerals as paleoenvironmental indicators in the Bathonian (Middle Jurassic) ore-bearing clays from Gnaszyn, Krakow-Silesia Homocline. Acta Geologica Polonica 62(3), 297-305.

Eberl, D.D., 1984. Clay minerals formation and transformation in rocks and soils. Philosophical Transactions of the Royal Society, London, A, 241-257.

Ekosse, G.E., 2000. The Makoro kaolin deposit, southeastern Botswana: its genesis and possible industrial applications. Applied Clay Science 16, 301-320.

Ekosse, G.E., 2001. Provenance of the Kgwakgwe kaolin deposit in southeastern Botswana and its possible utilization. Applied clay science 20, 137-152.

Ekosse, G.E., 2005. Fourier transform infrared spectrophotometry and X-ray powder diffractometry as complementary techniques in characterizing clay size fraction of kaolin. Journal of Applied Clay Science and Environmental Management 9 (2), 43-48.

Ekosse, G.E., 2008a. Thermoanalytical characterization, stable isotopes and paleoenvironmental considerations of kaolinite from two genetic sources. Fresenius Environmental Bulletin. 17(1), 29-42.

Ekosse, G.E., 2008b. Spatial distribution of Iron in soils and vegetation cover close to an Abandoned Manganese Oxide Ore Mine, Botswana.Journal of Applied Sciences 8(1): 14-25.

Ekosse, G.E., 2010. Kaolin deposits and occurrences in Africa: Geology, mineralogy and utilization. Applied Clay Science 50 (2), 212-236.

Ekosse, G.E., 2012. Kaolinite: Occurrences, Characteristics and Applications. Nova Science Publishers, pp. 1-30.

Ekosse, G.E., Mulaba-Bafibiandi, A., 2008. Granulometric Evaluation of Continental Bentonites and Kaolin for Ceramic Applications. Journal of Applied Sciences 8 (6), 1021-1027.

Eriksson, P.G and Reczko, B.F.F., 1995. The sedimentary and tectonic setting of the Transvaal Supergroup floor rocks to the Bushveld Complex. J. Afr. Earth Sci. 21, 487-504.

Eriksson, P.G and Reczko, B.F.F., 1995. The sedimentary and tectonic setting of the Transvaal Supergroup floor rocks to the Bushveld Complex. J. Afr. Earth Sci. 21, 487-504.

Eriksson, P.G., Altermann, W., Catuneanu, O., Van der Merwe, R., Bumby, A.J., 2001. Major influences on the evolution of the 2.67-2.1 Ga Transvaal basin, Kaapvaal Craton. Sedimentary Geology. (141-142), 205-231.

Eriksson, P.G., Hattingh, P.J., Altermann, W., 1995. An overview of the geology of the Transvaal Sequence and Bushveld Complex, South Africa. Mineralium Deposita 30, 98-111.

Eriksson, P.G., Schweitzer, J.K., Bosch, P.J.A., Schreiber, U.M., van Deventer, J.L. and Hatton, C.J. 1993. The Transvaal Sequence: an overview. Journal African Earth Sciences 16, 25-51.

Fernandez-Caliani, J.C., Galan, E., Aparicio, P., Miras, A., Marquez, M.G., 2010. Origin and geochemical evolution of the Nuevo Montecastelo kaolin deposit (Galicia, NW Spain). Applied Clay Science 49, 91-97.

Folorunso, D.O., Olubambi, P., Borode, J.O., 2014. Characterization and Qualitative analysis of some Nigerian Clay Deposits for refractory Applications. IOSR Journal of Applied Chemistry, vol 7 (9), pp. 40-47.

Galan, E., 2006. Genesis of clay minerals. In: Bergaya, F., Theng, B.K.G., Lagaly, G. (eds). Hnadbook of Clay Science. Developments in Clay Scienec, volume 1. Elsevier, Oxford, pp. 1129-1162.

Galan, E., Aparicio, P., Fernandez-Caliani, J.C., Miras, A., Marquez, M.G., Falllick, A.E., Clauer, N., 2016. New insights on mineralogy and genesis of kaolin deposits: The Burela kaolin deposit (Northwestern Spain). Applied Clay Science 131. 14-26.

Galan, E., Ferrel, R.E., 2013. Genesis of clay minerals. Journal of Developments in Clay Science, vol 5A, 83-126.

Gilg, H.A., Hulmeyer, S., Miller, H., Sheppard, S.M.F., 1999. Supergene origin of the Lastarria Kaolin Deposit, South-Central Chile, and Paleoclimatic Implications. Clays and clay minerals, vol 47 (2), 201-211.

Gilg, H.A., Sheppard, S.M.F., 1996. Hydrogen isotope fractionation between kaolinite and water revisited. Geochim. Cosmochim. Acta 60.529-533.

Gilg, H.A., Sheppard, S.M.F., 1996. Stable isotope geochemistry of clay minerals. Clay minerals, 31, 1-24.

Gilg, H.A., Weber, B., Kasbohm, J., Frei, R., 2003. Isotope geochemistry and origin of illite-smectite and kaolinite from the Seilitz and Kemmlitz kaolin deposit, Sexony, Germany. Clay Miner, 38, 95-112.

Hallberg, R.O., 1976. A geochemical method for investigation of paleo redox conditions in sediements: Ambio, special, Special Report, 4, 139-147.

Harris, C., Compton, J.S., Bevington, S.A., 1999. Oxygen and hydrogen isoopes composition of kaolinite deposits, Cape Peninsula, South Africa: Low- temperature, meteoric origin. Economic geology. vol 94, pp 1353- 1360.

Hartzer, F.J. 1995. Transvaal Inliers: geology and relationship with the Bushveld Complex. PhD. thesis 415p. Rand Afrikaans University, Johannesburg, South Africa.

Hartzer, F.J., 1995. Transvaal Supergroup inliers: geology, tectonic development and relationship with the Bushveld Complex, South Africa. Journal of African Earth Scienecs, vol 21 (4), pp. 521-547.

Harvey, C.C and Murray, H.H., 1997. Industrial clays in the 21st Century: A perspective of exploration, technology and utilization. Appl. Clay Sci 11, 285-310.
Heckroodt, R.O., 1991. Clay and Clay materials in South Africa. Journal of the Southern African Institute of Mining and Metallurgy, vol 91 (10), pp. 343-363.

Heckroodt, R.O., 1992. Kaolin Resources of the Republic of South Africa. Handbook 13. pp 102.

Horbe, A.M.C., 2011. Oxygen and hydrogen isotopes in pedogenic minerals-implication for paleoclimate evolution in Amazonia during the Cenozoic. Geoderma 163,178-184.

Hughes, J.C and Brown, G., 1979. A crystallinity index for soil kaolins and its relation to parent rock, climate and soil maturity. J. Soil Sci. 30, 557-563.

Ismail, S., Husain, V., Anjum, S., 2014. Mineralogy and Genesis of Nagar Parker Kaolin Deposits, Tharparkar District, Sindh, Parkistan. International Journal of Environmental Geology. 5(1), 33-40.

Jones, B and Manning, D.A.C., 1994. Comparison of geochemical indices used for the interpretation of paleoredox condiions in ancient mudstones. Chem Geol 111: 111-129.

Kabanda, T.A., 2003. Climate, A first synthesis of the environmental, biological & cultural assets of the Soutpansberg. Pp. 10-11. In: Berger, K., Craffort, J.E., Gaiger, L., Gaiger, M.J., Hahn, N., MacDonald, I. (eds). Leach Printers and Signs, Makhado.

Keller, W.D., 1976. Scan electron micrographs of kaolins collected from diverse environments of origin 1. Clays and Clay Minerals 26, 1-20.

Kogel, J.E and Lewis, S.A., 2001. Baseline studies of the clay minerals society source clays: chemical analysis by Inductively Coupled Plasma-Mass Spectroscopy (ICP-MS). Clays and Clay minerals. vol 49 (5), 387-392.

Kuehni, J., 2002. The early development of the Munsell system. Colour Research and Application, 27 (1), 20-27.

Lanson, B., Beaufort, D., Berger, G., Bauer, A., Cassagnabe, A., Meunier, A., 2002. Authigenic kaolin and illitic minerals during burial diagenesis of sandstones: A review. Clay minerals, 37, 1-37.

Lario, J., Spencer, C., Plater, A.J., Zazo, C., Goy, J.C., Dabrio, C., 2002. Particle size characterisation of Holocene back-barrier sequences from North Atlantic Coasts (SW Spain and SE England).

Lawrence, J.R., Taylor Jr, H.P., 1971. Deuterium and oxygen-18 correlation: clay minerals and hydroxides in Quaternary soils compared to meteoric waters. Geochim Cosmochim Acta 35: 993-1003.

Le Bas, M.J., Le Maitre, R.W., Streikeisen, A., Zanetin, B., 1986. Chemical classification of volcanic rocks based on the total alkali- silica diagram. Journal of Petrology 27 (3), 745-750.

Linlin, W., Bo, J., Dehua, P., Chengming, Y., Chunlin, Z., 2011. Characteristics and genesis of clay minerals in the Northern margin of the Qaidam Basin. Mining Science and Technology (China) 21, 141-145.

Lyons, T.W., Werne, J.P., Hollander, D.J., Murray, R.W., 2003. Contrasting sulphur geochemistry and Fe/Al and Mo/Al ratios across the last oxic- to- anoxic transition in the Cariaco Basin, Venezuela. Chem. Geol, 195, pp. 131-157.

Madejová, J. and Komadel, P., 2001, Baseline studies of the clay minerals source society: infrared methods. Clays Clay Miner., 49, 410–432.

Madi, K., Tsanwani, M., Zhao, B., Tongu, E., 2013. Insights on structural, petrographical, mineralogical and geochemical approach on the Grahamstown kaolin deposit: Genesis in the Eastern Cape, South Africa. International Journal of Sciences: Basic and Applied Rsearch (IJSBAR), vol 10(1), pp. 146-163.

Madhavaraju, J and Ramasamy, S., 1999. Rare earth elements in a Limestones of Kallankurich-Chi Formation of Ariyalur Group, Tiruchirapalli Cretaceous, Tamil Nadu. Journal of the Geological Society of India, 54, 291-301.

Madukwe, H., Ogungbesan, G., Aturamu, A., Ajisafe, Y., 2016. Provenance, tectonic setting, source area weathering and paleoenvironment of the Illaro Formation, Dahomey Basin, Nigeria. Journal of Environmental and Earth Science. Vol 6(10), pp. 95-119.

Mahjoor, A.S., Karimi, M., Rastegarlari, A., 2009. Mineralogical and Geochemical Characterisation of Clay Deposits from Soouth Abarkouh District of Clay Deposit (Central Iran) and their Applications. Journal of Applied Sciences 9(4): 601-614.

Manju, C.S., Narayanan Nair, V., Lauthambika, M., 2001. Mineralogy, geochemistry and utilization study of the Madayi kaolin deposit, North Kerala, India. Clays and clay minerals 4, 355-369.

Manoharan, C, Suthatsan, P., Venkachalapathy, R., Vasanthi, S., Dhanapandian, S., Veeramuthu, K., 2015. Spectroscopic and rock magnetic studies on some of Basic and Applied Sciences, vol 2 (1), pp. 39-49.

Mizota, C and Longstaffe, F., 1996. Origin of cretaceous and Oligocene kaolinites from the Iwaizumi clay deposit, Iwate, northwestern Japan. Clay and Clay Minerals 44, 408-416.

Moore, D.M and Reynolds, R.C., Jr. 1997. X-ray Diffraction and the identification and analysis of clay minerals. Oxford University Press, Oxford, pp. 378.

Mousa, D.A., Abdou, A.A., El Gendy, N.H., Shehata, M.G., Kassab, M.A., Abuhagaza, A.A., 2014. Mineralogical, geochemical and hydrocarbon potential of subsurface Cretaceous shales, Northern Western Desert, Egypt. Egyptian Journal of Petroleum 23. 67-78.

Murray, H.H., 2007. Applied Clay Mineralogy. Occurrences, processing and application of kaolins, bentonites, palygorskite-sepiolite and common clays. Developments in clay science. 2, pp. 179.

Murray, H.H., 2002. Industrial Clays Case Study. Mining, Minerals and Sustainable development No.64

Murray, H.H., 1999. Applied clay mineralogy today and tomorrow. Clay minerals 34, 39-49.

Murray, H.H., 1986. Clays. In: Ullmans encydopedia of Industrial chemistry. 5th edition, pp. 109-136.

Murray, H.H and Keller, W.D., 1993. Kaolin, Kaolin and Kaolin. In Murray, H.H., Bandy, W., Harvey, C., (eds), kaolin genesis and utilization. Special publ, vol.1. The clay miner. Sci., pp.1-24.

Nesbitt, H.W and Markovics, G., 1980. Chemical processes affecting alkalis and alkaline earths during continental weathering. Geochimica et Cosmochimica Acta, 44(11), 1659-1666.

Nesbitt, H.W and Young, G.M., 1984. Prediction of some weathering trends of plutonic and volcanic rocks based upon thermodynamic and kinetic consideration. Geochim Cosmochim A, 48: 1523-1534.

Ngole, V.M and Ekosse, G.E., 2012. Physico-chemistry, mineralogy, geochemistry and nutrient bioaccessibility of geophagic soils from Eastern Cape, South Africa. Scientific Research and Essays vol 7(12), pp. 1319-1331.

Ngole, V.M., Ekosse, G., Ayonghe, S.N., 2007. Physico-chemical, mineralogical and chemical considerations inunderstanding the 2001 Mabeta New Layout landslide, Camerron. J. Appl. Sc. Environ. Manage. vol 11(2), pp. 201-208.

Ngon Ngon, G.F., Bayiga, E., Ntamak-Nida, M.J., Etamie, J., Noa Tang, S., 2012. Trace elements geochemistry of clay deposits of Missole II from the Doula sub-basin in Cameroon (Central Africa): a provenance study. Journal of Sciences, Technologie & Development, vol 13 (1), 20-35.

Njoya, A., Nkoumbou, C., Grosbois, C., Njopwouo, D., Njoya, D., Courtin-Nomade, A., Yvon, J., Martin, F., 2006. Genesis of Mayouom kaolin deposit deposit, Weastern Cameroon. Applied Clay Sci. 32, 125-140.

Nyakairu, G.W.A., Koebel, C., Kurzweil., H., 2001. The Buwambo kaolin deposit in central Uganda: Mineralogical and chemical composition. Geochemical Journal 35, 245-256.

Odoma, A.N., Obaje, N,G., Omada, J.I., Idakwo, S.O., Erbacher, J., 2013. Paleoclimate reconstruction during Mamu Formation (Cretaceous) based on clay mineral distributions. IOSR Journal of Applied Geology and Geophysics. vol 1(5), pp 40-46.

Ojo, O.J., Adepoju, S.A., Alhassan, N., 2014. Geochemical and Mineralogical Studies of Kaolinitic Clays in Parts of Illorin, Southwestern Basement Rock Area, Nigeria. Universal Jourbnal of Geoscience 2(7): 212-221.

Olaremu, A.G, 2015. Physico-Chemical characterization of Akoko mined kaolin clay. Journal of Minerals and Materials characterization and Engineering, 2015, 3, pp. 353-351.

Papoulis, D and Tsolis- Katagas, P., 2008. Formation of alteration zones and kaolin genesis, Limnos, Island, Northeast Aegean Sea, Greece. Clay Miner, 43, 61-646.

Pirajno, F., 2009. Hydrothermal processes and mineral systems. Springer, Netherlands, pp. 1250.

Rimmer, S.M., 2004. Geochemical paleoredox indicators in Devonian-Mississipian black shales, Central Appalachian Basin (USA). Chemical Geology 2066, 473-391.

Roaldset, E., 1978. Mineralogical and chemical chamges during weathering, transportation and sedimentation in different environments with particular references to the distribution of Ytrium and Lanthanide elements. Ph.D. Thesis, Geol. Inst. Univ. of Oslo, Norway.

Roser, B.P., Korsch, R.J., 1986. Determination of tectonic setting of sandstone-mudstone suites using SiO2 content and K2O/Na2O ratio. Journal of Geology 94: 635-650.

Rozanski, K., Araguas, L., Gonfiantini, R., 1993. Isotopic patterns in model global precipitation in climatic change in continental isotopic records (ed A.G.U): Geophs. Monogr 78, 1-36.

Ruan, C.D and Ward, C.R., 2002. Quantitative X-ray powder diffraction analysis of clay minerals in Australian coals using Rietveld methods. Appl. Clay Sci, vol 21, pp. 227-240.

Ruiz Cruz, M.D., 2007. Genesis and evolution of the kaolin-group minerals during the diagenesis and the beginning of metarmorphism. In: Fernando Nieto and Juan Jimenez-Millan, eds. “Diagenesis and Low-Temperature Metamorphism. Theory, Methods and Regional Aspects” Seminarios SEM, 3, pp. 41-52.

Saiki, B., Parthasarathy, G., 2010. Fourier Transform Infrared Spectroscopic Characterization of Kaolinite from Assam and Meghalaya, Northeastern India. J. Mod. Phys. 1, 206-210.

Saiki, B., Parthasarathy, G., 2010. Fourier Transform Infrared Spectroscopic Characterization of Kaolinite from Assam and Meghalaya, Northeastern India. J. Mod. Phys. 1, 206-210.

Santos Jr, A.E.A and Rossetti, D.F., 2006. Depositional Model of the Ipixuna Formation (lae Cretaceous? Early Tertiary), Rio Capim Area, Northern Brazil. Latin American Journal of Sedimentaology and Basin Analysis, 13, pp. 65-87.

Santos Jr, A.E.A., Rossetti, D.F., Murray, H.H., 2007. Origin of the Rio Capim Kaolinites (Northern Brazil) revealed by analyses. Journal of Applied Clay Science 37, 281-294.

Santos, I., Costa, C., Quintela, A., Terroso, D., Ferraz, E., Roca, F., Dorzhieva, O., Krupstakaya, V., Vigasina, M., 2014. Mineralogical composition of sedimentary and residual kaolin dposists from Portugal. Communicacoes Geologicas, vol 101(1), pp. 195-197.

Santos, M.D.C., Varajao, A.F.D.C., Yvon, J., 2006. Geochemistry of a sedimentary lateritic kaolin deposit in Quadrilatero ferrifero, Brazil. Journal of Geochemical Exploration 88, 318-320.

Savin, S.M., Epstein, S., 1970. Oxygen and hydrogen isotope geochemistry of clay minerals. Geochim Cosmochim Acta 4: 25-42.

Sei, J., Morato, F., Kra, G., Staunton, S., Quiquampoix, H., Jumas, J.C., Olivier-Fourcade, J., 2006. Mineralogical, Crystallographic and Morphological characteristics of natural kaolins from the Ivory Coast (West Africa). Journal of African Earth Sciences 46, 245-252.

Shemang, E.M., Suh, C.E., Ekosse, G.E., Coetzee, S.H., 2007. Crystal morphology and indicative microchemistry of kaolinite from kaolin occurrences in Alkaleri Region, Northeastern Nigeria. GeoActa 6, pp. 15-26.

Sheppard, S.M.F., and Gilg, H.A., 1996. Stable isotope geochemistry of clay minerals. Clay minerals, 31, 1-24.

Sheppard, S.M.F., Nielsen, R.L., Taylor, H.P., Jr., 1969. Hydrogen and oxygen isotope ratios of clay minerals from porphyry copper deposits. Econ Geol 66, 515-542.

Singer, F., Sonja, S.S., 1971. Industrial ceramics publication, pp. 18-56. Chapman and Hall, London, UK.

Tan, K.H., 1996. Soil sampling preparation and analysis. Marcel Dekker Inc. New York, pp 392.

Thiry, M., 2000. Paleoclimatic Interpretation of clay minerals in marine deposits: an outlook from the continental origin. Earth-Science Reviews, 49, 201-221.

Tobia, F.F., Shangola, S.S., 2016. Mineralogy, geochemistry and depositional environment of the Beduh Shale (lower Triassic), Northern Thrust Zone, Iraq. Turkish Journal of Earth Sciences 25: 367-391.

Vaculíková, L., Plevová, E., Vallová, S. and Koutník, I.:2011, Characterization and differentiation of kaolinites from selected Czech deposits using infrared spectroscopy and differential thermal analysis. Acta Geodyn. Geomater, 8, No. 161, 59–67.

Van Reeuwijk., 2002. Procedures for soil analysis. Int. Soil. Ref. and Info. Centre, Wageningen, The Netherlands, Tech. paper 9, pp. 101 .

Vidal, P., 1998. Geochimie. Serie geoscience. Dunod, Paris, P.1990.

Werne, J.P., Lyons, T.W., Hollander, D.J., Formolo, M.J., Sinninghe Dameste, J.S., 2003. Reduced sulphur in euxinic sediments of the Cariaco Basin: sulphur isotope constraints on organic sulfur formation. Chem. Geol, 195, 159-179.

Wronkiewicz, D.J., Condie, K.C., 1987. Geochemistry of Archean shales from the Witwatersrand Supergroup, South Africa: source-area weathering and provenance. Geochimica et Cosmochimica Acta, 51(9), 2401-2416.

Wu, W., Xu, S., Lu, H., Yang, J., Yin, H., Liu, W., 2011. Mineralogy, major and trace element geochemistry of riverbed sediments in the headwaters of the Yangtze Tongtian River and Jinsha River. Journal of Asian Earth Sciences. 40, 611-621.

Zhou, C.H., and Keeling, J., 2013. Fundamental and applied research on clay minerals: from climate and environmental to nanotechnology. Journal of Applied Clay Science 74, 3-9.

Zuoping, Z and Chuanxian, L., 1995. The behaviour of rare-earth elements (REE) during weathering of granites in Southern Guangxi, China. Chinese Journal of Geochemistry. vol 15(4), pp. 344-352.